Layered Extrusion of engineering Metal Alloys (LEMA) using Semi-Solid Thixotropic Feedstock

By:

Abdullah Alharbi

A thesis submitted in partial fulfilment of the requirements for the degree of Doctor of Philosophy

The University of Sheffield
Faculty of Engineering
Department of Mechanical Engineering

Submission Date

31/08/2023

ABSTRACT

Additive manufacturing (AM) has gained significant attention in low- and medium-volume industries due to its ability to create custom products with complex shapes, design freedom, material savings, and short lead times. While most AM processes focus on thermoplastics, there is increasing interest in metal AM systems, including powder bed fusion processes. However, these methods often involve high acquisition and operating costs, limiting accessibility. To address this, this study focuses on developing and investigating the Layered Extrusion of Engineering Metal Alloys (LEMA) system as a cost-effective alternative metal AM approach. The LEMA system manipulates alloys in the semi-solid thixotropic state. Utilising semi-solid metal slurry in extrusion-based AM can result in metal components with substantially lower operating costs and reduced thermal stresses compared to laser-based method.

Experimental work initially conducted (Phase I) using the LEMA system involved in-situ creation of semi-solid thixotropic metallic alloys, particularly focusing on the Zn-Sn binary system, but improvements were made to the LEMA system for the subsequent phase to enhance performance. In Phase II, thermodynamic simulations and thermal analysis have indicated that Zn-40Sn holds promise for semi-solid thixotropic applications. Cold extrusion and heat treatment processes were employed to produce thixotropic feedstock with proper microstructures before being additively manufactured. The 3D printed components were evaluated and the result suggested that the adapted method for semi-solid billets preparation was feasible technique which then helped in a successful printing metallic material.

Additionally, printing experiments were conducted to study the effects of major process parameters on the quality of deposited single-layer. It was demonstrated that single layers could be printed under 1.5 mm diameter orifice, extrusion speed of 20 mm/min, substrate moving velocity of 200 mm/min, and extrusion temperature of ≈ 313 ℃. The optimized printing process parameters from these experiments were then utilized for multilayer printing. It was found that substrate temperature is a key factor for achieving good metallurgical layer bonding at the interface of the printed layers. The research results support LEMA's feasibility as an alternative for the metal additive manufacturing route and lays the groundwork for processing SSMs with higher melting points in the future.

DEDICATION

This thesis is dedicated to my parents who left the world. I know they would be proud, and I will forever be grateful for the knowledge and values they instilled in me.

ACKNOWLEDGEMENTS

"In the name of ALLAH, who is most Gracious and merciful. ALLAH's harmony and kindness be upon the last and final messenger and Prophet Muhammad (SAW)." ALLAH has blessed me with the patience and strength necessary to follow a straight path and complete my PhD studies. My utmost thanks to Allah Subanahutalah for His perpetual kindness and support during my research.

This thesis would not have been accomplished without the help of the following people (in no particular order), no matter how large or small the contribution.

First, I would like to thank my esteemed academic advisor, Prof. Kamran Mumtaz, for his generous guidance and help throughout this endeavour. I would like to sincerely express my gratitude toward him for continually being the reference point of clarity and expectation at each stage. He is a supportive advisor and teacher, as well as an admirable entrepreneur. Without his supervision, it would have been much more difficult to overcome the challenges associated with this work. It was an honour to have such a highly regarded academic as an advisor and to receive so much of his valued time, helping to ensure that I succeeded not only academically but also on a personal level.

I would like to express my sincere thanks to Dr. Masoumeh Faraji from Coventry University for her constant support and guidance during my PhD studies. Her patience, encouragement, and immense knowledge were fundamental for the successful completion of my studies. I will always remember those periodic meetings, which included enjoyable and exciting discussions about the findings of my research.

I am also grateful to all the university staff who helped me carry out the experimental part of my research and trained me in different skills. A special thanks goes to the technical staff in the Department of Mechanical Engineering, Gareth Barker, David Webster, Matt Kirkland, Richard Kay, Chris Todd, Wendy Birtwistle, Jack Leach, and Kurt Bonser for their constant support and patience. I am also indebted to the technical staff in the Department of Materials Science and Engineering, to Tesoro Monaghan and Sylwester Mikula in particular, who trained me in metallurgy and specimen preparation. I would like to thank Dr. Cheryl Shaw for her assistance with SEM analysis at the Sorby Centre for Electron Microscopy. I also want to extend special thanks to Dr. Oday Hussein for his help with DSC experiments.

I would like to thank my friends for their support and encouragement, especially Dr. Ashfaq Khan, who has been there for me at every step and always had time to listen to my thoughts and help me straighten them out.

Sheffield has been a great place to meet amazing people. To my Saudi community here, thank you for making this city a home to me.

I am indebted to my beloved country, the Saudi government, and its representatives the in Technical and Vocational Training Corporation. I sincerely thank them for their financial support for this PhD research.

Finally, but perhaps most importantly, I would like to thank people for their continuous support throughout my life and education. First, I would like to acknowledge the people who brought me into the world, my father Mohammed and mother Maqbula, who passed away before the completion of my education. I know they would be proud, and I will forever be grateful for the knowledge and values they instilled in me.

Thanks also to my dear brothers and sisters, who were wishing to see this day, for their encouraging words and timely support throughout my time in the UK. I also thank my relatives and friends all over the world for their kind wishes and emotional support.

I am immensely grateful to my loving wife, Mrs. Nesrin Bakour, for her valuable help, care, tolerance, and support, and for providing me with emotional stability, which I indeed required during my research. She is the source from where I take the strength and inspiration to achieve my goals. I also dedicate this work to her.

My deepest thanks to my loving daughters Refal, Lemar, Taleen, Lareen, Ransi, and Evana, who gave me the strength to undertake this task and were the source of my happiness. My sons, Ammar and Yazan, also inspired and motivated me to do my best. Without them, I would not be where I am today.

I owe the success of this project to all of you. I love you all and thank you.

NOMENCLATURE

Al	Aluminium
AM	Additive Manufacturing
ASTM	American Society for Testing and Materials
CAD	Computer Aided Design
CDF	Closed Die Forging
CNC	Computer Numerical Control
C_O	Donates the concentration of the alloy
D	Screw diameter
DED	Directed Energy Deposition
DMD	Direct Metal Deposition
DMLS	Direct Metal Laser Sintering
EBDM	Electron Beam Direct Manufacturing
EBM	Electron Beam Melting
FDM	Fused Deposition Modelling
f_L	Liquid fraction
F_S	Solid fraction
h	Channel depth
k	Equilibrium partition ratio
LEMA	Layered Extrusion of Metallic Alloy
LENS	Laser Engineered Net Shaping
LMD	Laser Metal Deposition
LOM	Laminated Object Manufacturing
Mg	Magnesium
MHD	Magnetohydrodynamic
MIT	Massachusetts Institute of Technology
MJM	Multi-Jet Modelling
m_L	liquidus line slope

N	Rotational speed
NRC	New Rheocasting
Pb	Lead
PBF	Powder Bed Fusion
PBIH	Powder Bed and Inkjet Head
PM	Permanent Mould Casting
R	Gas constant
RAP	Recrystallization and Partial Melting
SHS	Selective Heat Sintering
SIMA	Strain Induced Melt Activated
SLM	Selective Laser Melting
SLS	Selective Laser Sintering
Sn	Tin
SQC	Squeeze Casting
SSM	Semi-Solid Metal
STL	Transformed to a Stereolithographic
T	Temperature
T_L	Liquidus line
T_M	Solvent melting point
T_S	Solidus line
UC	Ultrasonic Consolidation
wt.%	Percentage by Weight
Zn	Zinc
ΔE	Activation energy
η	Viscosity coefficient
$\dot{\gamma}$	Shear rate
3D	Three-dimensional

TABLE OF CONTENTS

LIST OF FIGURES

LIST OF TABLES

1 INTRODUCTION

In contrast to subtractive manufacturing approaches, AM is defined as an industrial technology that uses 3D model data to produce a final object by depositing a material layer by layer. AM has become one of the most rapidly advancing technologies in the last decade and is used by industries, experts, students, academics, and market analysts. This method is employed not just to manufacture prototypes, models, and casting patterns but also to build fully functional parts made of various materials, including metals, ceramics, polymers, and composites[45]. The ability to create complex 3D components without costly hard tooling, dies, or moulds has made AM attractive for many applications. Furthermore, the AM process can significantly shorten the time required between the first conceptual design of the product, prototype manufacturing, and distribution to the market[46]. Multiple AM techniques have been established to create engineered parts with high geometric freedom. However, most approaches have been designed for materials that are not metallic, even though metal-based additive manufacturing has constantly grown in high-value industries, such as aerospace, automobiles, and medicine. This is because metal AM enables the production of fully dense components with high geometric complexity/customisation using a variety of high-performance metals. The most popular metal AM techniques are Electron Beam Melting (EBM) and Selective Laser Melting (SLM), which use high-power energy sources, such as lasers or electron beams, to completely melt metallic powder feedstock from a powder bed. While feasible, the complete melting and rapid solidification of the feedstock during these processes can generate large thermal stresses within the formed components[47, 48],resulting in undesirable defects, such as residual stresses and high porosity[27, 49]. As a result, post-processing steps, such as heat treatment or isostatic pressing, are required to modify the microstructure and enhance the mechanical characteristics[50, 51]. Metal support structures must also be included to hold the part and reduce geometric deformation caused by procedure-induced thermal stress. This results in time-consuming and costly post-processing operations for support structure removal[52, 53].In addition to low deposition rates, the powder bed system is primarily dependent on the use of powder-based feedstock materials with particular features, which involves sophisticated equipment to produce[54]. Furthermore, the hardware used in these high-power laser/electron beam systems is inherently expensive and energy-inefficient. These technical challenges and economic barriers prevent the widespread adoption of metal AM in new markets. Hence, there is a demand to develop a new low thermal stress-inducing, energy-efficient, low-cost metal AM process.

Eliminating the drawbacks discussed above is highly desirable for the practical 3D printing of structural metal products. Extrusion-based AM system generally consists of low-cost hardware and a low-power energy source. The material extrusion route, also known as FDM, involves heating (normally around 200°C) feedstock material to obtain a sufficient viscosity before depositing it through a nozzle onto a surface. This technique was previously limited to the plastics AM industry, but recently it has been implemented in the direct fabrication of functional metal parts[20, 55].

This may offer several advantages compared with laser and electron beam sources, including low manufacturing costs, high deposition rates, and the production of components with reduced thermal gradients[40, 56-59]. However, these methodologies are restricted in terms of material variety owing to the necessity for complete melting and generally possess low mechanical properties as a result of interlayer delamination[20]. Additionally, extrusion-based metal AM requires a sufficiently high viscosity of the printing feedstock at a controlled flow rate[59]. Some studies have focused on developing the extrusion-based AM of alloys in the semi-solid state to improve the flow of materials and process stability, mitigating the defects associated with conventional extrusion-based metal AM. These approaches mainly relied on semi-solid metals (SSMs), which were developed by manipulating the microstructure and rheological properties of the alloy. In SSM processing, the alloy is treated at temperatures between that of the liquidus and solidus, where solid particles are embedded in a liquid matrix, resulting in a solution with a more desirable viscosity[31]. The shear-thinning rheology of SSMs with the desired globular microstructure allows for controlled and stable manufacturing during the material extrusion and deposition process, which facilitates fully dense 3D patterns[37, 40]. Furthermore, the mechanical properties of the 3D printed part can be enhanced based on the tailored microstructure, which cannot be obtained using more traditional metal AM methods[35, 40].

SSM extrusion can be classified into two methods based on the way of achieving the material in the semi-solid state. In the liquid stirring methods, the SSM alloy with desired characteristics is prepared by partial solidification and stirring of the molten metal, and then the SSM alloy is deposited through a nozzle onto a substrate[37]. In contrast, an SSM alloy can be obtained by the reverse process, similar to the FDM method, in which preformed nondendritic metal feedstock is subjected to partial re-melting to form the required semi-solid microstructure before being extruded to form the component[60].

The implementation of semi-solid technology in metal AM using low-melting point alloys was initially proposed by Rice et al.[37]. They employed a rheocasting system that involves a reservoir surrounded by heating elements to melt the materials and a rotor to generate the desired SSM before being deposited onto a movable platform. This system is relatively

bulky, leading to more restrictions, and this approach is only suitable for fabricating large parts because of the deposition size. Finke and Feenstra developed a traditional FDM method using a semi-solid slurry to fabricate metal parts[60]. They have used several model alloys of Sn-based low melting point. The work was conducted by partially re-melting a metal wire to the desired semi-solid condition. Then, the materials were squeezed out through a nozzle onto a plate moving in the x-y plane. The microstructures of the printed specimens showed typical globular structures corresponding to SSMs found in the literature. However, a boundary was observed in the cross-section of two layers, indicating that complete interlayer bonding was not achieved. Chen et al. processed alloys by direct metal writing to fabricate structures using only metals with low melting points, including Bi-Sn alloys that melt below 300°C[40]. They printed a sample from an ingot of $Bi_{75}Sn_{25}$, and the materials were extruded in a semi-solid state through a nozzle before being heated and stirred by a grooved rotor to obtain the globular microstructure. Jabbari and Abrinia also developed a machine for SSM extrusion and deposition to process low melting temperature Sn-Pb alloys[35, 61]. The The strain induced melt activation (*SIMA*) method was used to prepare the metal feedstock and introduce the favourite globular feedstock microstructure. Then, the treated wire was processed using thixo-extrusion equipment, where a semi-solid slurry was extruded onto a surface according to a specific trajectory to form patterns. However, multilayer stacking was not achieved. Recently, an FDM process was developed to manufacture biodegradable Mg-Zn alloy parts[28]. Two-step hot deformation was applied to prepare the metal filament and refine the dendritic microstructure. Then, the filament was transferred to the modified 3D thixo-printing machine, where it was heated under a semi-solid temperature range to form a globular microstructure and subsequently printed on a moving substrate. Although the intended parts were produced, they failed to show proper bonding between the deposited layers. In the present research, the two SSM extrusion approaches were investigated to determine the feasibility of an extrusion-based process for producing 3D objects using Zn-Sn alloys.

1.1 Research Novelty

The metal extrusion-based technique has demonstrated its feasibility as a form of additive manufacturing. However, there has been limited exploration into its full commercialization potential. Furthermore, while the technique has shown promise, there has been minimal exploration of semi-solid formation in conjunction with the additive manufacturing process, which represents a significant opportunity for advancement. Such experimentation could potentially be a significant advancement

and lead to fabricate structural metallic components alongside the desired rheological characteristics at low processing temperatures.

A thorough examination of pertinent literature unveiled that the utilization of the extrusion-based AM method with semi-solid metallic alloys (SSM-AM) has consistently been confined to alloys with relatively low melting temperatures. To further unlock the highest levels of energy conservation and time efficiency in AM of metal alloys, it is advantageous to closely examine the suitability of direct extrusion of semi-solid slurries and creation of 3D structures within a metallic AM framework. To the best of our understanding, there have been no instances reported in the literature to process Zn-Sn materials in semi-solid additive manufacturing (SSM-AM). Therefore, the present research aims to leverage the scientific principles of thixotropy to control feedstock viscosity below the full melting temperature of Zn-40Sn alloy. To elucidate the fundamental concept of this methodology, it proposes the development of a novel additive manufacturing process called Layered Extrusion of Engineering Metal Alloys (LEMA). LEMA is considered as an extrusion-based AM method for manufacturing metal components. The study shows that extrusion-based AM technology is viable for cost-effectively producing metal parts with simple and low thermal stress induction[62, 63]. Consequently, LEMA can capitalize on these benefits.

An additional innovative strategy involved is introducing the desired thixotropic feedstock in AM metallic extrusion processes. This achieved by controlling the appropriate viscosity of the feedstock without the requirement to attain full melting to ensure successful extrusion and layered deposition.

Another novel approach of this study lies in its thorough investigation of critical machine variables essential for optimal operation, including nozzle diameter, extrusion speed, substrate moving speed, and nozzle-to-substrate distance. By systematically varying these parameters, the quality of printed parts and the optimal parameter settings for extrusion and deposition process can be identified. While the study does not aim for exhaustive parameterization, it aims to establish fundamental operating conditions ensuring consistent process performance and high-quality results.

Also, this study addresses a critical knowledge gap concerning the interlayer bonding dynamics within semi-solid metal additive manufacturing processes, emphasizing the necessity for comprehensive investigation. Additionally, this

research will extend its scope to encompass a thorough examination of feedstock preparation methods and the structural characteristics of printed components. By delving into these key aspects, this study aims to contribute valuable insights to the field of metal additive manufacturing, thereby advancing its capabilities and applications.

1.2 Research Aims and Objectives

Although polymer extrusion-based AM is well developed, with commonly employed processes, such as FDM[64], the present body of knowledge and technology cannot be immediately transferred to molten alloys owing to their considerably different rheological behaviours. Particularly, SSM alloys represent a thixotropic fluid with a required non-Newtonian fluid behaviour, making it difficult to apply directly in metal extrusion-based AM. System modifications or a novel metal extrusion AM system would be necessary. Implementing SSM alloys in an extrusion-based AM system facilitates controlled and consistent fabrication during the extrusion and deposition process, resulting in fully dense 3D parts. Some investigators have confirmed the possibility of extrusion printing of SSM alloys. However, existing extrusion-based methods rely on low melting points, preventing them from being widely applied in industry. This is primarily due to a lack of equipment and fundamental understanding of extrusion-based AM for SSM alloys. This thesis aims to close this important knowledge gap and validate SSM extrusion AM closer as an economically feasible industrial process. In this context, this project involves building a novel metal 3D printing process that enables freeform extrusion printing of SSM alloy structures, as well as investigating the underlying principles involved in extrusion-based AM of thixotropic Zn-Sn feedstock.

1.2.1 Objectives

The principal objective of this PhD thesis is to design and implement a process for creating semi-solid thixotropic materials with controlled viscosity for controllable extrusion and the fabrication of 3D metal shapes. Thus, it is necessary to design and build a specially developed system that enables experimental studies. The primary outcome is a low-cost metal extrusion-based AM system that produces less thermal stress and does not require the use of expensive high-source laser/electron beams. There are several key objectives of this study:

- Conduct basic research on thixotropic metal processing and the essential link between thixotropy and extrudability, and then determine an appropriate formulation for Zn-Sn metal alloys with the desired thixotropic properties suitable for extrusion layered manufacturing.

- Conduct experimental investigations on solid-liquid phase transitions that occur during the solidification of materials under specific conditions and identify the suitable thixotropic feedstock process.
- Manufacture the thixotropic feedstock, which begins with designing and building an extrusion apparatus capable of adapting non-thixotropic materials into a thixotropic form.
- Develop a novel AM system that meets the LEMA concept and examine the novel deposition system to demonstrate the feasibility of the process for Zn-Sn alloys, as well as optimise the essential process parameters required for creating reliable parts.

1.3 Thesis Overview

To build a novel metal extrusion-based AM method, similar to other metal AM processes, an understanding of the material properties, mechanical engineering design, system performance, and solidification processes must be developed. Thus, the knowledge related to the concept is broadly covered in seven main chapters, in addition to the appendixes. Each chapter is outlined as follows:

Chapter 1. This chapter provides the introduction, brief overview, and background of the overarching research aims and corresponding objectives.

Chapter 2. There is not much information available related to the LEMA system because it is a novel process. Therefore, similar research corresponding to the LEMA system and research in related disciplines are examined in the literature review. This chapter covers the literature review on AM and its potential advantages and applications. Background information is given on a variety of AM processes, with a special focus on direct metal AM technologies. Next, to overcome the existing limitations of the conventional AM methods, an overview of metal AM extrusion processes is discussed, including the current research challenges. Finally, this chapter concludes by presenting the results of AM with SSMs, including a summary of metal AM extrusion methods and their limitations.

Chapter 3. This study aims to examine a novel approach for creating 3D metal structures through the semi-solid extrusion of alloys, and a deep understanding of topics related to SSM is required for developing such a system. This chapter presents an extensive review of SSM processing, including the fundamental properties, rheology of SSM slurries, SSM compositions, and methods for producing non-dendritic feedstocks. Moreover, methodologies of SSM processing and their advantages and applications are featured to provide the context for the present study, followed by a brief description of the research gaps.

Chapter 4. Once the research and previous literature have been clarified, experimental work is performed to evaluate LEMA capabilities. As the LEMA system is a novel approach, two major iterations of the LEMA design are implemented during this project. This section demonstrates Phase 1 of the experimental methodologies used in this investigation. Then, based on the outcomes and lessons learned from Phase 1, the configuration of the LEMA system is re-designed. Thus, this chapter also proposes an alternative mechanism in the LEMA system to achieve improved results, specifically addressing the limitations identified in Phase I. Moreover, a detailed description of the experimental equipment and processes used and developed to obtain pre-alloyed feedstock and comprehensive characterisation is also provided.

Chapter 5. The important results of the study are presented regarding Phase I, followed by a comprehensive discussion regarding the outcomes of Phase I.

Chapter 6. The results and discussion of Phase II are described. The chapter starts by presenting observations of established alloys used in the developed AM extrusion method. Thermodynamic simulations for selected alloys, including the comparison between Thermo-Calc and DSC analysis, are illustrated, followed by a discussion of the microstructural characterizations of the as-received alloys. The metallurgical examination of the prepared feedstock before and after heat treatment is also presented and discussed. A comprehensive investigation of the effect of process parameters on producing a single layer is performed. Finally, the optimized process parameters used for printing multilayers are described, followed by the main conclusion derived from Phase II.

Chapter 7. The work is summarised in this chapter, stressing the overall findings of the research, and recommendations are suggested to elevate the LEMA process to the level of maturity required for practical applications.

2 LITERATURE REVIEW TO ADDITIVE MANUFACTURING

2.1 Background to Additive Manufacturing

Additive Manufacturing (AM) is one of the non-conventional manufacturing processes and can also be referred to as three-dimensional (3D) printing, additive fabrication, additive layer manufacturing, freeform fabrication, additive techniques, and additive processes[65]. The first AM system was brought into existence in the 1980s as a way of creating functional products [66]. At this point, AM was known as rapid prototyping [67], because the concept behind this invention was to generate models to assist designers in the virtual visualisation of the design. Thus, it allows designers to test and improve the part before committing to building.

In contrast to the subtractive manufacturing methods, where the removal of the materials is required, an AM process involves making an object from 3D model data by adding material layer by layer [19] to generate the final product shape. Firstly, the design of the desired object is created using a 3D computer-aided design (CAD) programme. In order to be recognised by the machine, the CAD file is transformed to a stereolithographic (STL) format[68]. The STL file is uploaded to the machine, and then the machine is organised to build the required part by depositing and fusing material in a layer-upon-layer format. The completed part can be discharged from the machine platform, or it might require different post-processing operations, depending on the particular AM method used, any other product shape, or finishing requested requirements.

2.2 The benefits and Limitations of AM Systems

Generally, additive technologies have distinct advantages over traditional processes of manufacturing namely, CNC machining and casting. Holmström et al.[69] illustrated some of these benefits, showing that AM provides higher degrees of design freedom so a complex product design can be achieved, resulting in greater customisation flexibility. Furthermore, AM results in faster creation of components and reduced production costs due to its reduced consumption of materials compared to machining processes which create significantly more waste material. As machine tooling is not needed, this accelerates the prototyping and component building processes and reduces the cost of new products owing to the tool-less concept. Further, AM is well suited for limited production batches, and AM products can be optimised for a variety of functions[69]. Another benefit of the AM system is the fact that the range of materials processed by AM techniques includes polymers, metals and ceramics [70]. Moreover, the range of materials is expanding as the technology is developing further.

Although AM techniques have numerous advantages, they also have challenges associated with the processes that limit the application of such techniques for the production of functional parts. Some of the challenges associated with AM techniques are long preparation time, the difficulty in producing uniform and the consistent properties of materials, a high cost of manufacturing, problems with surface finish and accuracy as well as the need for post-processing[71]. Another consideration that should be taken into account is that problems with the surface finish which could affect the integrity of the produced part [72]. As a result, these disadvantages may lead to delays and limit the development and applications of AM technologies.

2.3 Applications of Additive Manufacturing Technologies

The applications of AM have been growing rapidly in the last few years in many areas of industrial sectors, used either by individuals or larger businesses and enterprises which are adopting AM to produce end-use components on a large scale. A good example of this application is in the aerospace sector that shows its interests in AM due to its capability of making high-performance products and more complex parts. These include turbine blades, compressor support cases, and engine housings. AM can also be used to repair aircraft engine components [73].

Medical companies have also begun to use several applications because of the ability of AM to enable design customisation to fabricate complex-shaped parts. AM is now used in the development of custom implants such as skulls, knee joints, elbows and hip joints[74]. The application of AM in dental implants benefits notably from the capability of AM technology to construct complex geometries and structures, such as bridges, crowns and fixtures [75]. Not least of all, AM technology is a suitable method for making physical models for clinical practising, education, and device-testing purposes to help physicians and researchers with better visualisation and understanding of the actual treatments required[76, 77].

It is worth pointing out that automotive companies are attracted by these technologies which allow new specialised parts to be provided in a short time, eventually assisting them in reducing the expenditures involved in the manufacturing of vehicles. AM has been innovated to tailor and produce several parts for auto-sports through SLS, SLM and EBM techniques. Engineers could successfully take advantage of these technologies to make the F1 gearbox which is 25% lighter – having a reduced volume of nearly 20% and having better mechanical properties than the machined parts [73]. Besides, engine exhausts, drive shafts and braking systems represent another practical application manufactured by AM [78].

2.4 Additive Manufacturing Processes

Today, several types of additive manufacturing technologies have been introduced. The different AM techniques may be classified depending on the way the material layer is fused in forming products and the way the machine system is adopted. Additionally, classification can also be grouped according to the kind of materials being utilised, such as metals, polymers or ceramics.

The American Society for Testing and Materials (ASTM) Board F42 on Additive Manufacturing has proposed seven methods for AM. The following table provides a short overview of the main AM processes categorised by ASTM F42[65].

Table 2.1: AM processes considered by ASTM F42[65].

AM Process	Brief Description	Related techniques	Material
VAT Photopolymerisation	Liquid photopolymer selectively cured by light activation	Stereolithography (SLA)	Plastics, Polymers
Material Jetting	Droplets of build material selectively deposited	Multi-jet modelling (MJM)	Plastics, Polymers
Binder Jetting	Liquid bonding agent selectively deposited to join powder	Plaster-based 3Dprinting (PP), Powder bed and inkjet head (PBIH)	Metals, Polymers, Ceramics
Material Extrusion	Material selectively dispensed through nozzle or orifice	Fused deposition modelling (FDM)	Plastics, Polymers
Powder Bed Fusion	Thermal Energy selectively fuses region of the powder bed.	Selective laser sintering (SLS), Electron beam melting (EBM), direct metal laser sintering (DMLS) and selective heat sintering (SHS)	Metals, Polymers
Sheet Lamination	Sheets of material bonded together	Ultrasonic consolidation (UC) and Laminated object manufacturing (LOM)	Paper, plastic, metals
Directed Energy Deposition	Focused thermal energy melts materials as deposited	Laser metal deposition (LMD)	metals

2.4.1 Stereolithography (SLA)

Stereolithography(SLA), founded by 3D Systems in 1986, was the first commercial AM process developed on the market and is still the most commonly used apparatus [79]. As presented in Figure 2.1, it utilises a UV laser to cure the surface of liquid resin in a tank to produce the cross-section of the 3D object. The starting material used here is a photopolymer resin which comes in a liquid form. The process starts after the reservoir is filled with the liquid resin, and the build platform is then lowered by layer thickness. The UV light is applied to solidify the resin of each layer. When the layer is completed, the platform is moved down to build a new layer. The whole process is repeated until the desired 3D object is shaped. After completion, the printed part is removed and immersed in a chemical solution to eliminate the excess resin and supports, and is followed by post-processing in a curing oven[77]. This method is fast, with high accuracy, and provides models with a relatively good surface finish [78]. However, long post-processing times, the equipment and support structure required, and materials cost, are some of the drawbacks which may adversely affect this technology [74].

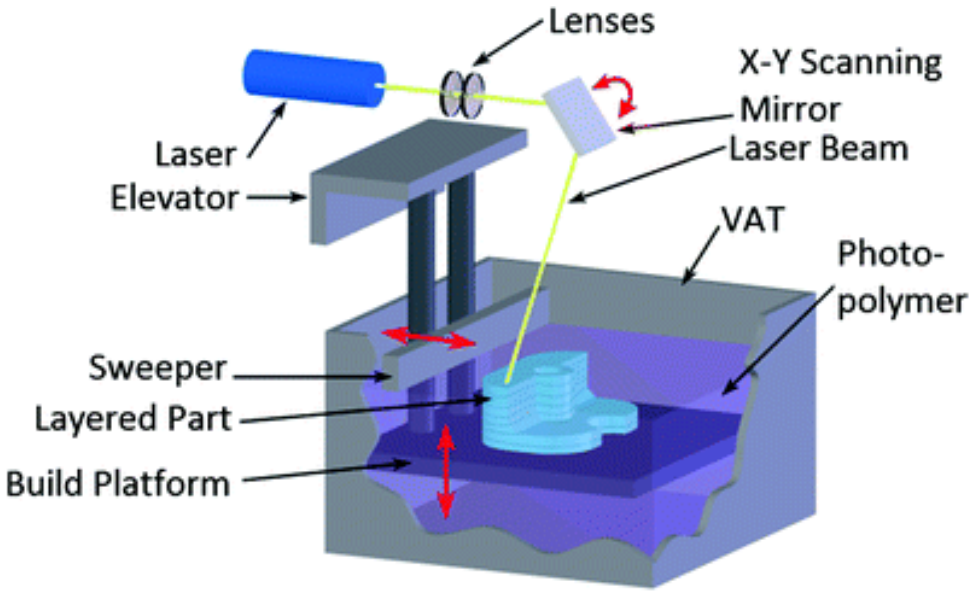

Figure 2.1 Schematic of the SLA process [11].

2.4.2 Material Jetting

Material jetting (MJ) manufactures physical models in a similar way to a 2D inkjet printer. However, instead of printing ink onto a piece of paper, a liquid of specific materials is deposited onto a build surface to form each layer and then hardened by specific approaches. The origins of this ink-jet printing process dating back to 1994 by a company called Solidscape[79]. There are multiple synonyms with material jetting that fall under this category including, but not limited to: Drop-on-demand (DOD)[80], Multi-jet

modelling (MJM)[73] PolyJet [81] and Thermojet [82]. Speaking generally, they are very similar ink-jet methods with slight differences. The printing process begins with a hundred material droplets being jetted where required by print-heads, which move in the x-y plane across a build platform. Following that, UV-light sources are used to cure the printed cross-section. After the first layer is finished, the platform descends, allowing the print-head to deposit the second layer upon the previous one. This process continues until the 3D model is fully obtained[83]. Figure 2.2 [5] below, illustrates the technology of Material Jetting. In general, the machine consists of more than one print-head – With one being required to dispense photopolymer materials for building the 3D object, and another to jet a gel-like substance to create support structures for overhangs that can be removed easily by a water-jet[84].

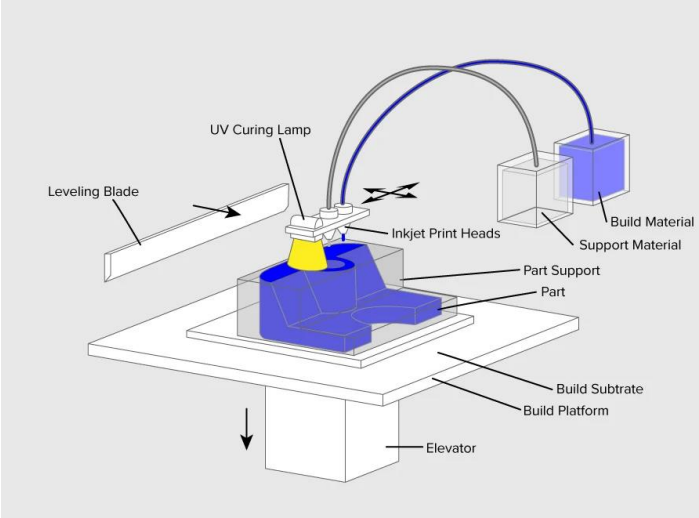

Figure 2.2 Material Jetting schematics [5].

One of the main features of this technology is the capability to print multi-materials with full-colour options and different physical properties as a result of the additional print-heads implemented in this process[85]. Good accuracy, build speed and office-friendliness are additional benefits that also make this technology popular for both industry and home-users [86].

Perhaps the most serious shortcoming of this method is that MJ parts are structurally weaker compared to others, such as stereolithography and selective laser sintering [67] Consequently, inkjet-based processes are reserved mainly for un-functional parts manufacture.

2.4.3 Material Extrusion

Today, material extrusion technology, which is also termed Fused Deposition Modeling (FDM) or Fused Filament Fabrication (FFF), is arguably the most prominent AM strategy

among people and businesses. This stems from the fact that FDM printers of all AM technologies offer the most affordable, simple, and office-friendly approach. FDM was introduced in the 1990s by Stratasys Inc., and it is currently normally used for applications such as demonstration models, design proofs and prototyping[87]. As seen in Figure 2.3[41], the basic concept of the process involves a material filament fed through an extrusion head and then drawn through a heated nozzle that has to be deposited layer-by-layer onto a movable substrate to produce the desired cross-sectional area. When the first layer is finished, the substrate is moved a step down in order to allow for an additional layer to be applied on top of the preceding layer, and the process is reiterated till the 3D object is completed.

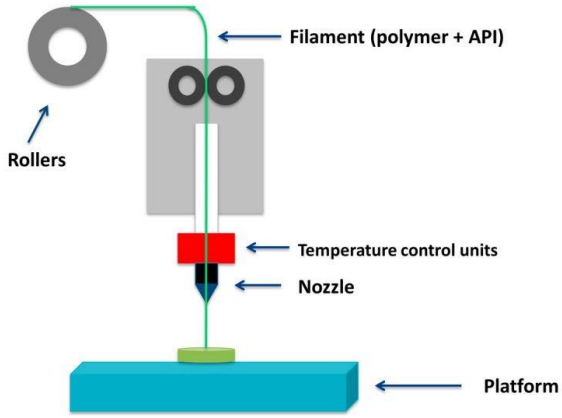

Figure 2.3 Schematic diagram of the Fused Deposition Modelling System [41].

One of the fundamental strengths of FDM is the wide range of processable materials with a variety of colours and types. They are mostly thermoplastics, for instance: Polylactide (PLA) and acrylonitrile butadiene styrene (ABS). Also, the investigation of engaging new materials in FDM printers was vindicated as it can now include metal, ceramics and carbon fibre[88]. Despite the many mentioned benefits of FDM technology, it does, however, have some weaknesses, as the accuracy and surface finish of the components can be poor compared to some other 3D printing technologies[82]. Moreover, the mechanical properties of the fabricated part and building speed need to be improved to make it successful in practice [88].

2.4.4 Direct metal additive manufacturing technologies

In the first stage, the rapid prototyping was invented to create 3D-models for visual purposes. However, in the modern day, these technologies are no longer used just for printed models. Because of its inherited advantages, it has developed from rapid prototyping to rapid manufacturing for end-use applications[89]. Even though the multitude of AM applications processes are polymer-based, AM options have been

expanded to manufacture components from alternative materials including: metals [19], ceramics[90], glass, concrete[91] and composites[92]. Among these, metal additive manufacturing has attracted a significant amount of attention and growth.

According to the annual worldwide survey on the growth of rapid prototyping and AM manufacturing, published by Wohlers Associates, in 2017, the sales of metal machines increased to an extent that 1,768 metal AM systems were sold, compared to 983 AM systems that were sold in 2016 – leading to an estimated increase of 80% in one year. As shown in Figure 2.4 [7], there has been a 650% growth in the last five years, and a 233% growth in the last two years.

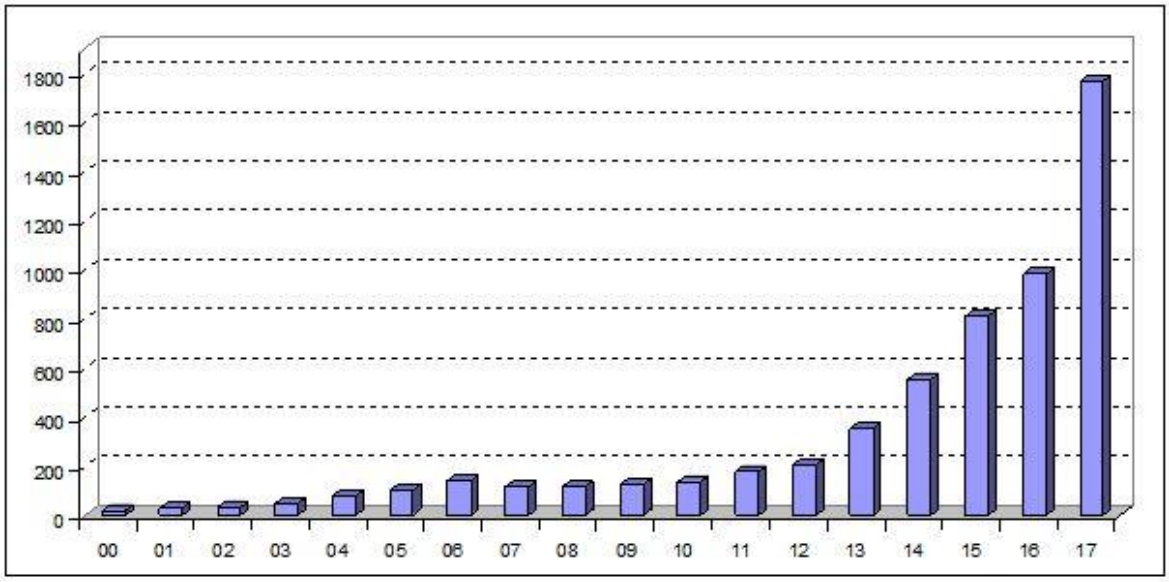

Figure 2.4 Annual sales of metal AM system 2000 to 2017 [7].

In the meantime, there has been a rising trend in metal materials revenue, as the global reference source reported a growth of 41.9% in 2018, an estimated $260.2 million, in comparison to the $183.4 million from the previous year, with growth exceeding 40% for at least five consecutive years. See Figure 2.5[52], for the sales of metals material market.

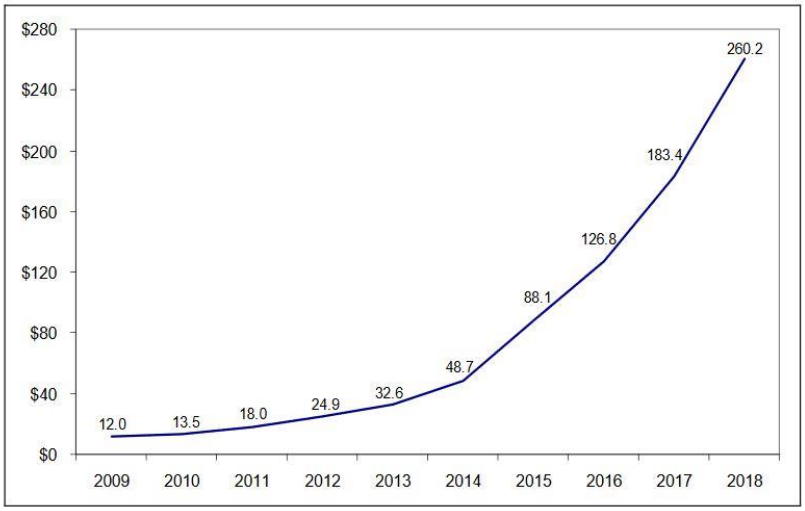

Figure 2.5 Revenue growth from metals for AM in 2019.

Such significant activity and growth among AM metal systems and materials is a telling indicator of the wider adoption of AM for diverse manufacturing applications. Moreover, AM worldwide suppliers and customers are becoming aware of the advantages of manufacturing metallic components using AM approaches.

Metal AM methods have been increasing due to the interest of commercial sectors, such as aerospace and medical-related industries etc. This is due to its feasibility of direct formation of better 3D components eliminating the need for tooling or machining[52], Also, AM metal benefits from less material waste, reduced manufacturing costs and shorter lead times for geometrically-complicated structures compared to conventional manufacturing systems.

The basic process of all AM metal-based fashions comprised of building up a metallic structure from a powder feedstock, wire, or sometimes sheet, in which the starting material is fused using an energy input such as a laser or beam and then converted layer by layer into a 3D-shape[93].

Although polymer-based materials attracted the most attention among the AM materials, additive manufacturing now uses metals extensively. Metal material options proceed to grow due to research centres, universities and AM manufacturers continuing to provide advances in AM metal materials and addressing their challenges. A variety of materials available for metal AM systems include: steels, aluminium alloys, nickel-based alloys, cobalt-chrome and titanium alloys. The development of new AM materials is advancing, thus, some research is being carried out to engage metal materials like high-entropy alloys[94], magnetic alloys[95], amorphous metals[96], and functionally-graded materials(FGM) [97] .

Typically, metal feedstocks can be used in the forms of powder, wire or thin sheets which are always used with sheet lamination technology. Such powder raw materials are normally used within the main powder-based AM systems, powder bed fusion (PBF) and directed energy deposition (DED), that are technologically employed to produce the metal component. A feedstock wire can also be used instead of a powder form in DED[98].

In general, metallic parts produced using AM systems offer similar features and sometimes compete with parts that are conventionally manufactured [19]. Gorsse et al.[39] presented a comprehensive overview of the microstructures and mechanical properties of three different additive-manufactured alloys compared to conventionally-processed alloys. The study has reported that AM-printed components can achieve characteristics better than ones prepared by conventional casting and forging routes, as shown in Figure 2.6.

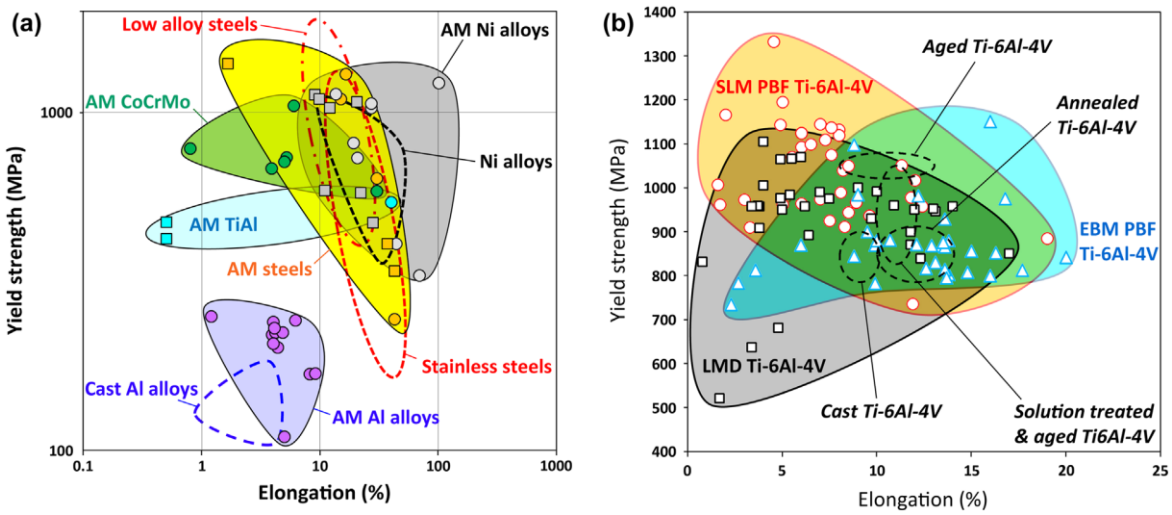

Figure 2.6 Materials property of alloys produced by AM and conventionally manufactured alloys (dashed lines), (a) steels, Ni alloys, Al alloys, TiAl and CoCrMo, and (b) Ti-6Al-4V alloys [39].

There are a number of diverse AM metal printing processes that are used in these applications throughout industry. In the literature, it found that there are numerous ways to categorise AM metal processes, including energy source, type of the material feedstock, state of the feedstock, processing techniques, material distribution, etc,[99]. For example, based on the energy source being used in AM, the processes can be branched out in three major categories: laser-based, electron-beam-based and arcwelding-based. All metal AM methods fall into one of seven standard categories which are issued by the ASTM F42 Committee on Additive Manufacturing, including: binder jetting, power bead fusion, sheet lamination, and direct energy deposition[65]. Though these are diverse categories, the metal AM processes share a relatively generic methodology. Each of the four classifications consists of distinct machine types, as illustrated in Figure 2.7 [32]. A summary of the process overview for the four AM technologies developed to fabricate

metal parts, together with their benefits, weakness and applications, is provided in the next section.

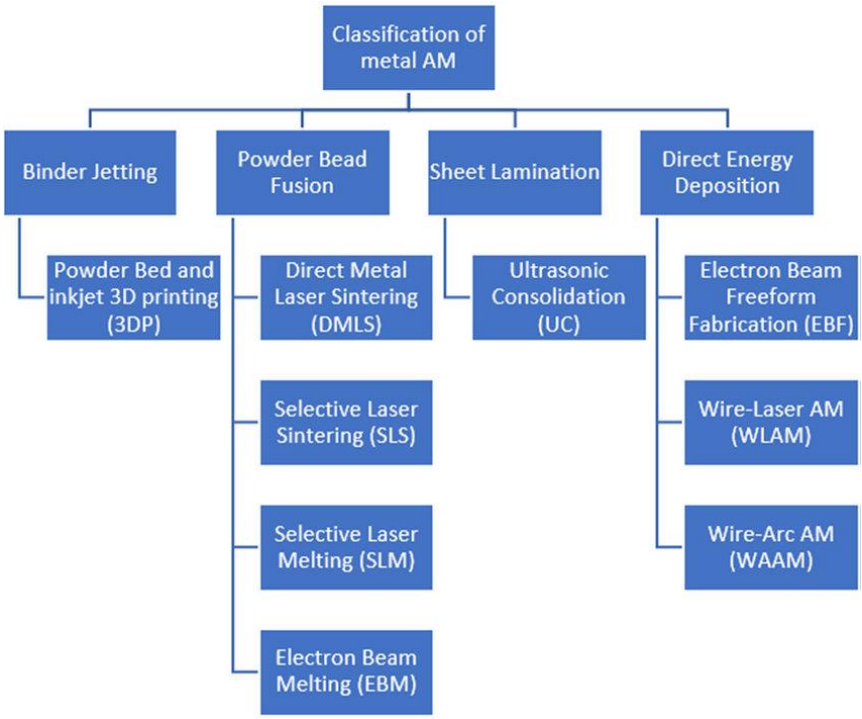

Figure 2.7 Metal AM systems classification [32].

2.4.4.1 Powered Bed Fusion (PBF)

Direct Metal Laser Sintering, Selective Laser Melting and Electron Beam Melting are considered to be the most common forms of metal AM processes relating to PBF for industrial applications. The general processes of PBF are shown in Figure 2.8[8]. The deposited metal powder over the powder bed is selectively fused/melted by a high-energy scanning electron or laser beam in order to form the cross-section of the desired part. The build platform is then decreased to let a new layer of powder take place over the previous layer using a roller. This procedure is iterated until a fully dense 3D part is fashioned. Once the part is completed and the system has cooled down, the unused powder is detached, and the part is moved towards further processing in order to further improve its quality.

.

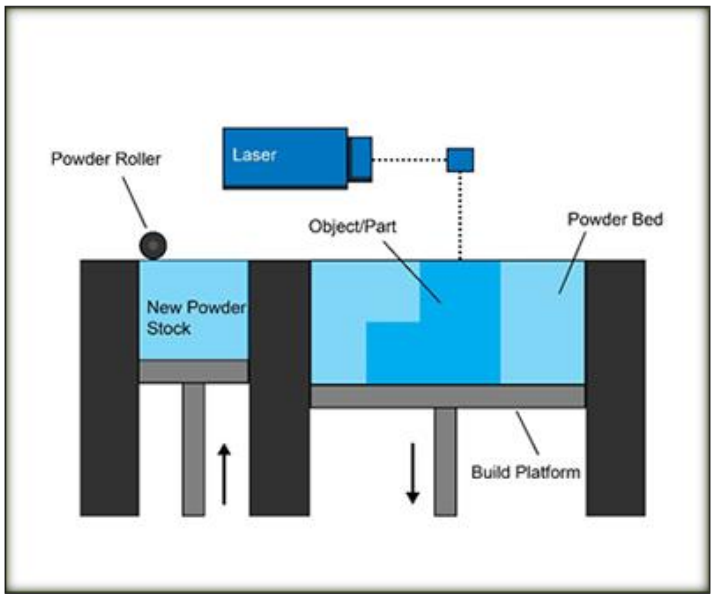

Figure 2.8 Illustration of the generic processes of PBF [8].

These PBF technologies can produce complex geometrical parts that are not easily made by other conventional manufacturing systems. Further advantages include a better surface finish, excellent mechanical properties and the utilisation of a wide range of metal alloys[100].

While metal AM processes, as a whole, have been fundamentally employed in many industrial applications, there are various challenges that still occur within FBF technologies. One of the most challenging aspects of such SLM/EBM systems is residual stresses that are formed as a result of the huge thermal gradients within the process due to the quick heating and freezing of the powder feedstock[100]. Additionally, these undesired stresses may harmfully influence the mechanical properties of parts and lead to increased post-processing times during heat treatments (employed to eliminate the geometric distortions produced). Other undesired defects are fractures, typically due to fatigue produced by the structure of the components[101].

Another major drawback to metal AM systems, such as SLM/EBM, is the general cost of the process. The process costs of maintenance, feedstock, hardware, etc., are high and will impede the development of the metal AM process within industrial applications for efficiently creating products[102]. Even though the metal AM processes are seen as competitors to traditional manufacturing approaches, another limitation is their inefficient use of energy involved in the transformation of electrical power to high laser/electron beam energy employed in AM technologies, such as SLM/EBM[103].

2.4.4.2 Binder Jetting

Binder Jetting is a manufacturing process that belongs to metal AM technologies, where a part is created using two materials: a metal powder, and a binding agent that normally

comes in a liquid form. In this process, the binder, which acts as an adhesive liquid, is selectively printed onto a pre-deposited powder bed. Then, the powder is bound together creating the first layer of the physical object. A schematic diagram of the process of Binder Jetting is illustrated in Figure 2.9 [27]. This method has a very large build volume and can print metal parts with a low cost compared to that of DMLS/SLM. However, this process does have its disadvantages, including a limited range of materials associated with the lower mechanical properties due to the higher porosity of the parts[104].

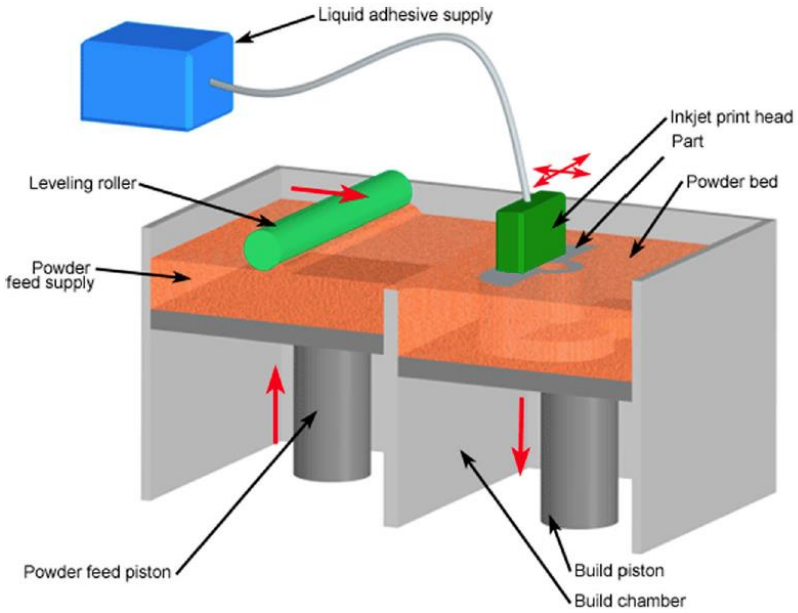

Figure 2.9 Schematic illustration of the Binder Jetting system [27].

2.4.4.3 Directed Energy Deposition (DED)

DED is a 3D printing system essentially employed to make 3D structures from metallic alloys. This method is well-suited for repairing or adding more features to existing parts [105]. The fundamental concept of the DEM process is based on melted metallic alloys that are deposited onto the desired surface via a nozzle. As shown in Figure 2.10[19] the nozzle is mounted to a multi-axis arm system to allow for material deposition at any angle. The materials (wire or powder) are being melted upon deposition by a high-energy source – either a laser or electron beam projector. After the deposited materials are fused, further material is introduced, and the practice is repeated layer by layer till the desired shape is completed.

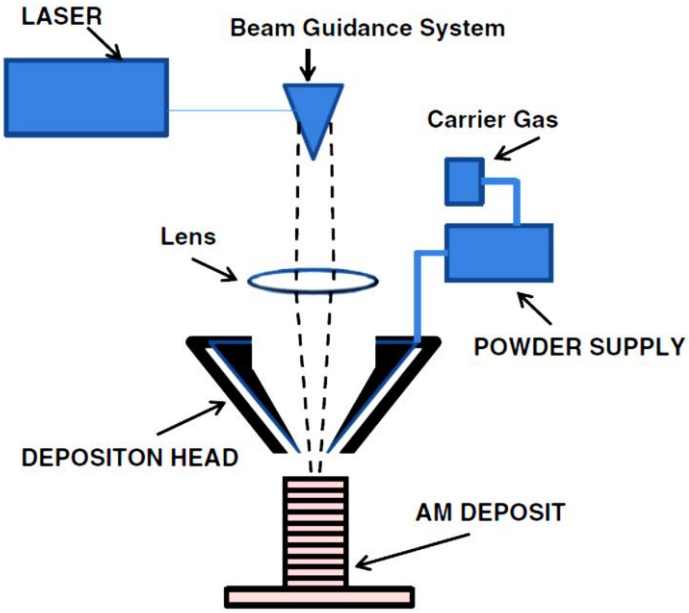

Figure 2.10 Generic design of a DED set-up [19].

Although there are many benefits of DED, such as relatively high building speed (compared to PBF), repair and manufacturing functions, and a larger area of a building (which can be seen in this process)[19], DED does suffer from some serious shortcomings that include higher surface roughness, which means post-processing is required in order to achieve the preferred features [106]. Another problem with this approach is that the thermal histories of the process have a serious impact on the fabricated microstructure and can result in the presence of residual stresses because of the melting and reheating cycles during the additive manufacturing process[67].

2.4.4.4 Sheet Lamination (SL)

Unlike other Metal AM processes that use powder or wire feedstock, SL uses material sheets which are stacked and then bonded together to construct the physical part. An additional cutting operation step is required to shape the desired cross-section of the layer. Ahn[105] states that there are two broad categories of sheet lamination: laminated object manufacturing (LOM), and ultrasonic consolidation (UC) processes. In LOM, sheets of material, which are supplied from a material spool, are placed onto a movable substrate. The layers are bonded together using a heated roller and then a knife or laser used to cut the target shape. After a layer is completed, the substrate is moved down before a fresh sheet of material is applied to the previous one, and the process is repeated until the entire part is completed. A post-processing procedure is essential, such as removing the remaining materials to acquire the favoured surface and finish[73, 107]. Figure 2.11 a)[108] illustrates a bonding process of LOM. Interestingly the UC process adopts a similar layer-by-layer concept but uses ultrasonic welding of the metal film

instead of an adhesive. As can be seen in Figure 2.11 b) [33], ultrasonic vibration by sonotrod, in association with pressure, causes the layer to melt and weld which is then followed by a CNC milling process to trim and achieve the required cross-section of the layer.

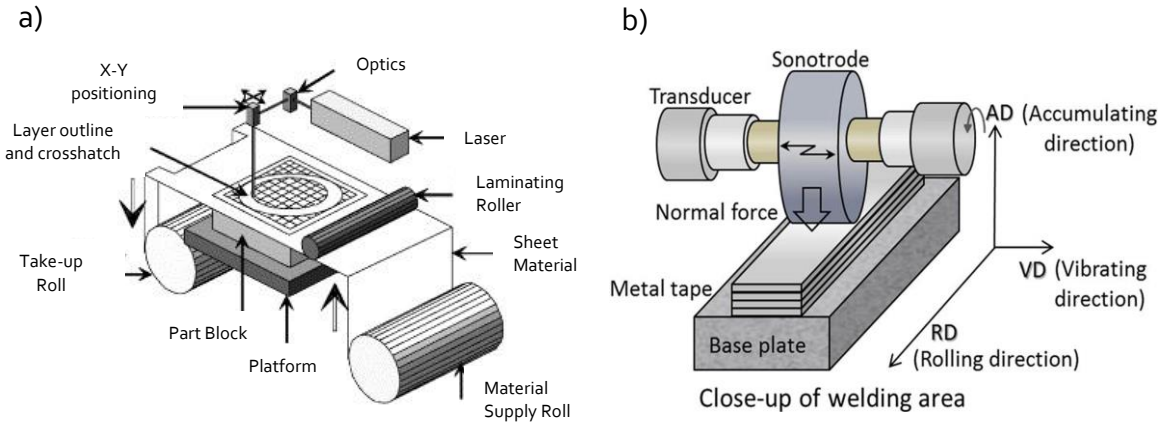

Figure 2.11 Schematic of the sheet lamination a) laminated object manufacturing[75] b) ultrasonic consolidation [33].

Sheet lamination techniques have proven themselves to be inherently fast, low-cost processes and more suitable for larger parts[27]. However, these methods suffer from some serious limitations, including: low surface finish, the anisotropy of mechanical properties, and lower strengths in the z-direction when compared with the longitudinal direction. Another problem with this approach is that it is hard to achieve complex 3D curved shapes[109]. Accordingly, the sheet lamination process has fewer applications for fabricating functional parts.

2.5 Overview of Metal AM Extrusion Processes and Current Research Challenges

Material extrusion additive manufacturing (MEAM), as one of the AM types, is a method of manufacturing 3D parts by softening and extruding the material feedstock via an orifice that travels in multiple directions to form the structure layer by layer. MEAM is a multifunctional and valued manufacturing technology that has experienced considerable industrial advancements in recent years. Additionally, it is one of the most commonly used methods in AM systems. According to the analytical agency Statista[110], on worldwide Additive Manufacturing market share, MEAM had the biggest market share of all AM processes, with approximately 71 % share of all the industrial AM systems. Additionally, with regard to the number of parts produced and the overall value of production, MEAM was recognised as the dominant AM technique.

The above was due to the reasonably priced and accessible nature of the systems, as well as being office-friendly and requiring less maintenance in comparison to other AM techniques [73, 111]. Because of these benefits, MEAM is being used in a range of industries, including; aviation, automobile, architecture, medical industries and many more [112, 113]. The MEAM process, unlike other AM processes, is ideally suited for multi-material extrusion and may be used to fabricate products from a diverse range of materials, primarily thermoplastic materials [52], which are constantly evolving. Nonetheless, MEAM technology has been modified for extrusion of many feedstock materials, including metal[38, 55], ceramics[114, 115], and composites[116, 117], to construct functional components[118], thanks to current advances and enhanced accuracy[64]. Most of the parts printed by a MEAM process require a support structure, otherwise overhanging structures will be collapsed or deformed, and these supports can be easily removed either mechanically or manually after the printing is completed[71]. Since the printing process is accomplished upon the support structure, this may have an impact on the mechanical properties of the final part. If the MEAM used a metallic feedstock to print, it may need a binder system which will be eliminated by additional post-processes such as debinding and heat treatment procedures[119]. When the post-processing is employed, a shrinkage may occur as a result of reduced porosity and the densification of sintered parts [120].

The first step in MEAM is the feedstock preparation and fabrication, and this can be formed as rod-shaped, granules, or a filament, according to the printer machine configuration [121]. As seen in Figure 2.12 [43], there are three basic approaches currently being adopted to allow intricate parts to be produced by extrusion-based AM, including: material extrusion with plunger-based, screw-based, and filament-based[122]. The following is a brief description of these mechanisms.

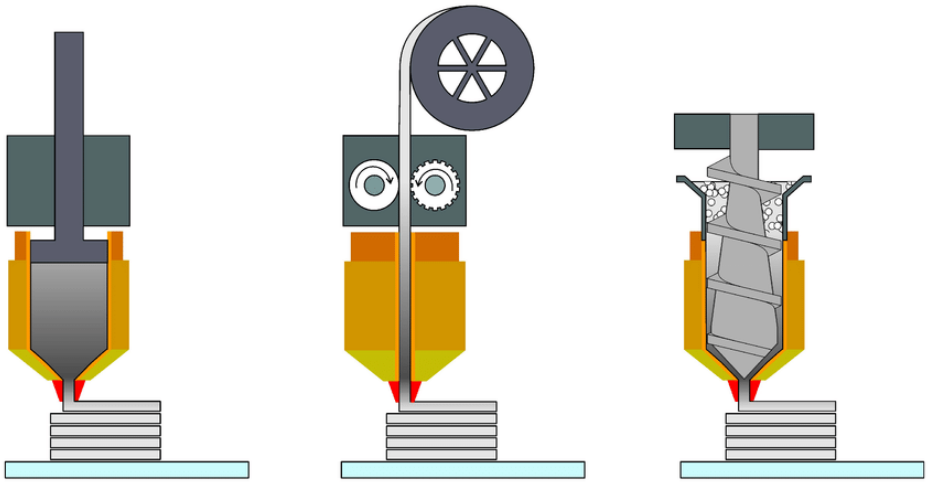

Figure 2.12 Schematic diagram of the three different approaches for extrusion-based AM [43]

- **Filament-based AM**

Filament-based extrusion is a well-known method for the creation of 3D products which was initially pioneered by Scott Crump in the 1980s, and Stratasys Inc. commercialised it in the early 1990s as Fused Deposition Modelling(FDM) [123]. However, it was introduced later as Fused Filament Fabrication (FFF), according to the starting material, which is filament-based feedstock. FFF is currently one of the most extensively employed and representative methods among MEAM technologies. This is due to its simplicity, being well-understood, safe, and generally a low-cost process. This process is mainly used for feedstock materials made of plastic, but it may be used for metal and ceramic applications too [114, 124].

The key elements of a typical FDM machine consist of a pinch roller feed, extrusion head, a nozzle connected to the extruder, and a building platform on which the 3D object is created. The basic concept of the process involves a spooled filament fed through an extrusion head using a stepper motor mechanism. The continuous filament functions as a plunger to force the materials through a heated nozzle and which are then deposited layer by layer onto a movable substrate to produce the desired cross-sectional area[125, 126]. When the first layer is finished the substrate is moved a step down in order to allow for an additional layer to be applied on top of the preceding layer and the process is reiterated till the 3-D object is completed. In metal FFF methods, the filament, which is produced in a single/twin screw or a plunger extrusion machine, comprises a metal-based powder with high consistency surrounded by a polymer-based binder. The amount of metal powder varies between 50 and 60% volume, and there are various feedstock materials used including stainless steel, tungsten, aluminium, titanium, etc.[127]. The optimum powder amount must be correctly determined to provide the desired properties in the filament. A

filament with too much solid loading powder will increase the viscosity and it may result in breakage during winding. If there is insufficient powder content, this will also make processing more difficult and distortion may occur during the sintering process. It is essential that the filament must be free of porosity, have a consistent shape, and a homogeneous distribution of metal powder, with as high a metal powder content as possible to reduce shrinkage.

Controlling the aforementioned factors properly will optimise the printing, debinding, and sintering stages, and will subsequently influence the mechanical properties and density of the sintered objects[120]. The binder system must also be taken into account when developing the composition of the filament since it has a significant impact on the manufacturing process and the quality of the final components. The binder is made of various components that help powder-based products form and maintain their structure. The binder agent is typically composed of various types of polymers, waxes, and additives to facilitate all of the functions that a binder system must perform[128]. Generally, the filament must be robust enough to withstand the pinching from the wheels without shearing. At the same time, it should be flexible enough to be spooled. Finally, it should avoid the buckling failure between the pinch roller feed and the entrance of the heated extrusion head due to excessive compression[125, 129].

- **Screw-based AM**

In filament-based material extrusion equipment, in order to extrude a suitable amount of material and so ensure a reliable procedure, special care should be paid to filament fabrication. For example, a filament with a constant cross-sectional area and certain flexibility is considered as further operation to the whole process. Therefore, a screw-based extrusion approach has been developed to avoid the shortcomings of the filament-based 3D printing system where not all the existing materials can be formed into a spooled filament that is also hard enough to be pushed by the feeding system of the FDM[43]. With the help of the rotating screw, this process may continually feed pellets/granules of material regardless of the component size being manufactured. The continuous and consistent rotation of the screw allows for the uniform feeding of pellets into the barrel. Accordingly, the screw extrusion-based method has the capability of controlling materials' rheology more accurately than other MEAM systems[130].

The general configuration of this process comprises a screw, barrel, nozzle and heaters. In a conventional screw-based extrusion machine, a single screw extruder is mounted vertically on a machine frame with heating elements connected to the barrel for temperature processing. The building substrate is managed by stepper motors to move the substrate in XYZ directions and control the material printing, and a computer is used to operate, regulate, and monitor the whole system[122, 131]. To start the process, the

feedstock materials, in the form of pellets/granules, are fed into the hopper attached at the top of the barrel and then the screw conveys the incoming materials toward the melting channel. The heaters deliver the adequate heat to the materials until the required viscoelastic phase is reached. After the materials are softened and screwed, the molten feedstock will be pumped up through the nozzle to allow the material deposition to finally create the part. Although this process offers several advantages, including a wide range of non-filament feedstocks and a continuous working system, there is still an opportunity for system enhancement – optimising process parameters(granules/pellets size, molten temperature) to enable more precise control for the system and hence ensure that the extruded material flows uniformly during the deposition process[43, 132].

Some attempts have been made to manufacture parts using the screw-based extrusion technology. Bellini et al. proposed a screw extrusion approach, based on the FDM system, in what they have called 'mini extruder deposition' to manufacture parts made from a combination of ceramic and polymer binders[132]. The system comprises a mini-extruder with uniform pitch and constant channel depth throughout the screw length, fitted on a high-precision positioning system. Despite the fact that the procedure of depositing parts was successful, they reported that the primary constraints of this technology were material aggregation in the feed section and air entrapment between granules.

A similar system of a screw extrusion-based AM setup was developed by Cruz et al. to overcome the drawback of the filament feeding method [133]. The process comprised designing a single screw of 90 mm length and 15 mm diameter, with a nozzle diameter of 2 mm. Two band heaters were attached to the surface of the barrel, allowing for processing temperatures of up to 250°C. The building substrate was able to move in XYZ directions with the help of step motors to governor trajectories, material extrusion and layer thickness. A logical controller and a computer were employed as an interface to control the printing procedure and various process parameters like extrusion temperature, speed of screw extrusion, and deposition material rate. Consequently, the developed extruder set-up was able to process a material feedstock having 61vol.% of carbonyl iron with a binder. However, there is a lack of knowledge as the investigators failed to provide additional information about extrudability and printed samples.

- **Plunger-based AM**

A plunger-based extrusion (also referred as piston-based) is similar to the other MEAM types. The apparatus consists of various elements, which include a heated cylinder, plunger/piston, nozzle, and substrate. The working principle of this method begins by placing the feedstock material in a reservoir and warmed to the temperature desired. Then, when the materials approach the required viscoelastic state, a mechanical displacement takes place so that the vertical plunger moves down and pressurises the

molten materials out of the nozzle – laying down the material on a substrate based on a pre-set shape produced by CAD software, creating the 3D part[131]. The plunger-based technique, compared to screw-based material extrusion, can be easy and low-cost, since multiple heating zones and complicated screw design are no longer necessary here [16]. As well as there being no need to further prepare the material into filament shape, one of the main advantages of this system, compared to filament-based extrusion, is that the rod feedstock can have a higher solid loading[127].

At present, Markforged Inc. and Desktop Metal Inc. are two businesses based in the USA that provide commercial MEAM machines for metal extrusion that employed plungers [134, 135]. Markforged names their technology "Atomic Diffusion Additive Manufacturing," (ADAM), while Desktop Metal names it "Bound Metal Deposition" (BMD). A rod is made from a mixture of metal powder and polymer that will be stored in a machine cartridge and then fed to the extruder. The machine comprises a heating unit so the rod will soften enough to enable the material to be forced out of the nozzle onto the building table to create the object layer-by-layer. The Markforged Inc. system has an ultrasonic vibrator with an energy source to ultrasonically bond the fresh layer onto the previously extruded layer. Desktop Metal Inc. , on the other hand, adopts a laser scan sensor attached to the printer and utilises an in-process inspection mechanism to check that the precise dimensions are being deposited[43]. After printing, the manufactured part goes through post-shaping processes, e.g., debinding and sintering cycles to remove the binder and realise dense parts.

Despite many positive attributes, there are some drawbacks to plunger-based systems. Rod feedstock fabrication is considered an additional step compared to the screw-based extrusion. Also, the system may need to be reloaded with materials feedstock during the manufacturing process, especially for a large object, affecting the printing continuity process. To solve this issue, Giberti et al. [21] presented an in-house developed AM system based on extrusion and deposition of metal powder and a polymer binder, as shown in Figure 2.13. Preliminary trials have been performed with different materials made of a mixture of metal powder (stainless steel or zirconia) with a polymer binder. The method relies on the usage of a MIM extruder to prepare the feedstock (feeding unit) alongside a plunger-based system (extrusion unit) to extrude the materials through the nozzle onto a movable table, which is based on a 5-axes parallel kinematics machine. The process begins with granulated materials being fed by gravity into the system through the hopper. After which, a heated feedstock is injected into the plasticising unit, where a screw that rotates continually is fixed at 45 degrees. Finally, the material moves to the extrusion unit, where a vertical piston pushes and pressurises the heated material through a nozzle on a 5-axes worktable, obtained with a parallel kinematics setting. It was possible to produce parts in

this way, and the need for a support structure during the deposition was minimised. However, the process does require debinding and sintering operations after extrusion.

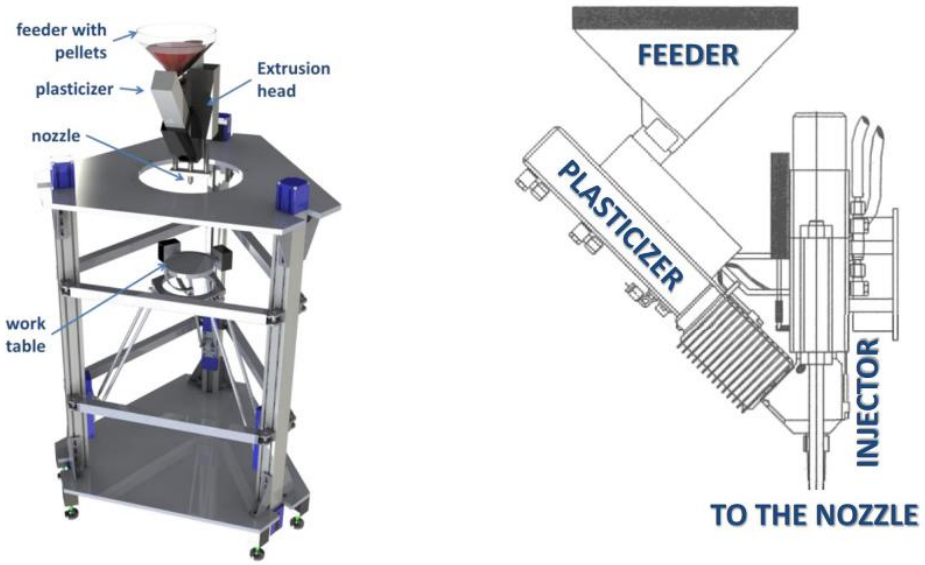

Figure 2.13 Proposed extrusion machine combining a screw-based and plunger system [21].

Recently, Waalkes et al. proposed a customised piston-based material extrusion system with Ti-6Al-4V feedstock produced by Metal Injection Moulding (MIM) with the goal of fabricating dense green components[16]. As shown in Figure 2.14, the system is built using a rod-shaped piston driven by a stepper motor and has a heating pad, a nozzle (0.4mm diameter), and XYZ linear motion stage. The MIM feedstock is uniformly granular and contains a 66% sphere-shaped Ti-6Al-4V powder that is embedded in a binder system. The proposed system successfully deposited green components with a satisfactory appearance. Further, they stated that the fabrication cost of the developed system was equivalent to FFF printing. However, this process can suffer from a heterogeneous material deposition during the building process due to the form of the initial feedstock being used "granules". This potential problem might be solved by utilising a rod-shaped feedstock instead.

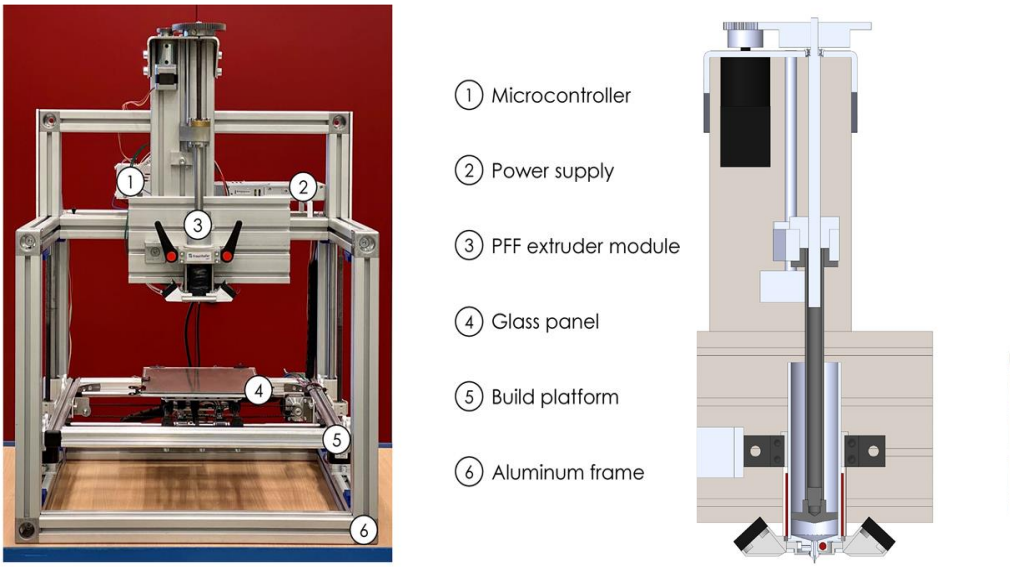

Figure 2.14 Customised plunge-based extrusion system [16].

The use of MEAM systems to print metal parts has the potential to offer advantages when compared to conventional metal AM techniques, including powder bed fusion processes. One of the main advantages is that MEAM does not necessitate the use of high-cost lasers or electron beam energies. Moreover, significantly lower hardware and maintenance costs, as well as the potential to reduce thermal stresses within the components in comparison with SLM/EBM[20, 60] make this system more accessible and open the door to new possible markets. Alongside the faster building rate of MEAM (compared with other metal AM technologies)[136], material feedstock deposited with a suitable viscosity at a low melt temperature can result in fully dense 3D parts produced from metallic alloys [64]. The ability to manufacture metallic parts using MEAM technology suggests applications in a variety of fields, including industrial prototyping, manufacturing tooling, aerospace, and medical instruments[88]. Despite the potential benefits that MEAM techniques offer, most of the broader applications of extrusion-based metal AM is limited to low-temperature and low-strength alloys. Moreover, due to the lack of a regulated atmosphere, there is a risk of oxidation between layers during the construction process[30]. The challenge here is that the viscosity of metallic alloys within the extrusion process should be sufficiently controlled for successfully deposited feedstock geometry, but that requires precise heating control.

The extrusion-based AM method is a process that corresponds relatively to the LEAM system that is being developed in this dissertation where molten materials with the desired viscosity are extruded onto a build platform via a heated nozzle to form a structure. Hence, further discussion will be restricted on metal with MEAM. The next sections discuss the state of the art in literature and the efforts conducted regarding the metal MEAM

systems that are most relevant to the LEMA project, including the fundamental benefits and challenges of these technologies.

2.5.1 Extrusion-based AM of metal-based composites

The MEAM (FDM) is a well-establish deposition process, especially for thermoplastic prototyping applications with high part stability, processing dependability, and appropriate accuracy. Yet, further investigation and progress are needed to expand its field of applications and maximise its capabilities as a workable manufacturing process. The fundamental operating principle of the FDM method opens the door and encourages development and use of additional materials such as metal and metal-ceramic/polymer in order to gain the potential benefits and subsequently broaden the FDM applications. The development of FDM has been ongoing to fabricate metallic structures from metal-based composite materials. The process requires post-processing steps, including de-binding and sintering processes to eliminate the binding agent and finally produce the desired metal part.

A lot of the early work has been done by researchers at Rutgers University to develop fused deposition ceramics and metals [64, 137]] by using a commercial FDM from Stratasys Inc. Their attention has been focused on using a variety of ceramic and metallic materials, such as silicon nitrate, lead zirconate titanate, aluminium oxide, hydroxypatite, and stainless steel to manufacture green parts through an FDM method. The produced part is subsequently subjected to a binder removal process and then sintering operations by firing out the binder in order to achieve fully dense products. As a result of the enhanced feedstock filament that meets the required flexibility, stiffness, and viscosity properties, they have been able to produce structural and functional parts for different applications [64].

Guohua Wu et al. have demonstrated the possibility of fabricating prototype metal components by processing a filament of polymer binder loaded with 58% volume fraction of 17-4 PH stainless steel powders using Fused Deposition of Metals (FDMet)[138]. During the FDMet procedure, the metal filament, which was fabricated via a screw extrusion process, was fed into a heated extruder of the modified FDMet system and deposited through a nozzle onto a moving substrate to create the 3D object. The following step is post-processing, which comprises removing the binder from the green part and then sintering the part to make it denser. The findings suggest that accurate and reproducible FDMet parts were found, nonetheless, some process parameter adjustment is required. .

Another piece of research conducted by Masood and Song(2004) developed polymeric/metallic composite materials for an FDM printer with the goal of achieving direct rapid tooling applications [38]. Initially, they used a single-screw extruder machine

to fabricate a filament wire of iron powder and nylon binder materials for FDM processing. The filaments produced using this composite were implemented successfully in an unmodified FDM printer to create inserts for plastic injection moulds. (See Figure 2.15). The investigated characterisation of the mechanical properties for developed materials has been determined to be desired, allowing for the production of flexible feedstock filaments which were employed successfully in FDM processing to produce functional parts. Even though they made progress, their results exhibited imperfect material features, such as insufficient conductivity properties in comparison to metallic components produced without a polymer content[20].]. In addition to the post-processing stage that is required for improving the part density, further enhancement of process parameters is required to improve the quality and accuracy of FDM-formed inserts.

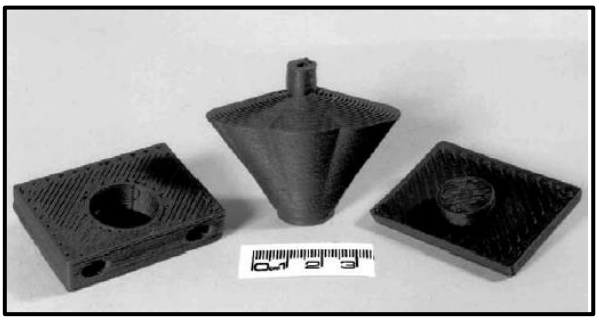

Figure 2.15 3D printed parts by FDM metal technology using the iron/nylon filament [38].

2.5.2 Extrusion-based AM of direct metal

One of the biggest drawbacks for processing metal/ polymer feedstock through FDM is that the green part requires additional post-processing, e.g., binder removal and sintering in order to obtain a dense metal component. As a result, some researchers have adapted the FDM concept to print a pure metal alloy directly rather than using metal-polymer feedstock as starting materials.

An investigation conducted by Mireles et al., 2012[20] used a modified FDM 3000 extrusion system to create a 3D structure from filaments of Sn60Bi40(non-eutectic alloy) and Bi58Sn42(eutectic alloy). In their trial, they have redesigned the extrusion head of a Stratasys FDM 3000. Figure 2.16 a) and b) illustrate the original configuration and the redesigned liquefier for the FDM machine that was used in this research, respectively. The curved liquefier (900 bend) of the FDM was replaced with a straight liquefier (highlighted by red dashed lines) to reduce the friction effects. The liquefier was also reduced in length to enhance transient response because of start/stop operations, reduce drive force and improve the heat transfer from the liquefier inlet to the nozzle. Also, modifications of the toolpath commands were needed to ensure a controlled extrusion of metals. Other

process parameters were developed, such as decreasing deposition head velocity, adjusting liquefier temperatures, and modifying the rates of materials' flow for successful deposition. For the eutectic alloy Bi58Sn42, the liquefier temperature was set at 210°C, and for the non-eutectic alloy Sn60Bi40, it was set to 220°C. The liquefier temperature was set to 2100C for the eutectic alloy Bi58Sn42 and 2200C for the non-eutectic alloy Sn60Bi40.

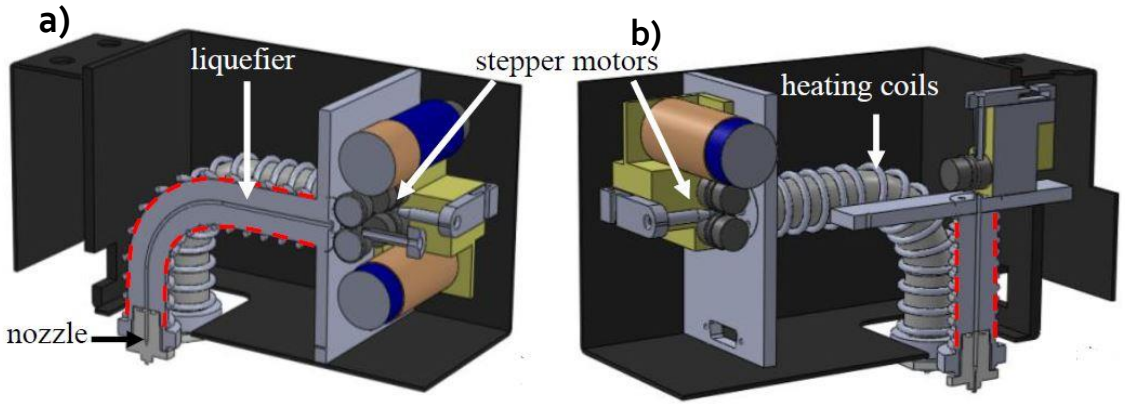

Figure 2.16 Shows the original liquefier configuration for a FDM 3000 and b) shows the altered liquefier design [20].

The experiment was performed and, consequently, they managed to deposit parts and a 3D-printed sample of six stacked layers from low-melting alloys, as presented in Figure 2.17. The layers of eutectic alloys had a print width of 1.24mm and a layer thickness of 0.74mm, while the print width was 1.12mm and the layer thickness was 0.71mm for non-eutectic material. The researchers also stated that due to their modifications to the FDM 3000 system, the deposition was more controlled and continuous throughout the process. Nevertheless, once again insufficient mechanical properties were observed in their products [139]. Moreover, the microstructure between layers also needs to be studied, and further complex 3D shapes have not been presented.

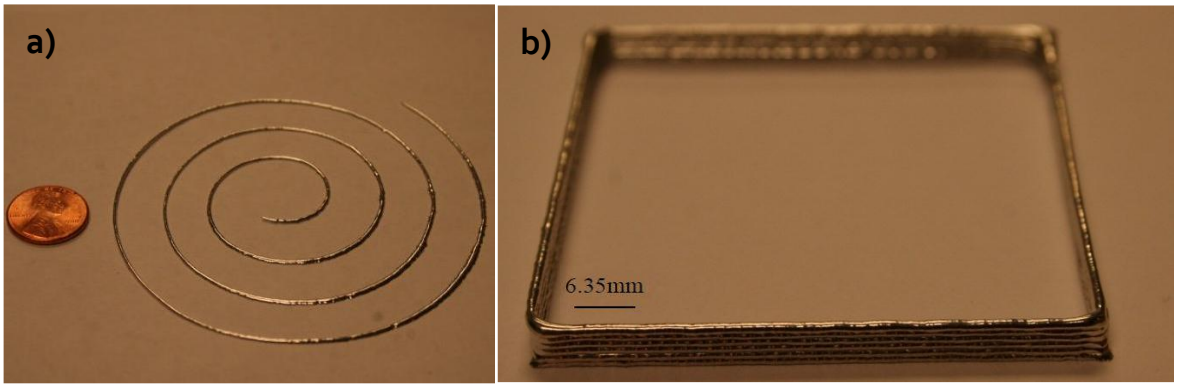

Figure 2.17 Shows geometries fabricated using FDM metal a) 2D prints and b) geometry of a 3D prints of 6 stacked layers [20].

A further attempt at using the FDM method to directly deposit metal was accomplished by Hsieh et al., where low-temperature melting alloys were extruded on a substrate to build linear patterns [30]. The investigators designed a tailored nozzle extrusion which was attached to a commercial Delta 3D printing system in order to process metal alloys instead of polymer. This technology used filaments made of Sn60Pb40 and Sn99.7Cu.03 solder with a diameter of 1.6 mm, and the experiment was carried out at temperatures ranging from 2200 to 2400 oc. In addition to adjusting the material and nozzle for printing, the extrusion parameters such as nozzle moving speed, extruding velocity and layer thickness were optimised. As a result, a continuous and uniform extrusion product was constructed with acceptable formability. Figure 2.18 demonstrates the consequence of a successful layer extrusion of a) ten-layer stacking of Sn99.3Cu0.7 and b) five-layer stacking of Sn60Pb40. Figure 2.18 c) displays the microstructure analysis of Sn99.3Cu0.7 print which reveals varying grain sizes between layers. It clearly shows the interface between subsequent deposition layers, which could be due to poor extrusion process control.

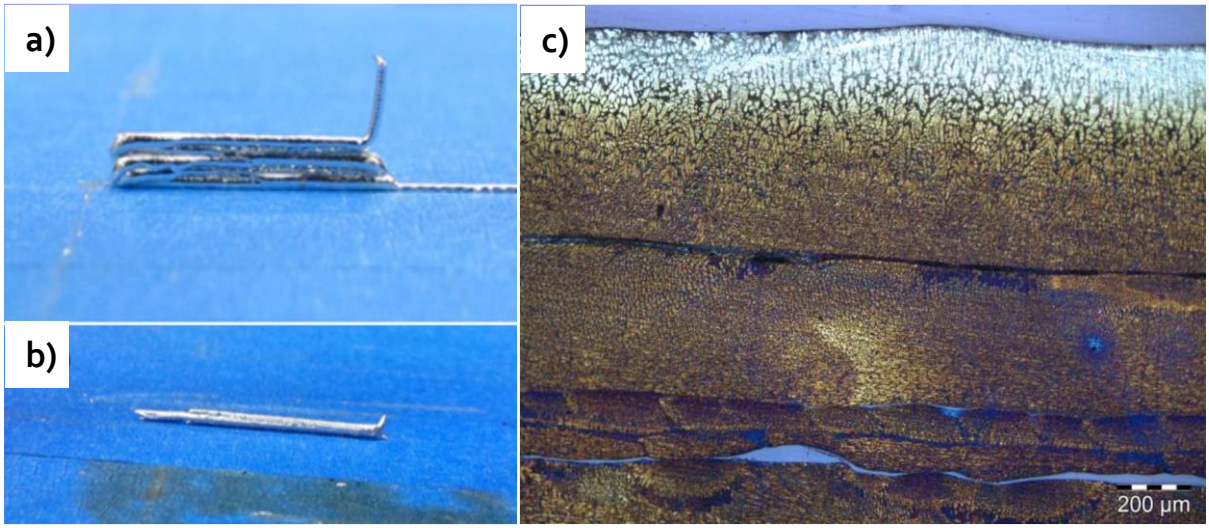

Figure 2.18 Shows a) 10-layer stacking of Sn99.3Cu0.7, b) 5-layer stacking of Sn60Pb40 and c) optical microstructure of printed layer for Sn99.3Cu0.7 [30].

Ma and Zhang[29] proposed a direct writing process for the printing of metal parts by using compressed gas as a driving force to deposit the material onto a substrate. They introduced it as a pneumatic extruding direct writing deposition process (PEDWD). The scheme of PEDWD is presented in Figure 2.19. In this examination, a eutectic alloy of tin-bismuth (Sn63Pb37) was chosen as a raw material and heated to a molten phase in a chamber before being pneumatically squeezed out through a nozzle using compressed nitrogen into the movable substrate to form the 3D patterns. Using several nozzles with different design structures, this technique produced numerous metal patterns, including metal lines and three-dimensional objects. Further examination was carried out investigating the microstructure, and they reported a good metallurgical bond between layers. However, besides the complicated system and the high energy consumption, due to the requirement to attain full melting temperature, there is a lack of sufficient knowledge about the mechanical properties.

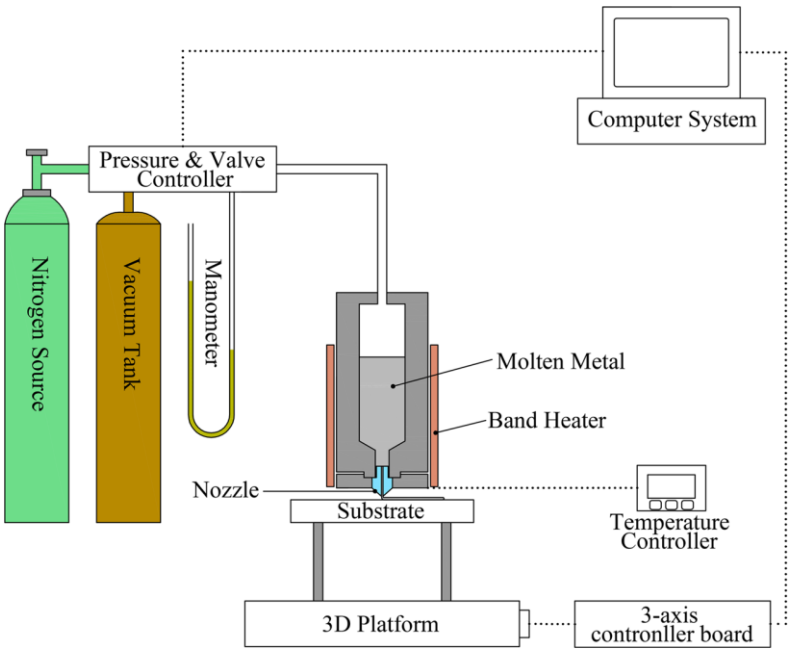

Figure 2.19 A schematic diagram of pneumatic extrusion methodology [29].

2.5.3 Extrusion-based AM of thixotropic alloys.

There are inherent limitations when preparing filaments, such as the limited range of materials that have the ability to be produced in a filament form which then can be spooled [43]. Material extrusion with a filament base can also exhibit several problems associated with the feeding processing. One of the most common weaknesses of the feeding mechanism of the FDM process is the filament buckling due to the excess compression during printing[140]. Buckling failure can cause the filament feedstock to jam between the driving wheels liquefier, and subsequently break the filament. Last but not least, the back-

pressure in the liquefier experienced during the printing stage constrains the portion of the powder volume in the feedstock filament, diminishing the chance of fruitful sintering of the green part[132]. Consequently, these problems may cause interruption of the process, stopping it from being a continuous deposition, and operator intervention is necessary. Hence, there is still a demand to develop a low-cost MEAM method of fully dense metallic parts, that avoid filament-based extrusion issues, without the requirements of post-processing and with no defects such as residual stresses and unwanted porosity within components.

Semi-solid processing is a near-net-shape technique that can produce metal parts in a semi-solid state with a high degree of mechanical properties and functional performance because of the special structure of the thixoformed part[141]. In semi-solid slurries, the metal alloy of solid–liquid mixtures lies in the zone between solidus and liquidus lines of the equilibrium phase diagram. The processing of semi-solid metal (SSM) is reliant upon the thixotropic property of alloys with globular microstructure rather than dendritic microstructure in the semi-solid state. If the microstructure is made up of solid spheroids in a liquid matrix, the viscosity is time- and shear-rate-dependent. When the alloy is sheared, it thins and flows, but when it is left alone, it thickens[142]. This slurry behaviour, unlike conventional die-casting processes where the flow is turbulent, leads to smooth and laminar slurry flow during die filling, which eliminates defects such as porosity and enhances mechanical properties. As a result, products can be produced with thinner cross-sections, resulting in a lower weight[143]. However, the dendritic structures obstruct the flow of the metallic alloy (during typical casting) owing to their morphology, allowing the particles to adhere to each other and significantly increase the shear strength of the metal alloy[31]. Hence, applications using alloys with a dendritic structure morphology should be avoided. It can be concluded that the rheological behaviour of the alloy in the semi-solid state is deemed more advantageous for use in processes where the grains have a more rounded shape and fine diameter. In comparison to materials with grains that have a dendritic geometry, materials having circular grain morphology tend to have lower viscosity and less liquid phase segregation, promoting better flow of the metal slurries and resulting in more uniform microstructures[144, 145]. The semi-solid metal processing will be discussed in detail in the next chapter.

The controlled microstructure and the unique material property of the flow behaviour in a semi-solid slurry contribute to forming successfully dense metal components with intricate structures [146]. This opens up the opportunity of an integrated technology by using semi-solid metal processing for additively manufactured parts [37]. Therefore, employing the semi-solid metal (SSM) processing with the extrusion-based AM could offer

greater advantages, i.e. controllable materials deposition, and would achieve an efficient, affordable and widely accessible metallic AM process.

There is a relatively small body of literature that is concerned with developing AM of metallic alloys which exploits the semi-solid metal extrusion approach and shows signs of success. Rice et al. (2000) pioneered the first research on the solid freeform fabrication process to deposit semi-solid alloys. As a result, two theses[147, 148], two journal papers[37, 149], and two patents[150, 151] were produced. Figure 2.20, a schematic diagram of the system for extrusion and deposition of semi-solid metal. They employed a rheocasting system that involved a steel reservoir and mixing chamber which were both surrounded by heating elements to melt the materials. Further, a motor-driven rotor was used to apply shear force and generate the desired semi-solid alloys. In this experiment, the reservoir was loaded with pieces of 85% Sn-15% Pb alloy and then heated to just above the liquidus temperature within an inert gas environment. The molten metal transferred from the reservoir to the mixing area while it was stirred by the rotor, allowing for breaking up any dendritic structure to form rounded solid particles surrounded by a liquid matrix. Afterwards, the semi-solid slurry was deposited layer by layer onto a movable substrate creating different shapes of metallic components.

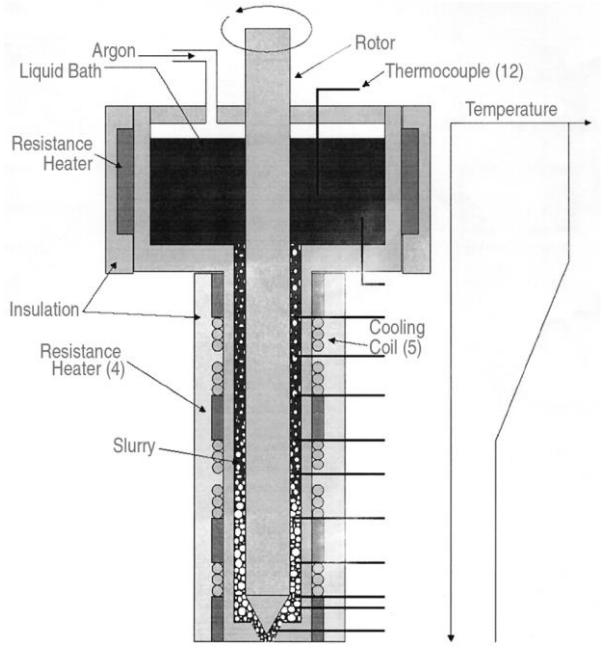

Figure 2.20 Diagram of the rheocaster process.

Figure 2.21 a) depicts successive layers of the prints produced using a solid freeform fabrication (SFF) process and b) depicts the microstructure of the interlayer region. The structure characteristic of the extruded material was investigated and showed that a favourable microstructure was seen with excellent bonding between the layers. This is seen in Figure 2.21 b), which shows that there is no metallurgical interface between the

extruded layers. Furthermore, tensile tests were carried out on both deposited and casting samples to determine the quality of the mechanical properties. The findings revealed that the UTS for the deposited component were comparable to what had been found in specimens that were produced by conventional casting processes. This study confirmed the feasibility of implementing a solid freeform fabrication process to produce near-net-shape metallic components from semi-solid alloys. The limitations, however, of this approach are that the rheocasting system was very bulky, leading to more restrictions, and it is only suitable for fabricating large parts due to the deposition size. Also, the main obstacle for this process is the layer thickness of the deposited sample, which was around 3.5mm, as shown in Figure 2.21 [37]. It means that complex and fine features cannot be produced using this process.

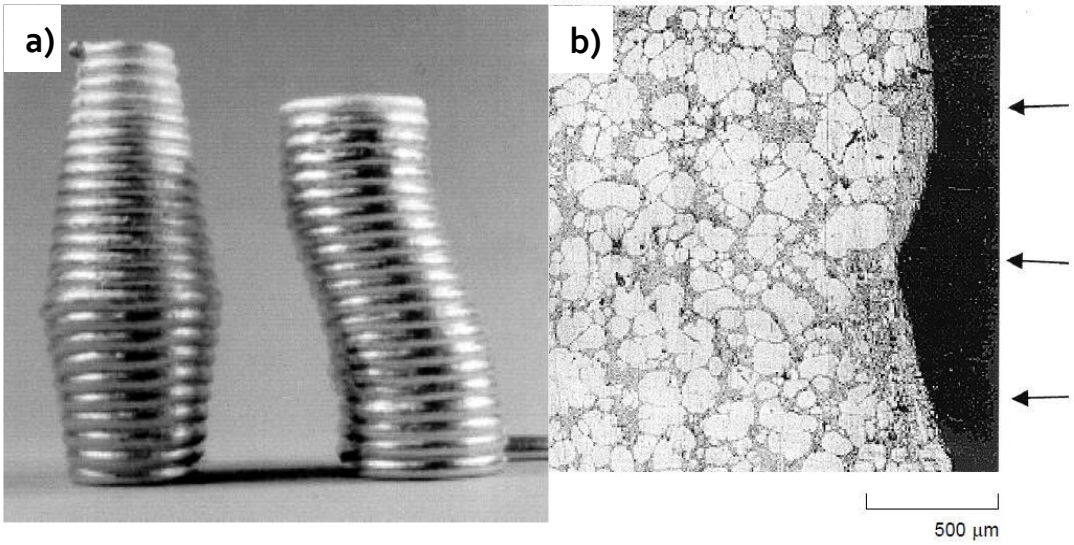

Figure 2.21 Example of deposited sample b) microstructure of the interface layer [37].

Another approach was done by Finke and his cooperative team at the Netherlands Organization for Applied Scientific Research (TNO) and the University of Twente, using traditional fused deposition modelling (FDM) for the extrusion and deposition of semi-solid metals. The scientific information of the study was presented through a Doctoral thesis[152],and two published papers[14, 60].

As can be seen in Figure 2.22 a), they have used solid freeform fabrication (SFF) based on the FDM technique to test several model alloys of Sn-based low melting points including Sn-Bi, Sn-Pb-Bi, and Pb-Sn. These materials were supplied in a pre-conditioned metallic wire form, and drive wheels were used to create a pressure force to push the materials into the heating channel. The work was conducted by partially re-melting the metallic filament to the desired semi-solid condition. Then the materials squeezed out through a nozzle to dispense onto a plate moved in an x-y direction. The z-axis was moved down manually in order to deposit a fresh layer on the previous one. It was possible to deposit multiple

layers, and for investigation purposes, the extruded material was examined by optical and electron microscopy. Figure 2.22 b) displays a typical microstructure of a printed layer by an extrusion-based AM system. The researchers concluded that, according to the examination that utilised an optical microscope, the microstructures of the printed specimens showed typical globular structures corresponding to semi-solid materials found in the literature. However, a boundary was observed in the cross-section of two layers indicating that fully interlayered bonding was not achieved. Also, it is unfortunate that the study did not include a mechanical properties examination of the extruded part. Notwithstanding these limitations, this work could validate the ability of the FDM process for the extrusion and deposition of semi-solid metals and confirm the work of other previous studies in this area[37].

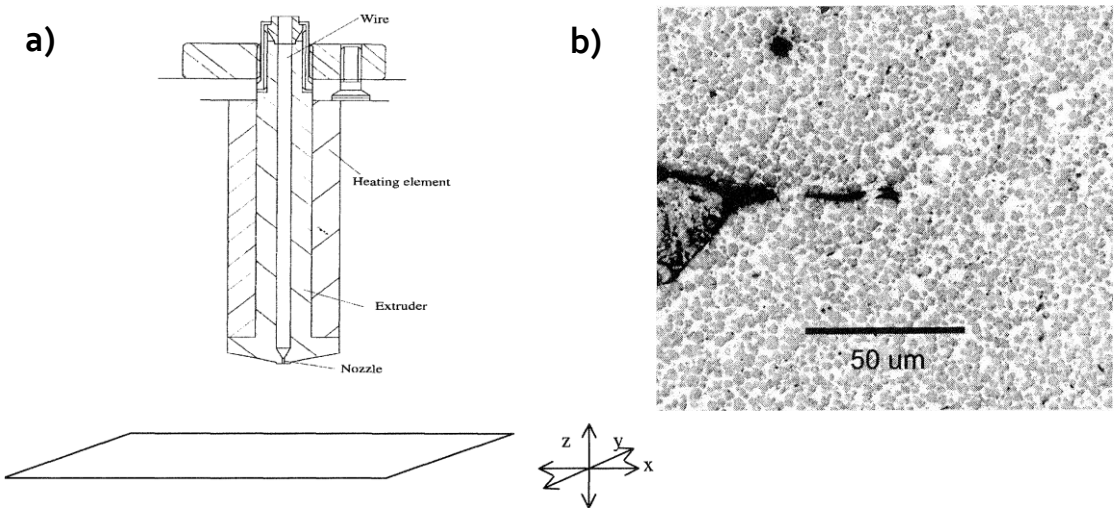

Figure 2.22 FDM-based apparatus for the fabrication of 3D metallic parts and b) microstructure of the deposited layers [14].

Work done by researchers in the Lawrence Livermore National Laboratory [40] used a process of direct metal writing (DMW) for fabricating 3D metal parts in the semi-solid state. Figure 2.23 demonstrates the DMW with the rheocaster method used in the study. The DMW system is made up of an alloy reservoir, a motor-driven, grooved, printing platform, and heating elements with a thermocouple for temperature reading. This DMW prototype was proposed to fabricate structures using only low melting point metals including bismuth-tin alloys that melt below 300°C.

The trial was started by inserting small pieces of (15mm in diameter) an ingot of a chemical composition of Bi75Sn25 into the DMW machine. Resistance heaters and an inserted grooved rotor were used here to heat the materials and apply a shearing force, respectively. Subsequently, the materials converted into a semi-solid state, and then a nitrogen pressure was applied to facilitate steady-state deposition. The materials were

extruded through a nozzle of 1 mm diameter into a pre-heated substrate after being heated and stirred. The distance between the nozzle and the substrate was about 0.7mm. Two layered filaments were extruded with overhanging structures, as illustrated in Figure 2.24 a). Moreover, the deposited Bi75Sn25 semi-solid alloy was examined using SEM/EDS to study its internal microstructures.

.

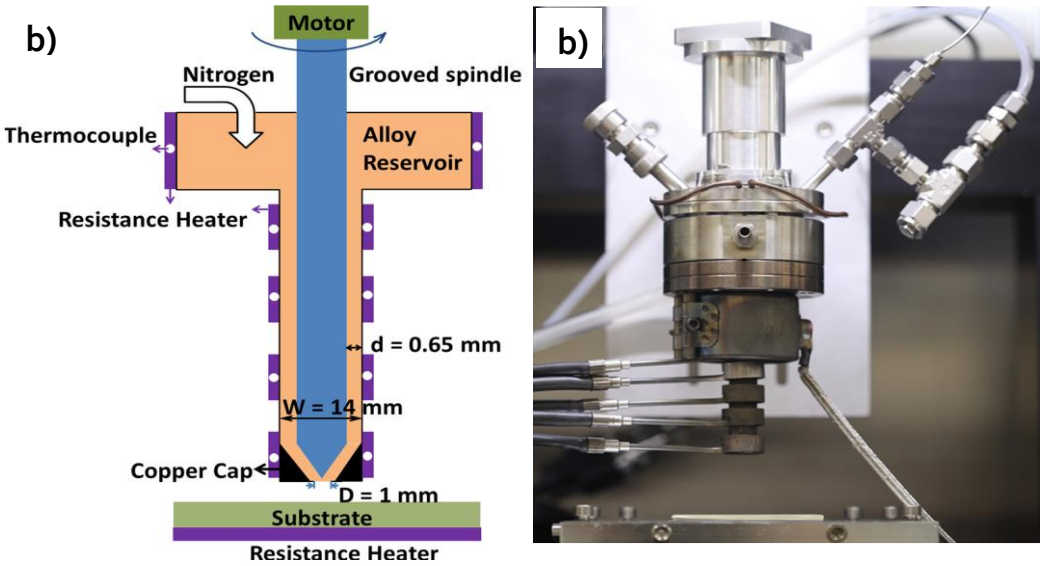

Figure 2.23 Schematic drawing and b) DMW process [40].

The results show that the microstructure of the printed filament contained a mixture of the polygonal primary Bi blocks phase and the Bi-Sn eutectic. This is attributed to the applied shear force during the DMW process which fragmented Bi dendrites, thus allowing Bi solid phases within the semi-solid slurries. Also, the authors reviewed the joint between the deposited layers and concluded that the pre-heating of the substrate material was a key control parameter for interfacial bonding. Figure 2.24 b) shows a micrograph of the bond between adjacent layers exhibiting a good metallurgical joint. However, the work demonstrated here employs a DMW system to print only metallic alloys of low melting points which do not exceed 200 °C.

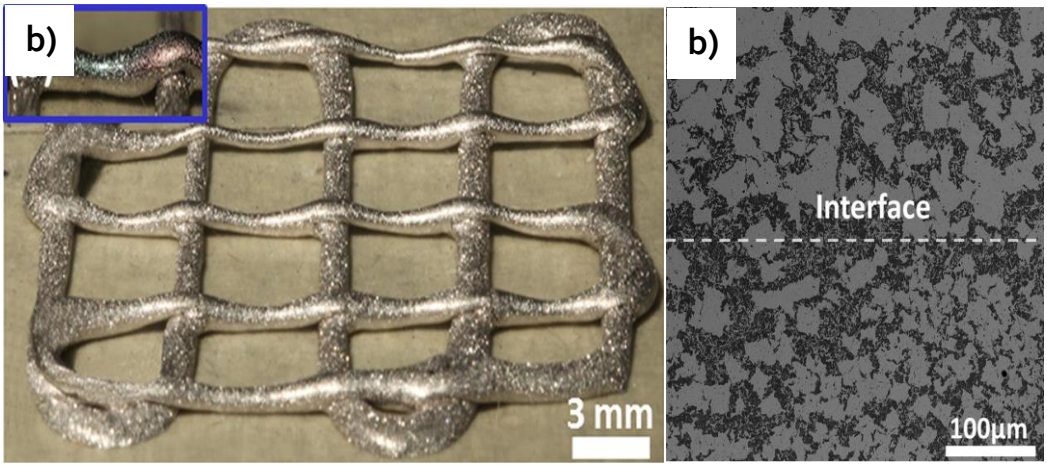

Figure 2.24 a) printed sample of Bi75Sn25 alloy and b) prints microstructures.

Jabbari & Abrinia conducted further experiments using the approach of extrusion-based AM of the semi-solid metal Sn-Pb alloy [35]. This work was documented as a metal additive manufacturing method: semi-solid metal extrusion and deposition (SSMED). This process used a metallic filament of a wire feedstock that had been pre-prepared with the required microstructure. They employed a modified FDM machine to convert the metallic feedstock to a semi-solid phase by partial re-melting, and then placed it on a platform to form metal patterns. In this trial, a strain-induced melt activation (SIMA) process was adopted in order to produce wire feedstock associated with thixotropic properties to be used as starting materials.

Two sets of as-cast cylindrical-shaped ingots of 25 mm diameter with a nominal composition of Sn–15%Pb and Pb–40%Sn were prepared for the SIMA process. At first, the material was exposed to an extrusion operation by a hydraulic press to reduce the ingot diameter and produce a filament wire of 3 mm diameter with directional microstructures. Then, the extruded filament was subjected to a warming temperature up to 40°C due to the high plastic deformation resulting from the extrusion step. The final stage of the SIMA process is the isothermal heat treatment. The deformed feedstock was exposed to a partial re-melting course to allow change to a semi-solid phase in a furnace and was then isothermally kept for a period of time before it was quenched in cold water to introduce the desired microstructure of the thixoformed metallic wire. The partial re-melting process was done at different temperature values and isothermal holding times. It was found that the re-melting temperature of 190 °C and 187 °C, which correspond to the solid fraction of 0.6, produced the optimum microstructure for Pb-40Sn and Sn-15Pb alloys, respectively[61]. To accomplish the SSMED procedure, an FDM-based machine was altered to fit the experimental need of this work. Figure 2.25 below, details the SSMED system set-up and shows an example of the print. The metallic wire feedstock which was prepared with the desired microstructure was fed through a heated extruder

via a feeding system and then reheated to a mushy region. Subsequently, the semi-solid material was extruded from the nozzle tip (in the range of 1–2mm nozzle size) onto a moving platform to complete a layer, and thereby parts. Various factors of SIMA and thixo-extrusion processes were investigated to determine which had the most bearing on the success of extrusion and deposition of the print.

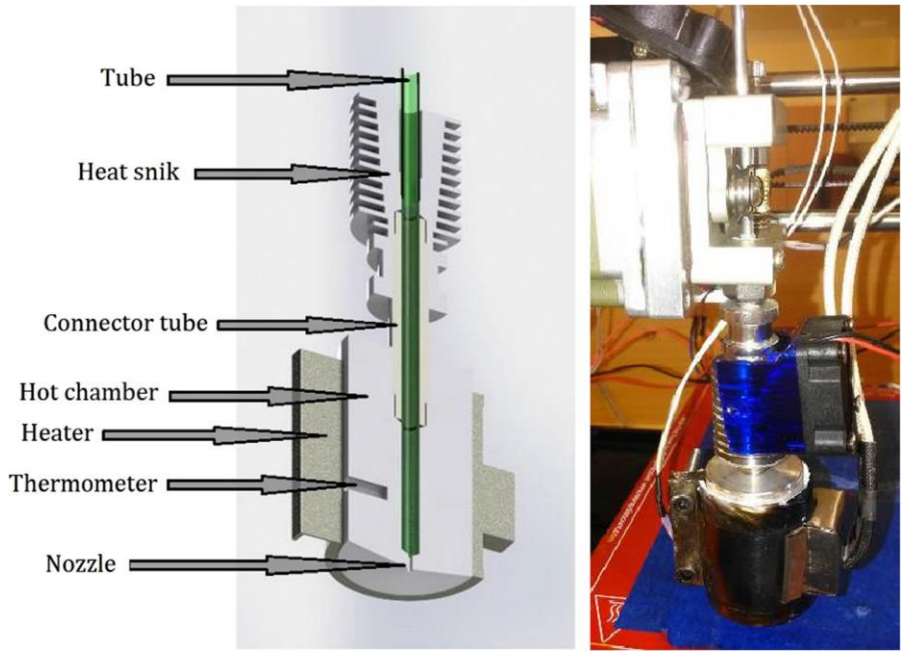

Figure 2.25 Diagram of the SSMED system developed [35].

Figure 2.26 demonstrates a sample of the printed part and SEM micrograph. Considering the resulted layer microstructure, it can be noticed that there is no apparent interface between the deposited layers, suggesting that the layers were printed properly. This was attributed to optimal conditions used for the processing parameters of SIMA during the semi-solid metal extrusion and deposition. Yet, since this is a filament-based system, a number of challenges are inherent in such methods, as described previously.

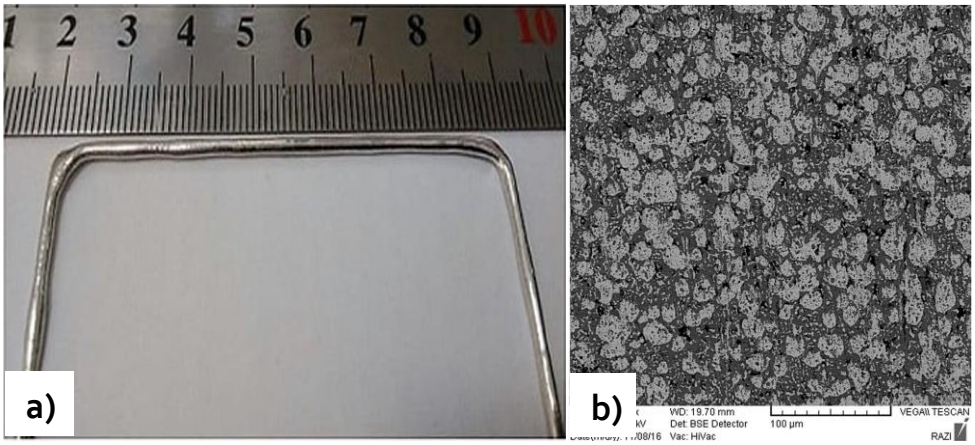

Figure 2.26 a) Printed single layer b) SEM microstructure of deposited layer [35].

Recently, Lima et al. investigated the feasibility of developing a thixo-extrusion-based additive manufacturing process.[28]. The objective of this work was to develop an FDM technique (also known as 3D thixo-printing) that enables additive manufacturing of metallic parts using biodegradable Mg-Zn alloy in the semi-solid state. Thus, a hot extrusion process was used to create a feedstock with controlled microstructures, which was then extruded via FDM at 420 °C. For the purpose of feedstock fabrication, the as-cast ingot of Mg-38Zn alloy was subjected to a two-step hot extrusion treatment using a hydraulic press. Two different nozzle diameters of the extrusion process were used, namely 5 and 1.75 mm, to yield extrusion reduction ratios of around 16:1 and 8:1, respectively. This mechanical deformation was carried out with a processing temperature of 330 °C. Subsequently, the cylindrical ingot of 20 mm was transformed into a metallic wire of 1.75 mm in diameter. The hot extrusion procedure is designed not only for wire feedstock fabrication, but is also employed to create a suitably thixotropic feedstock. It is believed that the hot mechanical deformation accomplished in the extrusion step is responsible for facilitating the dendrite-globule transformation mechanism during subsequent partial melting [26]. In order to create the Mg-38Zn filament (processed by semi-solid 3D printer), the extrusion head of a commercial FDM printer was re-designed, allowing the metal additive manufacturing of melting alloy up to 700 °C.

Figure 2.27 shows a comparison between the original configuration for an FDM extrusion head and the redesigned extruder implemented in this work. The thixo-printing process for the metallic filament was conducted at a temperature of 420 °C to ensure that the liquid fraction fell in between the range of 50% and 80%. The extrusion speed and the nozzle orifice diameter were selected to be 5.0 mm/s and 1.0 mm, respectively. During the building process, the distance of nozzle–substrate was set to be 1.0mm, and then the materials were deposited onto a substrate to form 3D metal patterns.

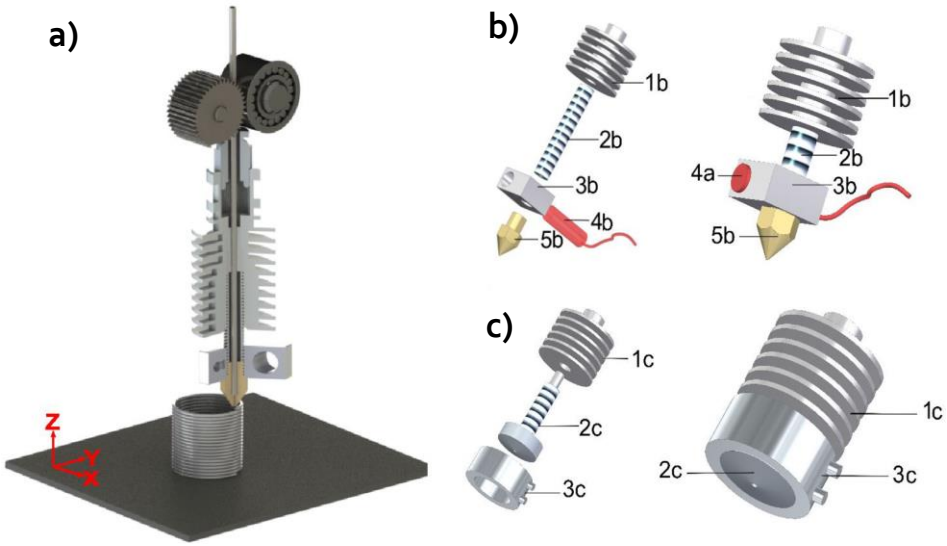

Figure 2.27 Show graphic of the commercial FDM b) original extrusion head c) redesigned extruder head [28]

The extruded material was layered on sandpaper and then metallurgical studies were performed on the prints. Figure 2.28 displays a sample of the 3D-printed feature and the resulting microstructure, indicating the feasibility of developed 3D thixo-printing to produce sophisticated structures with satisfactory microstructures. However, it was observed that there was a lack of information regarding the metallurgical joint studies between the deposited layers. The example microstructures depicted in this work are only for printed single layers, and no metallographic bonding investigations are displayed. It is assumed that the 3D thixo-printing method will still need to be developed in order to be a fully controlled system.

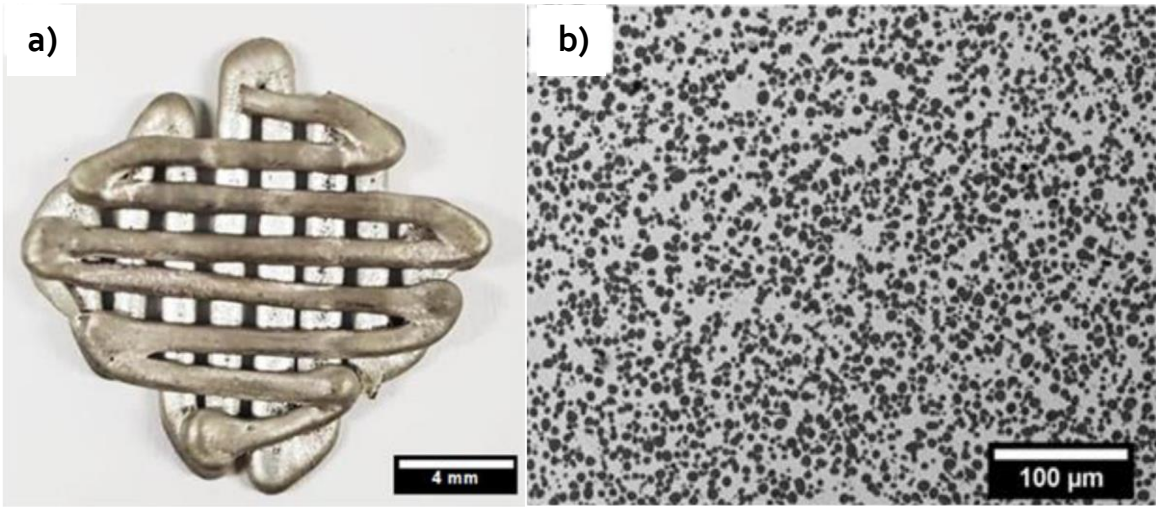

Figure 2.28 Macrograph features of the 3D specimen b) microstructure of printed filament [28].

2.6 Summary of Prior Arts on Metal AM Extrusion Methods

The material extrusion-based additive manufacturing of metallic alloy, which is one of the most widely known and rapidly developing AM systems, has sparked a lot of curiosity due to the simplicity and the low cost of this process. In addition, it could be a potential technology for offering complex and functional metal components for a variety of applications. Some research work has been done using the original concept of the fused deposition modelling (FDM) system for printing parts from a mixture of metal and polymer feedstock, and metallic parts have been successfully produced[38, 114]. These methods primarily rely on the polymer viscosity, (normally <60% is the typical loaded metal volume fraction) as well as on the strength and other anticipated characteristics of the metal powder. The polymer binder of the deposited component is eliminated after 3D printing, and it is then sintered, finally yielding a pure metal object.

While some of these techniques have been highly advanced, and can be suitable for the extrusion of metallic feedstock, there are still challenges and knowledge gaps that need to be addressed. For instance, such a proposed technique may require additional treatments after extrusion, including de-binding and sintering procedures to a convenient densification. Consequently, along with the post-processing steps attached, extra capital cost and effort in the production process, distortions and shrinkage defects during binder removal stages could also be observed. Also, with regard to filament extrusion-based processes, the limited range of the materials feedstock, which can be processed, is seen as a noteworthy drawback. The preparation and production procedure of the filaments themselves will result in increased process time and cost. Moreover, technical issues often arise from the use of the filament-based systems. Issues such as the blocking failure of the filament through the extrusion nozzle, backpressure, and the regular buckling that can be accrued because of the inappropriate compression during the extrusion process, can cause uncontrolled deposition and lead to a non-continuous process[43]. Further to this, despite some of the pleasant outcomes of the aforementioned filament-based methods, most of the conducted research has been focused on using low-melting alloys, such as tin and bismuth. This means it would not be suitable for high-strength alloys usable in the manufacturing of functional 3D-printed components.

As a result of the aforementioned boundaries, and filament feedstock downside during preparation and fabrication, some investigators developed FDM methods by exploiting the pure metal alloys rather than powder–polymer composites to directly print metal parts [20, 29, 30]. This work, however, shows either poor mechanical properties or highlights that the interlayer bonding between printed layers did not perform well. As a consequence of these problems, the metal AM extrusion approach has been transformed by some researchers, using a partially solidified metal alloy as a starting material. This method

employs semi-solid metal processing combined with material extrusion AM to create 3D parts. The rheological properties of the semi-solid thixotropic alloy allow for easily controllable deposition during printing, thus building dense 3D structures.

Prior investigations utilising semi-solid slurries in material extrusion AM have been conducted and have managed to extrude and deposit materials successfully [14, 37, 40]. Nonetheless, it was noted that they failed to address the challenge of the fabrication of intricate parts with overhanging structures and the design of semi-solid slurries of higher melting temperatures. The mechanical properties of the manufactured parts are a major factor from the functionality viewpoint of the components. Some of the aforementioned AM metal extrusion-based experiments introduced inadequate mechanical properties. Therefore, to prove the reliability and reproducibility of the process, more investigations need to be carried out with regard to the characteristics of the deposited sample. Generally, there is not much detailed information available within the literature regarding rheological properties, materials' deposition, and mechanical and metallurgical properties. Still, some aspects of the process parameters need to be understood and optimised in the literature in order to advance the AM metal extrusion systems – in particular, temperature conditions, extrusion speed, shear rate, and other aspects that could help to control the quality of the printed parts and thus provide reliable deposition. Nevertheless, as stated before, it is a worthwhile effort to offer the potential to form 3D-printed components using semi-solid slurries despite the imperfections of prior investigations.

3 SEMI-SOLID METAL (SSM) PROCESSING

3.1 Metal Additive Manufacturing Sing Semi-Solid Slurries

The 50th anniversary of introducing the Semi-Solid Metal (SSM) processing idea, also termed as thixoforming, will fall in the early 2020s. SSM was discovered around forty years ago by Spencer, at the Massachusetts Institute of Technology (MIT), during his PhD research when he was investigating the hot tearing of steels during solidification [31]. SSM is a method for metal forming exploited commercially using non-ferrous metals like magnesium, aluminium alloys and copper but equally applicable to any alloy with sufficient melting range to form a process window. In the SSM system, the metal alloy is treated when the metal is between a liquid and solid-state. At the present time, SSM processes have been applied in many industries due to their capability for manufacturing complex components. It is envisioned that using SSM for additive manufacturing to print fully dense components, has a great chance to be a promising AM technology due to the excellent mechanical and rheological properties of SSM alloys[37]. As accurate control of the metallic feedstock viscosity as proposed within SSM will allow successful layered deposition for AM extrusion[20]. Consequently, the exploitation of SSM and its advantages in Additive manufacturing technologies could reduce the cost and time of AM processing.

Since this research is based on extrusion of semi-solid slurries and building of 3D parts using the concept of additive manufacturing thus, it is important to have a better understanding of the fundamentals of semi-solid metal processing. A literature review about the solidification phenomena, the rheological behaviour of semi-solid alloy slurries and suitable materials are discussed within this section.

3.2 Fundamental of Semi-Solid Metal Processing

Conventional manufacturing techniques deal with metals where the alloy is treated in the form of a liquid state such as casting processes or solid state such as extrusion and forging methods. However, as indicated in the introduction semi-solid processing is a method of producing near-net-shape components where the metallic alloy is processed in a its semi-solid state. In the early seventies and during the examination of Spencer and his co-workers while they were investigating the hot tearing of Sn 15 %wt. Pb alloys by a rheometer that measure viscosity. It was observed that the viscosity of the alloy was much lower when it was constantly sheared while cooling from the totally liquid state to the semisolid state than when it was cooled into the semisolid state without shearing action[31]. The most important aspect of this procedure is the transition of associated microstructure from a dendritic to a spheroidal morphology. They reported that a

dendritic microstructure of the metal alloys was generated when the molten material is cooled to the semi-solid range with no shearing action. However, by shearing the material during the solidification process, dendrites are broken up creating spherical particles surrounded by a liquid. These conclusions had significant implications for the flow properties of semi-solid slurries. In the semi-solid processing, an alloy with solid near-globular grains microstructure and appropriate amount of solid fraction that dispersed in a liquid matrix, helps the material to flow into the die smoothly and fill the die cavity in a non-turbulent manner. The flow of liquid material within the die in a turbulent manner might cause the presence of air and die gases in the alloy and hence this can result in porosity, which has a negative impact on the integrity of the final product. Threfore, SSM processing introduces a high-quality near-net-shape component that has fewer weaknesses such as porosity, shrinkage, and gas entrapment compared with a similar component made from traditional casting methods[153].

Slurries with these unique microstructures have thixotropic characteristics which is necessary for semisolid processing. Thixotropy is a particular property of the materials and acts as an important behaviour factor if the semi-solid processes are to be successful. A definition of thixotropy was introduced by Mewis and Wagner (2009), as "the continuous decrease of viscosity with time when a flow is applied to a sample that has been previously at rest and the subsequent recovery of viscosity in time when the flow is discontinued"[154]. Examples of thixotropic behaviour are mayonnaise, ketchup and paints; they all become more viscous when stirred slowly and start to be less viscous when the gradual stir is increased. Alternatively, the property of thixotropy can be defined as time-dependent shear thinning as a result of changes in the microstructure of a material when shaken, agitated or sheared[155]. A dendritic and globular microstructure is presented in Figure 3.1 [34] together with a typical phase diagram that shows the semi-solid range used in thixoforming.

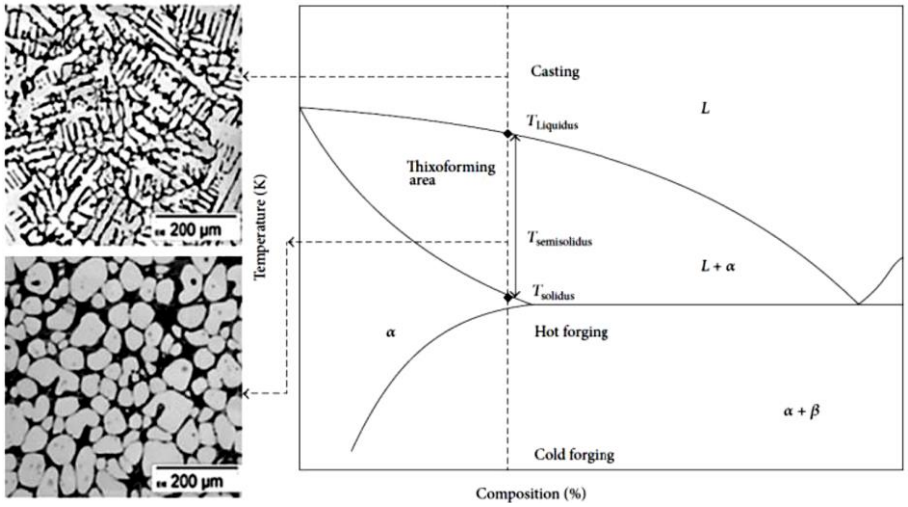

Figure 3.1 A generic phase diagram of a typical semi-solid alloy [34].

In general, a phase diagram of metal alloys is a schematic presenting a composition behaviour of the substance in relation to its temperature. The area that is above the liquidus line T_L is a liquid phase where the area the solidus line T_S indicates a solid phase. A combination of solid and liquid phases is shown between these two lines. The materials will begin to melt and then become semi-solid slurry when the metals are exposed to a temperature above the solidus lineT_S. With the increasing temperatures, the percentage of the liquid fraction will increase until the composition becomes entirely liquid above the liquidus lineT_L.

3.3 Rheology of Semisolid Alloys Slurries

Rheology is a term that used to describe the semi-solid and fluid properties of a substance. It is defined as the field of science that dealing with the studies of solid deformation and liquid flow[156]. The rheology can be applied to describe a wide range of materials from liquid to gases.

Generally speaking, the slurry of materials is either exhibiting liquid-like or solid behaviour. In the liquid-like, the slurry behaves like liquid when subjected to external force because of the distributed solid particles. In the solid-like, however, the slurry behaves like solid due to comprising an interconnected solid phase[42]. In the semi-solid processing, the solid-like slurry is involved which means it performs like a solid at rest yet flows like a liquid when sheared. This behaviour is demonstrated in Figure 3.2 where the alloy can be sliced and spread as easily as butter.

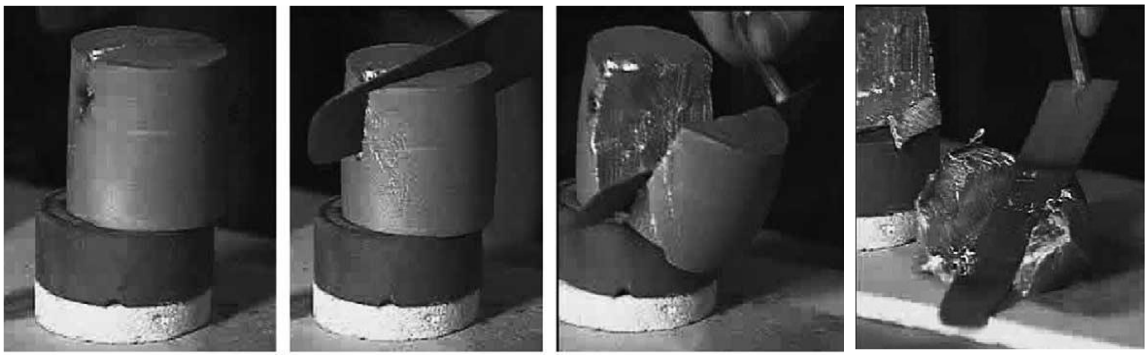

Figure 3.2 Illustrates a semi-solid billet that cut with a normal knife [22].

The rheological characteristics of semi-solid material is significantly influenced by the non-dendritic morphologies (scattered solid particles in the liquid medium) of the alloy, which in turn impact the alloy flow behaviour during processing. Semi-solid alloy with amount of solid fraction less than 60% typically exhibit two distinct rheological characteristic: thixotropy and pseudo-plasticity[1, 42]. Thixotropy and pseudo-plasticity are the two rheological behaviours shown by an SSM slurry under an external force. The property of thixotropy in SSM relates to the changes depending over time in the viscosity in a transient state as shown in Figure 3.3 , whereas pseudo-plasticity relates to the dependence of shear over steady-state viscosity[42]. Semi-solid processing method is mainly based on one or all of those rheological properties in the same process.

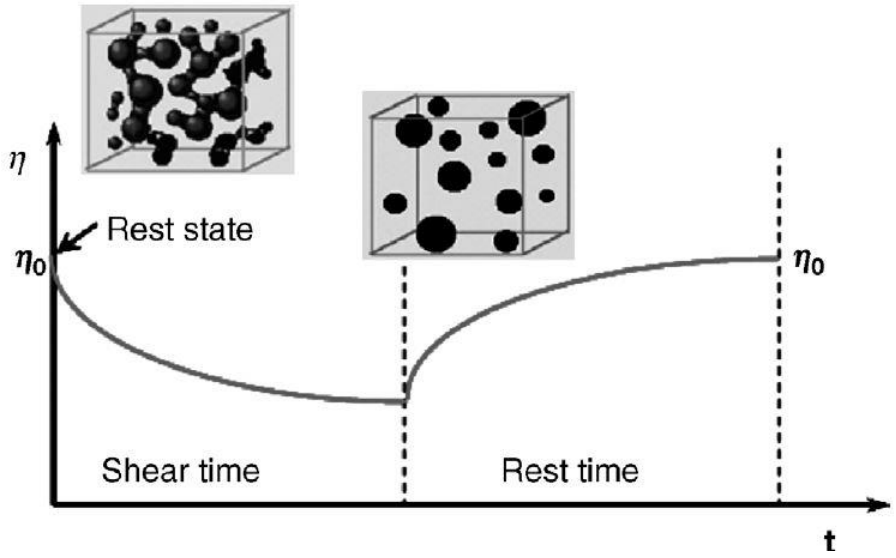

Figure 3.3 Graphic of time-dependent thixotropic behaviour [25].

Due to these rheological behaviours, SSM processing can gain vital advantages in developing SSM systems, such as by better control of die-filling. This will reflect in the integrity of the parts [157] (good mechanical properties, reduced porosity and shrinkage, etc.).

One of the most important conditions for rheological behaviour of SSM slurry is the property of viscosity (η). A vital role is played by viscosity in the concept of metal flow as the die-filling process relies on the control of viscosity during the SSM process[144]. In addition to that, the viscosity is also responsible for slurry flow and the forces necessary for the deformation of the materials that are being shaped [158].

Flemings et al[31] in their investigations illustrated that the viscosity of metallic alloys in the semi-solid range, at certain conditions can be affected by factors, such as solid fraction, shear rate and shearing time factor etc. The following provides brief overview of the importance process factors which affect the semi-solid viscosity.

3.4 Factors Affecting Rheological Behaviour of SSM

- **Effect of shear rate of viscosity**

The applied shear rate is one of the most fundamental elements impacting the viscosity of semisolid materials[159]. It generates non-turbulent or turbulent flow within the slurries during the solidification process. Normally, the semi-solid material will become more viscous when sheared slowly and it starts to be less viscous when the shearing is gradually increased and this viscosity reduction is caused by dendritic fragmentation and solid ripening phenomena within SSM slurries[22].

An examination was conducted by Joly and Mehrabian on Sn–15Pb alloy in order to investigate the behaviour of shear rate, solid fraction and cooling rate as well as viscosity in SSM slurries and the results can be seen in Figure 3.4 [42]. The Sn–15Pb alloy sheared at a 0.33 K min−1 cooling rate at different shear rates. Generally, they observed that, for a fixed rate of shear and cooling, it can be seen that the measured viscosity of stirred semisolid Sn–15Pb alloy increases with an increase in solid fraction. Nonetheless, the viscosity decreases with an increase in shear rate and decrease cooling rate for a given sold fraction[142]. The explanation of this observation is that due to the increase in shear rate and the decrease of cooling rate, the agglomerated particles are fragmented up and solid grains become more uniform and rounded[42] , and therefore grains spheroidisation procedure during shearing is presented in Figure 3.5 [31]. When such action is occurred it will also decrease the volume of liquid entrapped within spheroids and effectively reduces the size of spheroids at low cooling rates[23]. Consequently it allows the spheroid particles to pass over each other with less required effort, allowing for an unrestricted microstructure and a flowing of semi-solid slurries[1] which indicates that shear rate and cooling rate have a significant effect on viscosity.

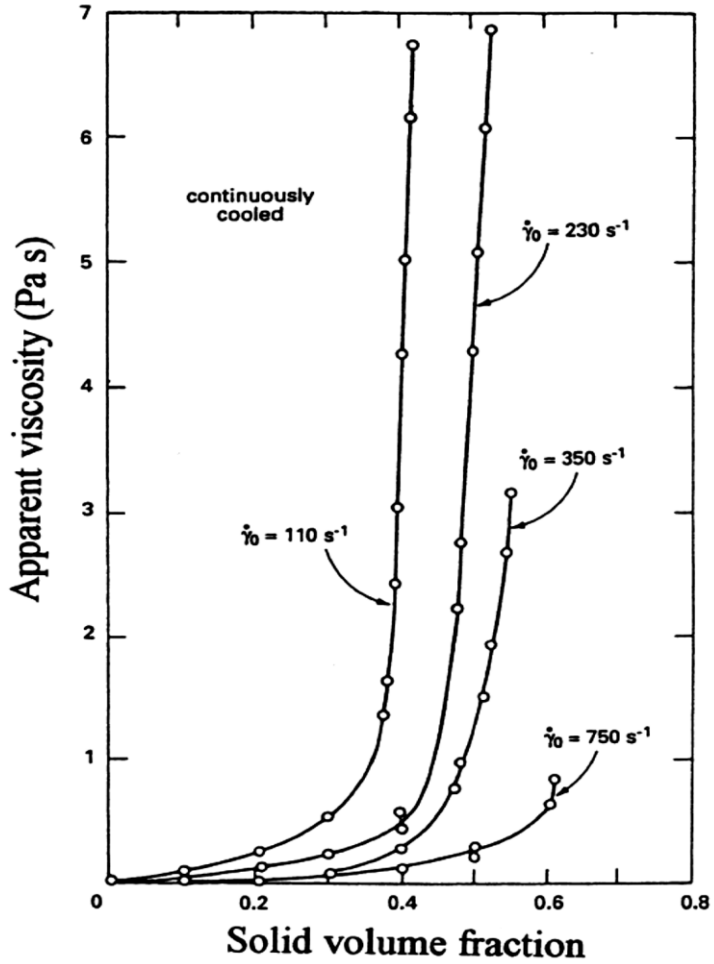

Figure 3.4 The solid fraction of Sn–15Pb alloy sheared continuously and during cooled at 0.33 K min–1 versus apparent viscosity at different shear rates [42].

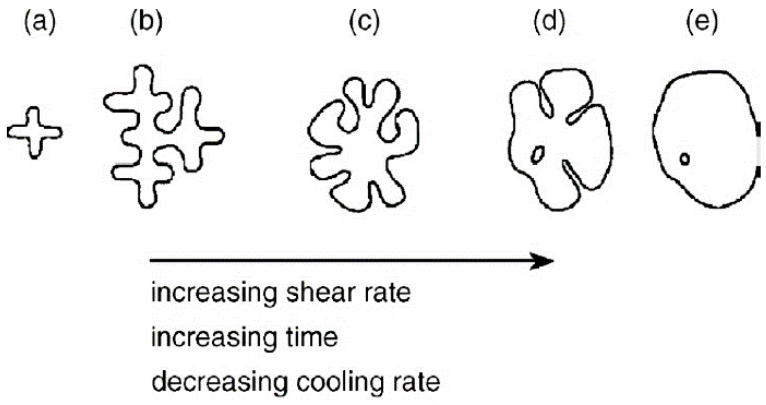

Figure 3.5 Graphic illustration of evolution of structure during solidification with vigorous agitation: (a) initial dendritic fragment; (b) dendritic growth; (c) rosette; (d) ripened rosette; (e) spheroid [31]

The shear rate of a single screw extruder can be calculated using Equation 3.1[160]

$$\dot{\gamma} = \frac{\pi * D * N}{h}$$

Equation 3.1

Where $\dot{\gamma}$= Shear rate in the screw channel, sec-1

D = Screw diameter

N = rotational speed in rpm

h = Channel depth

Note that this shear rates between the screw flight and the barrel wall are done using the same Equation 3.1. However, except h = distance between the barrel wall and the screw flight.

- **Solid fraction f_S:**

The solid fraction of the primary phase is one of the most essential metallurgical properties that has a major impact on SSM viscosity. The fraction of solid is identified as the percentage of the solid element and investigations have underlined the need of obtaining a low viscosity and a high fraction solid in SSM slurries[36, 144]. Generally, low viscous materials result in a better transition of metal slurry throughout the die-filling process and higher percentage of solid fractions during processing is necessary for preventing numerous flaws, obtaining intricate structure, and improving product quality. When the optimum solid fraction is attained within the slurries, the solid particles can be moved, slipped and rotated easily so the deformation of the mushy slurry will happen under less amount of external force, Figure 3.6 illustrates the mechanism of solid grains movement in a mushy metal condition[36].

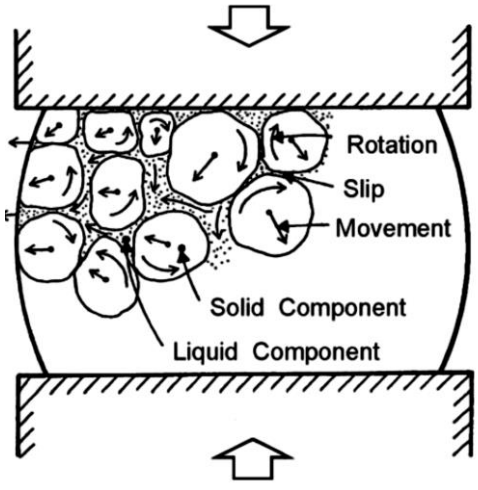

Figure 3.6 Solid components behaviour of a mushy metal [36].

The ideal volume of solid fraction varies from alloy to alloy but, in general, a high amount of solid fraction shows greater viscosity in SSM. A number of investigations reported that a suitable amount of solid fraction for SSM falls in the range of 0 .30 to 0.70[158, 161], while others stated that the effective solid fraction is between 0.5 and 0.6[23, 162]. The prediction of solid fraction is required to obtain the temperature-fraction solid relationships, which define the success of SSM processing or not. Several approaches are applied to predict the fraction solid in SSM processing, such as Scheil model or Lever Rule via a phase diagram.

In the Lever method, it is assumed that complete diffusion of the solid and liquid phases and this happens under equilibrium conditions over long periods of time. It can be calculated, at a given temperature T in the semi-solid range using the following equation[163]:

$$f_s = \frac{(T_M - T) - m_L \,.\, c_O}{(T_M - T).(1 - k)}$$

Equation 3.2[163]

Where the volume of the solid fraction is indicated by f_s, T_M is the solvent melting point, m_L is liquidus line slop, c_O denotes the concentration of alloy, and k is equilibrium partition ratio.

The another method of calculation the weight fraction of solid is by using Scheil model. This model proposes no diffusion in the solid phase (as opposed to the Lever condition which assumes diffusion in the solid phase and complete mixing in the liquid) and that diffusion takes place rapidly in the liquid phase leading to a non-equilibrium condition[164]. The fraction of solid at a given temperature T in the semisolid zone can be measured using the Scheil's equation [146, 163].

$$f_s = 1 - \left(\frac{T_m - T}{T_m - T_L}\right)^{\frac{1}{1-k}}$$

Equation 3.3[146, 163]

Where $f_s$the amount of solid fraction is, T_m is the solvent melting point, T_L is liquidus temperature of slurry and k is the ratio of the equilibrium partition.

Finally, computational thermodynamic softwaer such as Thermo-Calc & DICTRA[165], are also used to evaluate the percentage of solid fraction for equilibrium phase diagrams and Scheil model in multi-alloy systems.

- **Temperature**

In semi-solid metal processing, temperature represents a very significant factor like a solid fraction, as they can affect the rheological behaviour of SSM slurry and thus, influence the viscosity of the materials. It is believed that at high temperatures during SSM processing

may lead to reduced amounts of solid faction and hence, enhance the deformation and slurry flow[144]. There is a strong relationship between the impact of the temperature and fraction solid on viscosity in SSM alloy. The viscosity of the SSM alloy falls as the temperature rises as illustrated in Figure 3.7[4]. Temperature offers the activation energy to the fluid molecules, causing them to move. The motion takes place when the molecules of the liquid slide past each other, and the molecular chain and the force of attraction between molecules determine the ease of flow[166]. The viscosity-temperature relation is given in Equation 3.4[144] (only true for a system that there is no phase change due to the temperature difference). So, any variation in temperature normally influences viscosity.

$$\eta = \eta_o exp\left(\frac{\Delta E}{RT}\right)$$

Equation 3.4[144]

Where ΔE is the activation energy, η is the viscosity coefficient, R is gas constant, T is temperature.

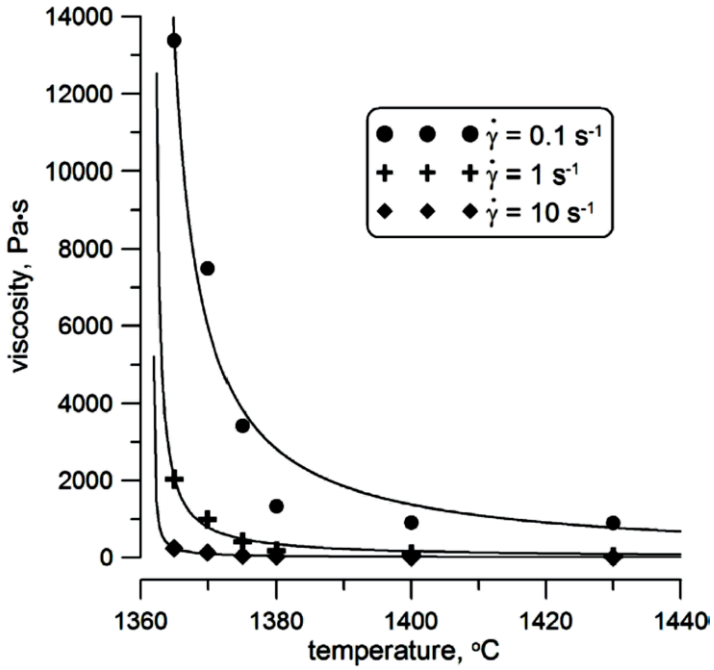

Figure 3.7 Effect of temperature on material viscosity [4].

- **Particle Size and Distribution**

Furthermore, particle size and distribution is one of the primary factors influencing the rheological properties of semi-solid alloys. There is interest, both practical and theoretical, to understand the effect of particle size and distribution in the rheological behaviour of SSM slurries. It is generally accepted that the smaller the particle size of materials, the lower viscosity, resulting in a better flow behaviour of the slurry. This phenomenon arises

due to the superior movement and reduced collisions among solid particles[1, 17]. Several experimental tests were conducted in order to characterise SSM behaviour and confirmed that the particle size, which is determined by the cooling rate and shear rate, influences the viscosity of the semi-solid metal[36]. Figure 3.8 shows how the cooling rate affects the size of solid particles and it can be clearly seen that the particle size is inversely proportional to the cooling rate.

The distribution of the solid particles within the SSM slurries is another aspect examined by investigators that has an impact on the rheological properties of semi-solid alloys which induce lowering viscosity and realizing high-quality parts. The agglomeration possibility of the dispersed particles in the liquid matrix could be reduced or improved with the application of external shear on the semi-solid slurries. The dynamic interactions between the solid particles within the semi-solid slurries lead to the development of agglomerates and therefore resulting the SSM slurries flow more difficult. After a period, under the influence of viscous forces, an equilibrium between the two opposing processes of agglomeration and de-agglomeration processes occurs, at which point viscosity changes to steady state and a uniform solid particles distribution is established[144, 167].

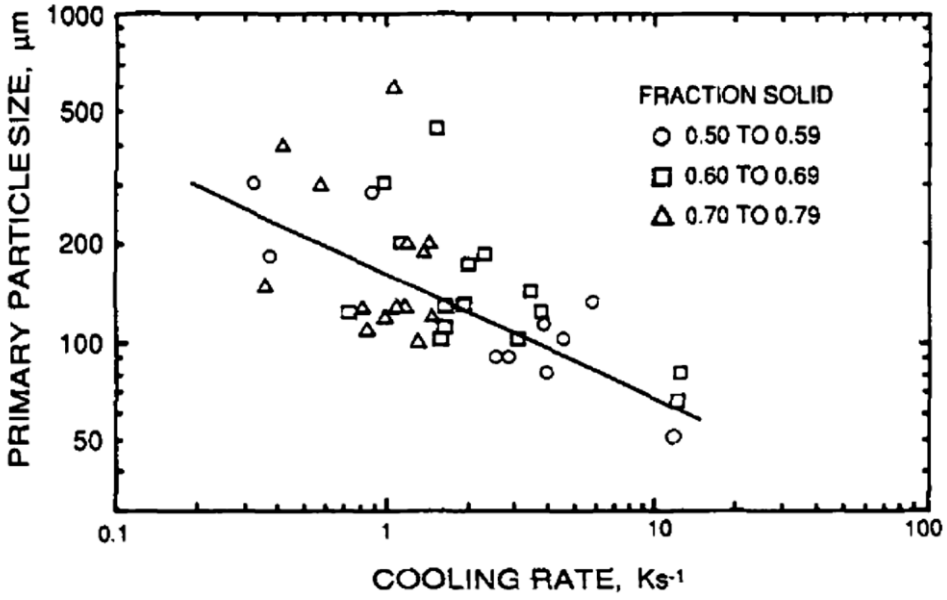

Figure 3.8 Difference of the grain size with the cooling rate for the Sn-15 wt pct Pb alloy [17].

3.5 Methods for Producing SSM Feedstock Material

Since the finding of the thixotropic behaviour of SSM alloys by Spencer in 1972, substantial studies into semisolid metal processing have been conducted and led to develop various processing routes. SSM processing technologies can be broadly divided into two categories namely Rheocasting and Thixoforming[42]. The Rheocasting begins with a liquid metal alloy that is sheared during solidification to create thixotropic SSM alloy, which is then transported directly into a die or mould to create the final component. In this route, the SSM slurry is made from a totally liquid alloy[168]. Thixoforming, however, is a near-net shaping processing which starts from the solid-state. In this approach a billet of feedstock having a spherical structure that has been specifically produced , cut to a required size, and then reheated to semi-solid regime to achieve thixotropic characteristics, and lastly forming the final product using various methods[169]. These SSM processing methods will be discussed later in more details in the next section.

As described above the first step in the thixoforming process is to produce a feedstock with a distinctive thixotropic microstructure, which is a critical step in achieving successful SSM processing. This unique structure is a non-dendritic primary phase with an appropriate amount of fine solid grains uniformly dispersed in a liquid matrix. A number of approaches for creating fine globular microstructures for feedstock manufacturing have been explored in recent years. The methods of producing this feedstock are classified according to the state of the starting material. This can be either from liquid metal via controlled solidification under a certain conditions, which are further can categorised into agitation and non-agitation routes, or from solid-state via substantial plastic deformation and recrystallization[34]. There are several techniques have been utilised to produce SSM feedstock out of a wide range of ferrous and nonferrous alloys such as Mechanical Stirring, Magnetohydrodynamic(MHD) Stirring, Spray Casting, Liquidus Casting, Ultrasonic Treatment, Grain Refinement, Strain Induced Melt Activated (SIMA), and Recrystallisation And Partial Melting (RAP),or a combination of these processes[1, 42, 170]. In this section, the most important of those techniques available for feedstock production are summarised below:

- **Mechanical stirring:**

The first processes route designed for producing feedstock for semi-solid processing is the mechanical stirring[171]. This method of vigorous stirring was primarily developed by the Massachusetts Institute of Technology, MIT[42] to achieve the non-dendritic microstructures during the solidification from the liquid state. The semi-solid slurry is agitated using an auger or screw[12, 172], impeller or fixed multiple agitators[42, 173] to a central shaft of the rotor and thus, mechanically breaking-up the dendritic structure. The

shear provided by the stirrer encourages the creation of non-dendritic structure during solidification. In spite of mechanical stirring employed a simple equipment and the stirring solidification process and flow behaviour of semi-solid alloy can be investigated through controlling processing factors such as stirring temperature , velocity and cooling rate[174]. The initial kind of mechanical stirring has yet to be commercialised. This was linked to a number of technical issues at the time, such as contamination of the metal slurry and erosion of the stirrer[17, 31].

- **Magnetohydrodynamic (MHD) Stirring:**

To address the issues associated with direct mechanical stirring, International Telephone and Telegraph (ITT) based in the United State established the magnetohydrodynamic (MHD) stirring process[1] (See Figure 3.9). in this process, the non-dendritic slurry is created using rotating electromagnetic fields during continuous or semi-continuous casting that leads to high shearing and accordingly, the dendritic structure is broken up in the semisolid phase to form the desired microstructure[143] and then SSM billets produced. The stirring process takes place deep within the liquid, which has already been filtered and degassed, hence avoiding contamination, gas porosity and stirrer erosion issues. As a result, MHD stirring has become the most widely used method for producing feedstock[171].

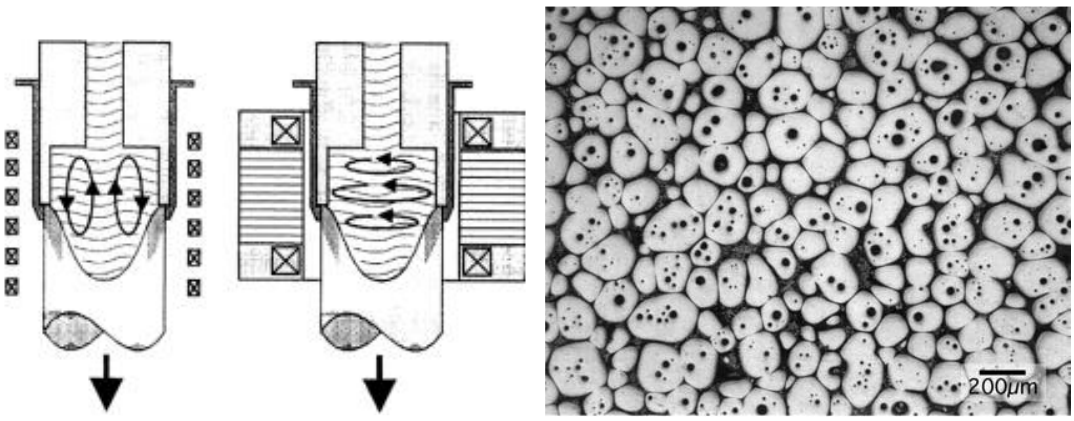

Figure 3.9 (a) Schematic of MHD technique[136], and (b) SSM microstructure realised using the MHD procedure [9].

- **Spray Casting:**

Spray Casting, also known as Osprey process, is alternative method for fabricating non-dendritic feedstock that eliminates the requirement for agitation the metal slurries during solidification. The general concept of this method is that the liquid metal stream is atomised into spray of very small droplets by means of a high gas jet, such as Argon and Nitrogen, as shown schematically in Figure 3.10. Following that step, the stream of droplets is deposited in the semisolid state onto a cooled substrate and then a globular structure is introduced on reheating that part in the state between solid and liquid.[1]. In addition to the advantage of this method to produce a fine-grained, homogeneous microstructure, it may have special advantages with high temperature alloys such as steels and super alloys. However, it believed that this process is more expensive production route comparing with MHD stirring process, as we as the billet sizes are typically not less than 60mm [24, 42].

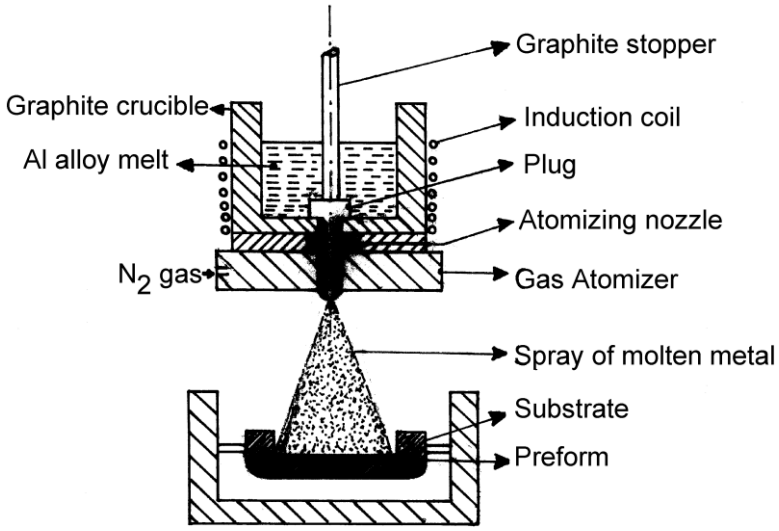

Figure 3.10 Schematic illustration of the experimental setup of spray processing [24].

- **Chemical Grain Refining:**

Chemical grain refinement is a non-agitation process that involves a modification of alloy composition to create feedstocks with the required spherical structure form liquid metal alloys for SSM process. It achieves by adding some chemical elements to the melt to control the nucleation process. For example, adding a Ti-B into aluminium alloys before casting leads to grain refinement and favours the formation of equiaxed microstructures instead of columnar growth[1, 34]. By using this method, It is possible to produce a low-cost raw feedstock with grain sizes of less than 0.1 mm. However to attain the desired properties this technique cannot be employed in isolation; it must be used in conjunction

with another method of producing feedstock, including liquid casting or MHD stirring process [42].

- **Liquidus Casting:**

Liquidus casting process, also called as a New Rheocasting (NRC), that was patented by UBE Industries Ltd.[175], is one of the non-agitation routes for spheroidal feedstock fabrication. The steps in the NRC process are illustrated schematically in Figure 3.11. In this process, the metal alloy is melted just over the liquidus temperature and then is poured into a holding crucible which is placed on a cooling carousel. By controlled cooling of the alloy into the semi-solid condition an appropriate solid fraction is obtained. Next, the crucible is transported from the chill station to the inclined sleeve before the semi-solid metal is cast into a mould by die casting and solidified with required thixotopic microstructure [176]. The NRC technique was the first industrialised rheocasting method and it was suitable for recycling scrap materials in-situ. However this process is presently not widely available commercially due to the high initial cost of the technique[34, 177].

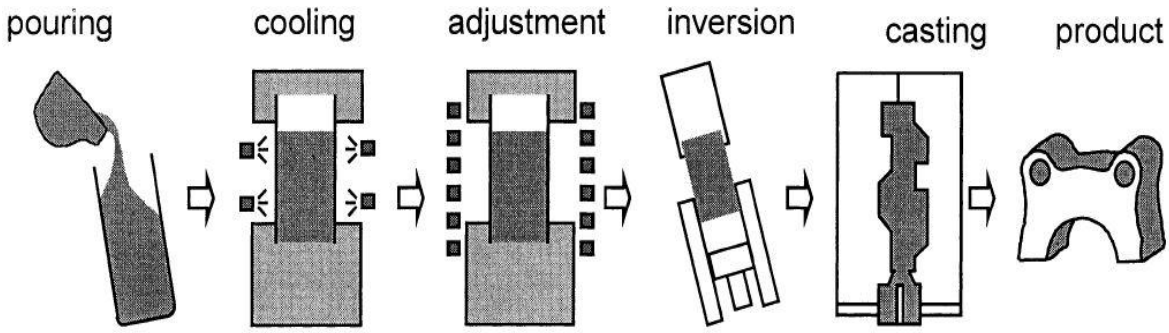

Figure 3.11 Schematic graph of new rheocasting(NRC) route [42].

- **Strain Induced Melt Activated (SIMA)/Recrystallization And Partial Melting (RAP):**

An alternative to the liquid agitation route is the solid-state working routes. In these thermomechanical methods, the creation of a non-dendritic microstructure is performed with no need for reaching the raw material melting point, i.e., the feedstock is shaped by deformation the metal in its solid-state. The material is deformed using traditional forging methods, subsequently warmed to a semi-solid condition. Strain Induced Melt Activated (SIMA)[178-182] and Recrystallisation and Partial Melting (RAP)[183-185] are the tow of the most efficient and widely available solid-state processes for fabrication SSM feedstocks. These approaches normally involve a heavy plastic deformation followed by recrystallisation routes during the re-melting phase to produce the globular structure. The

deformation step in SIMA and RAP procedures is the most important since it affects the grain size and homogeneity of the semi-solid microstructure[186]. The grain refinement of metal can be done by different deformation methods including rolling, extrusion, compression, drawing or forging[187]. If the deformed material is then subjected to a partial re-melting stage(semi-solid state and isothermal holding), recrystallization occurs during soaking, and once the liquid begins to form, it wets and penetrates grain boundaries, transforming the elongated microstructure to globular structure which comprising of spheroidal particles suspended in the liquid matrix. The difference between SIMA and RAP is that in the SIMA method the initial deformation of the material is carried out at a temperature higher than the recrystallisation, then cold work at room temperature. In RAP, however, the initial deformation is achieved below the recrystallization temperature (cold working)[22]. The morphological transformations of cast dendritic morphology after hot/cold deformation followed by re-heating to semisolid zone and thixoforming is shown in Figure 3.12. In SIMA, dynamic recrystallisation occurs during deformation temperature developing equiaxed grains structure. While in case of RAP dendritic deformed microstructure take places at cold deformation and it necessitate additional heating to cause static recrystallisation. Both routes result in development of globular primary phase morphology, i.e., thixotropic SSM alloy, when deformed materials exposed to reheating to the solidus-liquidus temperature zone. The SIMA method has been yielded high-quality thixoforming feedstock made from a range of alloys made from magnesium, aluminium, and zinc and has the ability to process wrought alloys as well as high-melting-temperature alloys like steel and super alloys [42, 188]. The solid-state production process via recrystallization seems to be a viable alternative to the liquid MHD process, as it uses less complex technology and equipment. However, RAP process is only suitable for processing feedstock with small diameter due to the level of uniform deformation required across the section [1, 143], that means working with larger billet diameters can be challenging and expensive.

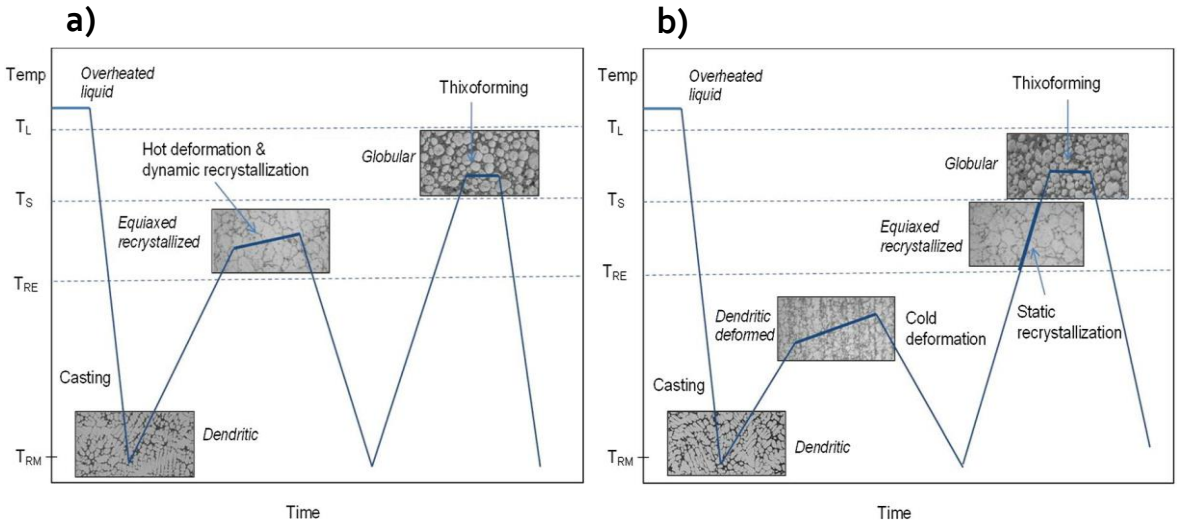

Figure 3.12 Schematic depicts of the stages of a) SIMA process and b) RAP process [26].

3.6 Semi-Solid Metal (SSM) Processing Methods

SSM processing is usually understood to include a wide range of processes. Nowadays, entire forming processes of component manufacturing, from thixotropic feedstock preparation through the last forming step, can be completed using semi-solid processing techniques. All of these the technologies can be broken down into two primary routes that are essentially different: namely rheo-route and thixo-route. The rheo-route is a method of introducing SSM alloy from a liquid state and then shaping it. In this process, the semi-solid slurry with desired thixotropic properties is placed directly, without any intermediate stage, into a mould or die to produce the final part. On the other hand, the thixo-route usually refers to techniques that include an intermediate solidification stage. In this thixo-route, the first step is material fabrication process where the feedstock material with the special non-dendritic microstructure is produced. The feedstock material is then reheated to a mushy zone to form the SSM slurry before being transferred to a metal die for component forming. If the component forming is accomplished in a closed die, it is referred to as thixocasting, if an opened die is used during this process, it is called thixoforging [1, 42]. Sometimes a term of thixoforming is applied to refer to both thixocasting and thixoforging, as well as a combination method in which the billet is driven into a die using a ram rather than a shot sleeve[22]. Figure 3.13 graphically depicts the differences between rheocasting, thixocasting and thixoforging. The rheo- and thixo-related technologies will be detailed as follow:

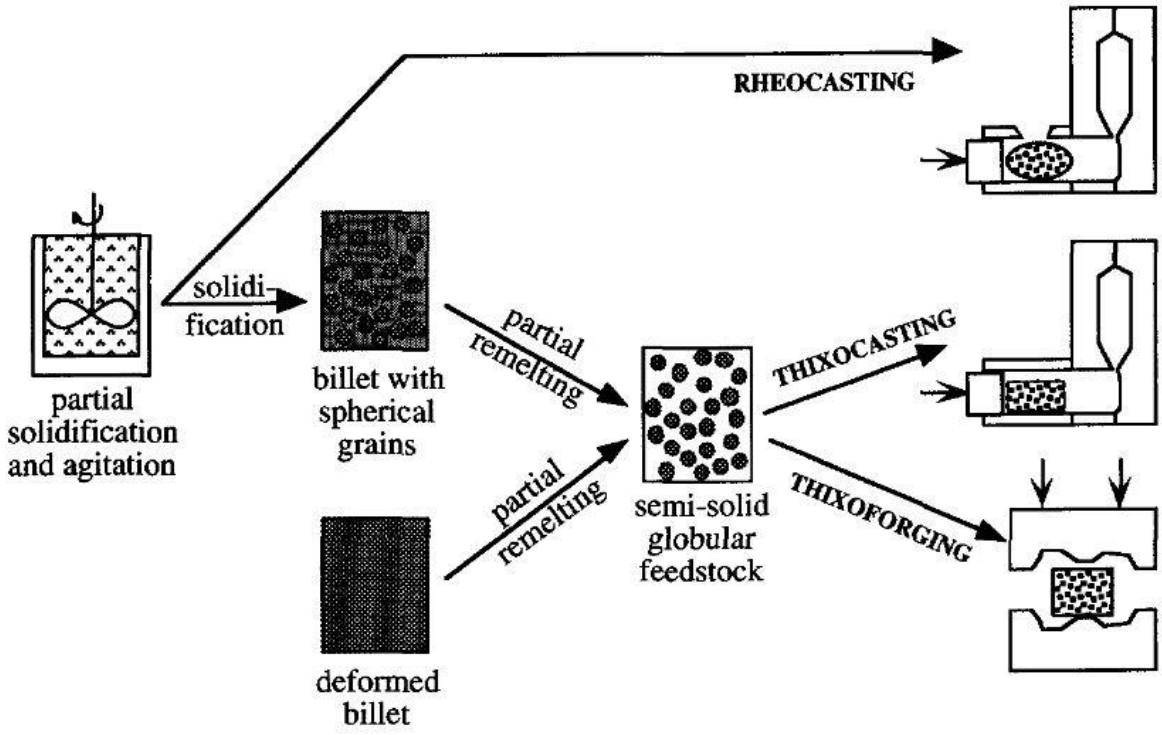

Figure 3.13 Shows a schematic illustration of different semisolid metal processing routes [6].

- **Rheocasting**

Rheocasting is a method of directly introducing semi-solid alloy from the liquid state, followed by a fabrication process[169]. Unlike thixocasting, which requires reheating a pre-modified billet, in the rheocasting process, the molten alloy is cooled down to a semi-solid state, while the non-dendritic microstructure required for semisolid processing is simultaneously created. As soon as the metal alloy has cooled and reached the desired temperature, the desired fraction solid between 10 and 30% [153], the obtained semi-solid metal is transferred into a shot sleeve, where it will be directly without any intermediate solidification phase pumped into a mould to form part[22, 168]. The semi-solid slurry with a microstructure of a fine solid grain , non-dendritic surrounded by a liquid matrix can be attained by (see the section on 'Methods for producing SSM feedstock material') a variety of methods during cooling including mechanical stirring, NRC or electromagnetic stirring[153]. The main benefit of rheocasting is that the molten alloy can be formed directly into non-dendritic SSM slurry at the casting machine, removing the need for specially produced pre-conditioned billet material, accordingly contributing to a significant reduction in operating cost compared to thixocasting route[169]. Also scrap and runners can be recycled on manufacturing site for use with the SSM forming process, lowering costs even further. However, product consistency is one of the potential challenges of rheocasting[177]. Since each casting is produced with a single shot of liquid alloy, therefore, it is hard to maintain the same level of consistency quality with new

components. Thus, semi-solid components formed by rheocasting tend to have less consistent properties than those formed by thixocasting.

- **Thixomolding**

The thixomolding process, which was invented by Dow Chemical, USA, in the early 1980s, is a semisolid metal processing method and generally similar to the plastic injection moulding process[18]. It has been established well, primarily in Japan and USA, to manufacture net-shape magnesium products including electronic and communications applications, e.g. laptop, cameras, and mobile phones[189-191]. Figure 3.14 shows the basic principle of the process where it can be seen that the whole forming processes are integrated in one single machine. The main components of this unit are hopper, heated barrel containing argon to prevent oxidation, reciprocating screw and preheated mould. In practice, this process include raw chips of magnesium are fed through the hopper into a heated barrel, which is accompanied by a rotating screw. The material is sheared and partially re-melted due to the rotating motion and heating in the barrel. As a result, a thixotropic of semisolid alloy is created in an argon atmosphere within the barrel. Finally, the rotational motion of the screw drives the alloy forward toward the nozzle, before it being injected into a heated mould to produce the thixomolded part[42]. In addition to this process can be adapted for mass production in continues manner the key benefit of the technique is that the manufacturing processes performed in a single step. Further, the liquid metal handling activities are no longer required, resulting in a clean and safe working environment. However, this approach cannot be used for aluminium applications as the aluminium melt often reacts with the barrel and screw elements and causing a considerable wear to the machine[192, 193].

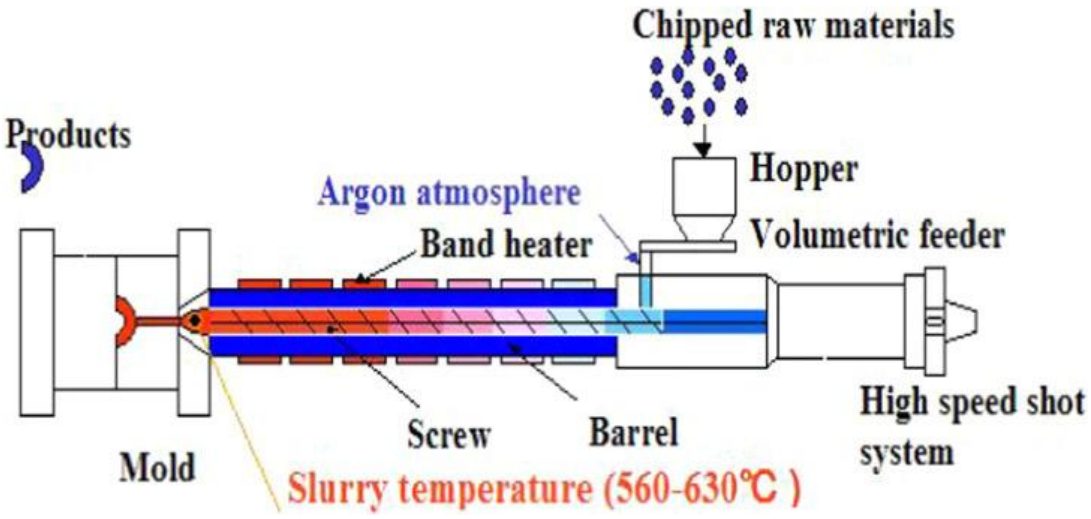

Figure 3.14 Schematic Illustrating the Thixomolding Process [18].

- **Rheomoulding**

This technology, similar to thixomolding, is derived from plastic injection moulding process. In the rheomoulding process, however, the liquid metal is utilised as initial materials instated of solid chips materials. There are two sorts of mechanisms that can be used in this process: a single screw[42] and a twin screw mechanism (latest version)[12] developed at Cornell University and Brunel University, respectively. In the twin screw mechanism (see Figure 3.15), which developed by Fan and co-workers, the liquid metal is fed into a barrel and allowed to cool to semi-solid temperatures while being agitated mechanically by a rotating twin screw. Due to the high shear rate of the rotating twin screw, the molten alloy altered to SSM slurries with a desired solid fraction. Then the semi-solid slurry is inserted into a die cavity through a nozzle to form the required object[143]. This method is suitable for mass production of components that do not require the use of especially pre-conditioned feedstock materials.

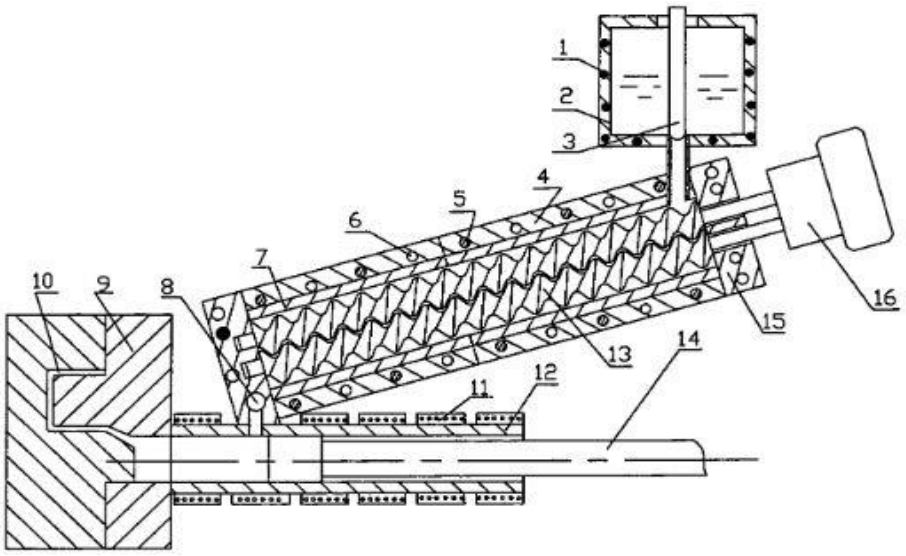

1, Heating elements; 2, crucible; 3, stopping rod; 4, barrel; 5, heating elements; 6, cooling channels; 7, barrel liner; 8, transfer valve; 9, die; 10, mould cavity; 11, heating elements; 12, shot sleeve; 13, twin-screw; 14, piston; 15, end cup; 16, driving system.

Figure 3.15 Schematic illustration of a twin-screw rheomoulding apparatus [12].

- **Thixocasting**

Thixocasting is a semi-solid forming process that involves injecting SSM slurries into a mould using a die-casting mechanism to create metal net-shaped components[1]. As sated earlier, the conventional thixocasting procedures are broken into two main steps: SSM feedstock fabrication and reheating it to SSM temperature zone which must be completed prior to forming procedures. In the thixocasting, a pre-modified billet, which has developed a fine-grained equiaxed microstructure, is initially produced by a feedstock

material preparation method such as MHD, mechanical stirring or thermomechanical process. Then, the fully solidified billet is re-heated to a temperature range between the solidus and liquidus temperature until it becomes homogeneous[153, 194]. The liquid fraction of the billet during the reheating stage is relatively high, i.e., usually more than 50%[22]. Next, by using a shot piston, the semi-solid slurry is then placed into a closed casting die to form the desired shape[195]. Typically, the shaped part is discharged from the mould and post-processing may be needed, such as grinding and machining. Reheating, which can be in radiant furnace or an induction heating furnace[143], the feedstock to the semisolid state is a critical step in the forming process. It helps to deliver a SSM feedstock with precisely controlled volume of solid fraction of fine and sphere-shaped particles consistently dispersed in a low melting point liquid matrix[42]. Therefore, precise and uniform heating temperature as well as heating period are key process parameters during the reheating phase that have a significant impact on the quality of the fabricated part. The thixocasting process has several advantages such as producing components of exceptional quality with superior mechanical and functional properties because of product consistency that comes from employing pre-modified billet. Though, The primary drawback of thixocasting is the increased forming costs caused by the premium attached to special billet produced as we as the difficulty of effectively recycling biscuits and runners[177].

- **Thixoforging**

The concept of this technique is similar to thixocasting process. However, the manufacturing process is conducted by open die rather being injected into a closed die in which the semi-solid ingot is positioned between two halves of the die (see Figure 3.16). After that, by hydraulically squeezing the two dies together, the final shape of the part is produced[196]. Normally this process utilises a significantly lower liquid fraction content prior to the forming i.e. between 30 and 50%, allowing the SSM ingot to be handled. This technology can make thixoforged parts with different wall thicknesses, sharp radii, and sharp edge thicknesses. Yet, due to the fact that the challenging in attaining reproducibility it has become less active in commercialisation[143, 158].

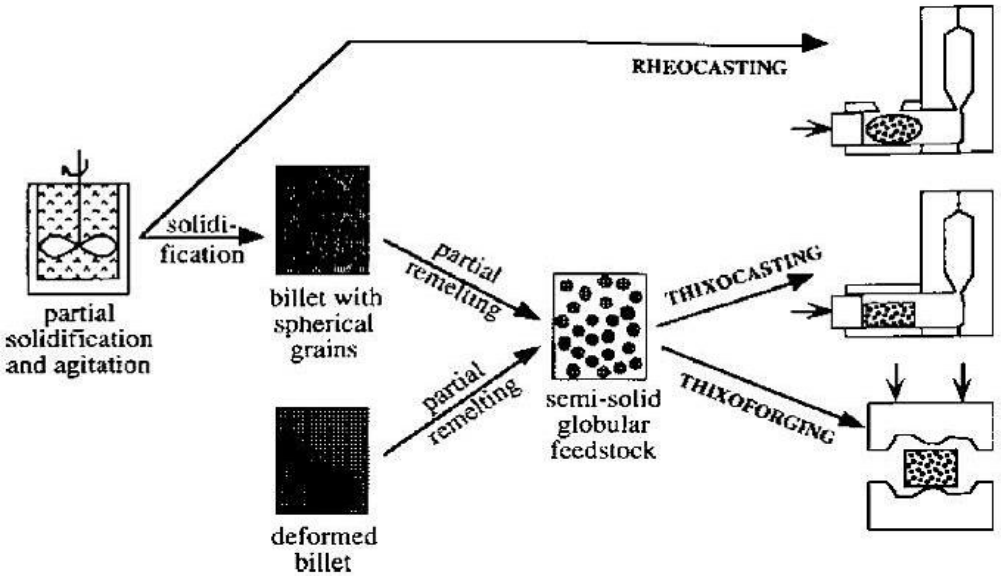

Figure 3.16 Schematic Illustration of distinct types for semi-solid metal processing [22].

3.7 Essential Criteria for Alloy Designing

It is obvious that obtaining a high-quality SSM alloy with a thixotropic microstructure and the subsequent smooth, non-turbulent mould filling is crucial to attaining the benefits of SSM processing. Achieving the advantages of SSM alloy processing advance the SSM technology that allows for the production of a wide range of near net-shaped metal components of complex geometries and excellent properties, in particular for the automotive and aerospace industries. However, It should not be assumed that all alloy compositions can be formed in semi-solid state and work for producing SSM components. These components are expected to be manufactured through proper design and alloy composition selection with optimised SSM processing parameters. There is a relatively limited number of metal alloys that are available and suitable for SSM processing as the present alloys were originally created for the casting process[197]. Despite the fact that there has recently been a continuous increase in interest and significant efforts are being made in alloy development particularly high-performance SSM alloys such as high-strength aerospace Al alloys [198]. Nevertheless, there is still a need to expand the range of metal alloys specifically designed for semisolid metal processing to pave the way for the development of industrial applications. However, one critical issue is determining whether the alloy of interest is suitable for semisolid processing. As a result, several criteria for determining the most suitable alloy for SSM processing have recently been presented[199]. Such alloys to be well suited to the SSM processing should have a number of compositional characteristics including a suitable freezing range, lower temperature sensitivity of solid fraction, the potential for age hardening, , morphology of solid phase

and good rheological properties and castability of the semi-solid alloy[42]. These criteria of alloy selection are described as follows:

- **Freezing range**

The freezing range of an alloy is one of the most important characteristics for SSM processing. The freezing range in semi-solid processing refers to the temperature difference between the liquidus temperature and the solidus temperature of an alloy. It is mostly influenced by alloy composition and processing conditions such as cooling rate. In semi-solid processing, the temperature ranges between solid and liquid states of the molten alloy have to be adequate enough to allow for a process window. Therefore, pure metals and eutectic alloys are not workable for SSM processing as the freezing temperature range is zero. Alloys with a large freezing temperature range, on the other hand, might experience some difficulties, such as poor liquid alloy fluidity and poor resistance to hot tearing[42]. Therefore, the freezing range is an essential factor which needs to be considered when designing an alloy for SSM processing.

- **Temperature sensitivity of solid fraction**

Obtaining a consistent solid fraction distribution during SSM processing is critical because this factor controls the rheological behaviour of the alloy, which has a significant impact on SSM workability. Consistent distribution of solid fraction can be attained by either maintaining a uniform alloy temperature, which is extremely hard in practice, or by selecting alloys with low-temperature sensitivity of the solid fraction, which is more feasible[200]. The temperature sensitivity of the solid fraction describes the variation in solid fraction with slight temperature changes, and it is normally determines by the slope of solid fraction (f_s) versus temperature (T)curve and denoted as $(\mathrm{d}f_s/\mathrm{d}T)$[201]. If the temperature sensitivity of the solid fraction is large, any negligible change in temperature prompts to a large variation in the solid fraction. As a result a little drop in temperature can result in significant rise in fraction of solid, and hence produced undesirable characteristic of SSM alloy due to uninform deformation and liquid segregation during mould filling process[202]. Therefore, the selected alloy for SSM processing preferably should have a very little temperature sensitivity of solid fraction. Liu et al[200], recommended that for optimal processability,$(\mathrm{d}f_s/\mathrm{d}T)$ should be less than 0.015 at the SSM working temperature, which is mean that a 1.5% change in solid fraction of the alloy is allowed for every for every 1℃ change in temperature.

- **The potential for age hardening**

The composition of the designed alloy for SSM processing should be age hardenable in order to optimise metal alloys. Age hardening is a heat treatment process which is used to offer several advantges including strength to metals, enhance mechanical and thermal properties as well as improve wear resistance[203]. Alloys intended for SSM processing

must have a significant ΔC in order to fulfil the criteria of the age hardenability of SSM processed components. ΔC is defined as the difference in the solubility of the element in solid solution between SSM processing temperature and aging temperatures[42]. Therefore, If an attention is paid during the selection of alloy composition, the possibility for age hardening can be obtained.

- **Castability**

Normally the metal forming process occurs between the solidus and liquidus state during the SSM processing in which the semi-solid alloy is then squeezed into a die cavity to produce a near-net-shape component. Consequently, the liquid phase is susceptible to the laws of traditional casting, and thus the castability of an alloy is an essential factor to achieve a successful SSM process[42]. Therefore, it is required to take into account the suitable fluidity of the liquid phase at the time of compositions selection to design alloy.

- **Morphology of solid phase**

Solid phase morphology plays a vital role for a slurry of SSM processing during alloy design. A perfect slurry for SSM processing should present an optimised semi-solid slurries with appropriate amount of fine size and rounded morphology of solid particles[42]. These particles are also uniformly distributed within the liquid matrix. As a result of such criteria for SSM alloy, allow a non-turbulent die filling and even microstructure of a slurry can be achieved after solidification providing the final component with improved properties. So, alloy development for SSM processing need to be selected carefully to enable the formation of an optimal SSM alloy.

- **Rheological Properties in the Semi-Solid State**

SSM processing is unique and favourable method compared to other traditional casting procedures due to the rheological characteristics of SSM slurries. Factors such as processing condition, morphology, size, and distribution of globular grains suspended in a liquid metal matrix and agglomeration of solid particles determine the rheological properties of the alloy in the semi-solid state[42]. These factors have on a major impact on the SSM alloy viscosity which in turn, influences the castability. Therefore, to take full advantages of SSM processing, favourable rheological properties of SSM slurry have to be considered.

3.8 Metallic Alloys for Semi-Solid Processing

Semi-solid metal processing is introduced as an alternative method to conventional casting and/or die casting processes. The ultimate goal of using the semi-solid process technique is similar to these conventional methods where they both manufacture semi-finished components. Therefore, the raw materials employed in those manufacturing techniques are relatively linked to each other. Consequently, the material alloys that

derived from these traditional methods have been engaged in both semi-solid processes, the thixoforming route, which involves preparing the feedstock materials in an additional stage and then subjected for heat treatment to form SSM alloy followed by forming process, and rheocasting routes, which involve slurry making in-situ where the SSM alloy introduced directly form liquid state and then followed forming operation[204]. Of course, not all the conventional alloys developed for traditional casting operations can be suitable for semi-solid metal processing.

The prospective material must be satisfying the specific requirements of semi-solid processing including small temperature sensitivity of solid fraction, wide solidification phase, the potential for age hardening, desired characteristics of rheology, castability of the metallic alloys, and the morphology of the semi-solid slurry. These considerations will lead to favourable thixotropic materials associated with non-dendritic microstructures that appropriate for SSM processing. The first investigation by Spencer at MIT that discover thixotropic behaviour of metallic alloys in the semi-solid state was performed in tin-leas alloys[31], due to low melting temperature of this model system. Since its discovery SSM processing of alloys has showed tremendous promise for industrial applications and was validated for a variety of metallic alloys including aluminium, zinc, copper, magnesium, titanium, ferrous, and super alloys[193]. The most important metal alloys for semi-solid processing will be examined in further depth in the following sections.

- **Aluminium Alloys**

SSM processing evolved primarily around aluminium alloys, which have the greatest commercial potential. It is one of the most well-known materials that have been extensively employed in manufacturing applications, particularly in the automotive and aerospace industries[205] Energy consumption can be conserved to process aluminium alloys by applying SSM process, where the power consumed in the die casting process to heat aluminium alloys is 35% higher than the consumption of required power in the semi-solid processing to treat the same aluminium alloys[23]. Every year, millions of components made from aluminium alloy are produced using the SSM processing route. Initially, conventional aluminum-based casting alloys were used in the development of SSM processing of aluminium alloys. Generally speaking conventional aluminum-based casting alloys from the 300 family have exceptional fluidity, corrosion resistance , castability, low coefficient of thermal expansion[141]. Therefore, alloys such A356 and A357 are among the most common traditional casting alloys which are semi-solid processed in commercial application[185]. Nevertheless, these alloys do not have the same mechanical properties as typically wrought alloys or high-strength aluminium casting alloys[185]. Hence, in order to achieve higher performance a number of investigation on the processing of high strength alloys , which are typically wrought, have

been reported such as the 2000 series, 6000 series and 7000 series[206, 207]. These high-strength alloys have been successfully processed using SSM. However, the majority of these alloys are inherent difficulties as wrought alloys are extremely difficult to cast or shape in the semisolid condition[208]. Several of practical examinations have confirmed that the wrought composition alloys experience challenges in thixoforming. For alloy such as 6061 shows steep slopes in the liquid fraction versus temperature curves resulting in narrow processing windows[209], hot tearing for alloys such as 2000 series as a result of too wide solidification ranges[185], and high susceptibility to hot cracking for 7075[207].

Table 3.1 indicates the measurements of thermal characteristics of some alloys that are cast and wrought for thixoforming process[42]. For wrought alloys, a slight change in temperature results in a significant difference in solid fraction and end up with inappropriate microstructures for semi-solid processing when the solid fraction increases due to a decrease in temperature, or uncontrollable SSM alloy when the solid fraction decreases due to a higher temperature. Table 3.2 represents some statistics for mechanical properties of some wrought and cast aluminium alloys [1]. It is perceivable that for the 356 aluminium alloy (AI-7Si-0.5Mg), the thixoformed specimens in T6 condition outperform specimens produced by the PM route in all mechanical properties and approach those obtained by CDF process. A similar observation can be found for A357 aluminium alloys in which the findings demonstrate that mechanical properties comparable to those obtained via the PM route, particularly in ductility. In the case of wrought aluminium alloys different results are presented, where they do not reach the greatest values of strength and desired ductility due to some issues associated, such as residual porosity, oxide inclusions and inherently vulnerable to hot tearing[1].

Table 3.1 Thermal properties of some Aluminium alloy [42].

Alloy/nominal composition	T_L	T_S	ΔT_{S-L}	T_L	T_S	ΔT_{S-L}	T_L	T_S	ΔT_{S-L}	$f_s = 0.3$	$f_s = 0.6$
Wrought aluminium alloys											
2024/Al–4·4Cu–1·5Mg–0·6Mn	638	502	136	640·6	507·0	133·6	640·6	515·8	124·8	0·0339	0·014
3004/Al–1·2Mn–1·0Mg	654	629	25	653·8	522·0	131·8	653·8	640·8	13·0	0·149	0·084
4032/Al–12·2Si–1·0Mg–0·9Cu–0·9Ni	571	532	39	571·5	519·0	52·5	571·5	535·4	36·1	0·0676	0·0244
5056/Al–5·0Mg–0·1Mn–0·1Cr	638	568	70	635·7	298·0	337·7	635·7	578·8	56·9	0·0335	0·0188
6061/Al–1·0Mg–0·61Si–0·30Cu–0·20Cr	652	582	70	652·1	532	120·1	652·1	590·5	61·6	0·0707	0·0331
7075/Al–5·6Zn–2·5Mg–1·6Cu–0·23Cr	635	477	158	634·9	471·4	163·5	665·4	517·7	147·7	0·031	0·0147
Cast aluminium alloys											
296.0/Al–4·5Cu–2·5Si	635	530	105	632·5	525·1	107·4	632·5	527·8	104·7	0·0192	0·0078
356.0/Al–7Si–0·3Mg	615	555	60	615·6	557·2	58·4	615·6	567·5	48·1	0·0118	0·201
357.0/Al–7Si–0·5Mg	615	555	60	614·9	557·2	57·7	614·9	560·7	54·2	0·0117	0·121
390.0/Al–17·0Si–4·5Cu–0·6Mg	650	505	145	661·4	510·2	151·2	661·4	510·2	151·2	0·06	0·0241
520.0/Al–10Mg	605	450	155	608·7	450·1	158·6	608·7	508·0	100·7	0·016	0·0094
771.0/Al–7Zn–0·9Mg–0·13Cr	645	605	40	644·8	468·2	176·6	644·8	612·8	32·0	0·0586	0·0349

Table 3.2 Mechanical Properties of some Wrought and Cast Aluminium Alloys [1].

Alloy	Process*	Temper	Yield stress, MN m^{-2}	Tensile strength, MN m^{-2}	Elongation, %	Hardness, HB	Ref.
Casting alloys							
356	SSM	T6	193	296	12·0	90	5
(Al–7Si–0·5 Mg)	SSM	T6	256	300	11·4	...	56
	SSM	T6	240	320	12·0	105	35
	SSM	T7	260	310	9·0	100	35
	SSM	T5	172	234	11·0	89	5
	SSM	T5	180	225	5–10	80	56
	PM	T6	186	262	5·0	80	57
	CDF	T6	280	340	9·0	...	58
	PM	T51	138	186	2·0	...	57
357, A357	SSM	T6	290	358	10·0	100	5
(Al–7Si–0·3 Mg)	SSM	T6	260	330	9·0	115	35
	SSM	T7	290	330	7·0	110	35
	SSM	T5	207	296	11·0	90	5
	SSM	T5	200	285	5–10	90	35
	PM	T6	296	359	5·0	100	57
	PM	T51	145	200	4·0	...	57
Wrought alloys							
2017 (Al–4Cu–Mg)	SSM	T4	276	386	8·8	89	5
2017	W	T4	275	427	22	105	57
2024 (Al–4Cu–1Mg)	SSM	T6	277	366	9·2	...	56
2024	CDF	T6	230	420	8·0	...	58
2024	W	T6	393	476	10	...	57
2024	W	T4	324	469	19	120	57
2219 (Al–6Cu)	SSM	T8	310	352	5·0	89	5
2219	W	T6	260	400	8·0	...	57
6061 (Al–1Mg–Si)	SSM	T6	290	330	8·2	104	5
6061	W	T6	275	310	12	95	57
7075 (Al–6Zn–Mg–Cu)	SSM	T6	421	496	7·0	135	5
7075	SSM	T6	361	405	6·6	...	56
7075	CDF	T6	420	560	6·0	...	58
7075	W	T6	505	570	11·0	150	57

*CDF closed die forging; PM permanent mould casting; SSM semisolid metal processing; W wrought.

Correspondingly, Figure 3.17 [42] is a schematic of mechanical properties of elongation vs yield strength for A357 and A356 alloys treated by sand casting, squeeze casting (SQC), permanent mould casting (PMC) and thixoforming. Generally, it can be seen that with respect to strength and ductility, better mechanical properties of thixoformed A356 and A357 are observed, but nearly equal to those obtained by SQC, compared to other conventional processes in the full heat treated condition (T6).

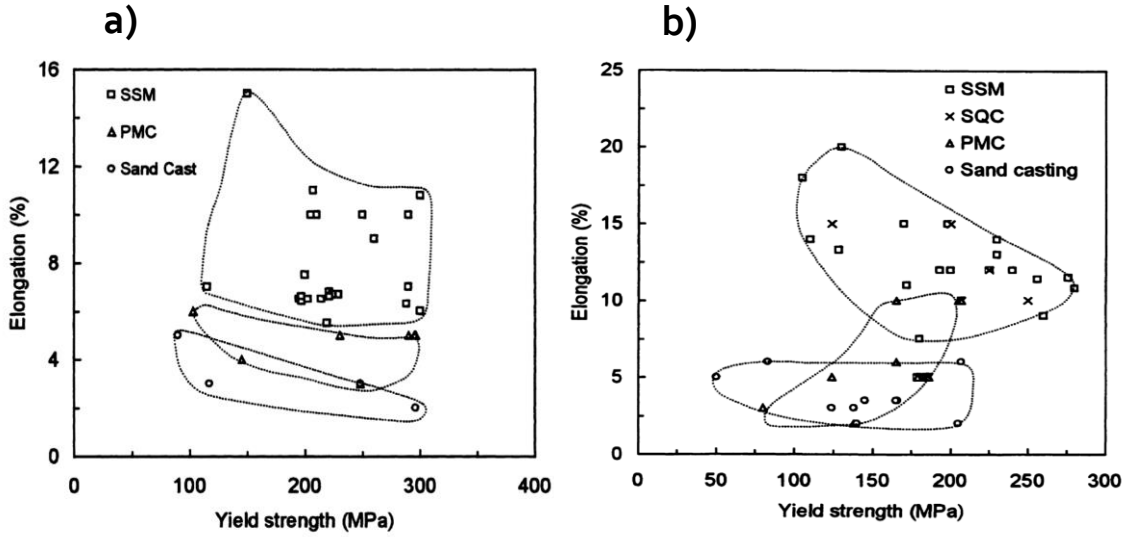

Figure 3.17 Some measurements of elongation of a) A356 alloy and b) A357 alloy plotted vs yield strength displaying an advantage of SSM processing (thixoforming) over traditional processing routes [42].

Figure 3.18 illustrates the fatigue strength behaviour of A356 alloy as thixocast in the T6 condition compared with others traditional casting processes[1]. This comparison proved that a substantial improvement of strength fatigue of thixocasting can be clearly observed compared with samples that are formed by other methods. This is observed due to the unique microstructure in the thixoformed parts[42]. Consequently, from the indicated results A356 and A357, aluminium alloys can be potentially employed in SSM processing, for instance, aircraft and automotive parts.

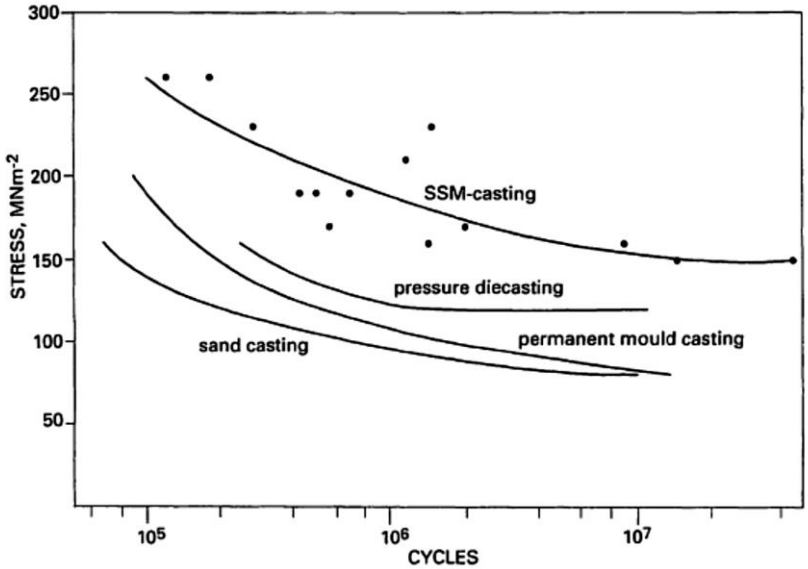

Figure 3.18 Fatigue measurements for SSM of A356 alloy (thixocasting) compared with other routes [1].

- **Magnesium Alloys**

Next to aluminum alloys the magnesium has been successfully tested to in semi-solid processing. Magnesium alloys have various benefits, which would include low density and high stiffness, strength and good conductivity. Due to the aforementioned benefits the demand for Magnesium alloys in the automobile industry and aircraft design has increasingly promoted, resulting in improved performance and fuel efficiency[210, 211]. The most common processing methods for magnesium alloys include casting, forging, extruding or rolling; however, when comparing parts processed using traditional methods (such as casting) with SSM processing, SSM primarily provides reduced defects and fine microstructure[212]. Thixomolding is a semi-solid manufacturing method to produce near-net shaped components in a single step, has attracted a lot of attention in recent years. This method, which is based on polymer injection moulding idea, is the most industrially advanced magnesium processing technique and was mainly developed for magnesium alloy (e.g. AZ91D, AM50A, and AM60B)[176, 213]. In addition to its potential efficiency and economy processing route, it tends to produce almost totally pore-free components and also magnesium alloy dose not react with the materials of the machine. Therefore, Thixomolding allows for the large scale production of a great number of components for applications primarily in the consumer electronics sector such as computers and mobile phones[193, 214]. Table 3.3 illustrates a comparison of tensile tests of some magnesium alloys processed via thixomolding and die cast. It can be seen that the measurements of thixomolded parts are higher especially in the ductility tests.

Table 3.3 Results from the tensile tests of magnesium alloys [36].

Material	Process	YS [Mpa]	UTS [MPa]	Elong. [%]
MgAl5Mn (AM50A)	Thixomolded	138.5	268.7	20.0
MgAl5Mn (AM50A)	Die Cast	112.1	232.2	13.0
MgAl6Mn (AM60B)	Thixomolded	147.5	278.2	18.8
MgAl6Mn (AM60B)	Die Cast	114.5	238.8	11.6

- **Steels**

Semi-solid metal processing is already employed in industry by researching low melting point alloys including aluminium and magnesium alloys, which are used for the majority of commercialised parts. Nevertheless, the application SSM processing for high melting point alloys such as steels was not used on a large scale. This is attributed to high processing temperature and narrow solidification range for low carbon steel[215]. Thixoforming of steels needs temperatures of around 1350-1450°C to process, while the temperature of aluminium thixoformed parts falls between 500 to 650°C. When compared to conventional processing technique of steel such as forging processes, SSM processing of steel has a number of potential advantages including low processing forces, complicated shapes achieved with a reduction in the number of forming steps and near net shape manufacturing[216, 217]. Other notable benefit include longer die life as a result of less thermal shock, better performance and weight saving of the parts with reduced porosity compared to traditional casting processes[218, 219]. Given these noteworthy benefits, increased emphasis is now being placed on the development of high-temperature semi-solid metal forming. The viability of thixoforming steels has already been demonstrated for a variety of steel grades, including carbon steel, high-speed steel, cold-working steel, and austenitic steels[36]. However, for selection an appropriate steel grades, it is important to note that final mechanical properties of the produced component is a key criteria for developing the steel grade. In general, it is acknowledged that steel alloys with a wider range of semisolid are most convenient for SSM process, such as steels X210CrW12, HS6-5-2, 100Cr6 and C38[216, 220]. Additional essential features are required while selecting a composition of steel alloys including small sensitivity to temperature and low solidus and liquidus temperatures [193]. The following Table 3.4 demonstrates the most important criteria and provide a general summary of the characteristic measurements identified for thixoforming of two types of steel grades [15].

Table 3.4 Summary of the most important aspects for the thixoforming of some steels grades [15].

Parameter	Abbreviation	Investigated range	
		HS6-5-3	100Cr6
Solidus Temperature	T_S	1219	1355
Liquidus Temperature	T_L	1401	1487
Interval for Thixocasting	T(10-25%)	18K (1269-1287°C)	28K (1391-1419°C)
Interval for Thixoforging	T(40-60%)	59K (1314-1373°C)	18K (1438-1456°C)
Entrapped liquid content	f_e	< 2 Vol.-%	10-15 Vol.-%
Average grain diameter	d	50-100 μm	300-400 μm
Shape factor	F	0.6-0.7	0.3-0.35

3.9 Advantages and Disadvantages of Semi-Solid Metal Processing

SSM processes have established as a unique casting process for applications requiring high mechanical properties, a complex geometry, or both. It is a cutting-edge technology that allows for the production of numerous parts for use in various applications, primarily the automotive and aerospace sectors. SSM processing , Similar to any other processes, has its own set of advantages and disadvantages. One of the most fundamental advantages is the non-turbulent die filling, which is caused by its highly and controllably smooth flow of SSM alloy during formation. In traditional die casting, the metal alloy is injected into the die in a turbulent manner, resulting in increased levels of porosity and poor quality of produced parts. In SSM process, however, a smooth flow behaviour of semi-solid slurries is introduced, with less level of shrinkage, gas entrapment, and porosity, leading to form components of high integrity associated with improved mechanical properties[221]. This means that SSM processed components formed with fine and uniform microstructures and this results in enhancement properties. Reduced shrinkage solidification, which may occur from the high faction solid and low heat content, allows the more complex and near-net shape to be made, subsequently eliminating unnecessary post-processing steps[169].

Another benefits of the SSM processing compared with conventional processes is that it reduced die degradation, the cost of which contributes significantly to total forming operation costs. In SSM processing, unlike conventional liquid metal casting processes, the metal alloy is processed in the solid-liquid region. Therefore SSM requires lower forming temperatures which reduce thermal cycling and wear on the die, extending die life[6]. The benefits of the SSM processing are outlined and highlighted in Table 3.5.

Table 3.5 illustrates some advantages of SSM processing [221].

Feature	Benefits
Lower temperature content	Faster part fabrication
	Reduced mould corrosion
	Forming a ferrous component
	High melting point material can be formed.
	Reactive materials can be formed
High solid fraction	Minimize shrinkage
	Minimize feeding required
	Decrease macro-segregation
	Fine particle structure
High and controlled viscosity	Reduce mould gas entrapment
	increased machinability
	Better surface finish
	Reduced oxidisation
Lower flow stress than solid metals	produced intricate components
	Reduced manufacturing costs
	increased production speed
Capability to integrate other materials	Able to combine with composites
Separation of liquids and solids	Purification

Despite the benefits mentioned above, SSM processing, like any process, has some limitations which may delay technological advancement of this process. One of the most well-known shortcoming of SSM processing is that the special equipment and highly skilled and trained operators required, which may be more expensive than those required

for traditional casting[6]. This could result in higher processing costs. Temperature is an extremely important factor in SSM processing which has a large influence on fraction solid and viscosity in the semi-solid state[42]. Slurries with a limited temperature range in the semisolid region necessitate precise temperature control.

Furthermore, despite the fact that the SSM process has been studied for four decades, process knowledge and experience must be continuously developed in order to facilitate the process applications for new products. Liquid segregation can be observed because of changes in the liquid and solid phase fractions, i.e. non-uniform heating, resulting in a part with a non-uniform composition[22]. Therefore, it is crucial to ensure uniform heating process throughout SSM processing. Other disadvantages include raw material costs can be high in comparison to casting, the number of material suppliers is limited, and finally controlling the ram speed during die filling is required as low ram speed may result in an incomplete die filling , whereas excessive speed contribute to turbulence flow and air-entrapment[169, 222, 223].

3.10 Applications of Semi-Solid Processes

Since the SSM processes were discovered, both academia and industry have become increasingly aware of their potential. It is now by far the most important process in terms of engineering application of all semi-solid process systems worldwide. At present, in terms of industrial applications, SSM process is a remarkably used method and has been widely employed by companies in a great variety of areas. This is attributed to the feasibility of SSM to introduce components with a complex design and exceptional mechanical performance at economic cost as comparing to traditional forming systems namely, casting and forging. There are many applications where the SSM process is an outstanding manufacturing method. It is competing with other methods of manufacturing for different sectors including military, aerospace, and, most particularly, automotive[42]. Automotive industry applications have gained the biggest benefits from SSM process because of the large number of components required by it. High-pressure and die casting processes are used widely for high-volume automotive parts. However, in the interest to avoid the potential issues associated with these processes such as porosity, gas entrapment shrinkage, etc., which limit the series of applications available. So the automotive industry adopted the SSM process as a viable alternative for producing high-integrity parts[224]. Moreover, automotive weight has recently increased as a result of supplementary equipment that satisfies different requirements such as electronic devices, high-class quality, and safety[225]. This raises concerns about fuel consumption and environment pollution problems. SSM techniques demonstrate weight reduction of automotive parts capable of meeting automative specifications at a cost-competitive with

other casting processes, allowing for more efficient material use as well as lower environmental implications[226].

The automotive components are made of materials ranging from magnesium to super-alloys, but aluminium alloys are one of the most well-known and widely utilised materials in automotive applications because of its potential efficiency and economy. Millions of automotive parts are produced every year that made from aluminum[6, 225]. Today SSM processing has established itself as a commercial technology for automotive industry applications to produce aluminum components techniques that can offer lightweight parts associated with higher ductility values and a better surface quality for a longer life cycle. For example, the part required a pressure tight, such as air conditioner compressor housing, master brake cylinders, fuel rails as well as other high strength parts like discs, wheels, engine mounts, steering systems, etc.[22, 23, 42]. Aluminium alloys such as Alloys A356 and A357 are ideal for the SSM processing[224, 227]. Figure 3.19 shows automotive parts that are produced by the SSM process such as engine suspension mounts, steering knuckle, and rear axle.

Figure 3.19 Demonstrate some automotive parts produced by SSM processing using MHD route [23].

The growth of SSM applications has been not only for automotive sectors but in other industries, such as consumer products, electronics, medical applications, etc. For magnesium alloys, SSM system is widely employed to produce thin-walled parts for an

electronic device, such as computers, mobiles, camera bodies, etc.[36]. In fact, broad industrial developments are going on to meet the expectations of the customers so that the advantages of SSM process are being utilised in more and more practical applications.

3.11 Research Overview and Hypothesis of LEMA

Over the previous years, additive manufacturing (AM) methods and their applications have been growing rapidly to create complex geometries with good mechanical properties. However, most of these technologies are focusing on non-metallic materials. Nevertheless, there is huge interest from several significant industries, such as aerospace, medical, and automotive, in metallic high function end-use parts. Some AM technologies are established for metallic applications for example, Laser sintering melting, electron beam melting and direct metal Laser Sintering. Yet, most of these methods require high power to melt deposit materials and consequently, great thermal gradients can be found resulting in undesired residual stresses. To tackle these drawbacks, supplementary fixtures and anchors are needed. This support means a lead to ineffective costing, extra time of post-processing and restrict the geometrical freedom of manufacturing design[228].

Further to these limitations, high manufacturing costs, low speed of material deposition and more power is consumed in these methods. Due to the previous shortcomings, extensive research should be carried out in order to improve metal additive manufacturing processes.

In this current experimental work, Layered Extrusion of engineering Metallic Alloys (LEMA) is proposed to produce a full density component. It is perceived by this idea that a semi-solid thixotropic metallic alloy is formed within the extrusion chamber to form a desired microstructure and then deposited on a target surface to generate a component. LEMA is recognized as an extrusion-based additive manufacturing technique for producing metal parts. The simplicity of the metal extrusion-based AM system offers some advantages including formed part with the low thermal history of stresses and low cost of processing. Additionally, as compared to SLM and EBM, the LEMA processes requires less energy because of the reduced temperatures and thus, minimising the potential of residual stresses[63, 229]. Additionally, the property of thixotropy in SSM alloy leads to controlled viscosity at a temperature lower than the point of melting enabling the deposition of the desired semi-solid material in a 3D fully dense product[40]. As a result, LEMA can leverage these advantages.

The main objective of this experiment is to develop a novel process of AM (LEMA) in order to make an extruded sample of metallic alloy with a suitable microstructure. This can be achieved by establishing the optimum extrusion parameters that include temperature,

deposition rates, shearing rate/force, and shearing time eventually identifying a sensible selection of alloys is a further aim of this work.

3.12 Research Gaps

The challenges and existing approaches for the AM of extrusion-based methods are discussed in detail in Chapter 2. The following are the knowledge gaps in the present literature:

- Over the previous years, additive manufacturing (AM) methods and their applications have been growing rapidly to create complex geometries with good mechanical properties. However, most of these technologies are focusing on polymer-based materials. This is likely due to the simplicity and the cost-efficient system concept associated with acquiring and operating the polymer AM method. Nevertheless, there is enormous interest from several significant industries, such as aerospace, medical, and automotive, in metallic high-function end-use parts. Some AM technologies are established for metallic applications, for example, Laser sintering melting, electron beam melting and direct metal Laser Sintering. Yet, most of these methods require high power to melt deposit materials, and consequently, great thermal gradients can be found resulting in undesired residual stresses. To tackle these drawbacks, supplementary fixtures and anchors are needed. This support means a lead to ineffective costing, extra time of post-processing, and restrict the geometrical freedom of manufacturing design[228]. Therefore, there is a critical need to expand the metal extrusion approaches and their applications to enable them an industrially suitable AM system. Layered Extrusion of engineering Metallic Alloys (LEMA) is proposed to fill this data gap. LEMA is extrusion-based AM with semi-molten alloy to deposit and form components. The simplicity of the LEMA system offers some advantages including the formed part with the low thermal history of stresses and low cost of processing[40, 56-59]. Additionally, as compared to SLM and EBM, the LEMA processes require less energy because of the reduced temperatures and thus, minimizing the potential of residual stresses. Hence, there is a need for a process that could manufacture high melting point metals at relatively lower temperatures, giving less residual stresses, with controllability of microstructure, little or no need of post processing and is economical
- Since this approach is extrusion-based AM method, a search of the literature revealed some studies, which based on the extrusion of metal/polymer filaments, have been made to print form 3D objects. They aim to improve the properties of the materials of the printed part including electrical and thermal conductivity,

however, it is argued that earlier research suffers from certain flaws including a limited range of filament materials that can be processed. Also, practical challenges that frequently arise from the use of a wire-based technology for example filament blocking and buckling. Furthermore, the fabricated parts required post-processing such as de-binding and sintering to remove the polymer binder and then attain dense metal components. This is not necessary when using the metallic alloy methodology described in this work. In this respect, this study specifically entails developing a polymer-free extrusion-based AM technique. So it can eliminate the above limitation of using metal/ polymer filament.

- To address the aforementioned effect caused by the employed composite filaments, it is becoming more important to develop an extrusion-based system that can build pure metallic parts. Therefore, some academics have proposed AM system based on extrusion of a feedstock made of low-melting-point metals below 220 °C to form 3D patterns. Despite the potential application that could benefit from a low-temperature alloy including electronic joining, fixtures, and electronic circuitry. However, the primary constraint here is that this method is only applicable to the low melting alloy and this limits the wider manufacturing application of metal extrusion with higher melting point alloys. Hence, research advancements are needed to accelerate the development of metal extrusion-based AM to deal with higher melting alloy to build high strength metallic components. Here we exhibit a method through which we were able to print structures of melting point alloy above 300°C. This has the potential to open up the door for new industrial applications such as those for the aerospace and automotive domains.
- Very few innovative investigations have employed semisolid metallic materials as feedstock in extrusion-based AM systems. That involves printing objects where the metal alloy in a semi-solid state with controlled liquid/solid phase ratios. The property of thixotropy in SSM alloy leads to controlled viscosity at a temperature lower than the point of melting enabling the deposition of the desired semi-solid material in a 3D fully dense product[40]. The capability to extrude and deposit the metallic material in the form of semi-solid slurry holds the potential to be a promising solution to many of the above-mentioned barriers. Although this approach is interesting, so far, very little attention has been paid to exploit higher melting temperature alloys as feedstock. Also, it was noted that a lack of fundamental understanding in some aspects, including interlayer bonding between the two layers and mechanical properties of the printed part, that still need to be fully investigated. Plus, demonstrating and extruding semi-solid alloy

with melting temperature exceeds 220°C, this approach will conduct a wider investigation to cover feedstock preparation, semi-solid extrusion parameters and printed structure examination.

4 RESEARCH METHODOLOGY

4.1 Approach /Method

The present study is intended to investigate and address the limitations discussed in the literature. In order to tackle the shortcomings in previous research, further and more extensive research should be carried out to develop a simple and low-cost metal extrusion-based AM system. It has already been discussed that the thixotropic property of the material alloy within the semi-solid processing enables the process to be controlled and hence improve the final product without having to reach the full melting point of the alloy. Also, given the multiple benefits of extrusion-based AM systems in general, and the promising capabilities of this method in particular (in terms of being suited for some metallic materials), it becomes a crucial technique and a cost-effective solution compared to conventional SLM/EBM processing[62, 120, 127, 230, 231].

The utilisation of thixotropic slurries successfully during the extrusion process allows the material deposition to be regulated, which is similar to what happens within the SSM processing. Therefore, the development of technology by using semi-solid metal (SSM) processing in conjunction with extrusion-based AM methods could address many of the challenges, improve the production process[37] and result in a more efficient, economical, and widely accessible metallic extrusion-based AM method. This combination is expected to play a significant role in future applications of metal AM technology.

During several years of investigation, two configuration designs were developed, called Phase I and Phase II. In the initial phase of the study, designated as Phase I, initial experiments were conducted to develop a semi-solid thixotropic metallic alloy within the extrusion chamber of the LEMA system to form the desired microstructure and then deposited on a target surface to generate a 3D component. These experiments involved testing various parameters such as temperature, shear rate, and time to understand their effects on the rheological behaviour of the material. A methodological study was then conducted where experiments in Phase I were repeated multiple times to ensure reliability and accuracy of the results. Average values were calculated from these repeated experiments to provide representative data. The experiments were designed to test the process and to identify any inconsistencies or variations.

During these experiments, it became evident that maintaining steady-state rheological behaviour of semi-solid slurries within the extrusion chamber was challenging and required precise process conditions, including temperature control

and desired shear rate and time. Additionally, there were limitations in achieving consistent deposition of the semi-solid alloy onto the target surface due to variations in the rheological behaviour of the material. While these challenges were not insurmountable, they significantly hindered the reliability and reproducibility of the results

To address these challenges, a redesign of the current system was necessary to eliminate many of these limitations. One such solution was controlling a metallic feedstock with a piston instead of a stirring mechanism, utilizing displacement control. Hence, in phase II, pre-treated feedstock with a suitable microstructure was reheated into a semi-solid state before being additively manufactured via AM metallic extrusion. This methodological approach allowed for more precise control over the rheological behaviour of the semi-solid slurries, thereby enhancing the consistency and quality of the final product. The details of both Phase I and Phase II approaches, along with the experimental procedures and results, will be discussed in the following sections.

4.1.1 Screw extrusion-based AM approach

A solution to the knowledge gaps listed in the existing literature would be to establish an utterly new AM extrusion system that can transform non-thixotropic material into thixotropic feedstock before controlled deposition. Therefore, a metal AM single screw extrusion-based method, as normally used in the FDM of thermoplastic, for in-situ creation of semi-solid thixotropic was developed to generate 3D patterns. An illustration of the proposed LEMA system can be seen in Figure 4.1. It shows the principle of a screw extruder AM machine, which was manufactured in-house specifically for metal AM processes. The system is filled with a non-thixotropic metallic alloy, which is then heated via conduction heating to a semi-solid state and followed by a shearing operation through a single screw. This creates a semi-solid slurry comprising of a mixture of spheroidal particles suspended in a liquid matrix duplicating a thixotropic structure.

The liquid mixture will serve as a carrier for the un-melted spheroidal solid particles during the deposition. The ultimate viscosity of the liquid matrix will be influenced by the proper selection and optimisation of liquid/solid fraction percentage. If the liquid fraction is too low, the slurries will remain rigid and will not flow, leading to nozzle obstructions; if the liquid fraction is too high, the material will extrude at an unmanageable rate. Additionally, because of deposit sagging, the deposited material may lose its geometric integrity. Hence, the optimum liquid fraction and shearing conditions provide a controllable feedstock viscosity[17] without needing to reach the material's full melting temperature,

permitting successful extrusion of the semi-solid alloy and layered deposition of metallic structures onto an electronic 3-axis platform.

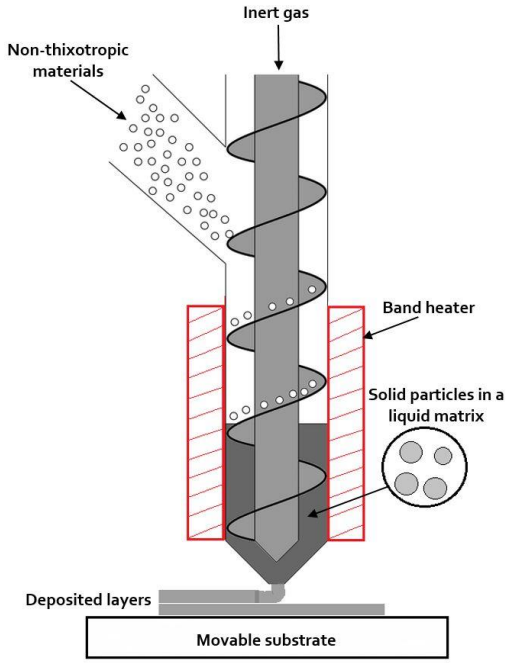

Figure 4.1 Depiction of the screw extrusion-based 3D printing principles.

4.1.2 Ram extrusion-based AM approach

Another alternative method that was suggested in this work to overcome the constraints and challenges in the literature is to use pre-treated materials with thixotropic properties to be printed and formed into 3D shapes. The diagram presented in Figure 4.2 depicts the main process methodologies used in this approach. As can be seen, the procedure involves two main stages. The initial stage of the Ram extrusion -based AM approach is the process of creating a feedstock having thixotropic features. Feedstock materials are associated with thixotropic properties facilitating the effective deposition of semi-solid slurries and the production of three-dimensional objects. At first, the machined ingot will be subjected to a cold extrusion using a hydraulic press to reduce the ingot diameter and produce oriented structures that are aligned with the direction of extrusion. Subsequently, it is heat-treated meaning that the deformed material is partially re-melted and then quickly immersed in cold water in order to offer feedstock with a globular morphology. The second stage of the approach is that, the thixotropic billet is inserted into a custom LEMA rig and held at specific temperatures before semi-solid extrusion using a hydraulic press onto an x/y/z gantry system.

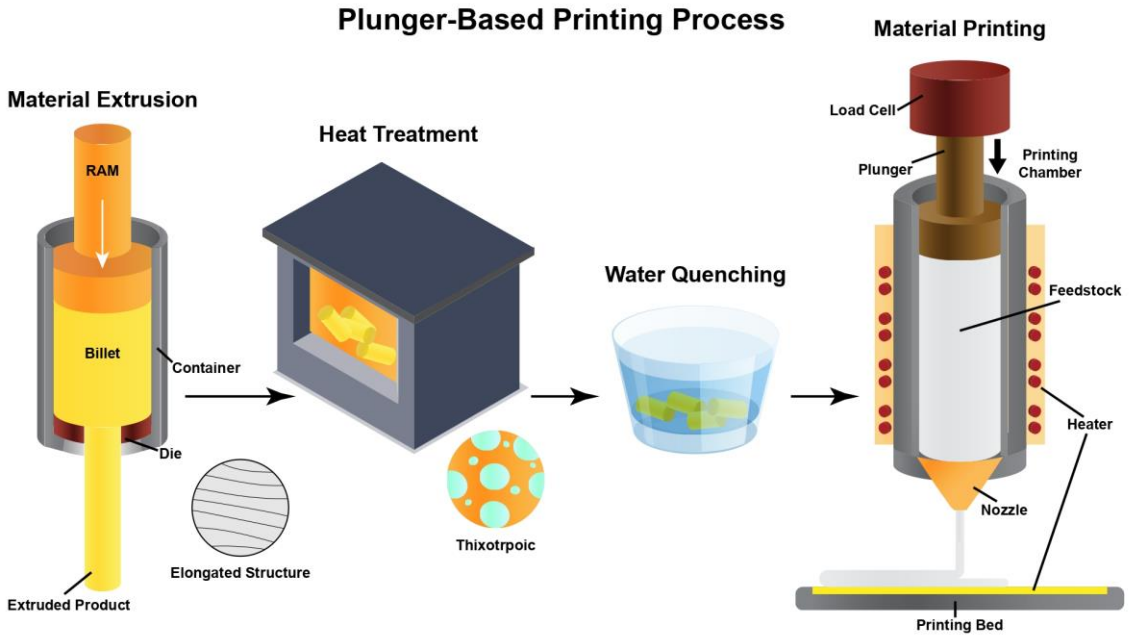

Figure 4.2 Flowchart illustrating the ram extrusion-based methodology.

4.2 Research Equipment

The research equipment utilized in this study plays a crucial role in conducting the research. Instruments such as optical microscopes, scanning electron microscopes (SEM) with Energy Dispersive X-ray Spectroscopy (EDS), a tube furnace, Differential Scanning Calorimetry (DSC), and a hydraulic press machine are essential for understanding material properties, conducting experiments, and developing novel manufacturing processes. In this section, the key equipment and their roles in the investigation and development of novel materials and manufacturing processes will be outlined.

4.2.1 Optical microscope

The majority of examined materials are invisible to the naked eye, hence the optical microscope having a significant role in sample analysis. The optical microscope, often known as a light microscope, is a system for closely investigating a small item to produce enlarged representations by means of a lens magnified with visible light. In this study, the optical pictures were acquired with the help of a Nikon Eclipse LV150 optical microscope, as illustrated in Figure 4.3. The microscope is made up of a number of components including an illuminator, eyepiece, lamphouse, objective lenses, movable stage controlled by a software programme and a built-in digital camera. This hardware/software combination of the optical microscope enables the use of capabilities such as autofocus function, high magnification, and high-volume analysis so that the sample microstructure can be inspected in more detail.

Figure 4.3 Optical microscope Nikon ECLIPSE LV150

4.2.2 Scanning electron microscope (SEM) and Energy Dispersive X-Ray Spectroscopy (EDS)

Scanning electron microscopy (SEM) is the most commonly used tool in material analysis, developed exclusively to observe surface morphology, topology and chemical composition of prepared samples. This uses a focused electron beam over the sample surface for producing magnified images[232]. As shown in Figure 4.4(a), the principles of operation begin with the electron gun, which emits a stream of electrons that are accelerated towards an anode by a voltage difference. The electron beam travels in a vertical track through the vacuum-sealed microscope. The beams are then focused onto the specimen surface by a set of electromagnetic lenses to form an electron probe. The probe then scans the surface of the specimen using scanning coils, allowing data about a specific area to be gathered[233]. As a result of the specimen–electron interaction, different types of signals are produced including secondary electrons (SE), backscattered electrons (BSE), and characteristic X-rays[44], which are then collected by detectors and converted into images that are presented on a PC.

Secondary and backscattered electrons can both be used to examine sample microstructures. SEs are formed on the surface of the specimen as a result of inelastic collisions of the beam electrons with the sample. Secondary electrons are extremely useful for revealing the surface topography of a sample[234]. Unlike SEs, BESs come from a wide area in the interaction volume, and they are caused by elastic collisions between the electron beam and the specimen. In addition to providing valuable information on crystallography and topography of the sample, BSEs images can be used to distinguish between different phases in sample microstructure, allowing more information to be gathered about the elemental composition of the sample[235]. Another vital radiation emitted when the electron beam interacts with the specimen is the characteristic X-ray,

which is known as Energy Dispersive X-ray Spectroscopy (EDS or EDX). These characteristic X-rays carry useful information about both qualitative and quantitative analysis, allowing users to determine the elemental composition of a desired point/area on the investigated specimen (qualitative analysis)[236, 237]. Plus, it can be used to estimate the percentage concentration of each element present within the specimen (quantitative analysis). Figure 4.4 (b) illustrates the interaction volume and the detection regions of the various signals generated.

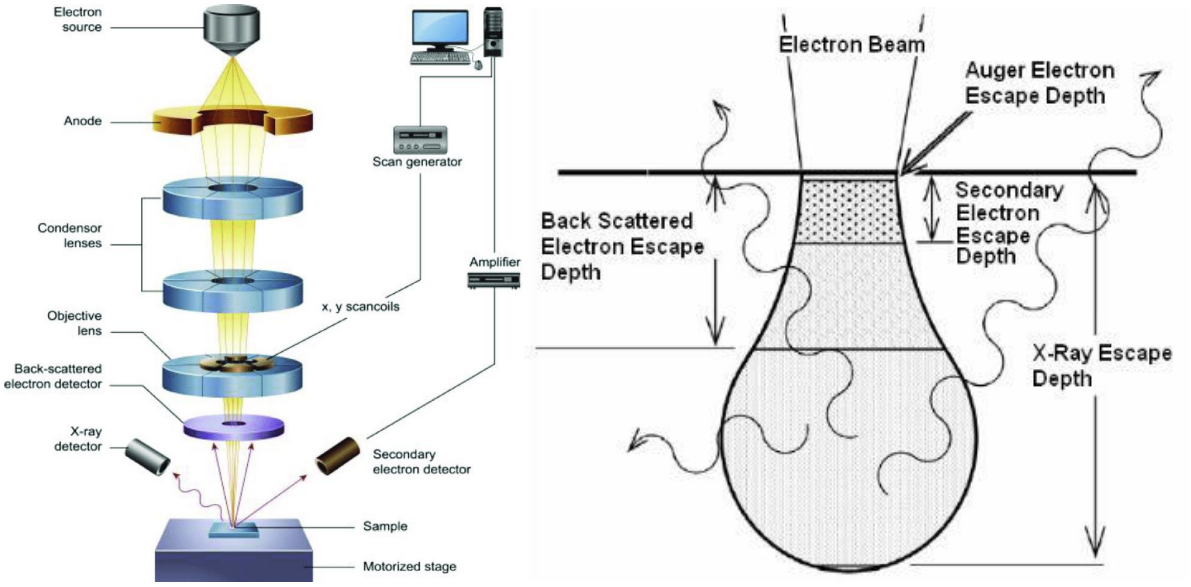

Figure 4.4 a)show SEM schematic diagram displaying the main components [13] and b) the effects of electron-beam interaction with a sample [44].

4.2.3 Tube Furnace

To carry out the RAP thermomechanical process, the required heat treatments were accomplished using an electric tube furnace (model STF 16/180 ,Carbolite Gero, UK) equipped with a temperature controller, as shown in Figure 4.5. The electric furnace is supplied with a recrystallised alumina work tube fitted with radiation shields in both ends of the tube to prevent heat loss and enhance temperature uniformity. This furnace comes with end seals manufactured from stainless steel with gas inlets to be secured to the end of the work tube to keep a modified atmosphere contained. The tube furnace is configured with a CC-T1 touchscreen temperature controller and equipped with a PID system to regulate the heating power and optimise the temperature within the work tube. Further, the furnace is capable of attaining temperatures of up to 1600°C, having silicon carbide heating elements in order to offer outstanding radial and linear chamber consistency.

Figure 4.5 Tubular heat resistant furnace

4.2.4 Differential Scanning Calorimetry (DSC)

In the science of the engineering, thermal analysis is a tool applied to describe the physical characteristic of the materials as a function of temperature over time when heating or cooling the sample under regulated conditions[238]. Thermal analysis is a useful and vital characterisation means, since it is capable of evaluating a wide variety of substances' properties, including: reaction enthalpies, heat capacity and energy phase transition[239]. Information about thermal behaviour profiles during extrusion and deposition of semi-solid materials is essential for controlling the processing parameters. The selection of processing temperature in the semi-solid range temperature is considerably influenced by the knowledge of fraction-liquid-temperature relations provided by the thermal profiles. There are a number of thermal analysis approaches that are widely used – chief among them being Differential Scanning Calorimetry (DSC).

DSC is the most commonly used tool in academia and industry for thermal analysis because of its simplicity and the high value of its analytical performance[240]. DSC has proved to be a very effective thermo-analytical tool for acquiring different characteristic temperatures, the fusion heat of each phase, the melting latent heat and the crystallization and melting temperature of the materials[241]. Moreover, it is possible to calculate the specific heats of the phase transitions as well as measure the estimated concentration of the phases. There are usually two substance locations for the DSC, one for the exanimated substance and the other for a reference substance. Both the sample and reference are cooled uniformly and kept at nearly the same temperature throughout the experiment. During the test, the DSC apparatus attempts to evaluate the temperature

differences in heat flow rate between the substance and reference material. Accordingly, the variations in the amount of heat flow for both materials are recorded as a function of temperature [242]. DSC can record results quickly over wide temperature ranges, and this technique also enables the testing of very small specimens. In this study, the apparatus used to perform the thermal analysis of metal alloys in order to evaluate the solidus and liquidus temperatures, the liquid fraction volume, and determine the optimum working temperature window, was the Perkin Elmer DSC instrument equipped with Pyris software (see Figure 4.6). The thermal profile information was also employed to estimate the liquid fraction for feedstocks preparation during isothermal heat treatment processes.

Figure 4.6 Perkin Elmer Pyris 1 DSC Differential Scanning Calorimetry.

4.2.5 Hydraulic Press Machine

A Schenck servo-hydraulic test machine was used to prepare SSM feedstocks for use in a metal extrusion-based AM system (see Figure 4.7). The machine applied a hydraulic system to convey force in order to insert the machined billet into the die. The hydraulic press was built in such a way that the force was applied in a vertical axis from top to bottom. This machine is equipped with a hydraulically regulated piston with a maximum load capacity of 250 KN and maximum stroke of 250 mm at a maximum velocity of 1000 mm/s. The operation of the machine press is controlled by a Moog™ Portable Test Controller integrated with a software system to monitor the test and collect data for subsequent data analysis, which is attached next to the machine area. The Portable Test Controller unit has an LCD front panel that can handle up to four digital servo control channels. A VGA display is also linked to the portable test controller to allow the operator

to view the data on a larger screen. This machine is capable of running tensile, compressive tests; static or cyclic modes are also available. The machine also has two emergencies stop buttons to ensure operator safety.

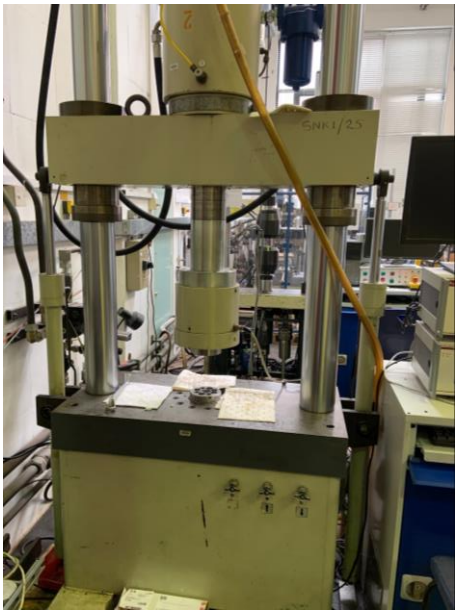

Figure 4.7 Hydraulic machine

4.3 Phase I: Screw Extrusion-Based Process

4.3.1 Introduction

When compared to laser or electron beam sources, extrusion-based additive manufacturing typically comprises cost-effective hardware with low-power energy sources[62, 229]. On the other hand, semi-solid metal (SSM) manufacturing is a near-net shape that enables the creation of a metal stream with controllable rheology in low processing temperatures typically between liquid and solid processing. This offers several advantages including free-porosity parts with less shrinkage and a controlled microstructure that allow for better mechanical properties. The development of a hybrid semi-solid forming and AM metal-based technology that use a semi-solid alloy as an input in AM technique would enable considerable cost and production-time savings and achieve an efficient, affordable and widely accessible metallic AM process[14, 40, 57].

The primary goal of this study is to investigate a novel manufacturing system capable of thixotropic processing and the 3D printing of metal alloys in a variety of devices and products. Hence, in phase I, a metal AM extrusion-based method for the in-situ creation of semi-solid thixotropic was developed – where the raw materials are heated and stirred within the extrusion chamber to prepare the semi-solid slurry, followed by the extrusion and layered deposition of metallic structures. The following part of this chapter moves on

to describe in greater detail the rig design of phase I, and the associated experimental procedure.

4.3.2 Experimental setup and methodology

In order to achieve the main objective of this work, an extrusion system (LEMA) is employed, which is shown in Figure 4.8 , to stir and deposit the semi-solid materials through the barrel and nozzle using a single screw and a heating source. A screw extruder, which is driven by a motor, was positioned at the centre point of the nozzle to induce shear forces in the semi-solid alloy through rotation. A movable platform, which is controlled by G-code, is placed under the extrusion barrel for printing. The whole arrangement is located inside an insulation chamber. The fundamental working principle of this system is that the raw materials are fed manually from the top hole of the extruder. The chamber is vacuumed to lower the oxygen content and then the Argon gas is flushed through the system to reduce the possibility of oxidation. The materials are then heated inside the barrel to around the melting point. Subsequently, the molten alloy is cooled to the appropriate temperature as it is stirred by a single screw before being deposited onto a movable platform to make the first layer of the object.

The mechanism of mixing involves the application of mechanical agitation to the molten metal within the extrusion chamber. This stirring action is achieved by the rotation of a single screw, which is positioned inside the barrel of the extrusion system. As the screw turns, it generates shear forces within the molten metal, breaking up any agglomerates and distributing the particles uniformly throughout the melt. This promotes the formation of fine, globular grains, which are desirable for semi-solid processing.

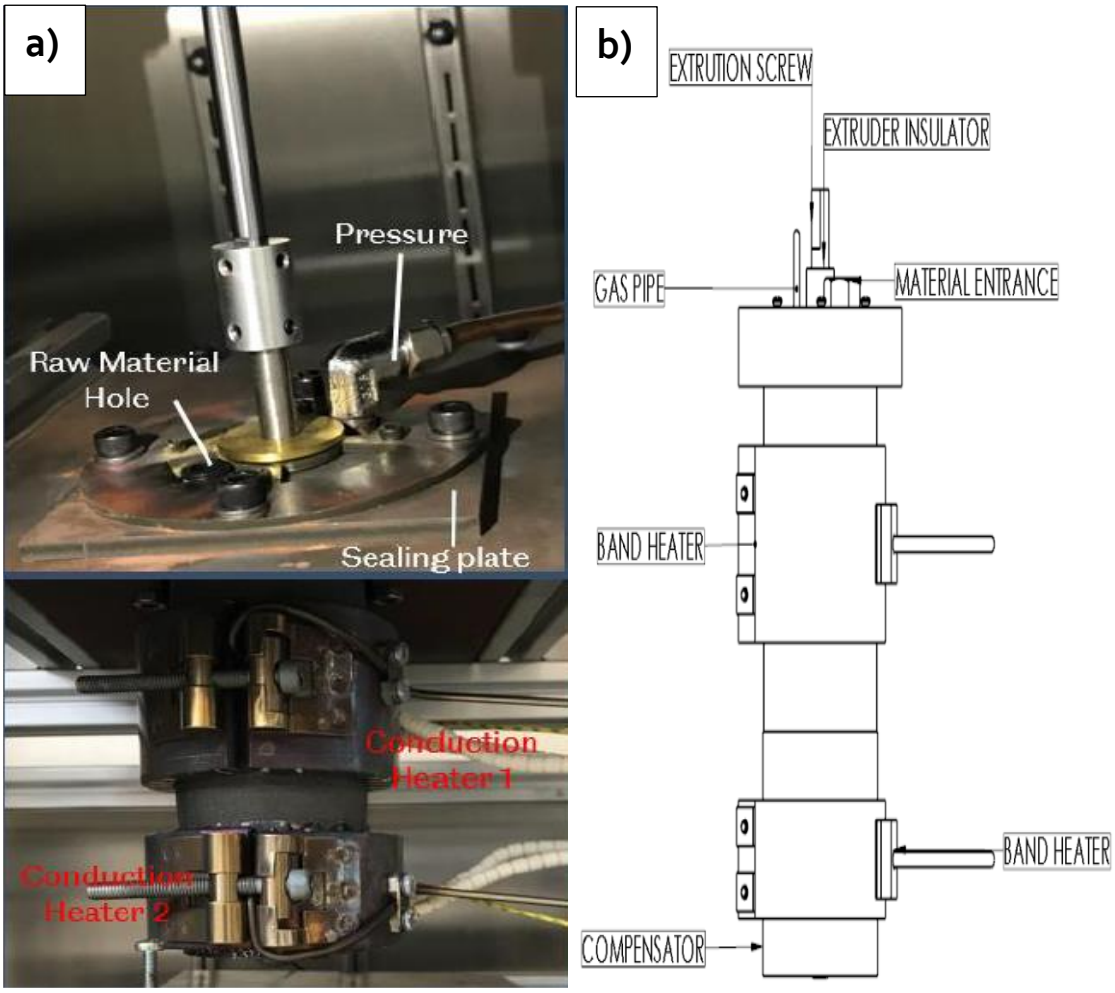

Figure 4.8 Overview of LEMA process a) actual process and b) schematic image

4.3.2.1 Experimental apparatus

- **Extruder barrel and screw**

As shown in Figure 4.9, a single screw is used to evaluate the feasibility of the LEMA system. Due to the high temperatures involved during the process, both the extruder barrel and screw were made from Ti6Al4V. To ease cleaning, the extruder chamber was made as two separated pieces as shown in Figure 4.10. In order to obtain higher shear rates and easy material deposition, the channel depth of the extrusion screw is designed to be greater than the channel depth at the screw tip, and the end tip of the screw is designed to mate with the extruder nozzle to ensure that the metallic alloy is prevented from coming out through the nozzle until is properly mixed.

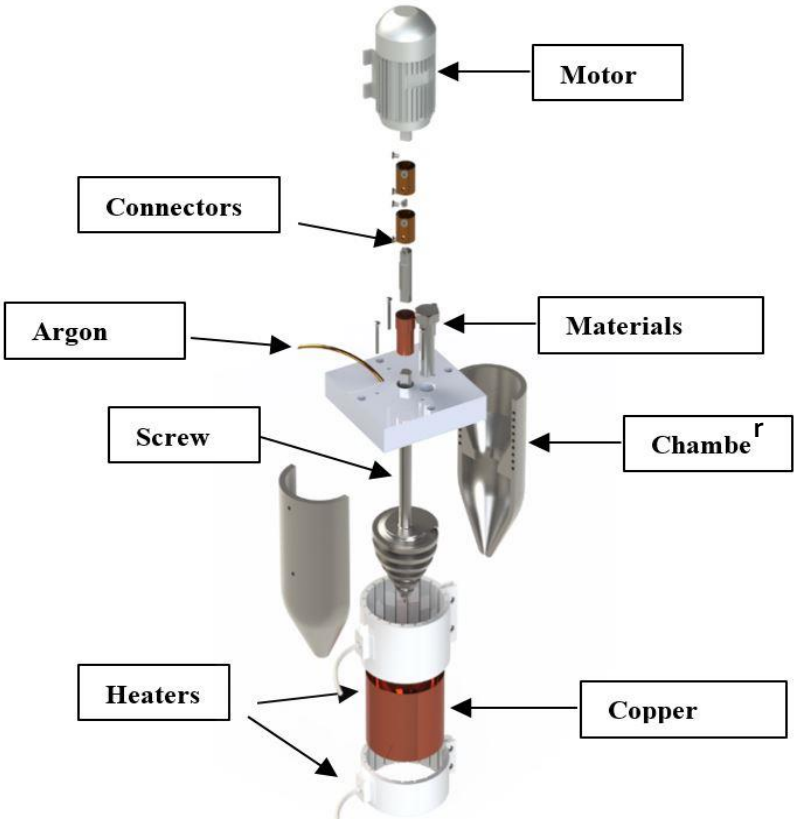

Figure 4.9 Exploded view of LEMA components

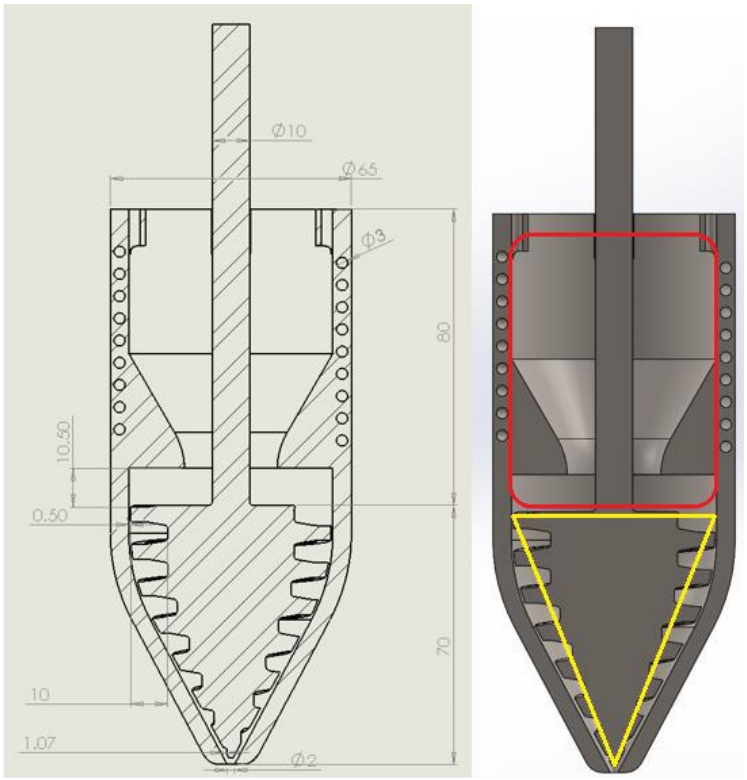

Figure 4.10 Illustration of a cross-section of a single screw in the LEMA Process

- **Heating Source, temperature control system and extruder motor**

For heating sources and better temperature control, two ceramic band heaters with wound inner resistance coils evenly threaded through insulated ceramics are used, as demonstrated in Figure 4.11. This type of ceramic band heater provides a better heating method leading to the perfect heat transmission of radiation, conduction, and convection so that the material can be melted and controlled efficiently.

.

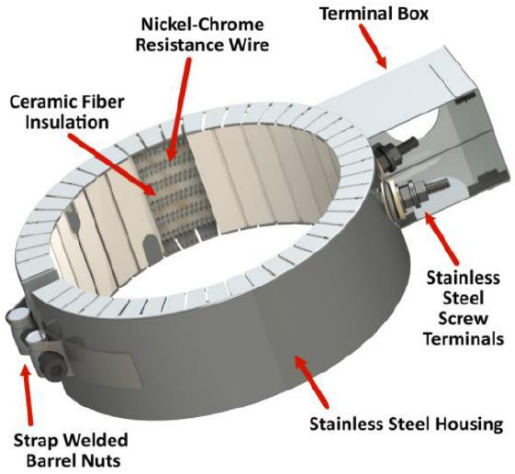

Figure 4.11 Ceramic band heater [3].

To control the heating and melting process, two thermocouples are used – one connected to the ceramic band heaters, and one attached to the extruder body. The signals from these thermocouples provide the target temperature in the semi-solid state with a precision range of 0.3°C. When this temperature is reached, the preferred condition of the alloy in the state between solid and liquid can be fulfilled. There are two supplementary thermocouples provided to ensure an adequate temperature, within a specified range, is achieved. One is placed in the middle of the extruder surface and the other one is positioned close to the nozzle tip using jubilee clips. Even though these thermocouples will not give exact temperature readings of the SSM itself, they help to provide additional evidence of the potential SSM temperature. The screw is driven by a large Nema23 motor with a holding torque of 1000mNm and 10mNm of turning torque to provide the shear rate to the semi-solid alloy. The motor is mounted on the top of the frame so that it cannot be moved. All elements, heaters, motor speed, feed rate and the printing bed are operated by means of a G-code. The whole control system of LEAM is based on Marlin firmware using Arduino software.

- **Movable Platform**

The typical manageable substrate transfers through three-dimensional Cartesian coordinates on the X, Y, and Z axes. That means the extruder can deposit materials in any position within the bed platform. In the current project, in order to deposit the semi-solid alloys, a movable platform is designed, as shown in Figure 4.12. The substrate can be moved in three different axes, x-y-z, and is controlled using Marlin firmware. This extrusion system involves the usage of seven stepper drives: four Nema23 stepper drives to control the Z-axis, two Nema17 stepper motors with a holding torque of 520mNm and a turning torque of 37Nm, and one to control the X Y-axis.

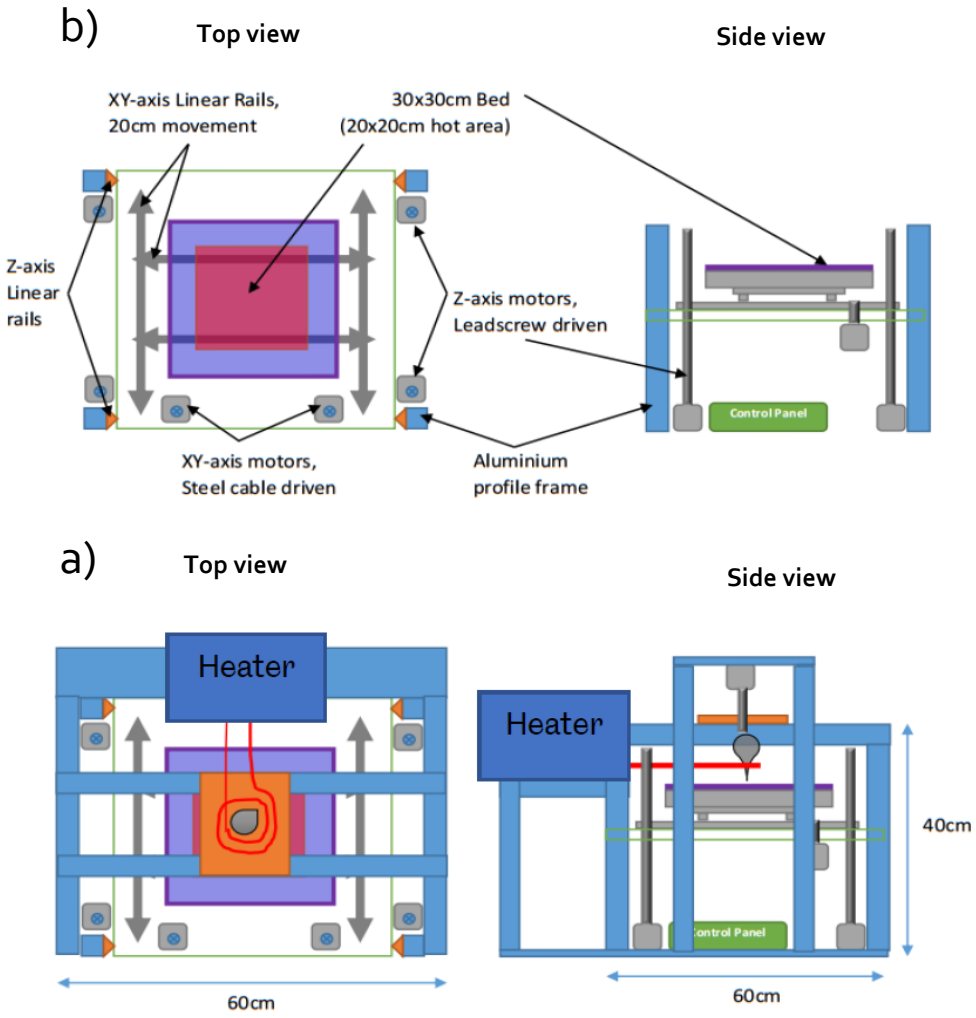

Figure 4.12 Schematic diagram of a) LEAM frame and b) movable platform in X, Y and Z direction.

- **Insulation chamber**

As shown in Figure 4.13, the extruder holder is fixed to the frame (made from aluminium strut profiles) and mounted on a four-column base. All parts of the screw extrusion arrangement are located in the insulation chamber which is used to protect the deposition mechanism from oxidation. The chamber is connected to a vacuum pump that enables the removal of as much air as possible from the enclosed area. The pump cannot produce an area that is 100% devoid of air, therefore, an inert neutral gas is provided by inflowing the argon, which is measured by a gas sensor, into the chamber. The inert atmosphere enclosure will reduce the oxygen concentration within the apparatus, thereby reducing any oxidation effects.

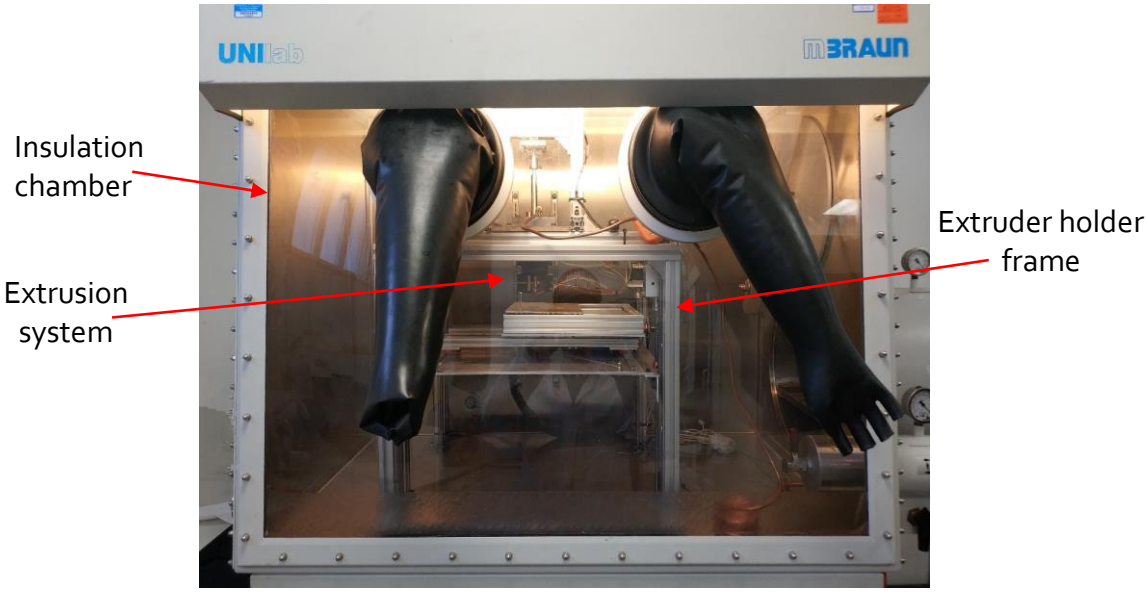

Figure 4.13 Aluminium frame for housing metal print head.

4.3.2.2 Materials selection

The requirements for an alloy suitable for the LEMA process experiments were determined using the essential criteria for alloy designing in Section 3.7. Parameters of alloy selection for SSM, such as the solidification range and the sensitivity of the solid fraction to temperature variations, are key factors that need to be considered in the alloy selection process. These parameters can be predicted from the solidification phase diagram of the alloy.

- Solidification Phase Diagram

Figure 4.14 shows a generic phase diagram of an alloy which typically includes details on microstructures, melting, cooling, and other properties. From this phase diagram the microstructure of dendritic and non-dendritic properties for a semi-solid alloy can clearly be seen. The area that is above the liquidus line T_L is a liquid phase, whereas the area under

the solidus line T_S indicates a solid phase. A combination of solid and liquid phases occurs between these two lines.

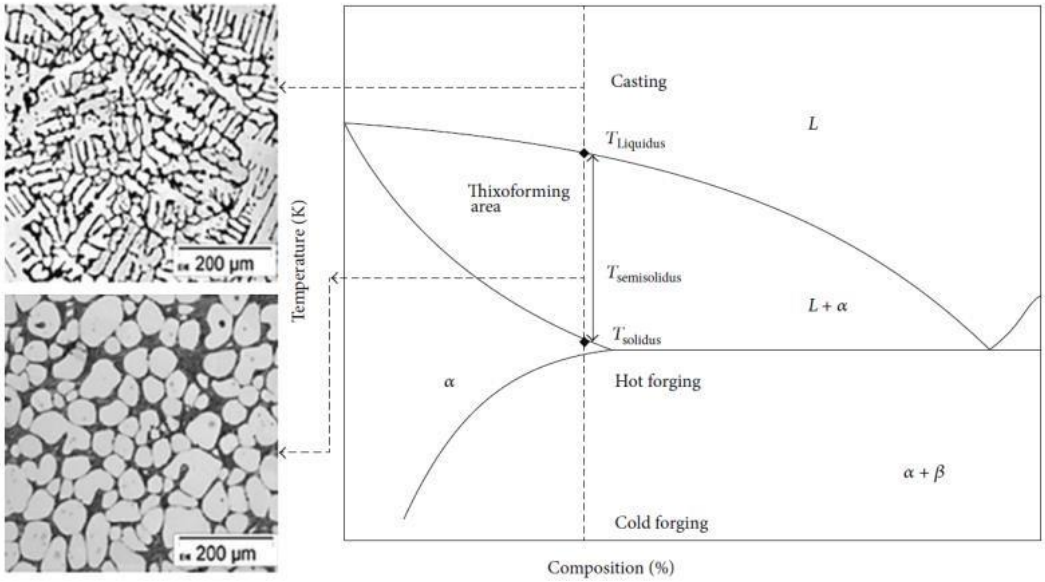

Figure 4.14 A generic phase diagram of a typical semi-solid alloy [34].

- Alloy Selection: Zinc-Tin Alloy

Based on the LEMA system capabilities, such as the achievable temperature and apparatus boundaries, zinc–tin alloy materials were chosen. In the current process, a composition of Zn-30 wt. %Sn was suggested due to its low-temperature melting point , which is more suited to the LEAM system as it offers a reasonable SSM solidification range.

- Phase Diagram Analysis

The phase diagram of the designated Zn-30wt.%Sn alloy was used to examine its solidification ranges, as illustrated in Figure 4.15. The liquidus line and solidus line of the composition Zn-30wt.%Sn are 360°C and 199°C, respectively, revealing that the temperature range of semi-solid alloys is around 161°C.

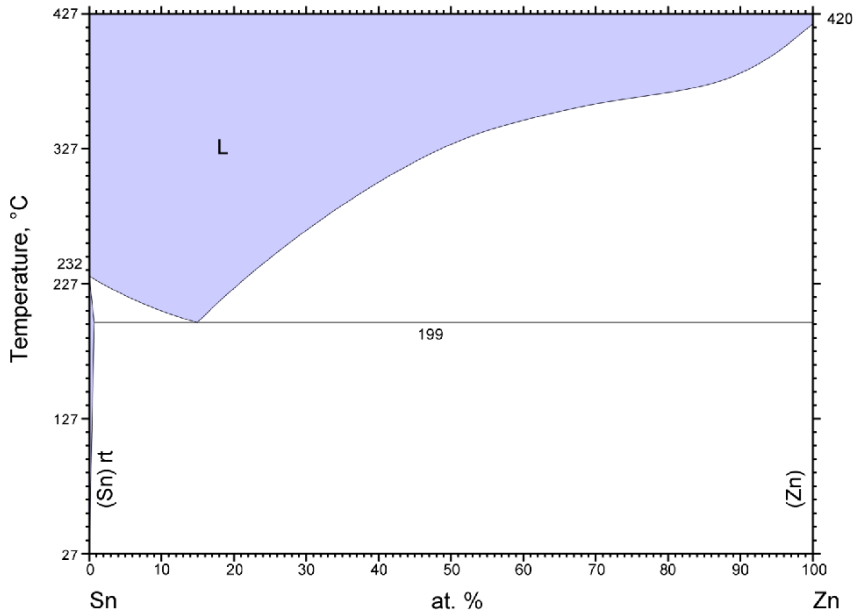

Figure 4.15 The phase diagram for Zn-Sn alloy [2]

- Liquid Fraction Analysis

The ideal liquid fraction of semi-solid alloys is generally between 0.4 to 0.6 as it forms and gives better properties of thixoforming [36]. An analysis using the lever rule was conducted to determine the liquid fraction of Zn-30wt.%Sn at 300°C. (See appendix 1 for Lever rule calculations)

4.3.2.3 Experimental Procedure

According to the above considerations, a composition alloy of Zn-30 wt.% Sn was chosen to examine the validation of the LEMA system. A total of 75g of raw materials were utilised – with 52.5 g being zinc and 22.5g being tin, and both materials were in a flake form.

- Preparation and Extrusion

Using the movable substrate, and by adjusting the 3-axis coordinators, the clearance gap between the end of the extrusion screw and substrate was fixed at 15 mm to allow adequate deposition of SSM alloys to be extruded. The composition of the alloys was added into the extrusion barrel from the top hole of the extruder and then sealed.

- Environmental Control

An advanced vacuum system was used, and Argon gas was flushed inside the insulation chamber via an intake valve fixed on a circular steel plate on the top of the extruder to allow for an inert environment. Accordingly, the oxygen amount, which was detected by an oxygen sensor, dropped to 18% approximately. Argon gas was used to avoid any

changes in chemical properties, such as oxidation of the printed part. The extrusion chamber was heated to above the melting point ≈ 420°C to achieve a molten alloy.

- Processing Parameters

Depending on the extruder wall thickness, it may require more time for heating to ensure that the composition of the alloys inside the chamber has attained the desired temperature of the liquid-solid matrix. It was proposed to allow 25 minutes of heating time before the materials were processed. The heating time was optimized based on in-process experimentation, with 25 minutes observed as sufficient to completely melt the alloy, ensuring consistent and uniform temperature. Therefore, Once the extruder was properly heated, the molten alloy was cooled to the desired and solid fraction (about 40%, indicated by temperature) while being continuously mechanically agitated by the screw extruder (anticlockwise) through a motor.

- Shearing and Deposition

The screw extruder was used to mix the metallic alloy and generate the desired semi-solid materials, i.e. until the dendrites were fragmented, sphere-shaped solid phase particles were created, and the preferred viscosity of the alloy was achieved. Throughout this process, a series of experiments were conducted, and the microstructure of the deposited materials was closely examined. This meticulous analysis allowed for the identification of the optimal shearing conditions required to attain the desired semi-solid alloy state. Once the semi-solid metal was obtained, pressurised argon was used once again to flush the material and allow the mixed material to be forced out through the orifice on the movable substrate while the screw rotated clockwise to the desired shear.

- Experiment Settings

The movable platform that can move in 3-directions was controlled by computer software. The speed of the substrate was set at 10 mm/s. The shearing rate was another important parameter that was to be studied – the suggested range of values to be tested were 50, 75, and 100 RPM. Regarding the shearing time, it was decided to apply a 7-minute initial shearing time. The 7-minute initial shearing time was chosen based on practical experience and preliminary experiments to ensure sufficient mixing of the alloy to achieve the desired semi-solid state without risking microstructure degradation. After completing the deposition, the temperature of the heaters was increased in conjunction with a flushing air to clean any materials left. Three experiments were performed and Table 4.1 shows a description of each experiment setting.

Table 4.1 Experiments conducted with Sn30-Zn70

Test No.	Materials Compositions	Proposed Extrusion Temperature (°C)	Shear rate (RPM)	Shear time
1	Zn-30 wt.% Sn	300	50	7 min.
2	Zn-30 wt.% Sn	300	75	7 min.
3	Zn-30 wt.% Sn	300	100	7 min.

- Microstructural Analysis

Deposited materials were optically microscopically examined to observe the microstructural characterisation as a function of processing parameters. To analyse the microstructure of the deposited alloys, one metallurgical sample was taken from each experimental condition. Metallurgical samples were taken from each experimental condition, sectioned from the middle to ensure representation of the centre using an IsoMet machine coupled with a cut-off wheel 10S20. For the mounting process, a Buehler SimpliMet 1000 machine was employed with a Bakelite resin where the temperature was set to 290 °C and a force of 290 bar was applied for 2 minutes followed by a cooling rate of 4 minutes. The mounting process is crucial as it provides a stable platform for consistent sample preparation, ensuring accurate and reproducible results during analysis

- Sample preparation

After the mounting step, a grinding process took place with an EcoMet 250 PRO grinder/polishing machine and with several grades of grinding papers. A 320, 400, 600 and 1000 grit-size silicon carbide papers were used for 1 minute at a grinding speed of 60 rpm and under a force of 30N. In the same machine, the polishing process was carried out where samples were polished using 3µm and 1µm diamond suspensions for 5 minutes at a polishing speed of 60 rpm and at a force of 30N. A chemical etching method was employed using a solution of 2ml of nitric acid and 98 ml of ethanol for 40 seconds to reveal the microstructure of the samples under the optical microscope. Prepared samples were usually washed with ethanol and air dried between the grinding, polishing and etching processes. Finally, for the optical evaluation of the microstructure, a Nikon microscope was used with the magnifications of 10x, 20x and 50x. Figure 4.16 displays the specimens after the sample preparations' processes.

Figure 4.16 Samples after polishing and grinding processes.

4.4 Phase II: Piston Extrusion-Based Process

4.4.1 Introduction

The key goal of this research is to develop a novel extrusion and deposition system that is capable of processing semi-solid thixotropic metal slurries. However, throughout the course of phase I, a number of design problems with the LEMA system and regions for development were perceived. These concerns were addressed during phase II by developing an extrusion and deposition machine that combine a universal testing machine (UTM) and a custom-made metal printing system. To effectively extrude and deposit thixotropic materials, it was suggested that the designed system comprises a piston mechanism as a driven system rather than a screw-extrusion-based system. This would mean that pre-conditioned thixotropic feedstock is used instead of in-situ thixotropic material generation within the barrel by a screw extruder which has several drawbacks, as described in the previous chapter. The generated thixotropic feedstock was then fed into the metal 3D printing machine to enable extrusion and deposition of metallic alloys in the semi-solid state. In the sections that follow, the experimental setup and procedure will be described in more detail.

4.4.2 Experimental setup and methodology of extrusion-based process

4.4.2.1 Materials selection and composition

In recent years, there has been a growing demand for manufacturing components using lightweight materials with acceptable mechanical properties. Zinc-based alloys have emerged as valuable options due to their superior characteristics and lower cost since their development. Some studies have considered zinc alloys as alternatives to pewter alloys in industrial applications due to their superior mechanical properties and cost-effectiveness[243] [244]. In various industrial applications, zinc-based alloys outperform traditional counterparts such as aluminium-casting alloys, copper-based alloys, bearing bronzes, and cast iron [245].

Zinc-based alloys offer numerous advantages, including cleanliness, low-temperature processing, reduced energy requirements, excellent castability, high mechanical strength, and enhanced bearing properties and wear resistance.[244, 246]. Among zinc-based alloys, the Zn-Sn alloy stands out as one of the best lead-free high-temperature solders, attracting significant attention from industries. Zn-Sn alloys possess unique properties such as high melting temperatures and the absence of intermetallic compounds (IMCs). In addition to their lower cost, they exhibit higher ductility and excellent electrical properties and oxidation resistance at elevated temperatures and in high-humidity environments[247-249]. Another important

feature of the Zn-Sn candidate is the relatively large solidification ranges of this alloy, which range from 150 to 175 K[250], making it suitable for semi-solid processing techniques. Lead-free, high-temperature solder research has received special industry interest and is considered necessary for a wide range of components and connections. These materials are increasingly being used in electronic apparatus for aerospace applications such as engine components and braking systems. Furthermore, the application of high temperature solder is growing within automotive, telecommunications, and energy-production applications[251].

The selection of the prospective candidate for semi-solid extrusion and deposition was guided by factors such as the temperature sensitivity of the liquid fraction df_L/dT within the targeted liquid fraction range, the solidification temperature range, and the temperature process window. The temperature sensitivity of liquid fraction (dfL/dT) is a critical parameter for semisolid processing in which represents how quickly the liquid fraction of the alloy changes with temperature. Therefore, this parameter is crucial for semi-solid AM methods because temperature fluctuations in the printing orifice can impact process stability. If an alloy has a high liquid-fraction sensitivity, it requires more rigorous temperature control for stable processing. Accordingly, ingot alloys with a non-eutectic chemical composition of Zn-40%Sn were chosen for this study, supplied by AIM Solder Limited, UK. Unlike eutectic alloys, non-eutectic alloys possess a solidification range of temperature, allowing them to remain semi-solid within a specific temperature range. In other words, at a particular temperature, the melted alloy starts to solidify and continues to solidify as the temperature decreases, until the final temperature is reached and the alloy is fully solidified. The alloys between the solidus and liquidus temperature ranges perform like paste, where the alloy is semi-solid. Furthermore, thermodynamic calculations conducted using Thermo-Calc software confirmed the suitability of the chosen compositions for semi-solid processing. (more details will be presented in the subsequent chapter). Another contributing factor for selecting these alloys was their melting-point temperature, which matched well with the specifications of the designed rig. Thus, the Zn-40Sn alloy was selected as the prospective candidate for semi-solid extrusion and deposition in this research, offering promising potential for advanced manufacturing applications.

4.4.2.2 As-received materials

The starting material was originally received as a triangular-ended ingot with approximate dimensions of 305mm (base length) *27mm (base width)*20mm (top width)* 20mm

(height). After that, two specimens were cut from the as-received ingot and machined into smaller pieces in order to conduct the microstructural investigation and examination processes using an optical microscope and electron scanning microscopy. It is necessary to analyse the microstructure of as-cast material in order to understand material behaviour before processing. This microstructure can be then used to compare to the microstructure formed after experimentation. The samples of the as-received material are shown in Figure 4.17.

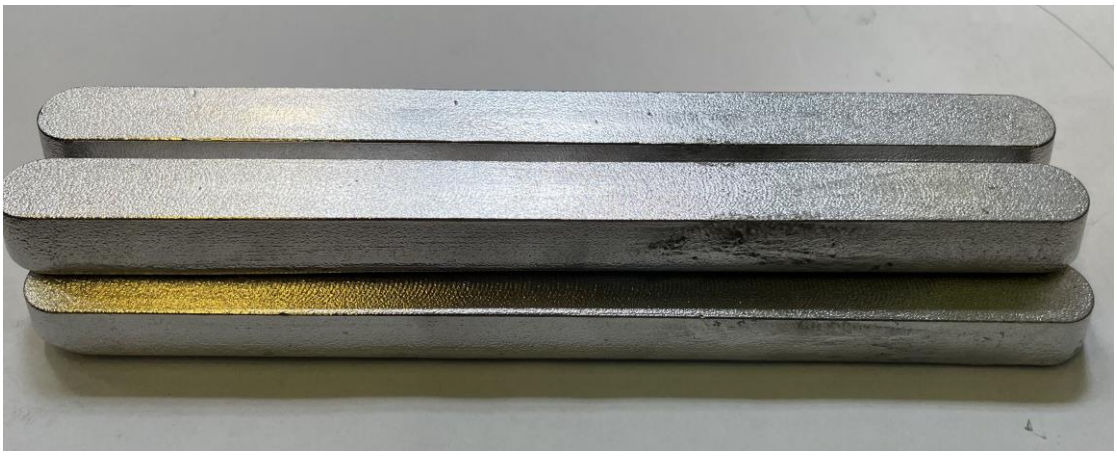

Figure 4.17 Shows the as received materials.

4.4.2.3 DSC analysis and liquid fraction

The metallic alloys being studied were as-cast 60% Zinc– 40% tin(cut from the centre of the ingot) with a weight of about 20 mg of material. The sample was contained within an alumina DSC crucible and placed into the heating chamber of the DSC. Another crucible, without a sample, was used as a reference material and sited into the DSC heating cell. Attention was paid when handling samples and the DSC crucible, so tongs were used for picking up objects in order to avoid sample contamination. Throughout the test, both samples were examined in a heat range from 30 to 400 °C and then cooled to 30° C at the same rate. The device was supplied by nitrogen gas with a flow rate of 100 ml/min in order to mitigate the impact of oxidisation of the specimen. In this trial, two consecutive cycles of DSC experiments were carried out at the same heating rate. It was stated [252] that the repeated cycle can be used to eliminate any thermal history that the materials may have gone through during manufacture. Between the steps of heating and cooling, a 10 min isothermal holding time was allowed in order to equilibrate the heating flow between the heating and cooling ramp. The following parameters have been used for the DSC. In the first ramp, the test temperature started at room temperature to 30 °C and was held at this temperature for 10 min. The sample was then heated at a rate of 10 °C per min to a

temperature of 400°C. After retaining the sample for 10 min at this temperature, the heating was reduced to 30 °C with cooling rate of 10 °C/min and again held for 10 min. In the second ramp, the temperature was elevated at the same rate again to a temperature of 400 °C. Figure 4.18 illustrates the temperature ramp profile used for the DSC test.

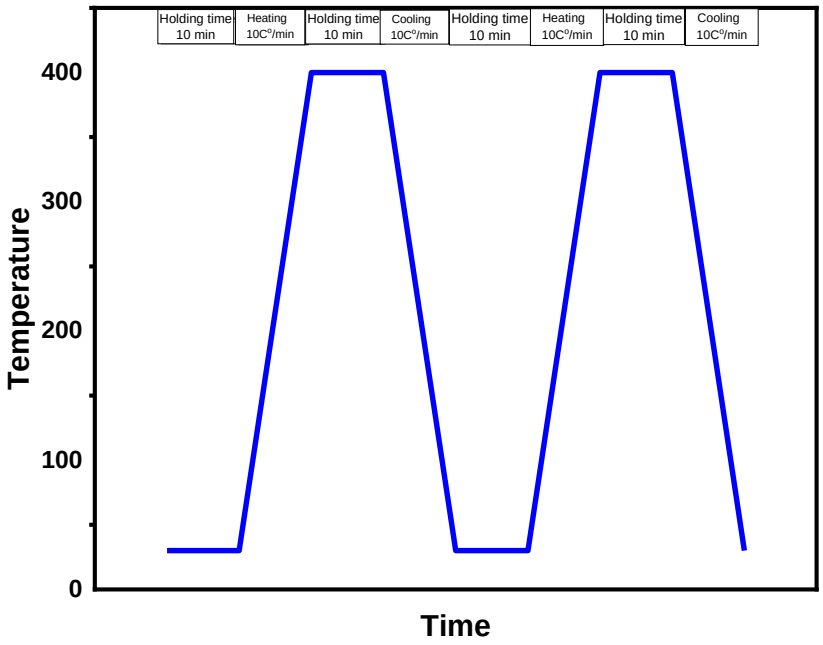

Figure 4.18 A diagram of the temperature ramp profile.

The raw DSC data was then analysed by the commercial Pyris software to evaluate the thermal behaviour profile to determine melting characteristics of the samples including liquidus and solidus temperatures and liquid fraction. In the DSC measurement, the reaction temperature was taken as the intersection of the baseline and the extrapolated tangent line of the heat flow peak. The assessment of the liquid fraction volume was evaluated using the Flynn method[253], which involves integration of peak partial areas. This technique can be used to determine the liquid fraction transformed into solid as a function of temperature and vice versa by integrating the partial areas between the obtained DSC traces curve and baseline using the solidus and liquidus values as a guide.

The liquid fraction feature is a key property for determining a material's thixoforming capability. As mentioned, it provides important measurement data including solidification range, solid/liquid phase amount, temperature sensitivity of the liquid fraction, and processing window of the examined material. Furthermore, the isothermal heat treatment temperatures to generate non-dendritic feedstock were determined using the fraction of liquid versus temperature (f_L vs. T) relationship. Hence, liquid fraction vs. temperature data of an alloy is fundamental for controlling semi-solid processing. Also, identifying the

theory and estimation approach for freezing/melting phenomena is a critical parameter to understanding the potential technology for alloy designing and improving the working window of semi-solid processing[10, 254].

In the DSC technique, the specimen is heated at a constant rate from a temperature where the alloy is completely solid to a temperature higher than the liquidus point, or cooled from above liquidus temperature to lower value. The development of the melting heat during the solid/liquid phase transition is computed. As such, the rate of heat energy amount can be calculated using the flowing equation [163, 255]:

$$\frac{d_q}{dt} = m\left[f_S C_{p,S} + (1 - f_S)C_{p,L} + \Delta H \frac{df_S}{dT}\right]\frac{dT}{dt}$$

Equation 4.1

Where dq is the heat supplied to a substance; dT is the change in temperature; m is the mass of the specimen; f_s is solid fraction; $C_{p,S}$ and $C_{p,L}$ are the heat capacities of the solid and liquid phases respectively; ΔH is the heat of melting, dT/dt is the heating rate, and dq/dt is is the difference between the rates of energy supply to the sample cell and the reference cell.

As the heating rate z is constant, the measured increase in the absorbed heat of melting can be used to compute the decrease in the weight fraction of the solid during melting using equation 6[254].

$$df_S = \frac{1}{zm\Delta H}\left(\frac{dq}{dt}\right)dT \Leftrightarrow \Delta f_S = 1 - f_S(T) = \frac{1}{zm}\int_{T_S}^{T}\frac{1}{\Delta H}\left(\frac{dq}{dt}\right)dT$$

Equation 4.2

A common approximation to Equation 6 is to assume that the heat of melting is temperature independent, and therefore the solid phase composition is linearly proportional to the number of melted materials [163].

$$f_S(T) = 1 - \frac{1}{m\Delta H}q(T)$$

Equation 4.3

The term $q(T)$ is the amount of heat absorbed from the start of melting till the alloy temperature touches T.

The liquid fraction is frequently assumed to be proportional to the absorbed energy during the transformation. As a result, the liquid fraction can be determined using the peak area of the transition, as illustrated in Figure 4.19. The total area of a melting peak is considered to be 100% liquid. The liquid fraction at temperature $T1$ ($To<T1<Tf$) can be calculated using the following equation[10]:

$$\%Liquid = \frac{Area(T_1 - T_0)}{Total\ area}$$ **Equation 4.4**

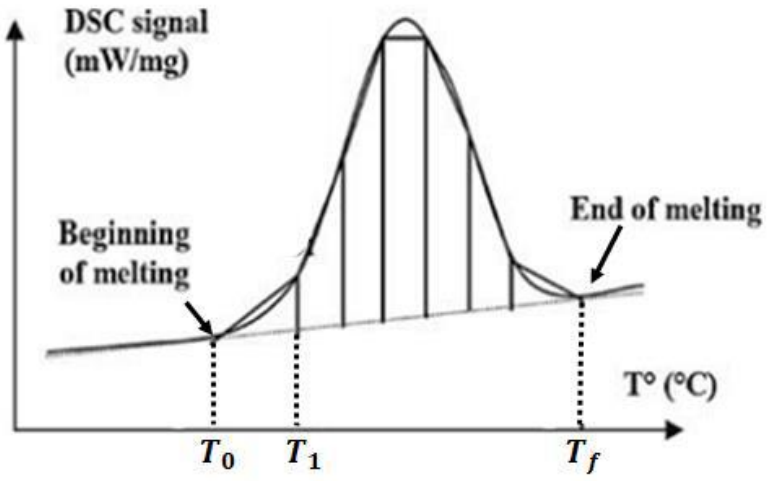

Figure 4.19 Shows estimation method of liquid fraction [10].

4.4.2.4 Thermodynamic prediction by Thermo-Calc

Nowadays, the rapid development of computational thermodynamics has offered a quick and reliable method for understanding material properties, enabling alloy design. The thermodynamic simulation enables the evaluation of solidification parameters without the need for actual material preparation. This is extremely beneficial as it requires less time-consuming experiments and therefore reduces cost. Thermodynamic modelling can be applied to supplement experimental investigations and as a guide for the development of the alloy, particularly prospective SSM candidates. There are numerous integrated computational software tools available to study the phase equilibria and solidification behaviour of alloys, including Thermo-Calc, Pandat, and Factsage – developed based on the CALPHAD (Calculation of Phase Diagram) simulation[256]. The CALPHAD technique is a dependable and multipurpose technique for producing phase diagrams that requires fewer experimental data than traditional methods[253]. The fundamental concept of the CALPHAD approach is the modelling of the Gibbs free energy of each phase as a function of temperature, composition and pressure. The results are then compiled into a thermodynamic database.

This allows the prediction of thermodynamic characteristics and phase diagrams of multicomponent systems. Additionally, it enables the tracking of each alloy during the isothermal heat treatment or solidification processes by calculating the distributions of the phase and compositions[202]. This information is critical for understanding and controlling the behaviour of industrial alloys.

Computational thermodynamics is used in this research to calculate the alloys' solidification sequences. The Thermo-Calc software package with database SSOL4 was used to evaluate the fraction of the liquid during the solidification process under both equilibrium and non-equilibrium (Scheil) solidification. Thermo-Calc is a commercial software package that is extensively used to calculate and understand almost all possible types of thermodynamic and phase diagrams of multi-component material systems for a wide range of materials. It is capable of processing multi-component systems with up to 40 elements and many different phases. [165]. Furthermore, various types of process simulations can be carried out. It can be used for complex heterogeneous interaction systems with highly non-ideal solution phases[257]. Depending on the database to which it is linked, it can be applied to analyse any thermodynamic system in the areas of chemistry, metallurgy, material science, alloy designing, semiconductors, etc.[165].

It should be noted that the thermodynamic calculation was performed using Thermo-Calc to estimate the liquid fraction under the equilibrium condition, based on the Lever rule, and the non-equilibrium condition, based on the Scheil–Gulliver model. In general, the terms equilibrium and non-equilibrium condition refer to two extreme situations of the solidification process. The equilibrium solidification mode (Lever rule) is based on the assumption that equilibrium diffusion takes place in both liquid and solid states. The non-equilibrium solidification (Scheil model), however, applies the following assumptions: (a) equilibrium interface; (b) no back diffusion takes place in the solid phase; (c) the composition is homogeneous throughout the entire liquid phase; and (d) solid and liquid phases have equal densities[258, 259]. The predictions of the Thermo-Calc simulations were compared to the results of the Differential Scanning Calorimeter (DSC) and are presented in the next section.

4.4.3 Feedstock fabrication of semi-solid alloys

The main reason for semi-solid processes being successful is the preparation of the semi-solid materials with a thixotropic microstructure. The microstructure morphology of this starting material for SSM forming is composed of fine, solid, near-spherical particles suspended in a liquid matrix with a large solidus-to-liquidus transition zone [42]. An advantage of this unique microstructure has a strong influence on the flow behaviour of semi-solid slurry in a positive way – so that parts can be achieved efficiently without typical defects that can be found in the conventional casting process. Furthermore, the produced components which present with a fine and non-dendritic structure benefit from better mechanical properties compared to other conventional manufacturing process[34]. SSM thixotropic materials can be manufactured from a liquid alloy, via controlled solidification under particular conditions, or from a solid, via heavy plastic deformation followed by recrystallisation[42].

There are a number of methods that have been introduced within the industry and applied globally for producing feedstock with a spherical microstructure in the semi-solid state. These include Mechanical Stirring, MHD, SIMA, Spray Casting, Cooling Slope Casting, Direct Partial Re-melting etc. Among these, the Recrystallization and Partial Melting (RAP) method, which was developed by Kirkwood et al., is one of most efficient and commercially accessible solid state routes to thixotropic feedstock owing to its low cost and simplicity[260]. This process involves two essential steps of deformation followed by isothermal heat treatment. Nevertheless, prior to the RAP process, a dendritic cast microstructure is prepared in a suitable form through a conventional casting process. Subsequently, during the RAP procedure, the material is exposed to a deformation by cold or warm working at a temperature below the recrystallisation temperature. Then, the deformed material is subjected to a partial re-melting to achieve a semi-solid state and isothermally held for a time to introduce the thixoformed billet[261]. The deformation stage may be done by a variety of different techniques, including rolling, forging, upsetting, and extrusion[188].

The microstructural evolution of non-dendritic formation for the RAP process consists of different stages. The first stage of microstructural evolution is that the strain energy is stored, which can be attributed to deformation of the cold working, within deformed materials as a form of dislocations and vacancies. Secondly, once the cold-worked material is heated, changes occur within the material structure where recovery and recrystallisation take place traced to dislocation climb and cross-slip, and combining vacancies. In the final stage, when the heating overrides the alloy solidus temperature (mushy zone), the liquid phase would then penetrate into the recrystallised grain boundaries. As a consequence, a slurry with desired globular solid particles is generated surrounded by a liquids matrix[186, 262]. In this work the RAP approach has adapted to fabricate semi-solid feedstock billets as a result of operational simplicity and low-cost equipment. Moreover, it is an ideal candidate for manufacturing small-diameter, semi-solid billets and has the capability to introduce high-quality feedstock from wrought alloys and high melting point alloys including steel and super alloys[42]. The next section gives a brief description of the procedures and methods used for billet fabrication which are proposed to be used in this study.

4.4.3.1 Overview of the apparatus design used for feedstock fabrication

The apparatus was designed, built and commissioned in order to produce the required billets to be used as feedstock in the LEMA system. In this present work, an extrusion test unit was used to reduce the diameter of the starting materials and prepare billets that were to be used for the isothermal heat-treatment process and then semi-solid extrusion and deposition. This extrusion test unit was a combination of a custom-made extrusion die and

hydraulic press machine. The die inlet area was designed according to the dimensions of the starting raw material. The custom-made extrusion die had a cavity with a conical shape in order to reduce the diameter and produce the required feedstock dimensions. Figure 4.20 illustrates the extrusion die assembly which is made of five different units: container, die, die backer, supporting plate and ram. The extrusion die set was developed with special requirements in mind to assure the success of the process. The material of the units is required to be made of high-deformation-resistance materials, and for this a H13 die steel, which has the desired properties, was chosen. These parts were fabricated using an advanced manufacturing technique, in collaboration with the manufacturing facility of Sheffield University. As can be seen in Figure 4.20, all units are bolted together by three secure screws which are mounted evenly around the perimeter and used after installation to correct any misalignment. The container unit, which is essentially a cylinder of 21 mm inner diameter and 29 mm in length, holds the work piece. The container is attached to the extrusion die unit and has an inner diameter the same as the extrusion die entrance diameter. The die is one of the vital units of the extrusion chamber as its orifice fashions the final shape of the extruded structure when the metal is squeezed through it. This extrusion die is a cylindrical shape having a conical entrance profile with an exit diameter of 9 mm. Also, the extrusion die is manufactured with a recess and tooth on the top and bottom surface of the die, respectively. These features enable the joining and plugging of the rig parts to each other.

Another benefit is that it prevents any alloy leaking between the connected parts when they are exposed to pressure during the extrusion process. The die backer placed at the bottom of the extrusion die helps to support the die against the force required to force metal flow. The outline of the backer entrance opening is typically assumed to be somewhat larger than the diameter of the die exit, to facilitate a smooth flow of material. The die backer is designed with a vertical slot along its side to discharge the extruded billet. The supporting plate is mounted on the base of the hydraulic press and holds the whole extrusion die set. The last part of the extrusion chamber is the ram which is fitted to the crosshead of the testing machine. The ram has a circular cross-sectional area and, using the provided extrusion force, the ram is moved down to push the feedstock through the container cavity.

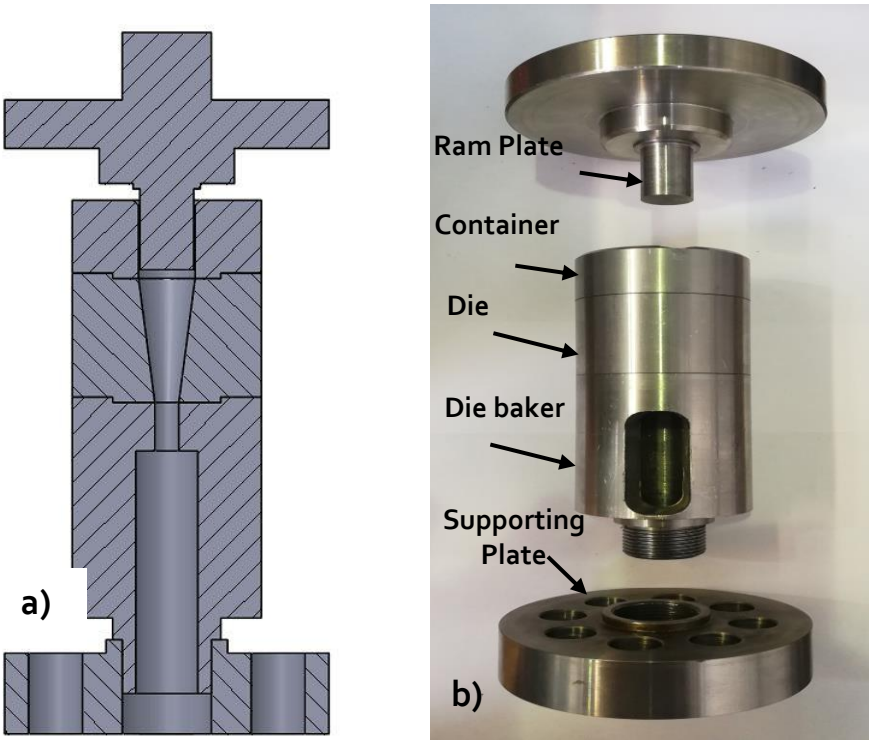

Figure 4.20 (a) schematic showing a cross-section of the assembly die extrusion and (b) disassemble parts of the setup.

4.4.3.2 Experimental procedure of billets production

The raw material was originally supplied in form of 305 mm *40 mm*20 mm cast ingots. The as-cast ingots were then machined into small cylindrical bars with a diameter of 20 mm and a length of 25 mm, as can be seen in Figure 4.21. The basic operation of the extrusion process is similar to that of a traditional press machine, which uses a large force to inject material into a die. The extrusion process was carried out at room temperature using the Schenck hydraulic press. This cold working is described as the plastic deformation of materials below the recrystallization temperature. The reduction area of the extrusion was 55% when investigated. Before performing the experiment, the extrusion die set was fixed onto the bed of the hydraulic press. The container, ram, die, and sample were lubricated in order to reduce friction between the die, container and billet (that may cause defects), resulting in the material to flow more favourably. Another advantage of applying lubricant is to reduce the extrusion force used during the cold extrusion. Additionally, to prevent any potential unwanted heat generation, the ram speed was maintained at 3 mm/min. The extrusion load and the displacement of the piston during the test were measured and recorded by a computer attached to the machine.

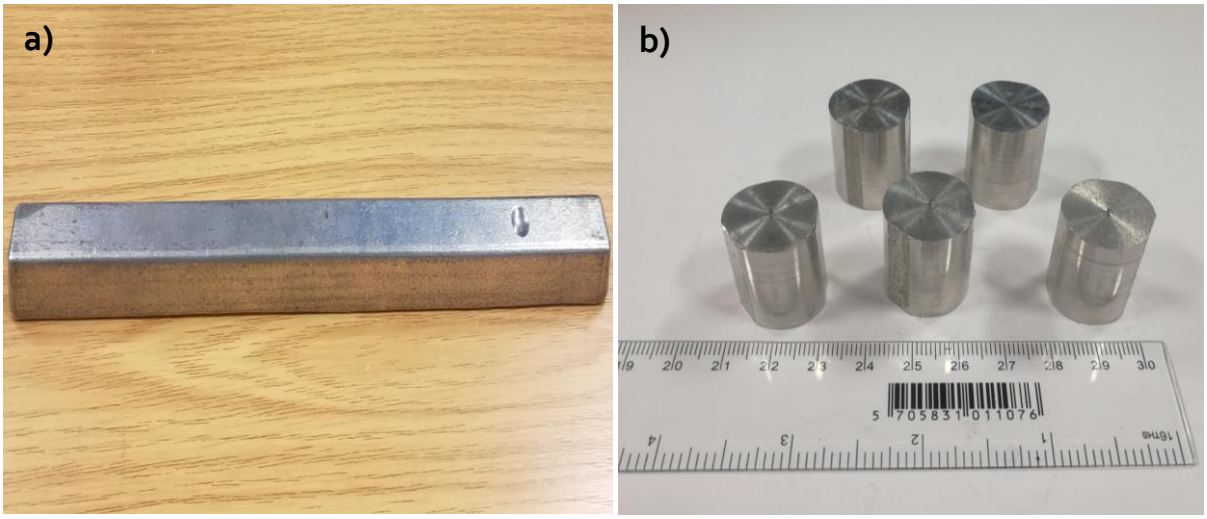

Figure 4.21 a) starting material b) machined bars.

A schematic view of the hydraulic test unit and extrusion die setup used in this research are presented in Figure 4.22. In the beginning, the cylinder sample was placed inside the container for a compression operation. The crosshead of the testing machine was instructed so that the ram was hydraulically lowered and positioned just before the top of the sample surface. Then, the application of the extrusion force resulted in the ram moving down toward the sample. Accordingly, the cylinder sample was pushed into the container and extruded through the die. When 95% of the sample length in the container was extruded, the machine was stopped. After the trial was completed, the ram then moved back to its highest point to allow the extruded billet to be discharged from the die backer and a new sample was uploaded. The whole metal extrusion procedure was repeated to produce the other samples. A photograph of the extruded billets is presented in Figure 4.23.

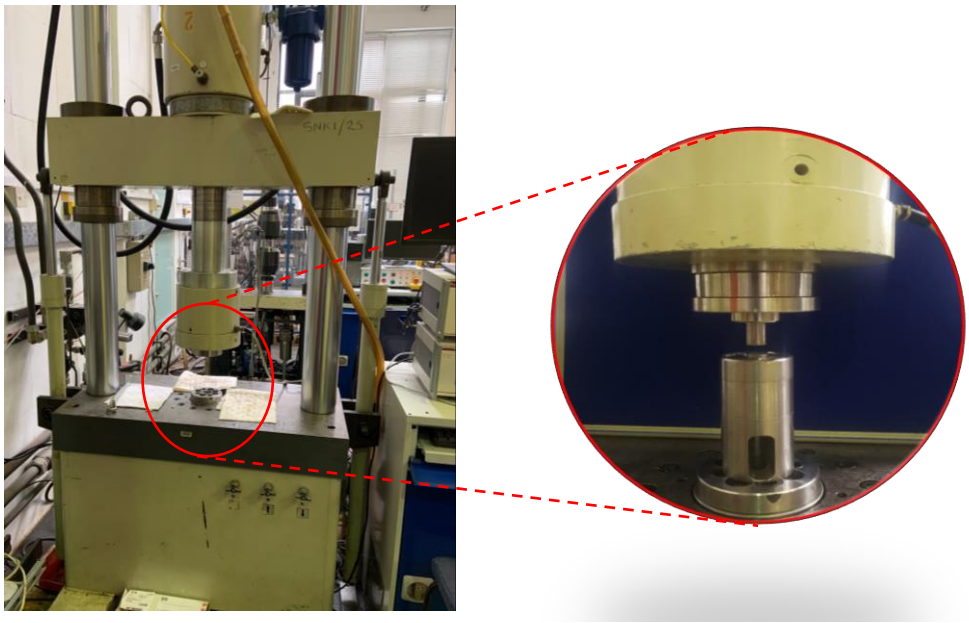

Figure 4.22 Experimental setup of the extrusion process using a hydraulic machine.

Figure 4.23 Alloy billets deformed by extrusion.

4.4.3.3 Partial melting of recrystallized structures

The final step in the feedstock preparation, after the solid-state deformation, is the partial-melting process. The temperature of the feedstock materials during the partial re-melting process has a big impact on the success of the thixoforming procedure. The material must be warmed to a suitable SSM temperature before the thixoforming process. This stage is essential in order to control the billet microstructure and transform the recrystallised structures of the cold-worked materials into a thixotropic structure with spheroidal particles[26]. The amount of energy stored with the alloy during the cold working is

thought to be a critical factor in the process of grain nucleation as it serves as a driving force for recovery and recrystallisation[261]. When the adequately cold-worked microstructure is exposed to partial melting within the semi-solid range, high-energy liquid metal penetrates the high-angle boundaries of recrystallised grains, forming a SSM alloy of a fine and globular microstructure[34]. The samples are then quenched immediately in water to retain their semi-solid microstructure and hence obtain the semi-solid billet.

The heat-treated samples were supported by a protective tube made from Alumina which was designed according to the temperature melting point of the examined materials. The cylindrical protective tubes were used to maintain the shape and keep the roundness of the samples during the heat treatment process. To observe the actual heating temperature of the specimen during the experiment, a K-type thermocouple was inserted in a drilled hole in one of the two sides of the examined sample. The heating rate and temperature fluctuation of the electric furnace were set at 10 °C/min and ±1 °C, respectively. To study grain formation and spheroidisation during microstructure evolution in the semi-solid stage, the specimens were placed into the electric furnace after the furnace reached predetermined temperature values. After the pre-set temperatures were stable, the deformed samples were isothermally held using different holding times.

The second stage of heat treatment is the quenching process, where the sample was immersed promptly after the completion of partial re-melting and the required isothermal holding times into ambient temperature water. The most significant advantage of this procedure is to capture the morphology of the developed microstructure during the semi-solid state. The resulting microstructures were studied to determine optimum holding times and temperatures that would produce the optimal globular solid particles for semi-solid extrusion. The effects of these parameters on the morphology and spherical nature of the grain size were also investigated. Table 4.2shows the experimental parameters for heat treatments of the examined alloys.

.

Table 4.2 Semi-solid isothermal treatment conditions for Zn-40%Sn.

Liquid fraction %	Isothermal holding temperature (°C)	Isothermal holding time (min)					
		A	B	C	D	E	F
0.40	282.5	2	5	8	11	15	20
0.50	313	2	5	8	11	15	20
0.60	334	2	5	8	11	15	20
0.70	347	2	5	8	11	15	20

4.4.4 Metal LEMA test apparatus components and design

In the literature, various approaches have been established and presented to extrude and deposit semi-solid metal to fabricate layer-based three-dimensional components. In this current research, an extrusion and deposition test unit (LEMA) was used to process the feedstock billets. The principle of thixo-extrusion was applied in this work in which the feedstock material, containing a globular microstructure, was heated up to a SSM range temperature in-situ, inside the extrusion barrel, by means of band heating system. Then, an SSM alloy was forced through a print head under pressure provided by a UTM machine to enable controlled deposition onto a platform. The arrangement was the combination of a UTM machine, thixo-extruder developed for deposition, support frame, and an x-y axis moving table. The arrangement was designed with specific requirements in mind to ensure the successful accomplishment of the operation. This will be discussed, in further detail, below.

4.4.4.1 Design overview

In this experimental work, the employed system (LEMA) is a hybrid of a UTM and a custom-made metal printing machine. This configuration was selected because it required only a simple experimental step-up and had a low processing cost, to process metal alloys and therefore print 3D metal shapes. The complete rig was designed, built, and tested at The University of Sheffield. Figure 4.24 shows a schematic diagram of the improved LEMA system, highlighting the main components, such as: cylinder, nozzle, heaters, and plunger drive system (detailed pictures are given in the appendix 2). The piston extrusion-based rig is mounted on the base of a UTM machine. The movement of the piston is controlled by a load cell through a machine controller. The printing method begins as follows: first, the pre-alloyed billet is fed into the barrel before the partial re-melting process of the billet is started. Next, once the material is being brought into a desired semi-solid state, a command is sent through the control system to the load cell to drive the piston down in

order to generate substantial pressure, pushing the molten feedstock to flow out of the nozzle and depositing it onto a worktable.

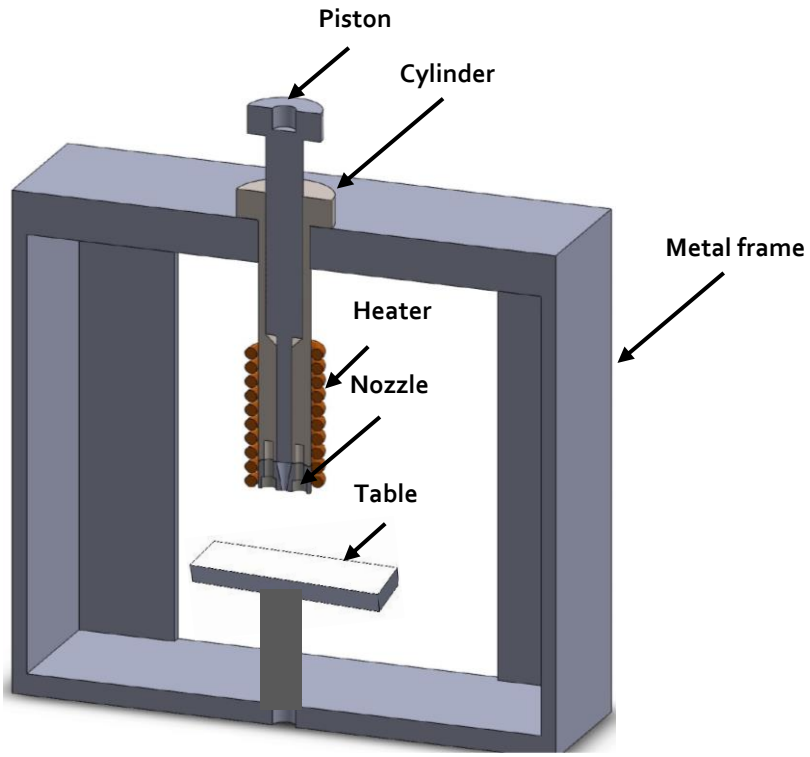

Figure 4.24 Schematic diagram of rig cross-section.

4.4.4.2 Universal testing machine (UTM)

A Tinius Olsen H25KS universal mechanical testing machine was used to transmit force with the aim of pushing the material feedstock to the extruder barrel. This is originally used for material testing including tension, compression, flexure, and shear strength testing. The maximum force capacity of this testing machine is 25 KN. A load cell integrated into the upper crosshead allows for the measurement of the force applied during the compression of the sample. The operation of the machine is managed by the machine controller, which is attached next to the machine testing, as shown in Figure 4.25. A computer-controlled software programme (Horizon data analysis software) was used to operate, screen, and record estimation information for later analysis.

Figure 4.25 Tinius Olsen tensile/compression test machine.

4.4.4.3 Metal support frame

The rig's metal frame, which was made from the alloy steel, was built to be sturdy and capable of withstanding the expected applied force from the UTM. The metal frame consisted of a thick upper plate, a lower plate (30mm), and beams, as demonstrated in Figure 4.26. The function of the upper plate was to carry the extrusion barrel and nozzle, while the lower plate was used to assemble the whole custom-made metal printing machine. Beams were welded in each corner connecting the two thick plates to ensure system rigidity. A slot was cut in middle of the lower plate to allow for the extrusion metal frame to be screwed onto the UTM machine. This was critical in aligning the extrusion chamber in order to ensure that the ram accurately entered the extrusion barrel. A clear Perspex acrylic sheet was used to cover the front of the extrusion chamber during operation. This type of material was used for the purpose because of its transparency which therefore allows for monitoring of the printing process and quick intervention if needed. Finally, to ensure full protection, a steel sheet cover was used to enclose the extrusion chamber from the back. More general information on the metal chamber can be found in appendix 3.

Figure 4.26 The support frame design

4.4.4.4 Piston, extruder barrel and nozzle (thixo-extruder)

In order to accomplish the experiment for material extrusion, a custom-made piston-based-extrusion testing apparatus was designed and manufactured at the University of Sheffield. The materials of this custom-made machine were chosen from highly heat resistant material due to its requirement to process feedstock billets in high-temperature conditions. The extrusion machine set-up (thixo-extruder) may be broken down into three major parts: piston, extrusion barrel, and nozzle, as can be seen in Figure 4.27. The complete thixo-extruder set was designed in a way so that the different parts can be substituted based on the requirements of the worker. Also, because of the high operating temperature, it may lead to thermal expansion of the metal parts, and piston thermal expansion may mean piston seizures in the barrel wall. The three parts were made from mild steel material to provide uniform thermal expansion and maintain a desired clearance between the piston and barrel wall. At the top of the extrusion barrel is a circular disc so the extrusion barrel can be mounted on the metal support frame. The piston is designed to extend through the entire length of the extrusion barrel. The metal frame was designed to be solid and to withstand the anticipated printing force applied by the piston. The piston was machined to two different diameters, 9 mm and 25 mm, to inject the semi-solid metal into the extrusion chamber and to be used as a guide, respectively. The interior bore of the extrusion chamber was designed with high dimensional accuracy to match the piston dimensions. The printing nozzle is a core part of the thixo-extruder and can varied based on the application of the extrusion and deposition set-up. At the top of the nozzle is a thread to fit the nozzle to the extrusion barrel. This nozzle design could be easily detached and switched with different lengths and outlet diameters for various applications. At the

lower end of the nozzle is a 45-degree angle cone, ending in an opening for metal deposition. The size of opening can also vary according to the desired thickness of the material layers. (See appendix 2for more details about the thixo-extruder design.)

Figure 4.27 Thixo-extruder arrangement.

4.4.4.5 Heating Source, Temperature Control System

Heating sources are a key contributor to the printing process and play the greatest role in the rheological behaviour of materials. If the temperature is insufficient, this will affect material viscosity and result in an undesired material deposition. Hence, to maintain a steady temperature in the extrusion chamber so that the system remains isothermal, two coil heaters (240v and 1000w capacity) are specially designed for the thixo-extruder. They are capable of achieving a temperature above 700 ° C and have been placed in direct contact around the cylinder for heat conduction and better regulation of temperature. The coil heaters were supplied with full-contact clamping bands that act as an operating guard over the crucial parts. Further, thermal insulation was applied on the coil heater to provide the added benefits of minimizing the heat loss so that the temperature is kept constant, safety purposes, and also reducing the surface temperature of the clamp. The heating system was connected to a dual control box (K39 Ascon Tecnologic, PID temperature controller manufactured by Elmatic, Cardiff) with the help of thermocouples monitoring the points of interest, including the temperature of the extrusion chamber and the inserted billet. The PID controller shows two temperature readings: the set-point value

and measured value. The set-point value represents desired temperature entered by the operator, while the measured value represents the actual temperature detected by the thermocouple. The PID control box governs the temperature of the coil heater based on the thermocouple input. For maintaining the temperature of the heating system, the PID controller operates a solid-state relay, which turns the power supply of the heating system on or off to reach the required temperature level.

4.4.4.6 Temperature recording

Thermocouples are used to gauge the temperature of materials in the extrusion chamber. Therefore, to monitor and provide more precise temperature control to the PID controller, two individual J-Type thermocouples are used and attached to the coil heaters. The highest temperature that this thermocouple can withstand is 770 °C. This form of the thermocouple is completely insulated against the heating wire and is made up of pure nickel lead, sheathed with glass fibre and coated with silicone. The benefits of this configuration are longer cartridge life, fast and accurate reading temperature, energy-saving, and also protection of the heater lead from the oxidation in the elevation temperatures. An additional mineral-insulated Type K thermocouple (1.0m diameter x 1.50m long, Inconel® Alloy 600 sheath) connected to a simulator thermometer is used to monitor and control the temperature of the inserted billet. This type of thermocouple has a temperature range of -25 °C to 700 °C which will suit the working temperature of experiment. The thermocouple is located on the inside of the cylinder from the top and towards the centre of the billet. The advantage of this set-up is that it allows for accurate temperature readings and feedback of the semi-solid alloy when reaching the desired temperature ranges. Regarding the uncertainty of the sensors, standard calibration procedures and adherence to manufacturer specifications were followed to minimize measurement errors and ensure the reliability of temperature data. This involved regular calibration checks and verification against known reference temperatures to maintain the accuracy of the temperature measurements throughout the experimental process.

4.4.4.7 Print bed.

The print bed should be optimised in order to maintain good material adhesion and avoid early delamination, which can result in edge warping and print failure. In this research, the print bed was designed and optimised for a piston extrusion-based AM system. The motorised bed is moved in an x-y direction and is controlled through Arduino programming to maintain a precise movement. The x-y table controller unit is made up of hardware components such as a DC power supply for the motors, essential switches to carry out the motion of each axis, and controllers for each axis.

The print bed is controlled via a USB connection between the print bed and the computer, using printer controller software called Printrun, as shown in Figure 4.28. Printrun is an open-source 3D-printing software integrated with slicer utility designed and programmed by Kliment Yanev. It is composed of three primary 3D-printing applications: pronsole (command window to send G-code), printcore (a standalone non-interactive G-code host), and pronterface (G-code command entry with graphical user interface)[263-266]. The operator can send commands directly to the 3D printer to execute calibration, tuning, and printing. It provides all the visual data to start and control the printing process. Further, the Pronterface software is supported by most of the main operating systems such as Windows, Linux and acOS.

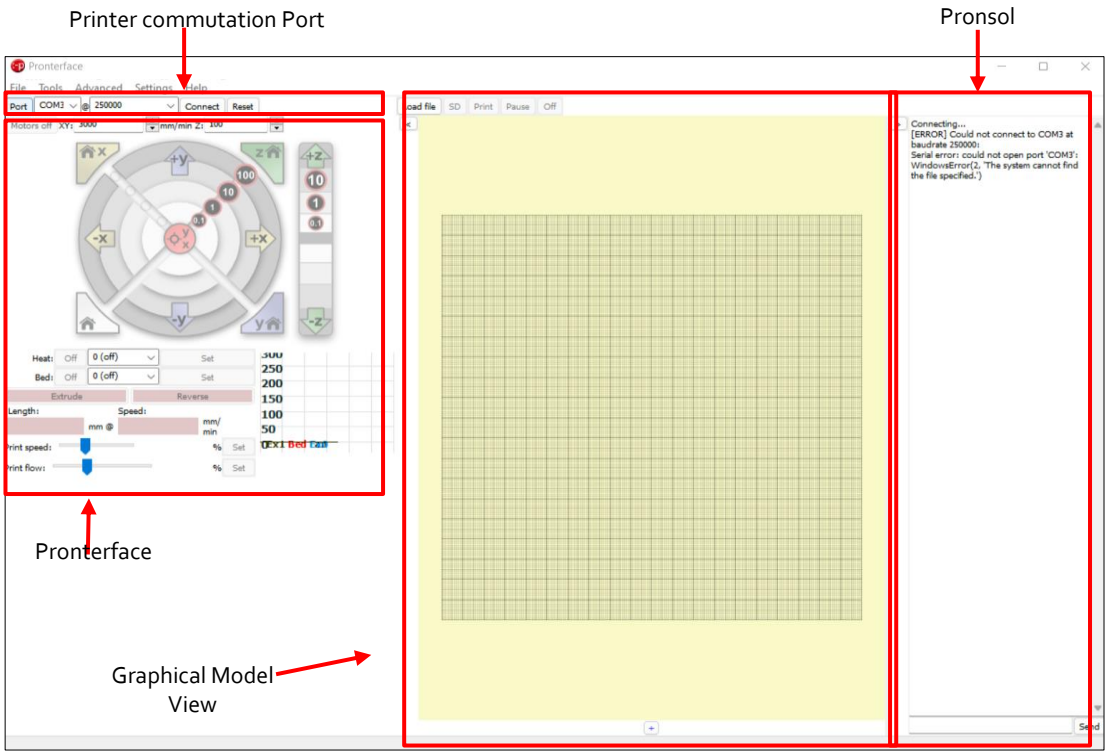

Figure 4.28 Printer communication programme.

4.4.5 Extrusion and deposition metal alloys procedure

Various approaches have been developed and introduced in the literature to examine the validation of extrusion and deposition SSM feedstock to build a 3D object. In this present work, a metal extrusion-based AM method was used to evaluate the feasibility of extrusion and deposition of a semi-solid metal alloy. The principle of thixoforming was applied in this experiment to help with the preparation of SSM feedstock with thixotropic properties in which the feedstock billet is deformed through an extrusion process followed by partial

re-melting in the semi-solid range in order to recrystallise and achieve fine, non-dendritic microstructures. Then, the pre-treated feedstock is fed into the custom-made metal printing machine for component forming.

Before beginning the actual experiment, a number of aspects and process preparations need to be taken into account. The metal chamber that carries the extrusion barrel was placed at the bottom of the UTM machine and adjusted, positioned, and well secured with the aid of the screw located beneath the metal frame. To minimise the adherence of the semi-solid alloy to the inner wall of the nozzle and barrel, a Boron Nitride (BN) ceramic spray was applied. BN is a dry film protective coating used in metal forming processes and applied mainly to surfaces that come into contact with molten metals to prevent corrosion ,reduce chemical attack, and provide longer life. Further, it is vital to ensure that the ram is free to move and is aligned perfectly with extrusion barrel. This was accomplished by inserting the ram into the extrusion barrel prior to tightening the screws. Next, the coil heating elements were placed around the extrusion barrel, covering the nozzle as well. To avoid any heat losses and keep the material isothermal, the coil heater was surrounded by an insulation blanket and a clamp band was used to enclose this thermal insulation.

The experiment was started by the pushing of the power supply button for the PID controller, coil heaters, and PC. Subsequently, the heaters were set to a specified temperature and a short wait ensued until the temperature reading stabilized. Afterwards, the feedstock billet was placed inside the extrusion barrel and a K-type thermocouple was inserted into the extrusion barrel opening to monitor and record the temperature of the molten alloy inside the barrel. The ram was lowered down to a position before the opening of the extrusion barrel and the x-y platform was moved up to close to the nozzle tip. The clearance gap between the nozzle tip and the substrate should be determined carefully, as too small a clearance gap may cause a blockage of the nozzle tip during the deposition, while greater distances result in less control of the prints. Finally, when the temperature of the billet reached a desired semi-solid state, a command was sent through the control system to the load cell to drive the piston down in order to generate substantial pressure, pushing the molten feedstock to flow out of the nozzle and deposit it onto a work table which moved relative to the extrusion.

The piston-based material extrusion experiment was conducted using various nozzles with different outlet diameters: 1 mm, 1.5 mm, and 2 mm. Previous studies on material extrusion of semi-solid alloys have revealed that temperature is one of the key factors in controlling the extrusion process, since it affects the volume liquid fraction, apparent viscosity, the rheological characteristics, and the extrusion quality of the semi-solid alloys[60]. Therefore, selecting an appropriate operating temperature that matches the correct liquid fraction range (40%-70%) should be taken into account for the smooth

operation of the extrusion process. Given this, 282, 213, 234, and 247 ◦C were considered as thixo-extrusion temperatures which correspond to the liquid phase fractions 40%, 50 %, 60 %, and 70% respectively, according to the results of the DSC investigation. Various parameters of the LEMA system condition, including, extrusion rate, substrate speed and liquid fraction were tested through the designed system. Further, the printed sample with different conditions was studied. The process parameters of the LEMA experiment are shown in Table 3.4.

Table 4.3 Key experimental parameters of Thixo-extrusion process.

Parameter	Nozzle diameter	Extrusion rate	X-Y moving speed	Liquid fraction
Value	1-2mm	20-50mm/min	20-50 mm/min	40%-70%

4.4.6 Specimen preparation and microstructural characterisation

The preparation of metallographic examination for specimens from solder alloys such as zinc, lead and tin alloy introduces particular challenges. It is not simple to achieve consistent metallographic outcomes with soft alloys. Most of the difficulties in the preparation process of the solder alloys are due to the low hardness of such alloys[267]. During the grinding and polishing stages, the abrasive particles can be embedded into the soft materials which can easily result in distortion of the microstructure[268]. Therefore, this would have a significant impact and could be misleading when interpreting the true microstructure. Also, as a consequence of the deformation and heating induced by the polishing practices, a soft alloy surface can be easily recrystallised[269]. This means that false structure information is likely to be presented. It is vital, thus, that special care must be taken during laboratory polishing, grinding and mounting of such soft alloys in order to control and reduce these obstacles in sample preparations.

4.4.6.1 Sectioning

The initial step in specimen preparation is the separation of samples from material. Because zinc alloys are relatively soft, specimen sectioning should be conducted with special techniques. As seen in Figure 4.29, a Beuhler AbrasiMet 250 precision cutting machine equipped with silicon carbide cut-off wheels was used to cut the materials to the required size so that they could be fitted for the mounting process. Coolant water was also applied to avoid any potential heat generation, recrystallisation or local tempering, which may have altered the microstructure. In this research, the metallographic preparation and microstructural characterisation were carried out at all different stages of the processes. Thus, small sections were taken from the as-received, as-deformed, as-heat treated, and as-deposited samples to identify the microstructure of the alloys.

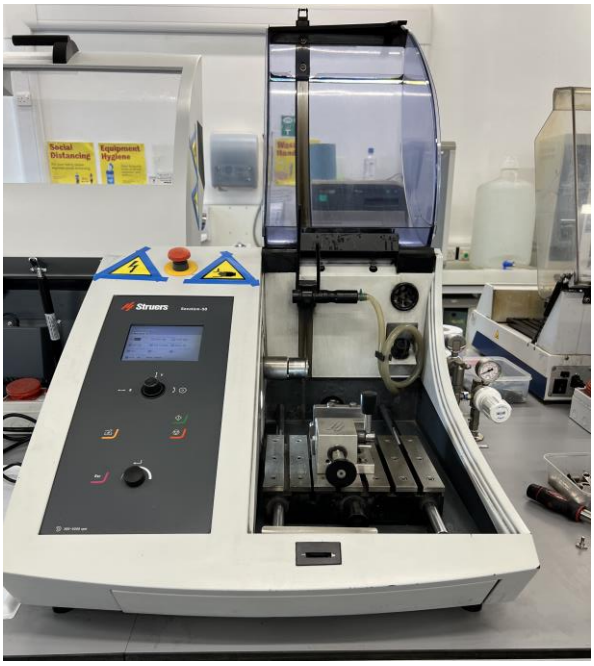

Figure 4.29 Beuhler AbrasiMet 250 precision cutting apparatus.

4.4.6.2 Mounting

Mounting is a process of embedding the specimen in a resin to support and protect it during the remaining steps of metallographic grinding and polishing preparation. Samples can be hot mounted using a mounting press or cold mounted using castable mounting resins at room temperature. The majority of zinc samples are mounted with traditional cold mounting wherein two agents are mixed, cast over the sample inside the mould, and then allowed to react to form a solid part. Hot mounting should not be used for zinc alloys as pressure and elevated temperatures, which are normally present in this process, might deform the sample and cause recrystallisation, respectively[270]. Therefore, in this project the samples were cold mounted in a plastic cup using epoxy resin (mixing ratio:25 parts of EpoFix + 3 parts Hardener, Struers). Subsequently, the mould comprising the material and epoxy mixture were placed into a vacuum chamber at room temperature and kept overnight for solidification.

4.4.6.3 Grinding, Polishing and Etching Sample

The next step is the grinding and polishing process, and this can be considered as the primary stage in sample preparation. The main objective of this step is to remove deformation as a result of the sectioning stage. This step will then produce a sample surface that is cleaned, levelled and highly reflective so that the interest features of the surface sample can be easily identified under microscope examination. The mounted samples were ground on an automated Buehler AutoMet 250 Grinder-Polisher machine (see Figure 4.30) using 4 different sandpapers, 280, 360, 600 and 1000-grit silicon carbide

(SiC) grinding papers in sequence, with a continuous stream of water which helped to eliminate heat and flush out any loose abrasive particles .This process is based on the use of progressively finer grain size abrasives for each successive stage. The force pressure and the grinding time at each grinding stage was set to be 20 N and 2 minutes, respectively. The rotational base speed of the grinding machine was set to 200 rpm and the head speed was 60 rpm. Between each stage, the sample was washed thoroughly and cleaned to eliminate any embedded abrasive particles in the sample surface.

Figure 4.30 The polishing machine containing a six-specimen holder.

The ground samples were then submitted to the subsequent treatment, the polishing process, and employed the same machine that was used for grinding operations. Nonetheless, the SiC papers and water were replaced by polishing cloths and micron-sized suspensions. The polishing step removes the distorted layer induced by grinding, and makes the specimen surface smooth and therefore more appropriate for imaging analysis. In this study the mechanical polishing stages were done using a MicroFloc polishing cloth and different grades of diamond suspension. The initial polishing was carried out with 3 µm followed by a 1µm particles-size polycrystalline diamond water-based suspension. Then, the fine polishing was done using a MasterPrep alumina suspension of 0.05 µm particle size . The polishing pad was washed with water and after each round of polishing, the sample was rinsed with water and then sprayed with an ethanol solution before being

dried using an automatic dryer. The grinding and polishing parameters used in this research are summarised in Table 4.4

Table 4.4 Procedures of grinding and polishing used for metallographic sample preparation.

Process	Cloth/Pad	Abrasive/Size	Lubricant	Relative Rotation		Force (N)	Time (mm)
				Head Speed	Base speed		
Grinding	SiC	280 grit	Water	↻60rpm	↻200rpm	20	2:00
Grinding	SiC	360 grit	Water	↻60rpm	↻200rpm	20	2:00
Grinding	SiC	600 grit	Water	↻60rpm	↻200rpm	20	2:00
Grinding	SiC	100 grit	Water	↻60rpm	↻200rpm	20	3:00
Polishing	MicroFloc	3µm Diamond suspension		↻60rpm	↻150rpm	18	5:00
Polishing	MicroFloc	3µm Diamond suspension		↻60rpm	↻150rpm	18	5:00
Polishing	MicroFloc	MasterPrep 0.05µm Alumina		↻60rpm	↺120rpm	18	4:00

The last phase of sample preparation that might be used is etching in a suitable etchant composition. The etching is a chemical or electrolytic procedure normally actioned soon after metallic grinding and polishing processes. The prepared sample is exposed to a solvent agent that selectively alters specific microstructural features of the sample. This step is essential in order to optically reveal different features of the sample microstructure including grain size, boundaries and phases[271]. The method of etching used in this study was to immerse the finely polished sample in a Nital solution (2% Nitric acid in ethanol) using a tongue for 15 seconds. Subsequently, the examined sample was dipped in a beaker of distilled water to eliminate any residual solution remaining on the sample. In addition to distilled water, ethanol was further used to provide the samples with additional good cleanliness. The sample was dried using an automatic dryer. To assess whether the etching had been completed properly, the etched samples were placed through an optical microscope for an initial visual investigation. If the etching had not been done sufficiently, ie over etched, the sample would have to go through the final stage of grinding, re-polishing and etching again to eliminate any contamination on the sample surface.

4.4.6.4 OM observation and image analysis

Once the etching process was performed, the specimens were ready for further investigation to examine the microstructure changes before and after deformation, after heat treatment, and post-printing processes. The optical microscope was used to capture the microstructure images of the prepared samples. It employs visible light and a number of lenses connected to a digital camera system to magnify the spotted images. The optical images were taken at various magnifications including 10x and 20x to observe the revealed microstructure and grain boundaries. Yet, when smaller features required to be inspected, a higher magnification of up to 50x was used. The optical microscope is linked to a personal computer (PC) associated with software for subsequent data analysis and storage (see Figure 4.31).

Figure 4.31 Optical microscope

4.4.6.5 Grain size measurement

The evaluation of quantitative metallographic measurements of the studied specimens required information such as average diameter and sphericity of the primary solid grains. The ImageJ software analyser, an open-source image processing software platform, was used to perform statistical analysis for specimens obtained from the isothermally heat-treated process in the semi-solid state and thixo-printing. To process the microscopic image using ImageJ, micrographs have gone through a multi-step approach for metallographic evaluation. Firstly, the images were transformed to an 8-bit grayscale in order to reduce the size and allow for thresholding. Then, thresholding took place to convert it into a binary (black-and-white) image; the black areas represent liquid fraction and white areas represent primary particles. Once the image was smoothed, with small particles removed, and grain segmentation based on their circularity applied, the software automatically calculated the desired morphological parameters. Figure 4.32 illustrates an example of (a) the original micrograph and (b) the final processed image highlighting the presence of the globular particles in the liquid phase represented by the white area.

In this work, the equivalent diameter and sphericity of primary solid grains were used to define average grain size and shape factor that are both determined by ImageJ software. The following formulae were applied to compute the average diameter of the grain size (D) and the shape factor (SF)[272]:

$$SF = 4\pi A/P^2$$

Equation 4.5

$$D = 2\sqrt{(A/\pi)}$$

Equation 4.6

where A and P are the area and perimeter of the examined primary grain, respectively. The shape factor (circularity) assesses how spherical the grains are that occur within a microstructure. A value that is close to 1.0 is regarded as a perfectly spherical solid grain, whereas a value that approaches 0.0 suggests that the shape is becoming increasingly elongated.

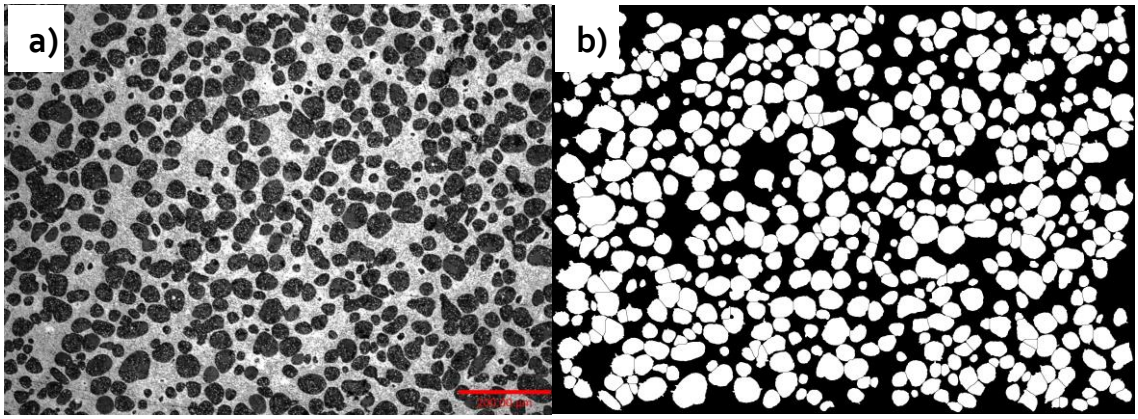

Figure 4.32 Micrograph for the (a) original image and (b) binary image, small sections were taken from the as-heat treated to identify the microstructure of the alloys

4.4.7 Scanning electron microscope (SEM) and energy dispersive X-Ray (EDS)

In this work to view the microstructure that light microscopy is unable to resolve, scanning electron microscopy (SEM) with an ultra-high-resolution field emission gun was used to gain microstructural information of the prepared specimens in greater detail. SEM imaging was accomplished using an FEI Inspect F50 Scanning Electron Microscope, as shown in Figure 4.33. Prior to imaging, a silver paste was applied (including to the bottom of the specimen) to improve the conductivity. The specimens were then carbon-coated (Agar Auto Carbon Coater, ~ 5 nm thick) using a Quorum Q150T ES machine to achieve high-quality images without any charging impact. The images were taken using the secondary electron detector (SE) and the backscattered electron detector (BES). The SE detector is used to examine the topological features of the sample surface, whereas the BES detector can be used to offer more detail on the different phases of material

microstructures. Images of both secondary electrons (SE) and backscattered electrons (BSE) were acquired with a high electron beam at 20 kV accelerating voltage to improve microstructure compositional contrast on specimens. The sample was placed on an aluminium stub and located inside the microscope, and then the chamber pressure was operated at 5.00 x 10-5 mbar. In order to produce high-resolution surface imaging, the spot size and working distance were set at 3.5 and 10 mm, respectively.

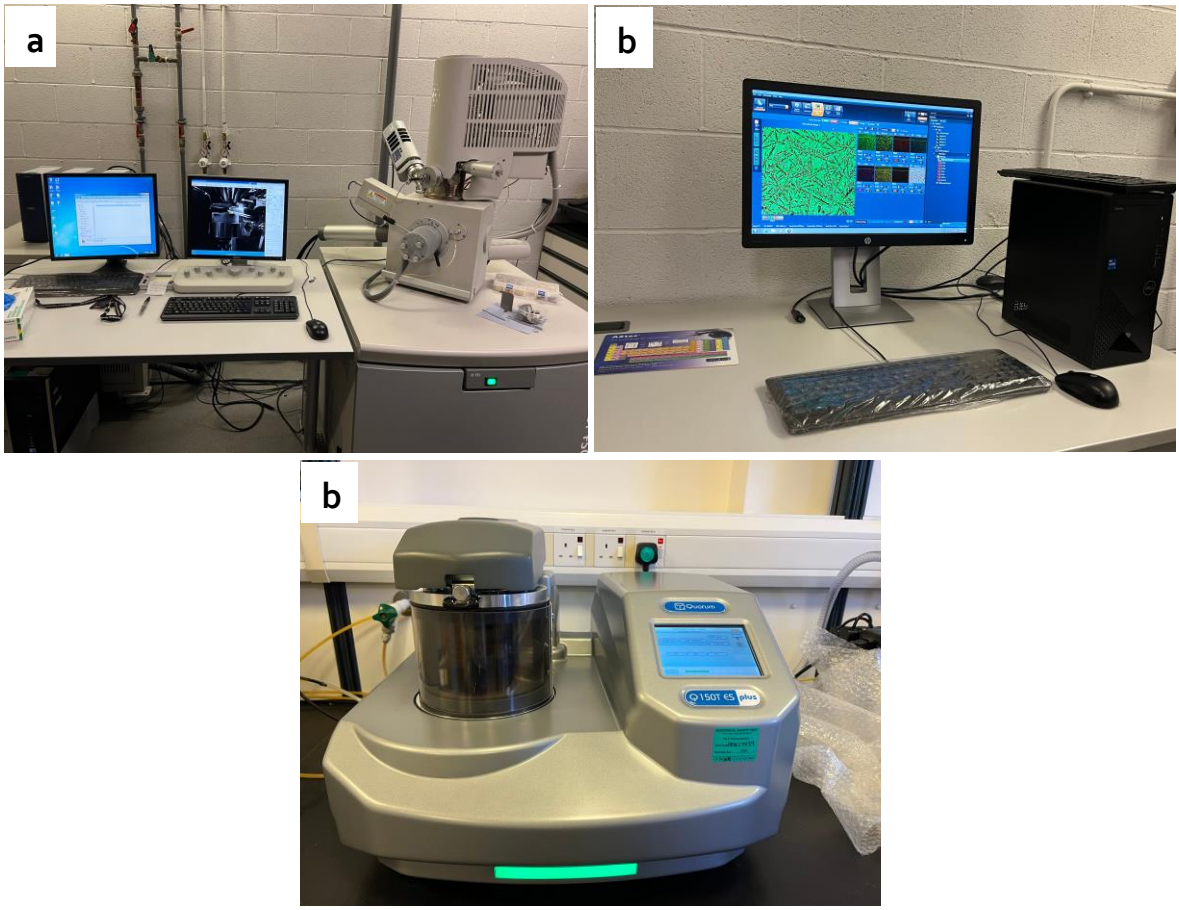

Figure 4.33 Photographs showing a) FEI Inspect F50 SEM, b) EDX AZTEC software to identify chemical analysis, and c) Quorum Q150T ES machine for carbon coating.

Furthermore, the Energy Dispersive X-ray spectroscopy (EDX) analysis was employed to verify the chemical composition of the samples. An energy dispersive X-ray spectrometer (Oxford Instruments X-max system) attached to an FEI Inspect F50 SEM was used for the quantitative EDX analysis. The condition for this examination, regarding the accelerating voltage and beam current, were set at 15kV and 0.8nA, respectively. The working distance between the EDX detector and sample surface was set at less than 10 mm in order to collect sufficient data. The information produced by the EDX detector was then analysed by AZTEC software, which can acquire and digitise photos after capture. Further, elemental distribution was conducted on some specimens using X-ray mapping. This mode is helpful for identifying element distribution within the observed phases.

5 A SEMI-SOLID THIXOTROPIC METALLIC ALLOY FOR 3D PRINTING

In phase I, a layered extrusion of metallic alloy system (LEMA) was developed which used a single reciprocating screw to break up and force the semi-solid alloy through the barrel and nozzle to be deposited on a substrate. This preliminary examination was tested with this system, and the outcomes were evaluated to assess the potential of the LEMA technique as a metal AM process in the future. The experiment was carried out in accordance with the methodology described earlier. However, it is worth noting that to conduct the tests at the calculated temperature of the liquid fraction 0.4 based on Lever rule, there was no observed extrusion of the alloy as the screw was not able to rotate. This might be due to the fact that high solid fraction of metal alloy was formed and this made the material extrusion was more difficult. So the heating temperature had to be increased to around 350°C to enable the screw extruder spinning. This temperature value corresponds to the solid fraction of 0.5; thus, the materials were more liquid-like with this lower solid fraction, and the extrusion process was easier. Also another point should be mentioned here is that although surface finish is very important in 3D printing industries, the surface finish of the prints such as the one depicted in Figure 5.1 is not as perfect as that found in other professional 3D printing processes. These parts have been printed with little consideration has been given to surface finish quality, as the goal of the project is to demonstrate extruding and depositing concept of semi-solid materials. Three tests were conducted and all the observations of the tests are presented below with more details.

5.1 Materials Extrusion of Zn-30 wt.% Sn

To conduct Test 1 and obtain a semi-solid thixotropic material with a liquid fraction of 0.5, the process parameters from Table 1 were applied, and the procedure outlined in Section 4.2.23 was followed. Once the semi-solid slurry reached the desired criteria, it was deposited through the nozzle. As shown Figure 5.1, the materials were successfully extruded and deposited onto an aluminum substrate. A short transient state was observed during extrusion and deposition, with the extruded material initially more liquid, followed by a transition to a steady-state flow.

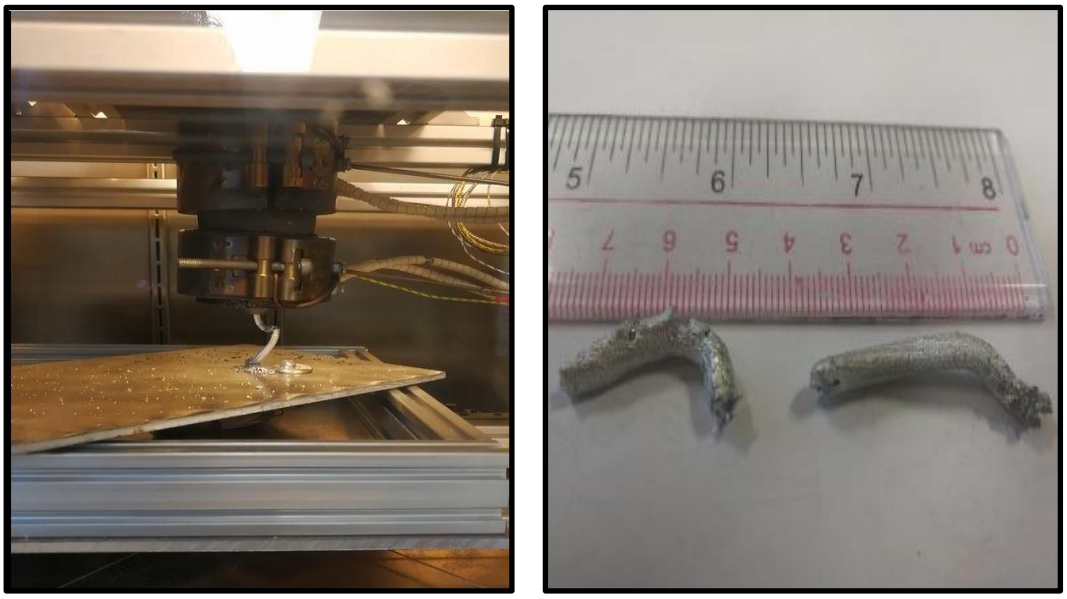

Figure 5.1 Initial printed sample from the LEMA system

After completing this trial, the temperature was increased to drain out any remaining material inside the nozzle. However, as observed in Figure 5.2, material had clearly become stuck between the screw flights. A significant amount of effort was required, including placing the screw in a furnace and performing cleaning and machining processes to remove the excess material.

Figure 5.2 Materials feedstock left within the screw.

In the second attempt, the motor speed was increased to 75 RPM, while the process temperature remained the same at 335°C. Seven minutes of shearing and 25 minutes of heating time were required to obtain the desired semi-solid alloy. The LEMA framework successfully deposited the material, as seen in Figure 5.3. However, due to the long distance between the nozzle and the movable substrate, the extruded material began to freeze before reaching the substrate, resulting in a strip-like form (See Figure 5.3a).

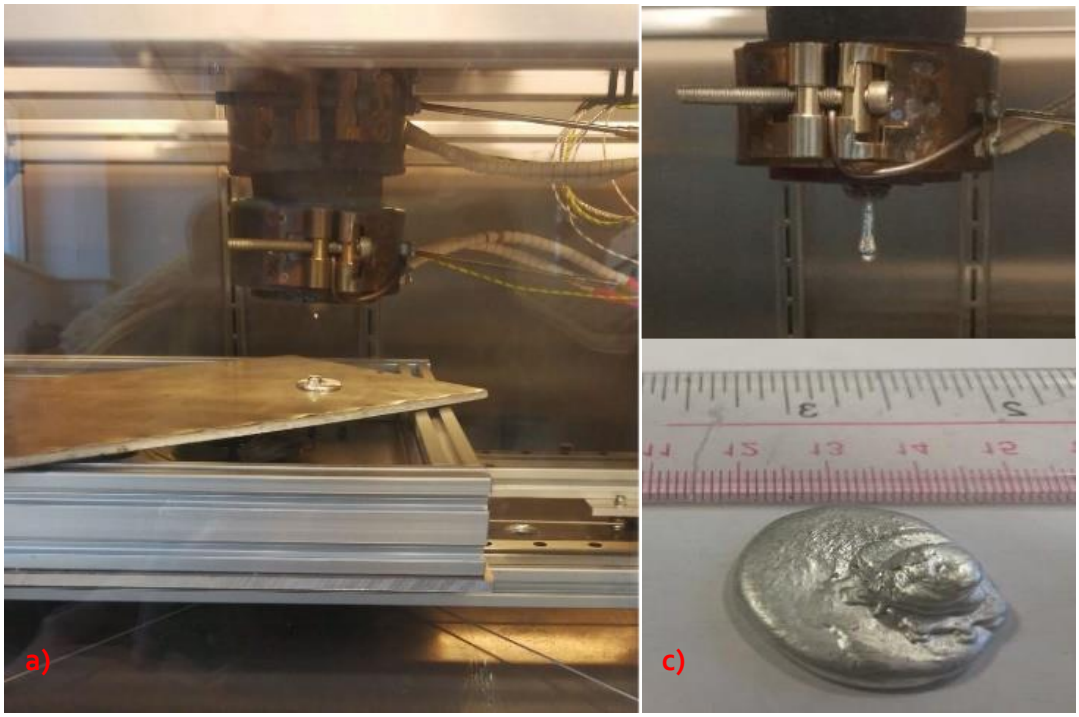

Figure 5.3 Printed layer of semi-solid alloy.

In the third attempt, the same process parameters and feedstock materials were used, with a Sn-30 wt.% Zn composition. Twenty-five minutes were given for the material to achieve the molten alloy, and stirring actions were applied continuously for 7 minutes while cooling to the desired extrusion temperature. The only difference was the shearing rate, where the motor speed was set at 100 RPM. Again, the materials were extruded successfully, and Figure 5.4 presents the results obtained from Test 3. Additionally, Figure 5.5 shows polished and etched cross-sections of the microstructure of the extruded specimens at different shear rates.

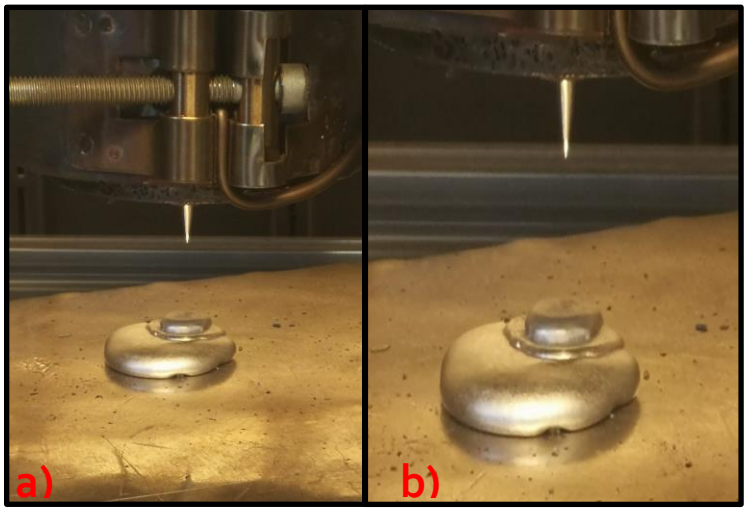

Figure 5.4 Deposited sample obtained during test 3.

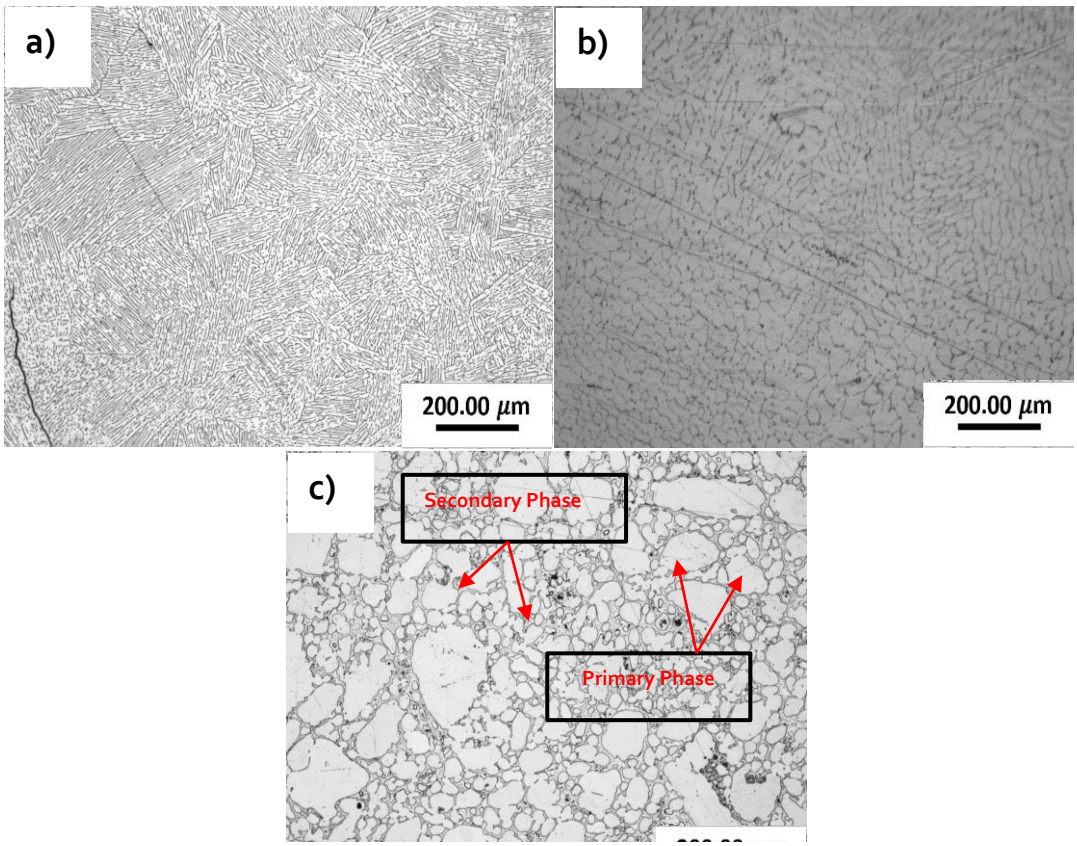

Figure 5.5 Optical micrographs showing microstructures of the Zn-30 wt.% Sn samples deposited at different shearing rates: a) 50 RPM, b) 75 RPM, and c) 100 RPM.

5.2 Discussion

The results presented in Figure 5.1, Figure 5.3 and Figure 5.4 illustrate the corresponding extruded samples at screw speeds of 50, 75, and 100 RPM, respectively. In the initial trial, the alloy emerged at a constant rate but exhibited rigidity and unsuitable behavior, likely due to insufficient shearing rate. However, at 100 RPM, the material extruded instantly with no rigidity, indicating a more liquid state, as observed in Figure 5.4. This result can be elaborated by the fact that raising the shearing rate by increasing the motor speed up to 100RPM resulted in a viscosity reduction of the metal slurry. Thus, the extrusion of the material mixture was too liquid, and it immediately fell out of the nozzle. Nevertheless, Adjusting the screw speed to 75 RPM allowed the alloy to be extruded onto the platform, displaying thixotropic behavior, akin to butter. Thixotropic behavior is crucial in semi-solid processing, as the viscosity of semisolid slurries depends on shear rate and time; increased agitation leads to fluidization, while viscosity rises with decreased shear rate. This phenomenon happens due to fragmentation and spheroidisation of dendritic crystals as the shear rate increases [23, 42, 273].

The microstructures of the deposited samples were optically characterized, and their cross-sections are shown in Figure 5.5. These micrographs reveal different magnifications of semi-solid microstructures for Sn-30wt.% Zn alloy extruded at different shearing rates. While some micrographs show a concentration of non-globular structures, others exhibit spherical shapes. The formation of a non-dendritic microstructure is critical for semi-solid processing. For instance, Figure 5.5a) depicts a microstructure from the sample extruded at 50 RPM, lacking evidence of a globular microstructure and instead showing strip-like structures throughout the sample. This finding is somewhat surprising given the fact that other research shows that semisolid alloy has non-dendritic structures with thixotropic properties. A possible reason for this could be that there was not enough shearing rate to break up the dendrites which resulted in a lack of diffusion between zinc and tin. However, Increasing the screw speed to 75 RPM, as shown in Figure 5.5b), led to a slight improvement, with the beginning of globular microstructure formation due to greater shear rates.

In the third test, represented by Figure 5.5c), the micrographs reveal significant growth in non-dendritic feedstock alloys of SSM. The microstructure shifted from dendritic to near-rounded grains, likely due to the increased shear rate. Where the shear rate was developed by increasing the motor speed from 50 RPM to100RPM for test 1 and 3, respectively and thereby allowing to break up dendritic growth and formulate near or spheroidal particle shapes. In accordance with the present result, this phenomenon was previously demonstrated for the effect of shear on solid particles shape[31]. However, despite these optimistic results, the particle size and distribution were not uniform as required for SSM processing. The observed grain shapes differed from the spheroidal particles reported in the literature. Those parts were fine, more rounded and the better primary globules microstructure. Hence, diverse consequences were found but these issues can be resolved. It can be resolved by applying different process parameters, alloy compositions and optimising the extruder design including heating elements and process control. So that, the investigations can be extended to employ engineered alloys including aluminium alloys, magnesium etc., as well as the disposition process, such as joining between two deposited layers. Additionally, the images in Figure 5.5c) show less entrapped liquid within the spheroid particles. Where the more entrapped liquid, the more porosity in the particles and this will lead to insufficient mechanical properties. Overall, the presence of entrapped liquid can result from inadequate shear and cooling rates during solidification[156].

- **Strategies for Improvement in Phase I**

In Phase I, several strategies could have been employed to enhance scientific knowledge, ensure result reliability, and improve repeatability. Firstly, a more extensive literature

review could have been conducted to better understand the phenomena related to semi-solid metal extrusion and additive manufacturing. This would involve studying established research in the field to identify key variables, mechanisms, and challenges. Additionally, experimental design improvements, such as conducting systematic parametric studies, could have been implemented to explore the effects of various process parameters on the outcomes. This would involve systematically varying factors like temperature, shear rate, and material composition to understand their individual and combined effects. Furthermore, the use of advanced characterization techniques, such as in-situ monitoring of material properties during extrusion, could have provided deeper insights into the underlying phenomena. Employing statistical analysis methods to analyze data and quantify uncertainties would also have been beneficial in ensuring result reliability and repeatability. Overall, a combination of thorough literature review, systematic experimentation, advanced characterization, and rigorous data analysis would have enhanced the scientific understanding and reliability of the outcomes in Phase I

5.3 Conclusion

This study of phase I was undertaken to demonstrate the capability of using a novel of AM extrusion-based process for deposition of semi-solid feedstock. This novel process is known as Layered Extrusion of Metallic Alloys (LEMA). An integrated screw-extruder and system were designed and employed to produce and deposit semi-solid alloy. The LEMA system was able to layer material successfully for additive manufacturing. These structures were produced by applying different process parameters including volume fraction of 0.50, imposing a screw speed of 50-100 rpm for 7 minutes. The printed samples of Zn-30 wt.% Sn alloy were then analysed to evaluate the microstructures. The implication of various distinctive shear rates was considered, and their possible effects were outlined. It was found that, while depositing material with a motor speed of 50 RPM failed to develop a typical microstructure of semi-solid alloys due to the insufficient shearing rate, further increasing the motor speed to 75 RPM resulted in microstructure improvement. However, motor speed of 100 RPM was better among all as its resulted micrograph has shown evidence of globular α-Zn microstructure typical for semi-solid fabrication processes. These outcomes seem to be consistent with other research which found that the shearing rate has a large effect on the apparent viscosity of an alloy. However, this result is subject to certain boundaries. The most important limitation lies in the difficulty of sustaining consistent rheological behavior of semi-solid slurries in the extrusion chamber. This demanded precise control over parameters like temperature, shear rate, and time. Furthermore, there were challenges in ensuring uniform deposition of the semi-solid alloy onto the target surface due to fluctuations

in the material's rheological properties. A parameter of shear rate was suggested to be one of the main reasons which could have affected the findings through these trials. It was found that by the properly managing shearing rate of the molten alloys (depositions form closely matching those mentioned in the literature review), the increased shear rate could lead to an improvement of homogeneous matrix alloys.

Overall, according to the macrograph of final prints, this test demonstrated that the integrated apparatus is capable of processing raw alloys in the thixotropic state and subsequently depositing directly through extrusion deposition. Further, the optical analysis concluded that although the current LEMA system is not totally capable to deposit materials of a high melting point. However, it could manage to print zinc alloys, i.e. low melting alloys, successfully with a moderately globular microstructure with thixotropic properties. As a result of that, the effort paves the potentiality of AM Extrusion-based module in the rapid production of inexpensive metal-3D-printing within the industrial applications. Nevertheless, more controlled trials will need to be done considerably including several alterations of the system, such as extruder design, temperature and extruder control, etc. that have to be established. These suggestions would be a fruitful area for further work.

6 A PISTON DISPLACEMENT PRINTER

6.1 Alloy Compositions

The main concept of extrusion and deposition of metallic filament alloy comes from the additive manufacturing of polymers using the fused deposition modelling technique. However, metallic alloy differs significantly from 3D printing with polymer materials using FDM. One of the most prominent differences is the rheological properties between molten polymer and semi-solid slurries. In both material conditions, the material exhibits a shear-thinning non-Newtonian behaviour, which is typical for pseudo-plastic materials. However, the low glass-transition temperature of polymers allows for filament softening over a wide temperature range, therefore, allowing readily extrusion through an outlet [35]. On the other hand, semi-solid alloy must be treated within a limited temperature range where the metallic alloy is in the region between solidus and liquidus lines in the equilibrium phase diagram [42, 274], with a desired morphology and fraction of solid. In this research, it was important to establish that alloys can fit within the scope of the developed AM extrusion method, i.e. materials that can be processed at semi-solid processing temperatures up to 380℃. The alloy used in this project is Zn-Sn alloy, which is widely employed in electronics applications and in connecting parts. The phase diagram of the Zn-Sn binary system, illustrated in Figure 6.1, is a simple one of eutectic type. This phase diagram clearly shows that some of these compositions can be used to create semi-solid slurries. This potential of using such alloy opens up possibilities for metal 3D printing applications, similar to those that use polymeric materials.

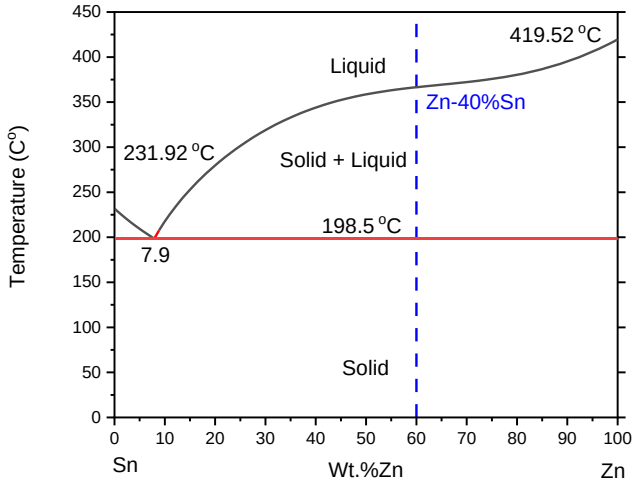

Figure 6.1 The phase diagrams of the Zn-Sn binary systems generated by Thermo-Calc software.

6.2 Thermodynamic Prediction by Thermo-Calc

The thermodynamic simulation is a good method to employ in understanding the solidification behaviour of the alloys. Thus, it was used as part of the alloy development process to help select the compositions that are best suited for the specified use here. The Thermo-Calc software was employed to study the liquid–solid transformation under non-equilibrium (Scheil) conditions using an SSOL4 database. The simulations should produce results that are close to reality for the proposed alloy systems. In this work and through preliminary thermodynamic calculations, predicting the melting range of the selected alloy as well as the solid/liquid phases for the determined temperature was possible. Despite carrying out multiple thermodynamic simulations, only the composition that demonstrated greater solidification intervals and lower liquid fraction sensitivity values within the working range will be considered in the context of this project. Figure 6.2 (a) shows the liquid fraction curves predicted by Thermo-Calc as a function of temperature for various compositions simulated in relation to the Zn-Sn system (the working temperature range is highlighted by dashed lines), and Figure 6.2 (b) displays the liquid fraction sensitivity to temperature (dfL/dT). The sensitivity is the derivative of the liquid fraction and reveals how much the liquid fraction changes with temperature. Moreover, to achieve a stable and controllable process, the sensitivity should be as low as possible in order to avoid significant variation in the liquid fraction. Studies have proposed that for better semi-solid processing, the value of (dfL/dT) should be less than 0.015 or $0.03°C^{-1}$ [200, 207]. This implies that a fluctuation of 1°C in temperature during the process would cause up to a 1.5% or 3% change in the liquid fraction.

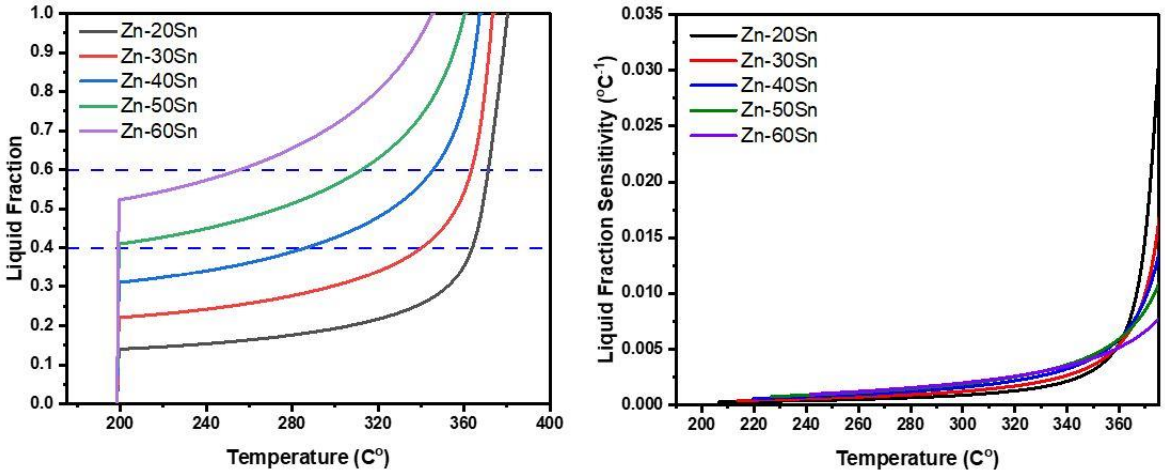

Figure 6.2 Illustrates simulated melting curve graphs for alloys of the Zn-Sn-system: (a) liquid fraction (Lf) versus temperature for Zn-XSn alloys, with X ranging from 20%–60%; (b) the sensitivity of the liquid fraction for the solid–liquid transition of different.

6.3 Analysis by DSC

Following the thermodynamic calculation stage, the alloy selected based on the criteria stated in the previous section was analysed by DSC to establish the fundamental thermal reaction properties of Zn-Sn alloys. Using this power compensation DSC equipment, the heat flow profiles achieved for the specimen were evaluated in terms of solidification behaviours. A small sample (~5 mg) was taken to perform the test for the thermal behaviour profile of the raw material during its melting and solidification processes. During the DSC test, the prepared specimen was heated from 30°C to 400°C at the rate of 10°C/min, held for 10 min and then cooled at the same rate as the initial heating temperature. At least three cycles were processed to avoid any thermal history. In addition, both the heat flow and the temperature behaviour were observed to obtain heating and cooling curves. The liquid fraction to temperature was then integrated from the information on the heat flow vs. temperature recorded from the solidification curve of the examined alloy.

6.3.1 DSC traces results

The phase transformation in the semi-solid interval generates peaks in the DSC curve during the solidification or melting reaction. Generally, a peak pointing downward on the DSC curve represents an endothermic transition while the peak pointing upward donates an exothermic transition. The measurements for the phase transition temperatures were evaluated in accordance with the recommendations in the literature [242, 255]. The eutectic reaction temperature was determined by the onset temperature of the first DSC peak during heating, and the peak temperature of the second peak was chosen as the

liquidus temperature. The onset temperature of the peak was calculated by investigating the intersection point between the baseline and the extrapolated tangent line of the heat flow peak, as discussed in section 4.3.2.4. A similar procedure was used for the DSC heat flow traces for the cooling curve. Figure 6.3 demonstrates the variations of the endothermic and exothermic peaks on the DSC curve for the as-received Zn-40Sn binary alloys at a heating/cooling rate of $10℃/min$. It can be observed that during heating, peak 1 is long, rising dramatically before suddenly dropping, whereas peak 2 is shorter and wider. In the cooling curve, on the other hand, both peak 1 and peak 2 are sharp. It is well understood that the DSC peak related to the melting of the eutectic portion of a microstructure is comparable to the one seen in a pure metal [275]. Consequently, the first DSC sharp peak during heating corresponds to the eutectic reaction: (Sn) + (Zn) ⟶ liquid. The temperature of the eutectic reaction indicates the beginning of melting, i.e. solidus temperature. The obtained onset temperature (198°C) of the eutectic peak corresponds very well to the predicted value for the Sn-Zn phase diagram (198.5°C), as shown in Figure 6.1. A related paper revealed that the eutectic reaction of the Zn-40Sn system would occur at a temperature of 199.6°C [275]. The minor variation can be credited to deviations among the experiment examinations. A similar discrepancy in eutectic temperature phenomena was also mentioned in various literature sources [248, 276, 277]. The second peak of the endothermic curve (heating process) of the binary alloy is related to the complete melting of the solid phase (Zn), which is related to the liquidus temperature; whereas in exothermic reaction (cooling process), it is considered as the first stage of solidification. The second thermal effect of the heating curve appears at approximately 365°C, which is slightly lower than the simulated liquidus temperatures of the binary Zn-40Sn alloys phase diagram (366.6°C) in Figure 6.1 . However, this is consistent with the value of the liquidus temperature reported in a previous study [247]. During the cooling process from a liquid state, the undercooling of the investigated sample was shown to have temperatures around 11°C higher and 5°C lower. The DSC undercooling is defined as the difference in temperature between the endothermic (heating peak) and exothermic peaks (cooling peak) [278]. The onset, end and peak temperatures during heating and cooling runs for each peak are tabulated in Table 6.1.

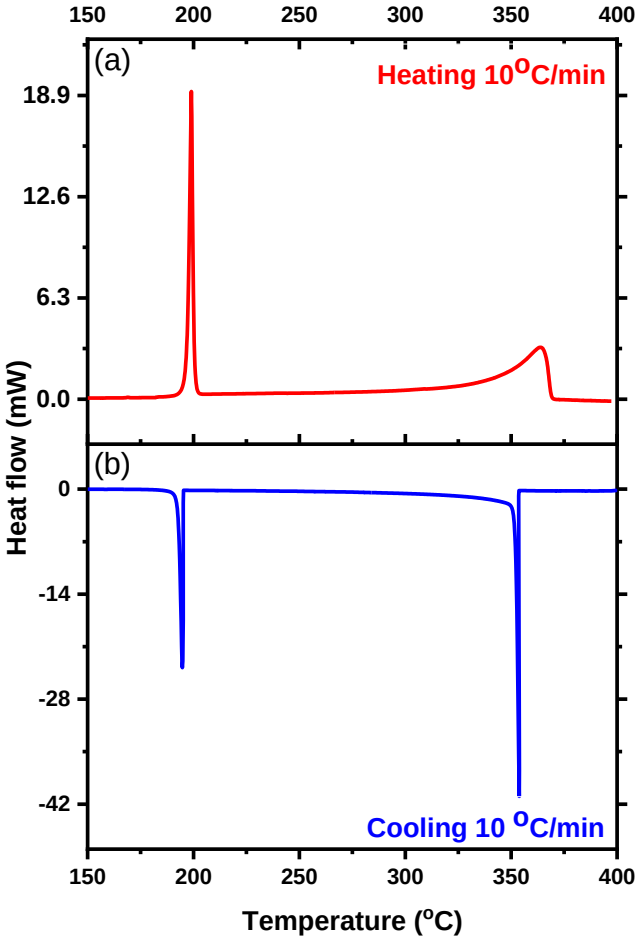

Figure 6.3 Shows the DSC traces for (a) melting and (b) solidification of as-received Zn-40Sn alloys.

Table 6.1 A comparison of the DSC results with the thermodynamic calculations for Zn-40Sn alloy.

	1st Peak			2nd Peak		
	Onset	Peak	End	Onset	Peak	End
Heating Cycle	198	199	205	340	365	270
Cooling Cycle	354	354	340	196	194	188

6.3.2 Liquid fraction calculated by DSC

As a function of temperature, the liquid fraction plays a vital role in the current work, enabling the successful extrusion and deposition of semi-solid alloy. Figure 6.4 displays the liquid fraction-temperature relationships derived from DSC traces of the heating curve for Zn-40Sn alloys. This curve was achieved after integrating the peak partial area under the DSC curve. It can be observed that the trend for the experimental curve changes suddenly when the eutectic phase begins to melt upon heating. This transformation takes

place over the temperature range during the heating or cooling curve. The figure also depicts two simulated curves, the first corresponding to an equilibrium process and the second to a Scheil process (non-equilibrium). It can be seen that the liquid fraction calculated by both equilibrium and Scheil conditions is identical. This is due to the fact that the Zn-Sn alloy phase diagram is a simple eutectic type and has a limited solubility of elements in one another, so the Scheil process will be the same as the equilibrium process [279]. In the DSC experimental curve, it is revealed that the liquid fraction curve obtained by DSC coincides with those calculated for the binary Zn-Sn phase diagrams of the alloys in Figure 6.1. Furthermore, a comparison of the simulated (equilibrium and Scheil) and the DSC liquid fraction curves shows very little variation within the proposed working window between 40% and 50% liquid fraction. The simulated working temperature range is approximately 64°C, while the experimental temperature range is nearly 53°C. Consequently, the thermodynamic calculations coinciding well with the actual thermal behaviour of the examined alloy obtained experimentally should also be considered.

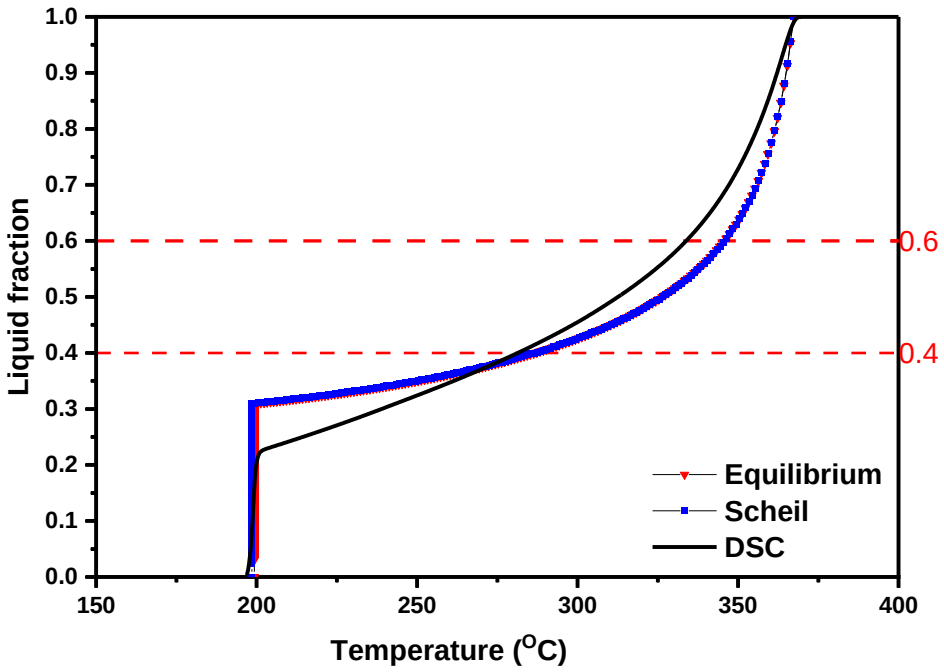

Figure 6.4 Calculated liquid fraction vs. temperature obtained by DSC heating curve compared to the predicted value of Thermo-Calc.

6.4 Microstructure of the As-received Ingot

The raw material was metallographically examined under a scanning electron microscope (SEM) to determine the distribution of the different phases at low and high magnifications. Figure 6.5 exhibits SEM images of the typical microstructures of the as-received Zn-40Sn alloy. As illustrated, the microstructure of the hypereutectic Zn-40Sn alloy comprises a bright phase and a dark colour phase indicated as eutectic β-Sn/α-Zn phase and primary α-Zn phase, respectively [247]. Observables are the randomly oriented primary α-Zn dendrites phases (zinc-rich, plate-like shape) surrounded by eutectic mixture β-Sn/α-Zn phases. The eutectic mixture can be observed in greater detail under higher magnification on the right side in Figure 6.5 (b). The eutectic structure is made up of a relatively small size of scattered α-Zn particles dispersed in a eutectic β-Sn matrix. It should be mentioned that the fraction of the primary α-Zn phase decreases as the Zn content decreases, while the fraction of the β-Sn/α-Zn eutectic increases [280], as expected from the phase diagram in Figure 6.1.

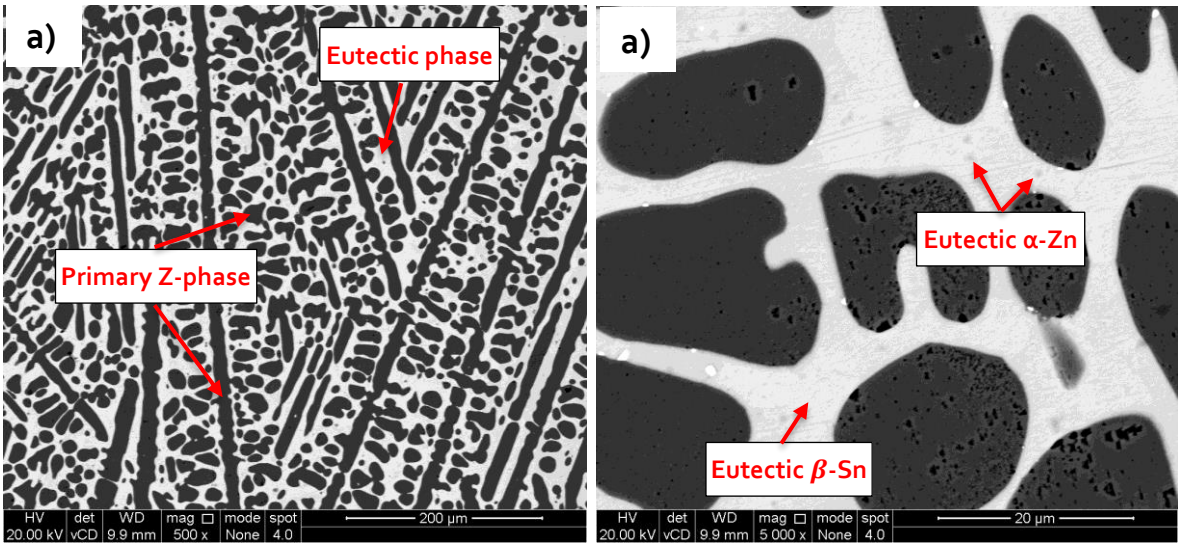

Figure 6.5 SEM micrographs of microstructures of as-cast Zn-40Sn alloy: (a) lower magnification composed of primary α-Zn and the eutectic Sn-Zn phases, and (b) higher magnification comprised of insert details of the eutectic matrix (β-Sn+α-Zn structure).

6.5 Microstructure Development of the Deformed Billet

As discussed earlier, the fabrication of semi-solid billets with a liquid phase surrounding near-spherical solid particles is a significant step needed for SSM processing. This thixotropic feedstock billet required for semi-solid processing can be produced by employing a mechanical melting process, a method known as liquid metal treatment. This process eliminates the dendritic morphologies typically found in the casting process and

transforms them into novel globular features. Nonetheless, another way to prepare the feedstock billet of a metal alloy is through solid-state deformation of the as-cast material before isothermal heat treatment [188, 281]. The solid-state hot or cold deformation imposes a strain level sufficient to disrupt the cast structures and trigger recrystallisation, enabling successful dendrite-to-globule transformation during subsequent isothermal heat treatment [188, 281]. Figure 6.6 shows the optical microstructure of the Zn-40Sn alloy in the longitudinal section after the cold working process. The microstructure of the deformed sample is characterised by an alternating pattern of elongated α-Zn plate-like grains and a surrounding eutectic mixture distributed around the α-Zn grains. The heavy plastic deformation caused the dendrite Zn- phase to break, resulting in the distorted microstructure displaying the textured features aligned along the extrusion direction. This distortion and stored strain energy in the extruded material provide the driving force for the recovery and recrystallization of new grains during the reheating phase.

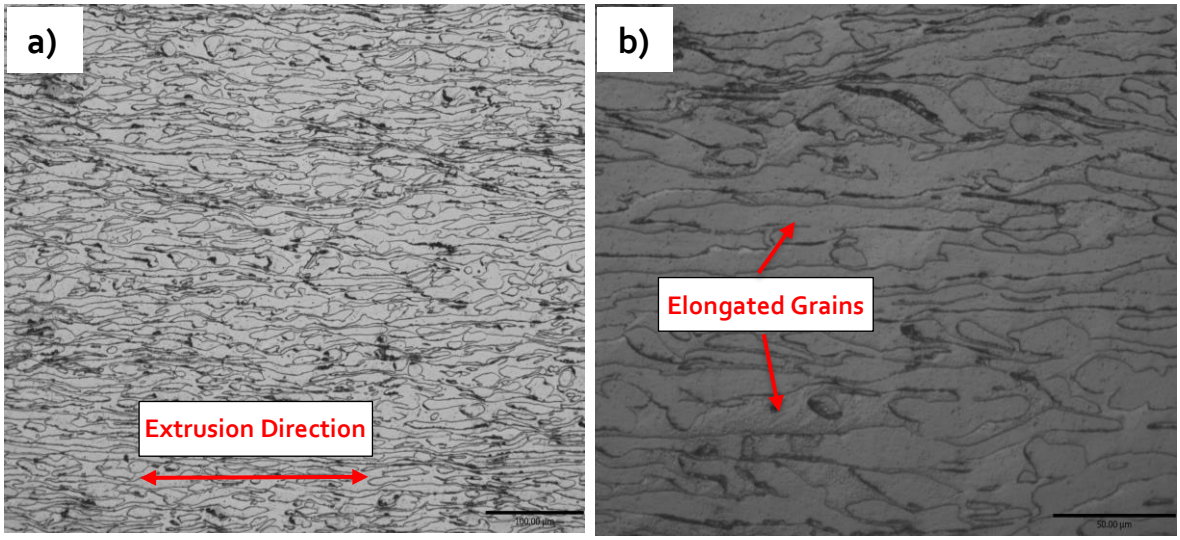

Figure 6.6 An optical micrograph of as-deformed Zn-40Sn alloy microstructures (a) at lower magnification and (b) at higher magnification.

6.6 Microstructure Development of Deformed Billet During Partial Re-Melting

It is well known that the rheological properties of semi-solid billets are affected by several parameters, including temperature, shear rate, time, and solid phase morphology [17]. Moreover, the rheological characteristics of materials in SSM processing are believed to be more attractive for industrial applications when solid particles have more spherical morphology and smaller diameter [145]. Materials with spherical particle geometry have lower viscosity values and less liquid phase segregation than materials with dendritic morphology, facilitating the flow behaviour of SSM slurries and creating more

homogeneous microstructures [144]. Because of this, semi-solid isothermal heat treatments were carried out to support the results of thermal analysis and thermodynamic simulations. These treatments were also used as a supplementary means to investigate the mechanisms involved in liquid formation and solid particle spheroidisation via the metallographic evaluation of the specimens subjected to heat treatments. Following solid-state deformation, the billet undergoes partial re-melting, in which only a fraction of the alloy is transformed into liquid. The heat treatment process was carried out over different temperatures in the transformation of the cold-worked microstructure of the samples into a non-dendritic microstructure before being water-quenched. Figure 6.7 shows an optical microscope microstructure evaluation of semi-solid billets after isothermal treatment at different heating temperatures and holding times.

The Zn-40Sn materials were heated to temperatures ranging from 282°C to 247°C, with soaking times varying from 2 to 20 min. Based on simulation and DSC analysis data, these temperatures correspond to liquid fractions ranging between 30% and 70%. The bimodal microstructures exhibit two distinct phases: darker for the primary phase and lighter for the eutectic phase. Under nearly all conditions, a semi-solid microstructure with a liquid phase surrounding nearly sphere-shaped solid particles was established. The microstructure is composed of almost α-Zn globular or equiaxed grains with a liquid film around them. The spheronisation process is an important stage of semi-solid microstructure development in the semi-solid isothermal heat treatment process, causing irregularly shaped solid grains to round out. During the isothermal heat treatment, the eutectic phase melts, firstly creating a liquid phase around the solid grains, and then the solid grains tend to transition to a spherical shape. This globularisation mechanism is readily visible in Figure 6.7. It is evident that by increasing the isothermal temperatures and soaking times, the quantity of the liquid phase at grain boundaries grows and penetrates between the adjacent grains. Consequently, solid grains gradually develop globularly. However, at 282°C for 2–8 min, some elongated grains can be clearly seen, indicating that the liquid phase (30%) created during partial re-melting at 282°C for 2–8 min is inadequate for complete spheroidisation. Furthermore, a prolonged isothermal holding time or a higher isothermal temperature could result in significant coarsening of solid particles, rendering them undesirable for thixoforming. This can be seen with the extension of the isothermal temperature to 347°C, where the coarsening of solid grains in the Zn-40Sn alloy is found to be very substantial, and the fine solid particles almost completely vanish. When the isothermal holding time further increases, the reduction of the solid fraction occurs, where the α-Zn solid phase starts melting and re-solidifying in the form of a fine dendrites matrix.

Nearly all the grain growth phenomena observed in these experiments can be attributed to two different mechanisms: coalescence and Ostwald ripening. These mechanisms are generally believed to operate simultaneously and independently during partial re-melting as soon as the liquid is formed. Coalescence is the process by which two or more small particles merge upon contact to form a large and irregular solid particle caused by the curvature of the grain boundaries [282-285]. When two or more particles collide, they form solid necks on the grain boundary and spheroids due to material transport in the neck area. Coalescence is thought to promote solid content due to an increase in solid-solid bonds; therefore, it is typically dominant at the early stage of partial re-melting and the low content of the liquid fraction [286]. Correspondingly, the Ostwald ripening mechanism, which dominates at longer-time and high-liquid fractions, involves the growth of large solid grains and the dissolution of small solid grains. Because of the difference in the curvatures of solid particles, larger particles with low curvature grow gradually, whereas small particles with high curvature dissolve rapidly during the Ostwald ripening process. Meanwhile, the crystalline grains become more spherical [284, 286-288]. Thus, the consequence of coalescence is a development in grain size as well as a decrease in roundness, while Ostwald ripening contributes to an increase in average grain size and a decrease in the number of solid grains. Therefore, grain growth is driven by both the coalescence and Ostwald ripening hypotheses.

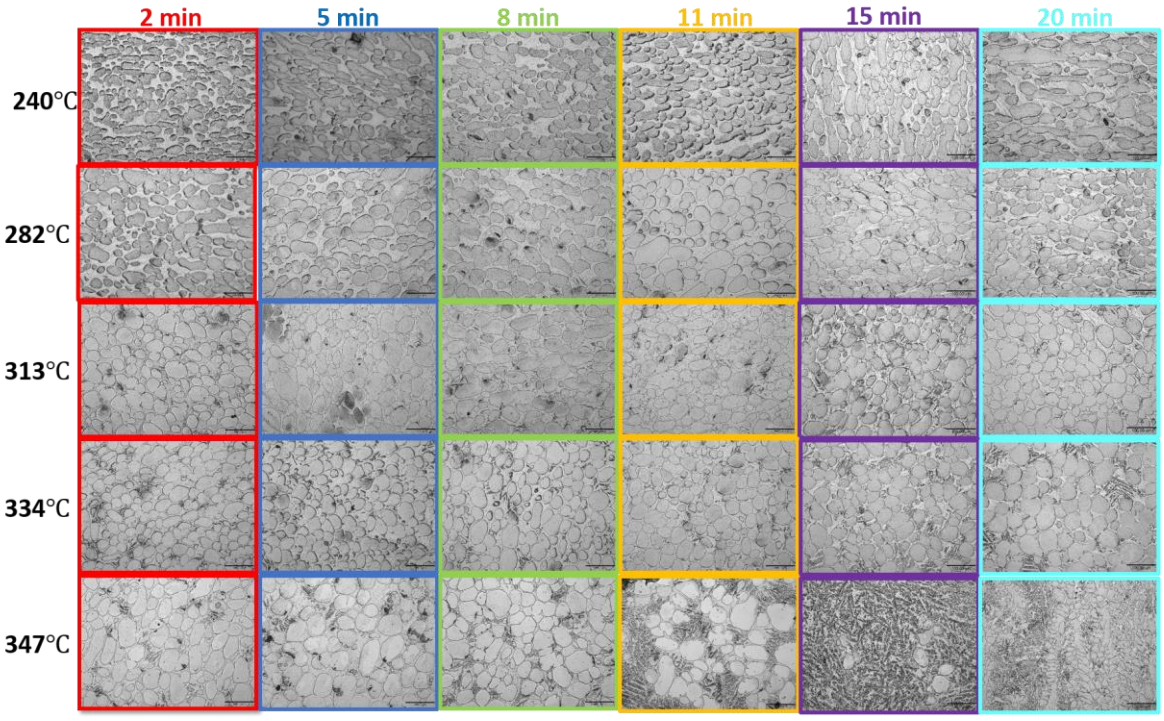

Figure 6.7 Displays the semi-solid microstructure evolution of Zn-40Sn materials as isothermal temperatures increased from 240°C to 347°C and prolonged the soaking time from 2 min to 20 min.

The average size and shape factor of the solid grain can be used to assess the microstructure of semi-solid thixotropic billets. Semi-solid materials with a smaller average of solid grain size have better mechanical properties after thixoforming, whereas materials with a greater shape factor enhance thixoformability processing [289]. The average grain size (diameter) and shape factor (circularity) were calculated using equations 1 and 2, respectively [272]:

$$SF = 4\pi A/P^2$$

Equation 6.1

$$D = 2\sqrt{(A/\pi)}$$

Equation 6.2

where A is the area of the solid particle and P is the perimeter of the examined primary particle. If the SF is equal to 1.0, this indicates that the grains are perfectly spherical.

Figure 6.8 illustrates the relationship between average grain size and shape factor under various semi-solid treatment conditions determined by quantitative metallography through the analysis software ImageJ. The average grain size and roundness of the microstructure conducted at 347°C for soaking times ranging from 11 to 20 min were very difficult to establish due to its irregular shape; therefore, the process condition of isothermal temperature at 347°C was not considered here. Figure 6.8 (a) shows that when the material is subjected to a given partial re-melting temperature, the average grain size increases continuously with increasing holding time. Additionally, in the case of the materials that were treated to the same isothermal holding time, the average grain size of materials reheated at higher temperatures is larger than that of those reheated at lower temperatures. However, when the material was exposed to isothermal temperatures of 313°C and 334°C for 5–8 min, the average grain size for the material reheated at 313°C was slightly larger. But when the holding time is longer than 8 min, the average grain size for the material reheated at 334°C is somewhat larger than the material reheated at 313°C under the same condition length of isothermal holding time. Additionally, Figure 6.8 (a) shows that increasing the holding time to exceed 5 min for all temperature treatment conditions causes the solid particles to coarsen. Hence, the average grain size increases along with the isothermal holding time. The primary mechanism for the structural coarsening of solid particles is the coalescence ripening phenomenon. The coalescence ripening phenomena was the main structural coarsening mechanism of solid particles during the period of the isothermal soaking process [42]. Contrasting the grain size measurements, Figure 6.8 (b) presents the effect of holding times on the shape factor at different temperature ranges for the as-deformed semi-solid billet alloy. Here, the general shape factor trend of the solid particles of all specimens slowly increases initially, but its reduction is apparent as the holding time is further elevated, suggesting that the

roundness of the solid grains improves at first, followed by worsening. However, when the holding time was 5 min at 313°C, the shape factor touched 0.82, demonstrating the best globularity among the solid particles. This outcome is inconsistent with the findings of an examination conducted by Fan et al. [287]. The shape factor rises initially due to the spheroidisation degree of the merging solid grains and then falls, owing to the irregular growth of large grains caused by Ostwald ripening [282, 290]. Given the comprehensive study of the influence of isothermal temperature and holding time on the size and sphericity of grain particles, it can be concluded that the average grain size of ~0.60 µm and the shape factor of ~0.82 are appropriate processing parameters for the Zn60-Sn40 alloy. From this viewpoint, semi-solid treatment conditions of 313°C and 5 min are the most suitable processing parameters to produce ideal semi-solid billets that have a relatively rounded microstructure and moderate grain size. Such features (small particles combined with high sphericity) have the potential to minimise liquid phase segregation as well as the force required to promote semi-solid material flow [28].

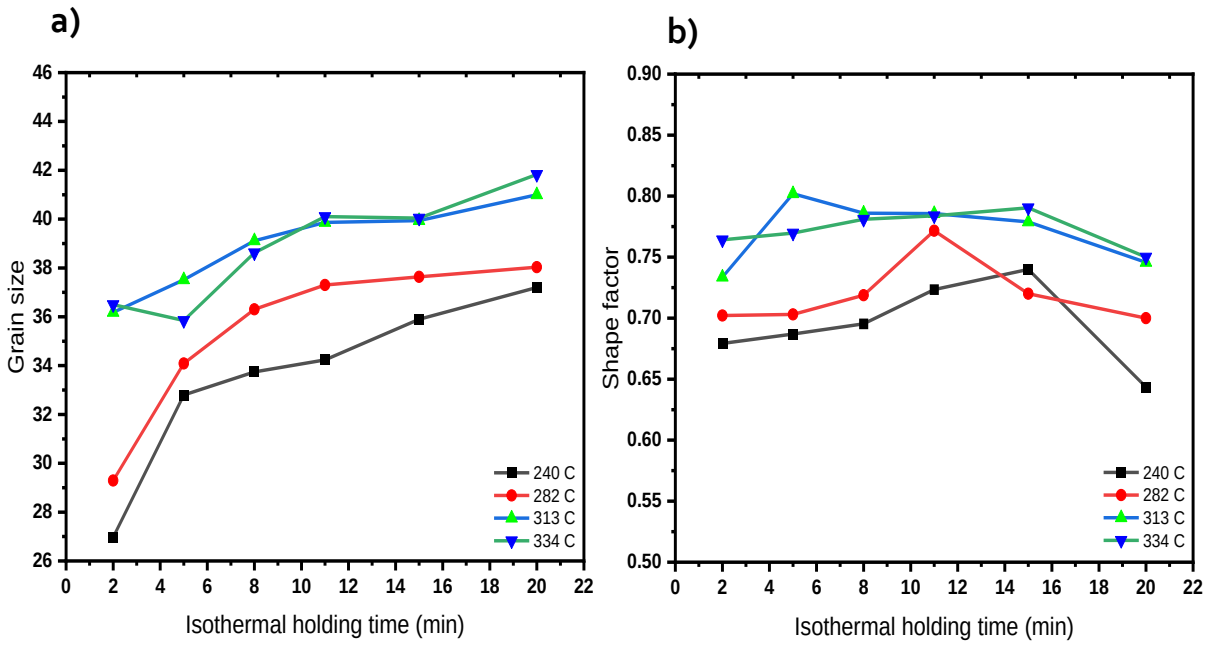

Figure 6.8 Shows (a) the average grain size and (b) roundness of Zn-40Sn alloys fabricated under different semi-solid treatment conditions.

6.7 Optimisation and Investigation of the Influence of Printing Parameters

The deposited metal layer is the fundamental element in the fabrication of 3D functional metal objects, as the 3D printed part is made up of a sequence of single layers. The geometrical dimension and the surface condition of the single layer have an immediate impact on the component's quality and shape. Therefore, it is vital to be able to control the metal prints during the manufacturing process. To achieve this, several key process

parameters need to be studied, which may affect the formation of a uniformly extruded metal line. The extrusion and deposition process parameters—such as nozzle diameter, extrusion speed, substrate moving speed and nozzle-to-substrate distance—play an important role in the continuous deposition of the metal alloy. Adjusting these parameters allows for the fabrication of an excellent single layer. The main factors considered in determining the general level of excellence of the single layer include the geometry shape quality and the width of the layer. The geometry shapes' quality of the printed layer was evaluated and assessed visually based on the degree of layer uniformity, i.e. stability and appearance. To investigate the effect of an individual parameter on the layer width and shape quality, only the selected parameter is changed while the other parameters remain constant. It was possible to establish a correlation between the process parameters and the printed metal layer. Furthermore, multi-layer parts can be achievable following the experimental identification of a suitable process window for the manufacture of a single layer. Hence, each of the above-mentioned parameters was iterated, and the optimal process parameters were chosen to successfully build a series of 3D metal components using the layered extrusion of engineering metal alloys (LEMA) technology.

6.7.1 Effects of nozzle diameter

The deposited structure of the first layer is the foundation of a 3D metal part, and it may affect the adhesion of the metal to the substrate and the quality of the final print. The use of AM metal extrusion to produce small structures requires that the deposited layer should be thin, and decreasing the width of the metal line via the optimisation of the nozzle diameter is one effective means to meet the requirement. Choosing the optimum nozzle diameter is very significant and would offer an ideal printing process, not only in terms of mechanical properties and geometrical accuracy of the produced part but also for extrusion time [291]. In general, larger nozzle diameters extrude more material, resulting in thicker and wider lines with less extrusion time; however, this can lead to a loss of print resolution. On the other hand, utilising a smaller diameter size of the nozzle can generate objects with greater detail. However, a lower flow rate of deposited material through the nozzle causes a longer extrusion time [292]. Thus, the nozzle diameter is a key factor in obtaining stability and maintaining the consistency of the printed line during the process. Given the importance of the nozzle diameter in the flow of liquid metal and printed part quality, preliminary experimental work with four distinct nozzle diameters (0.75 mm, 1.00 mm, 1.5 mm, and 2 mm) was employed in this research to identify line shape during material extrusion and establish which nozzle diameter would be best suited for the remaining printing processes. The critical process settings listed in Table 6.2 , including extrusion temperature, extrusion velocity, X-Y substrate velocity, and the distance between the moving substrate and the orifice tip, were kept constant throughout the

operating process. To evaluate how the different nozzle diameters influenced the sizes of the printed metal lines, the width of each printed line was determined, and the average values were used to evaluate the printing resolution.

Table 6.2 Configuration of extrusion parameters to investigate the impacts of nozzle size.

Printing parameters	Value
Extrusion Temperature ($℃$)	$\approx 313℃$
Extrusion speed	$20\ mm/min$
X-Y moving substrate velocity	$200\ mm/min$
Orifice tip-to-substrate distance (mm)	$3\ mm$

The initial test was performed using a 0.75 nozzle diameter. However, in addition to the increased extrusion force, the metal slurry was clogged at the nozzle tip and, hence, did not allow for proper deposition. The nozzle clogging was resolved by increasing the heating temperature in the extrusion chamber to allow material to exit the nozzle. However, higher temperatures resulted in deposited material with a high fraction of liquid and, as a consequence, uncontrolled material extrusion, decreasing the process resolution. The reason for this is not clear, but it may have something to do with nozzle diameter, where the orifice tip diameter of 0.75 mm can be considered too small for the application involving the extrusion of semi-solid material containing solid particles capable of accumulating in the nozzle opening and causing obstruction. This result mirrors those of the previous studies that have examined the extrusion and deposition of semi-solid metal alloys. Jorge Mireles et al. experienced the same issue, and in trying to resolve it, they modified the nozzle diameter of an FDM 3000 system from 0.406 mm to a larger diameter of 1.588 mm to minimize nozzle clogging and eliminate buckling at the liquefier entry [55]. A study was performed by Chen and colleagues [40] in which they successfully realised direct metal writing of metallic alloys in the semi-solid condition with the use of a nozzle diameter of 1 mm. Similarly, Jabbari and Abrinia investigated three different nozzle outlet sizes, 0.5 mm, 1.0 mm and 2.0 mm for semi-solid metal extrusion and deposition [61]. Their experimental data suggested that metal extrusion using an outlet diameter of 0.5 mm was not practicable for low volume content of solid fraction (fs < 0.3) because of the aggregation of solid particles and clogging of the nozzle opening. Nevertheless, the clogging phenomenon was negligible for nozzle diameters between 1 and 2 mm. Recently, Lima et al. demonstrated the feasibility of using a fused filament fabrication technique to process biodegradable Mg-Zn alloy in the semi-solid state. The investigation was performed at 380, 400 and 420°C, corresponding to a liquid fraction between 0.5 and 0.8; and they concluded that a continuous extrusion flow was successfully performed without

obstructions and discontinuities only at the highest temperature and nozzle diameter of 1.0 mm. Consequently, based on the above-mentioned information, the nozzle diameter of 0.75 mm has been excluded from this investigation to mitigate potential solid particle accumulation and nozzle-tip blocking.

Figure 6.9 exhibits a comparison of metal lines produced by various nozzle inner diameters. As demonstrated, all three nozzles managed to deposit metal structures. Despite the fact that the printed layer is continuous, different widths can be seen at some locations of the printed lines. The relationships between the diameter of the nozzle and the measured width of each single line are summarised in Table 6.3. Extrusion through the 0.75 mm nozzle was not feasible because it required higher liquid fractions to prevent the accumulation of solid particles, where higher amounts of solid fraction would lead to blockages in the nozzle. However, A nozzle diameter of 1.00 mm was able to extrude a continuous single layer with a width of 2.65 mm. Additionally, under the same printing parameters, layer widths of 2.25 and 2.7 mm were formed using nozzle diameters of 1.5 and 2 mm, respectively. As can be seen, layers deposited by a 1.5 mm and 2 mm nozzle diameter are 50% and 36% larger in width than their inner nozzle diameters, respectively. In contrast, the layer extruded through a 1.00 mm nozzle is 165% bigger than the exit nozzle diameter. These conflicting experimental results could be associated with the nature of the nozzle. In the narrow nozzle, the metal slurry was stressed, and some of the deformation energy was elastically stored. Hence, when the material exits the extrusion nozzle, the melt is no longer restricted by the wall of the print nozzle, reducing stresses occurring on the materials, and releasing the elastically stored energy [124]. This phenomenon may result in considerable variation in the extruded print from what is expected. In comparison with the metal line fabricated by the nozzle whose diameter is equal to 1.5 mm, the metal lines fabricated by nozzle outlets of 1.00 mm and 2.00 mm were thicker; this feature is undesirable in 3D printing fine structures. From these results, it can be concluded that the different nozzle diameters determine the road width, which, in turn, affects the accuracy of the finished components. Hence, based on a comparison of the average layer width with different nozzle channels, a nozzle exit of 1.5 mm was adopted as the suitable one.

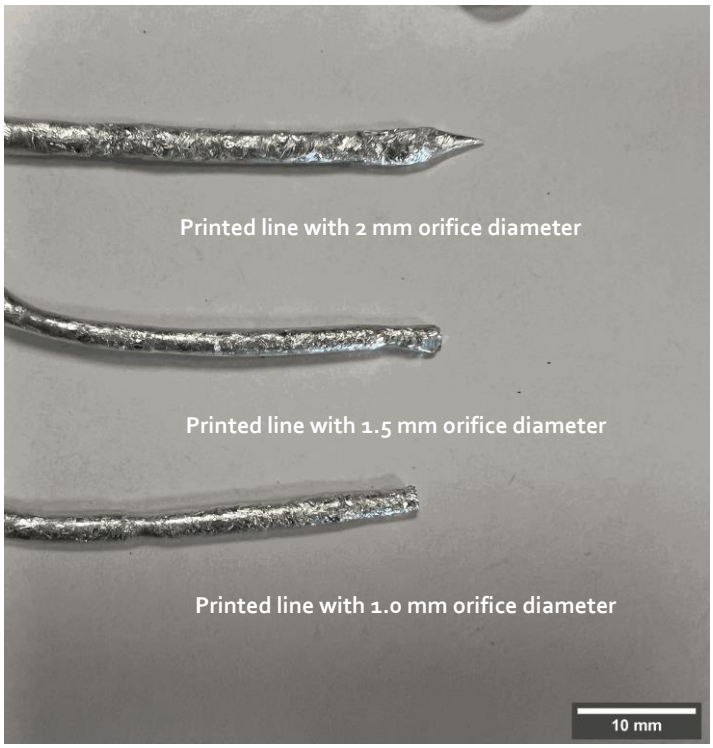

Figure 6.9 The metal lines fabricated with different nozzle diameters.

Table 6.3 Mean values of layer width extruded with varied nozzle diameters.

Nozzle inner diameter (mm)	Average value	% Difference
0.75	n/a	n/a
1.00	2.65	165%
1.5	2.25	50%
2.00	2.7	35%

6.7.2 Effects of extrusion speed

The influence of extrusion speed is a critical parameter in the 3D printing process. Data from preliminary studies have identified that the formation of the extruded material shape can be linked to the extrusion speed [293]. In this test, a plunger-based extrusion driven by a universal mechanical testing machine was used in the printing process. The extrusion speed can be controlled via the machine controller box. Hence, the moving plunger pushes the molten material into the extrusion barrel before being deposited onto a substrate. To obtain a proper metal print, the extrusion speed must be controlled within a certain range. During the material deposition process, the extrusion speed influences the molten metal flow rate. If the extrusion speed is too high, more molten metal will be layered, and it may cause a failure in controlling melt flow, which, in turn, results in the failure of the entire print. If the extrusion speed is too low, it may lead to inconsistent layer formation.

Therefore, managing the material metal flow rate during the printing process is vital. The consistency of printing an even metal path can be enhanced by taking into account the evolution of the thickness of the deposited line owing to the alterations in extrusion speed. Furthermore, by choosing the optimum extrusion speed, other defects can be avoided, including the microstructure coarsening process and segregation of the semi-solid alloy [60]. To verify that the extrusion speed does indeed affect the road width of the printed part, experimental extrusion investigations were conducted under extrusion speeds of 10, 20 and 30 mm/min. The other major process parameter values are shown in Table 6.4. Single layers were extruded with an orifice diameter of 1.5 mm, and the width of the extruded single layer was determined and subsequently plotted for comparison, as presented in Figure 6.10.

Table 6.4 Configuration of extrusion parameters to investigate the impacts of extrusion speed.

Printing parameters	Value
Extrusion Temperature ($\mathcal{C}$)	≈ 313 ℃
Nozzle diameter	$1.5\ mm$
X-Y moving substrate velocity	$200\ mm/min$
Orifice tip-to-substrate distance (mm)	$3\ mm$

The extrusion process was started with a minimum extrusion speed of 10 mm/min, as shown in Figure 6.10. Although the average width was recorded here (≈ 1.9 mm), the deposition process was unstable, mainly owing to a lower extrusion rate. This may cause a variety of issues related to the unstable dimensions of the deposited specimen. The approximately steady physical measurements were observed when the extrusion speed reached 20 mm/min. At this stage, the nozzle of the 1.5-mm outlet was able to deposit a straight line with an average width of 2.3 mm. However, when the extrusion velocity increased to 30 mm/min, more material was forced out from the orifice of the nozzle, contributing to the dramatic increase in the width of the measured line (≈ 4.1 mm). It is essential to control the extrusion speed, which affects the material flow rate and, hence, the width of the fabricated line. Therefore, an extrusion speed of 20 mm/min resulting in a stable line width with minimal variation, was selected in this study.

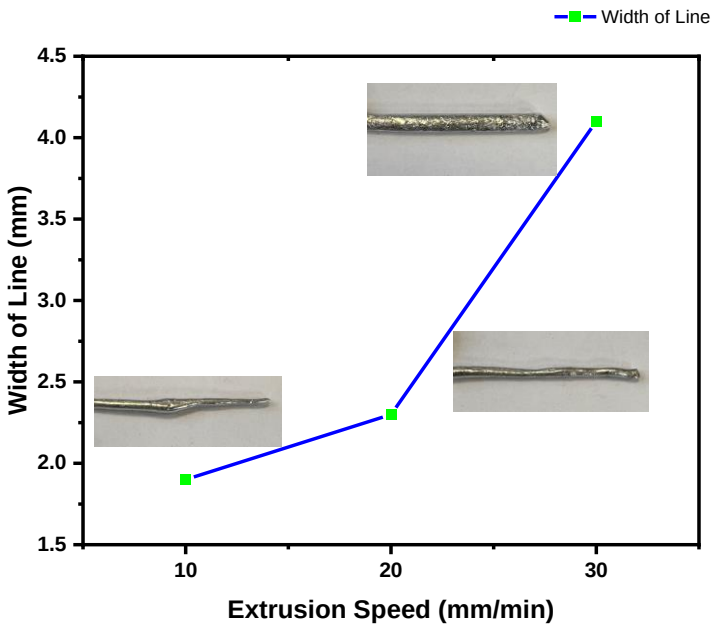

Figure 6.10 Effect of the extrusion speed on the width of the printed line.

6.7.3 Effect of nozzle tip-to-substrate distance

The nozzle-bed distance is one of the critical factors in print quality during the extrusion process. In the proposed metal 3D printing machine, the thixotropic alloy flows across the space between the nozzle and the moving substrate, which shapes the deposited lines. Accordingly, the distance gap will impact the printing resolution. In practice, at higher nozzle-to-substrate distances, the print route can become unstable, resulting in the breakup into discrete prints due to inadequate adhesion to the platform. Furthermore, a high tip-to-substrate distance increases the travel duration of the printed line through the air in relation to the drying time. This causes the materials to solidify before reaching the building platform, resulting in unacceptable substrate adhesion and imperfect layer bonding. On the other hand, too-small nozzle-to-substrate distances cause the departing material to smear or even damage the nozzle tip [61, 294, 295]. Therefore, accurate spacing is essential for manufacturing structures with the desired width line. To demonstrate a practical application and choose the appropriate tip-to-substrate distance, metal lines were printed with three different distance values ranging from 1.5, 3 and 5 mm. The other key process parameters are shown in Table 6.5 . A gauge block was used to determine the distance between the nozzle tip and the substrate. To evaluate the influence of the distance on printing resolution, the morphology and width of the deposited metal lines were examined.

Table 6.5 Configuration of the extrusion parameters to investigate the impacts of nozzle tip-substrate distance.

Printing parameters	Value
Extrusion Temperature ($℃$)	≈ 313 ℃
Extrusion nozzle	$1.5\ mm$
Extrusion speed	$20\ mm/min$
X-Y moving substrate velocity	$200\ mm/min$

Figure 6.11 shows the influence of the nozzle-to-substrate distance on the extruded material's morphology and width. Based on the observed data, it was clear that a nozzle-to-substrate distance of about the same size as the nozzle diameter resulted in over-extruded material with an uncontrollable and excessive spreading of printed material (line width ≈ 4.5 mm). This finding was expected, given the limited space available for extrusion. The extruded material spread horizontally over the X-Y platform as it was squeezed between the bed and the extrusion nozzle, explaining the observed rise in measured line width. When the distance between the nozzle and substrate was increased to twice the diameter size of the nozzle, a relatively well-defined material could be formed. Furthermore, at a higher nozzle tip-to-substrate distance, which is about three times the size of the nozzle diameter, the gravity and dragging impacts become more pronounced, resulting in a stretched printed metal line whose width considerably reduces. To conclude, when there is a 1.5 mm gap between the nozzle tip and substrate, the variance of the printed line width is negligible, demonstrating that the optimum nozzle-to-substrate distance forms a cross-section of the deposited metal lines.

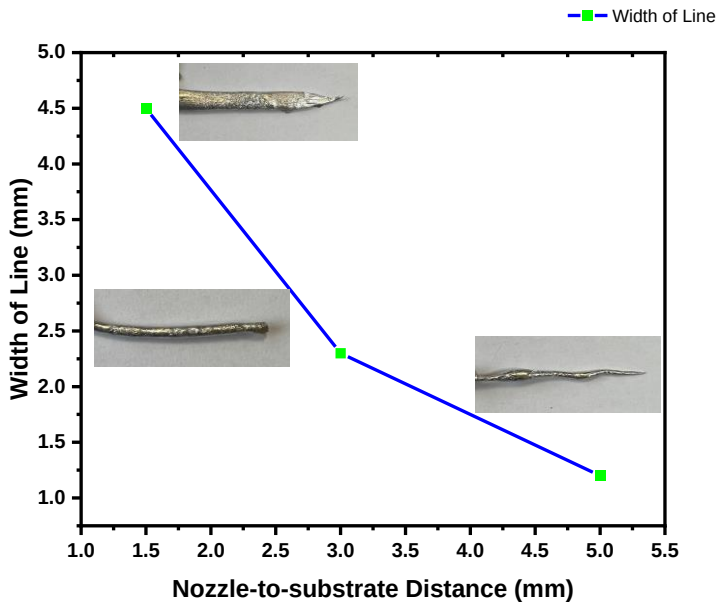

Figure 6.11 Effects of the nozzle-to-substrate distance on the print morphology and width

6.7.4 Effects of X-Y substrate moving speed

The last step in the optimisation and investigation of the impact of printing parameters on the quality of the final printed components is to optimise the X-Y substrate speed. If the substrate speed is very low, the deposited material may become sandwiched, resulting in forced flow. On the other hand, a quicker moving substrate speed is normally favoured to reduce overall building time and lower costs. However, if it exceeds the critical threshold, a stretching or sagging phenomenon in the printed metal line is triggered. An additional increase in the moving substrate speed may result in necking, followed by breakup [294]. To investigate the effects of the platform moving speed on printing resolution, three tests of moving speed were used: 100 mm/min, 200 mm/min and 300 mm/min, while keeping the other parameters constant, as shown in Table 6.6. The extrusion system uses two stepper motors that rotate in small steps to provide X- and Y-axis motion. The moving substrate can move freely along the X and Y directions under the control of computer software. The layer width is directly verified by assessing the printed material. To confirm the accuracy of the layer width, the value was measured at various positions, and the average value was determined.

Table 6.6 Configuration of extrusion parameters to investigate the impacts of substrate moving speed.

Printing parameters	Value
Extrusion Temperature ($℃$)	≈ 313 ℃
Extrusion nozzle	$1.5\ mm$
Extrusion speed	$20\ mm/min$
Orifice tip-to-substrate distance	$3\ mm$

Figure 6.12 demonstrates the influence of substrate velocity on the line width at varying printing speeds. It can be seen that at the lowest moving substrate speed of 100 mm/min, the average line width was 4.7 mm. This can be attributed to the fact that at slower-moving substrate speeds, printing time is higher, and therefore, the amount of extruded material has more time to spread. However, the average width of the printed line decreased considerably to 2.4 mm as the platform moving speed increased to 200 mm/min. When the moving plate speed was higher (300 mm/min), the trend of the decreasing printing line width became more pronounced. The average print line width decreased to 1.20 mm, and the shape quality of the deposited single layers was significantly affected. Moreover, in this case, it is challenging to achieve effective metallurgical bonding between metal layers. This is because insufficient melted metal can be extruded onto the previously established layer with restricted length as a result of the high speed of the substrate. In summary, this test has proven that an optimal substrate speed of 200 mm/min can be recognized as ideal for obtaining a suitable line width.

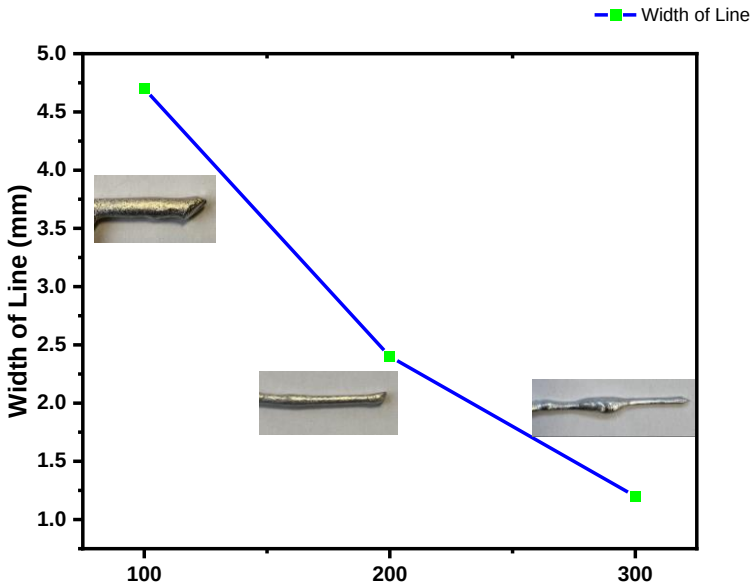

Figure 6.12 Influence of substrate velocity on the print quality and layer width.

.

6.8 Printing single layers with optimized process parameters

The investigation of printing process parameters is not only important for testing printability but also for the optimisation of the extrusion-based AM system, eventually producing satisfying outcomes. In this research, intensive preliminary assessment, calibration and configuration were carried out to establish the most effective printing technique. Therefore, based on the studied results, the feasible process window shown in Table 6.7 was adopted for the fabrication of single layers. The equipment of the extrusion and deposition was tested to demonstrate the entire printing process with a 1.5 mm nozzle. The thixotropic feedstock of the Zn-Sn alloy was fed into the hot extrusion chamber and reheated to a predetermined semi-solid temperature before being deposited into a substrate via a nozzle tip. The developed novel AM system was then able to deposit desired metal lines controlled by CNC software. Figure 6.13 illustrates the production of metal prints made of Zn-40Sn alloy, which includes different length lines and shapes with sharp 90-degree angles. It should be taken into account that the finished surface of deposited parts, such as those depicted in Figure 6.13, is not as uniform and smooth as that achieved in other metal additive manufacturing methods. These parts have been 3D printed with little regard for surface-finish quality. Surface finish is a very important aspect of metal 3D printing and will undoubtedly be the primary objective in future work. As can be observed, there was a noticeable hump at the beginning and toward the end of most of the deposited lines. This is thought to be due to acceleration/deceleration ramps in the platform velocity. Owing to the acceleration and deceleration of the bed, the overlap of the printed metal line developed at these ends. This might be addressed by modifying the software that controls the extrusion and deposition procedure and making the necessary adjustments, such as a postponed start and early stop for material delivery, which cannot be fulfilled under the scope of this study.

Table 6.7 Extrusion process parameters for generating single layers.

Printing parameters	Value
Extrusion Temperature ($℃$)	≈ 313 ℃
Extrusion nozzle	$1.5\ mm$
Extrusion speed	$20\ mm/min$
X-Y moving substrate velocity	$200\ mm/min$
Orifice tip-to-substrate distance	$3\ mm$

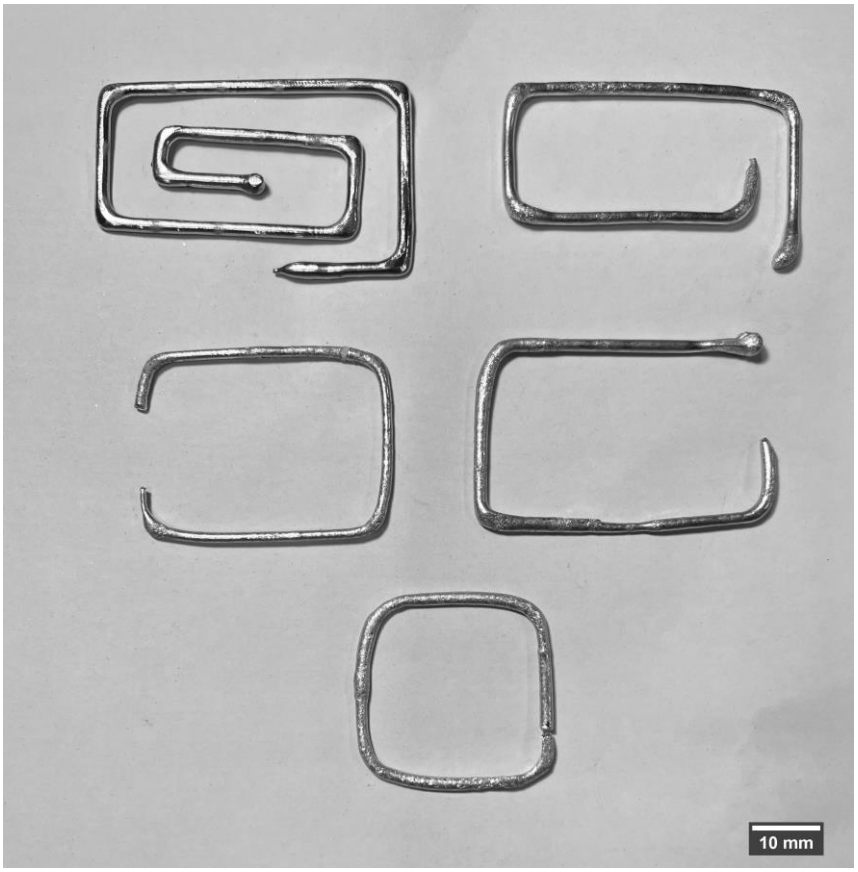

Figure 6.13 Examples of printed layer by the extrusion and deposition system of semi-solid alloy.

To investigate the impact of the adaptation of the parameters over the deposited Zn-Sn semi-solid alloy on the interior microstructures, a cross-section sample of the deposited line was taken for characterization. These specimens were carefully polished, etched and examined under an optical microscope and SEM equipped with energy dispersive spectroscopy (EDS). The investigation confirmed what had been expected as the microstructures obtained were made up of two distinct phases, α-Zn globular phase surrounded by eutectic Sn-Zn phase as shown in Figure 6.14 (b), which is in line with semi-solid materials processing established in the literature.

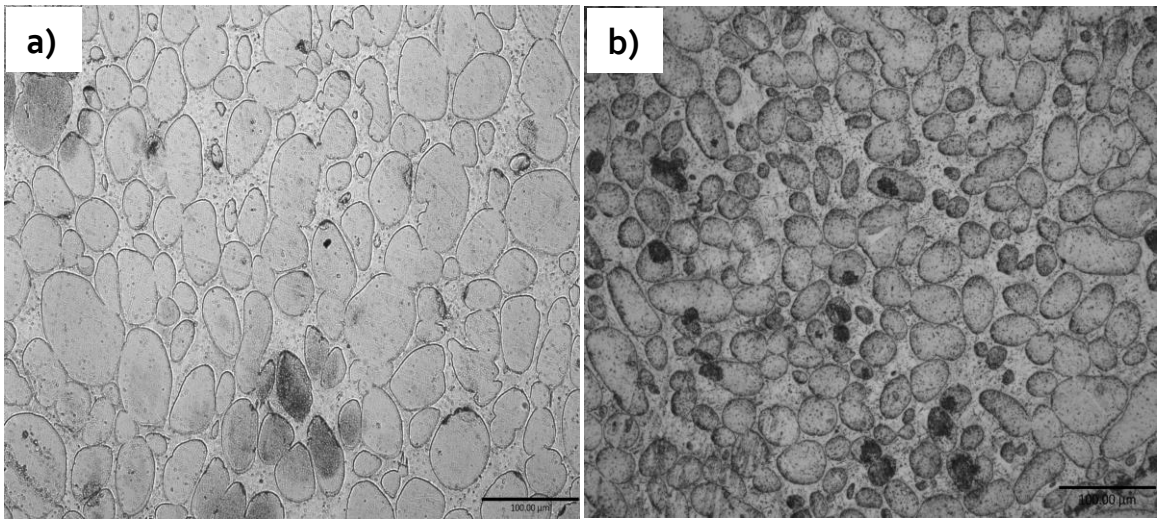

Figure 6.14 Shows (a) microstructure of the Zn-40Sn alloy after isothermal treatment in the semi-solid state at 313°C for 5 min and (b) microstructure results of deposited single-layer.

To provide a better understanding of the differences in microstructure between the initial heat-treated feedstock and the deposited specimen, the qualitative comparison method was employed. The quantitative method included assessing particle size to determine the average values for the diameter and sphericity (shape factor) of the primary solid particle structures. The sphericity indicates the presence of a perfect sphere that occurs within a microstructure. A value approaching 1.0 corresponds to a perfectly spherical morphology, while a value decreasing toward 0.0 suggests a more complex structure. Those microstructure factors mentioned above are key parameters in SSM processing and have an important impact on the viscosity of the semi-solid slurries, which affects their flow and rheological behaviour [34, 296]. It is widely assumed that the optimum microstructure for SSM alloy should present fine and rounded solid particles that are uniformly distributed in the liquid matrix to improve the thixotropic flow behaviour and consequently facilitate the component-forming process [34, 36, 167, 297]. Quantitative metallography evaluation was accomplished using the ImageJ software to examine the primary solid phase measurements for the semi-solid additive manufactured layer. The information gained was utilised to compare the findings of static heat treatments and semi-solid extrusion and deposition. Figure 6.15 illustrates the average grain size measurements for isothermally heat-treated sample microstructure compared to single metal line microstructure after the deposition and extrusion process, which includes primary grain diameter and circularity. It is apparent from this graph that there was a difference in the microstructure primary phase measurements between specimens processed under different processing conditions.

During the isothermal heat treatment for the specimen processed at 313°C for 5 min, the measured average particle size diameter was ≈ 37.5 μm; in contrast, the average particle size of the deposited samples decreased to approximately 31.6 μm. Another important aspect that significantly affects SSM was examined—the average shape of the primary solid particle. This also indicated changes in the average microstructure circularity values when the comparison was conducted between processes. The quantitative data for the investigated extruded layer displays that the primary solid particles showed an average sphericity value of more than 84% compared to 80% for that of the semi-solid treated sample. Taken together, these results provide a clear indicator that the metal print processed with the LEMA process is associated with a smaller grain size diameter and more globular structure compared with other samples produced with the different process. This was attributed to the semi-solid material being sheared during the extrusion and deposition processes, which improved microstructural refining that subsequently aided the printing procedure [35, 40]. These findings suggest that the shear applied in the nozzle tip promotes thixotropic properties. It is generally acknowledged that the microstructure grain size measurement is the most suitable for thixoforming consisting of globular grains of average size less than 100 μm and with an average shape factor that is greater than 0.6 [170, 298]. In this investigation, the LEMA process produced microstructures of finer solid particles with an average shape factor value of more than 0.84, suggesting that the microstructural properties of Zn-40Sn metal extruded were desirable for semi-solid application.

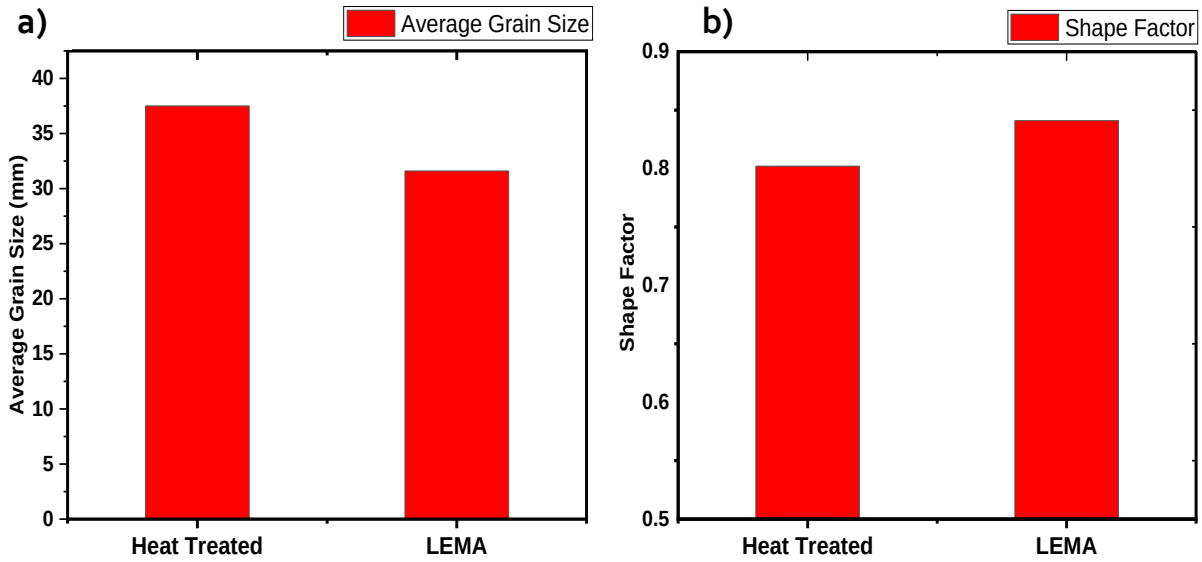

Figure 6.15 A comparison of quantitative data between samples produced by LEMA and isothermal heat treatment (a) mean grain diameter and (b) mean shape factor.

6.8.1 SEM and EDS analysis of the printed sample

Scanning electron microscopy and EDS were used to analyse the microstructure of the printed sample. Figure 6.16 depicts SEM images of the final microstructures, illustrating the deposited Zn-40Sn alloys with the anticipated geometric properties. In the left-hand side image, Figure 6.16 (a), the dark and bright colour phases represent the primary α-Zn and the eutectic mixture Sn-Zn phases, respectively. It can be observed that this microstructure is composed of globular α-Zn grains, which is typical for semi-solid processing embedded in eutectic phase. The eutectic Sn-Zn mixture can be seen in more detail by inspecting the SEM image on the right-hand side, Figure 6.16 (b).

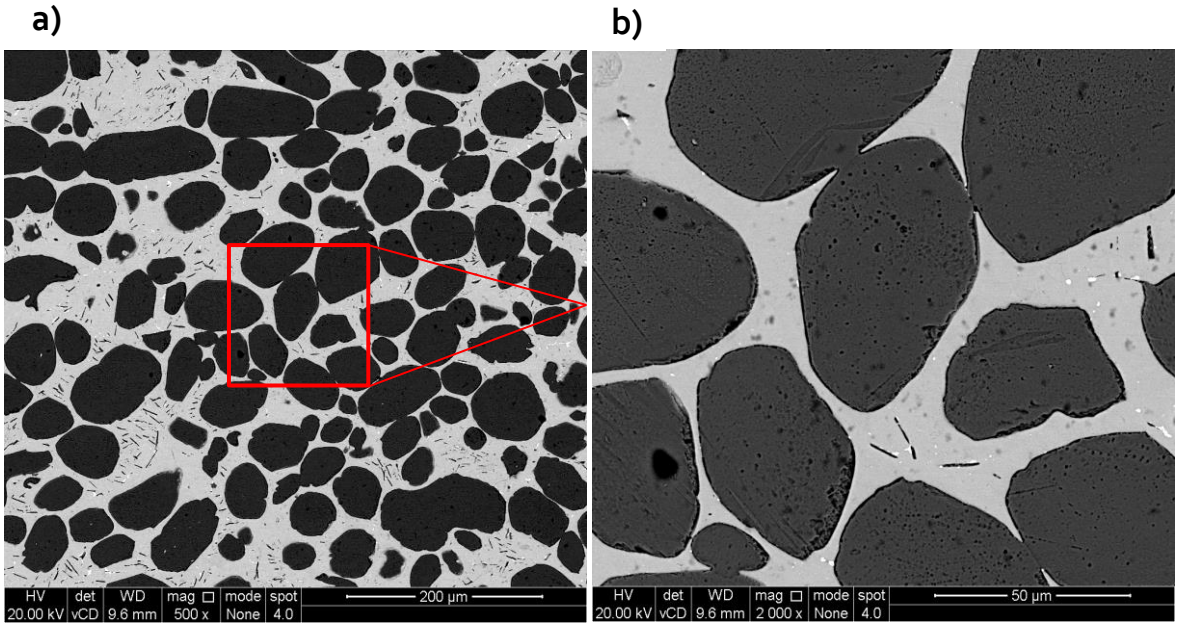

Figure 6.16 SEM micrographs of microstructures of as-deposited Zn-40Sn alloy: (a) lower magnification showing the primary spheroidal α-Zn phase surrounded by the eutectic matrix and (b) higher magnification showing insert details of the eutectic Sn-Zn mixture.

To establish the elemental composition of the different phases contained in the microstructure of the extruded specimen, EDS has been used. Back scattered electron and SEM micrographs were used to identify a phase, which was then targeted for EDX investigation. EDX analysis has been done at three different locations (spectrum 1, spectrum 2 and spectrum 3) marked in Figure 6.17. At first, the general compositions of the alloy specimen were identified by examining as large an area as possible on the surface (spectrum 1). The overall compositions of the examined area were found to be 57.5 Wt.% Zn and 38.3 Wt.% Sn based on the EDS data. This indicated that the average composition value of the examined surface area in spectrum 1 is close to the nominal alloy composition (Zn-40Sn). The EDS analysis at spectrum 2 corresponds to the eutectic mixture showed 95.7 Wt.% Sn and 4.3 Wt.% Zn, which indicate that the eutectic mixture is approximately

pure Sn. EDS analysis in spectrum 3 represents the globular α-Zn phase whose chemical composition consisted of 96.5 Wt.% Zn and 0.7 Wt.% Sn, demonstrating that the α-Zn globular phase with a high melting point belongs to a solid solution of Sn dissolved in the Zn matrix. Based on the above analysis results, it can be concluded that the liquid phase segregation was limited, and this was attributed to optimised process parameters during the metal part fabrication. This was confirmed by EDS results for the examined deposited materials, which showed that the chemical composition of the departing semi-solid alloy through the extrusion nozzle remained relatively stable. Such characteristics lead the slurries to smoothly eject from the nozzle without clogging or liquid leaking during the extrusion and deposition processes. The statistical validation involved analysing the distribution of the liquid phase across multiple SEM images and EDX spectra, measuring the percentage of the liquid phase in various regions of the sample, and comparing it against predetermined thresholds for uniformity. To ensure the repeatability of results, multiple samples were prepared under the same conditions and analysed using the same techniques. This ensured consistent results across the analysed specimens.

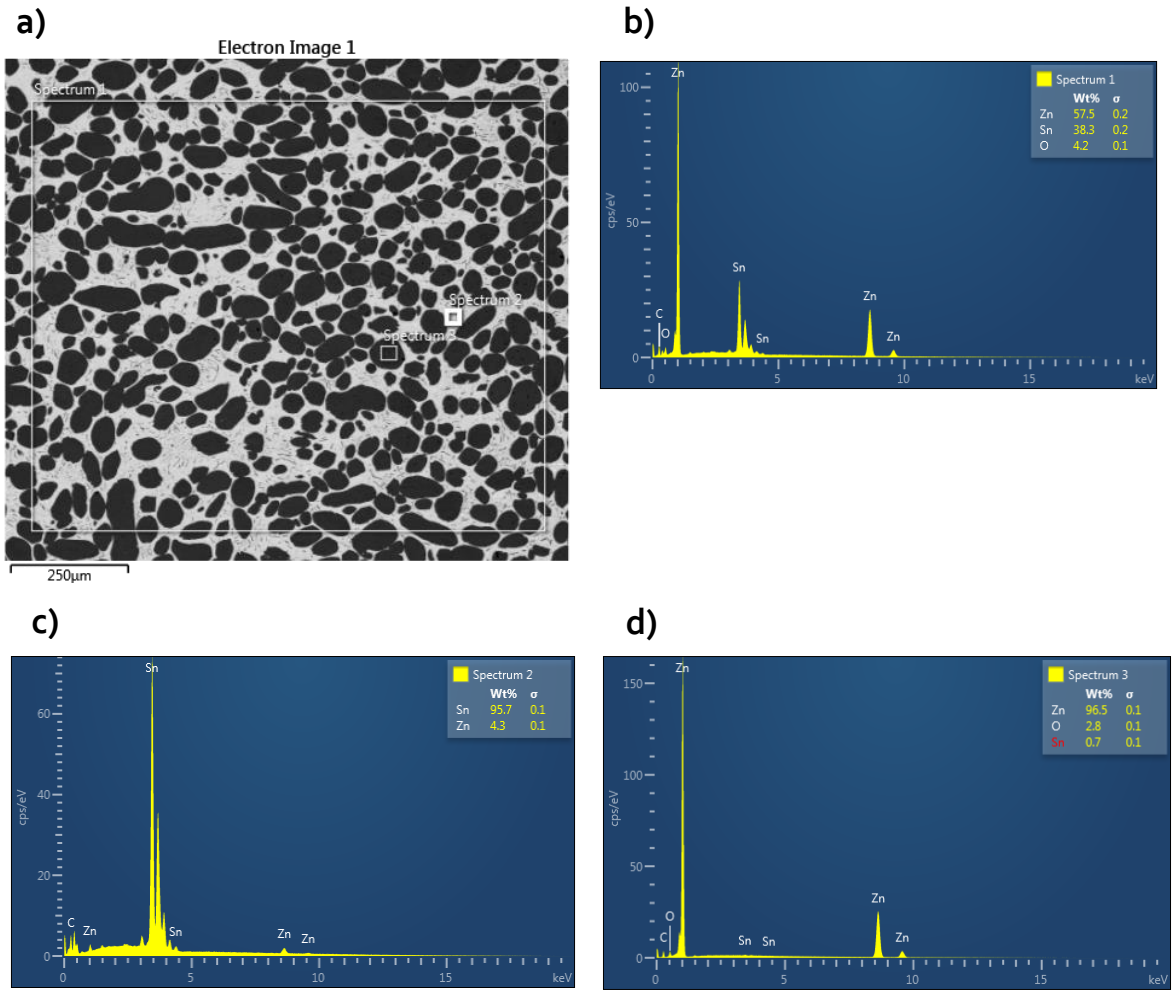

Figure 6.17 (a) SEM-BSE images of the deposited print, (b) EDS spectrum of overall composition, (c) EDS spectrum of eutectic phase and (d) EDS spectrum of primary globular phase.

6.9 Printing Multi-Layers with Optimized Process Parameters

One of the objectives of this experiment was to create multilayer depositions. In general, for multilayer creation, after the first layer is deposited, the moving substrate is moved downward for a predefined distance in the z-direction, and a fresh layer is placed over the previous one. The building process of the multilayer parts is more challenging than that of single layers due to repeated heating for layer deposition [299]. During the printing process, only the initial metal layer is extruded directly onto the platform substrate. Consequently, the subsequent layer is deposited onto the previously formed layer. Hence, the previously built layer will undoubtedly be subjected to more frequent thermal exposure compared to those deposited later, resulting in varying microstructures within the print [45]. To investigate the feasibility of the LEMA method for the production of multilayers, the optimised process parameters to generate single layers were selected based on the above-mentioned evaluations and examinations. Thus, these optimised process parameters were as follows: The extrusion temperature was kept at ≈ 313°C, the nozzle tip diameter was 1.5 mm, the extrusion speed was 20 mm/min, the platform moving velocity was set to be 200 mm/min and the gap between the nozzle and substrate was 3 mm. A variety of tests were conducted to highlight the fundamental connections between selected process variables and geometric final results by evaluating the cross-section of the metal lines. The thin-walled metal components were made by depositing layers only vertically. Figure 6.18 shows a series of metal parts that were fabricated using a LEAM machine based on the optimised process parameters. Notwithstanding experimental constraints, as a demonstration, it was feasible to extrude not only individual layers of material but also multi-layers. The geometry of this multi-layer print would require hours to create using existing direct metal printing techniques, such as powder bed fusion processes. Although the deposited multi-layers were relatively continuous, some defects existed, such as accumulation and depression of metal material, which may be due to inaccurate extrusion process control. A possible solution for these shortcomings will be discussed below.

Figure 6.18 Demonstration of deposited multilayer of the Zn-40Sn alloy at ambient bed temperature.

For the initial microstructure assessment of the multi-layer, a transverse cross section of the metal thin-walled parts was selected and cut from the mid-length location, thus ignoring positions near the corners. A metallographic investigation was performed to analyse the microstructure in various layers. Images of the cross-section of the thin-walled parts are revealed in Figure 6.19. This figure depicts the exact location of the interface between the two consecutive layers of the print, highlighted with the red dashed lines. Although the overall microstructures of all extruded samples appeared globular, which is typical for semi-solid alloys, insufficient interfacial bonding with micro-cracks was found at the interface. The state of the interface is one of the most vital aspects in producing a successful joining of metals using semi-solid slurries. There are two possible explanations for the weak interlayer adhesion behaviour demonstrated here: The first one is related to oxidation problems, which can occur at the interface and subsequently affect the connection between the deposition layers [149]. The interface must be free of oxides or impurities that could affect interfacial bonding during the formation of the multi-layer deposition process.

Another factor that might influence the connection between adjacent layers is the interface temperature [14]. The temperature of the semi-solid layer being deposited and the formerly placed layer determine the adhesion between the two layers. If the temperature at the contact area is too elevated, it may cause failure in controlling the flow of semi-solid slurries, resulting in unacceptable surface quality. If the temperature is excessively low, it introduces a poor metallurgical joint during the layer-wise material building process. In this way, the interface condition will have implications not only for the metallurgical connection between the layers but also for the surface quality and strength of the finished prints [300]. This evidence suggests that the optimised processing window from the single-layer tests appears to be limited to generating only the first layer. As a result, a processing method adaptation such as preheated substrate was examined in the process to enhance metallurgical bonds at the interface.

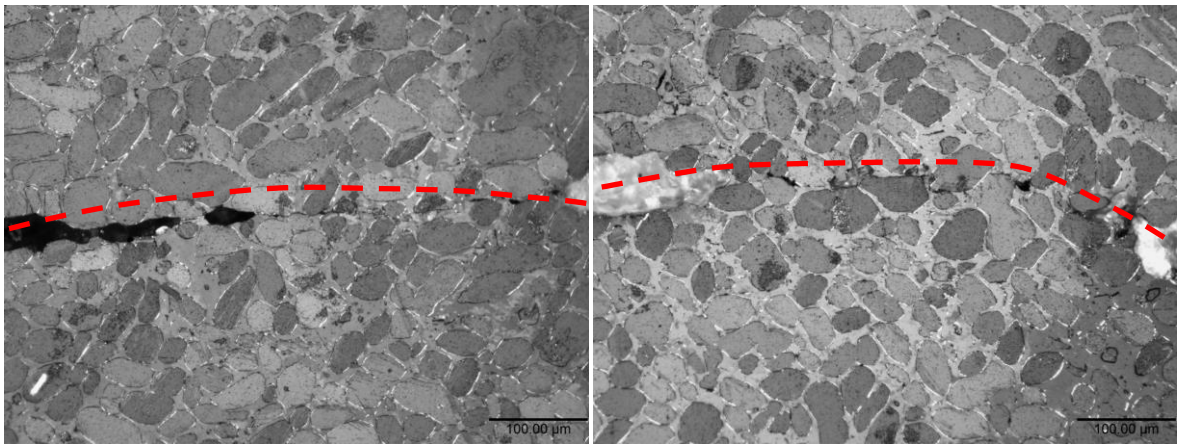

Figure 6.19 Example of extruded materials microstructure showing the inadequate interfacial bond between layers.

To ensure reliable interfacial adhesion between the current layer and the prior layer, a heated substrate stage was made of aluminum sheet and mounted on the X-Y platform with screws. Several tests with different substrate temperatures were conducted. In all cases, it was found that a substrate temperature between 175°C and 195°C was sufficient to remelt and coalesce successive metal materials. Therefore, the Zn-40Sn alloys were deposited onto a plate with a moderate heating temperature of 185°C, which is close to the solidus temperature of the investigated materials. Figure 6.20 shows some deposited patterns produced with the adapted preheated platform, exhibiting reasonable shape formation and adhesion between printed layers. Although there is continuous deposition of the semi-solid layers, at some points, they thicken and fluctuate in size. The substrate experiences acceleration and deceleration as the direction of its travel changes, so the substrate velocity is not stable. As a result of the unstable acceleration, more material accumulates in areas where the rate of acceleration is lower. To mitigate material build-up at low-speed spots, like in corners, more investigation is required in optimising the software of the substrate velocity and making the necessary modifications, which is beyond the scope of this research.

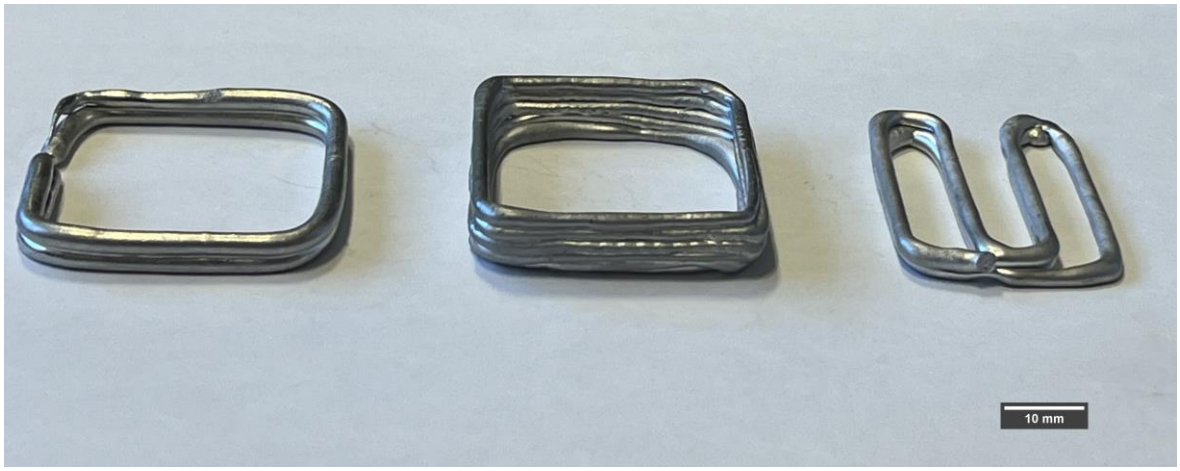

Figure 6.20 Demonstrates some metal parts that were built at a substrate temperature of 180°C.

To better understand the interlayer adhesion of the deposition and the microstructure revolution that appears during semi-solid extrusion and deposition, specimens from the extruded metal parts were analysed. Initially, cross-sectional views of the interface between deposited metal layers, manufactured with the assistance of a heating substrate, were examined. The specimens were carefully sectioned perpendicular to the layer interfaces, ensuring accurate representation of the boundary between layers. These sections were then meticulously polished to a mirror-like finish to facilitate optimal clarity for microscopy analysis. Subsequently, the polished sections were subjected to etching using a suitable chemical solution to reveal the microstructural features at the interface. The optical microscopy examination revealed a consistent globular microstructure across the layers. Importantly, when the printing plate was heated at 185°C during processing, no distinguishing boundary was apparent at the layer interface (See Figure 6.21). However, a continuous interface between layers and cracks became evident when the metal deposition was conducted at ambient bed temperature (Figure 6.19). These observations indicate that the interfacial bonding between layers is influenced by the temperature of the fresh semi-solid layer and the already-formed layer. This finding corroborates the conclusions of Chen et al. [40], who demonstrated the significant impact of bed temperature on layer adhesion. Hence, the interface temperature must be in the semi-solid range, allowing the solid particles to interlock with each other and finally achieve adequate metallurgical bonding at the interface. In summary, the above results underscore the importance of proper substrate temperature selection as a critical process parameter affecting 3D part fabrication.

Consequently, it was determined that depositing semi-solid Zn-40Sn alloy with a pre-heated substrate temperature of 185°C was necessary to achieve successful interfacial joining between layers during the process.

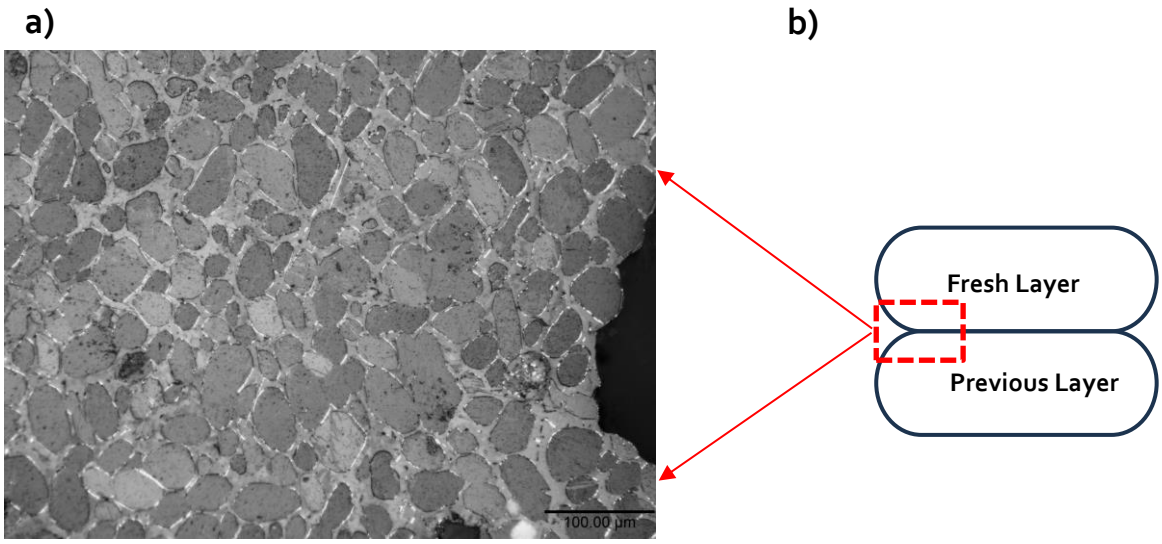

Figure 6.21 (a) shows the cross-sections of the interfaces between two consecutive layers and (b) demonstrates the location where the samples were taken.

In conclusion, based on the results depicted in Figure 6.25, the success of LMEA can be evaluated. Interfacial bonding between layers was indeed observed, indicating a degree of success in achieving multilayer printing of the semi-solid alloy. Interlayer bonding and multilayer printing were achieved primarily through the control of process parameters such as nozzle temperature, extrusion speed, and substrate heating. Factors influencing bonding strength and part integrity include material composition, layer deposition temperature, and surface preparation. Besides heating the material to re-melting, other options for enhancing interlayer bonding could include incorporating bonding agents, optimizing nozzle design for better material flow, or post-processing techniques like surface roughening or ultrasonic bonding. Although some technological obstacles must be addressed to overcome challenges, such microstructure results demonstrate the promising potential of the LEMA system for extrusion-based metal direct additive manufacturing.

6.10 Conclusion

In conclusion, the LEMA process is a novel extrusion-based AM technology that may be presented as another option of an AM process that can be applied in the industry. This enables an economical and low-cost AM process to fabricate metal parts by employing semi-solid thixotropic feedstock. In phase II, unlike phase I, the LEMA process was applied using pre-treated feedstock with a non-dendritic microstructure for processing. The development of lead-free solders has garnered significant interest in high-temperature applications, including in the electronic industry. The Zn-Sn alloy was chosen as a candidate for this manufacturing technique to address the increasing need for reliable substitutes for lead-containing alloys. Thermodynamic simulations and differential scanning calorimetry analysis were employed to evaluate the solid–liquid transformation with temperature and identify the appropriate composition for semi-solid AM. As a result of the findings, the Zn-40Sn alloy was chosen to be processed by the LEMA method.

The as-cast Zn-Sn alloy is not ready to be processed for layer-based extrusion in a semi-solid condition. So it was required to implement a process to generate consistent and qualified semi-solid alloys. The preparation of semi-solid material with thixotropic properties to be used in metal printing is a critical factor in the whole process. In the preparation, the as-cast Zn-40Sn material was distorted by a custom-made extrusion dye, which was designed and built in-house to produce metallic feedstock with a final diameter associated with a desired plastic deformation energy. Subsequently, a heat-treatment process was carried out by exposing the cold worked material to partial remelting to obtain the required microstructure of feedstock. Isothermal heat processes were performed at various temperatures in the semi-solid state to analyse the development and coarsening of globular microstructures. Nearly all heat-treated specimens, regardless of the condition, had globular microstructures, suggesting their potential for semi-solid processing. However, the microstructural examination showed that the semi-solid heating temperature of 313°C with 5 min isothermal holding time, which corresponds to a liquid fraction of ≈ 0.55, yielded the most appropriate processing condition to create a suitable semi-solid feedstock with a finer and globular solid phase.

Experimental identifications were performed to determine the influence of the principal process variables on the print quality of material during extrusion-based metal printing. The impacts of orifice diameter, extrusion speed, nozzle tip-to-substrate distance and x-y substrate moving velocity were specifically investigated. It was found that each of the process parameters plays an important role in the success layer produced. As a result, the optimum condition of the optimised process parameters has been adopted to produce single-layer specimens. A cross-section of the extruded single layer was examined, and the microstructural evolution exhibited that the deposited sample showed a finer and more

globular morphology in comparison to the heat-treated samples due to the shear applied through the nozzle.

Following the experimental establishment of an achievable process window for the manufacture of single-layer samples, an attempt has been made to use these optimal process window parameters for multilayer deposition. Microstructural analysis of the multilayers demonstrated clear inadequate bonding between the two layers. It was found that the interface temperature between the already deposited layer and the incoming layer is a critical parameter for good interlayer bonding. So it was realised that the optimised processing window parameters to produce a single layer appear to be limited to the first layer. Therefore, a preheated substrate was proposed and tested, addressing the problem of joining between the layers. The optical microscopy images of the investigated multilayer cross section suggested that good metallurgical bonding was realized when selecting the appropriate substrate temperature. In conclusion, whereas important design aspects must be developed and additional research on semi-solid thixotropic feedstock and methods needs to be carried out, the positive results obtained in this research suggest that the LEMA process appears to have potential in developing a new type of metal extrusion-based AM system. Further, it might be used for a wide variety of industrial semi-solid alloys with an acceptable semi-solid region, such as aluminum alloys and titanium alloys.

7 THESIS CONCLUSION, LIMITATIONS AND FUTURE WORK

7.1 Conclusion of The Thesis

Current metal AM methods and their processing materials have advanced to the point where they are now able to be utilised to produce high-value end-use components for a variety of applications, including aerospace, automotive and medical applications. This is due to the capabilities of these direct metal AM systems, such as powder bed systems that use a laser or electron beam source to generate dense 3D net shape structures with complex profiles. However, the high energy densities caused by the laser or electron beam source applied to fully melt the deposited powdered feedstock may introduce limitations, including residual stresses and large thermal gradients within the components. As a result of this requirement, a powder bed system can be costly to acquire or operate. The additional expense provides an economic obstacle, limiting industries and other sectors from accessing this up-and-coming and innovative manufacturing process. Therefore, there has been considerable interest in developing a new processing method, mainly to compete with powder bed systems and avoid the limitations mentioned. The method investigated in this research, which aims to deposit semi-solid alloys using a developed extrusion-based AM system (LEMA), promises several benefits for the future of metal AM, including lower manufacturing costs and savings on the usage of energy. Using such thixotropic metal 3D extrusion and deposition technology will allow the fabrication of fully dense 3D metallic parts due to the unique microstructure and controlled rheological properties of semi-solid alloys, which, in turn, improve the mechanical properties of the produced parts.

To ensure the aims and objectives of this work are fulfilled, two fundamental approaches were established, termed Phase I and Phase II. The main difference between them was the preparation of the semi-solid materials. Phase I involved the in-situ creation of semi-solid thixotropic materials. The non-thixotropic feedstocks were heated within the system to a specific temperature, stirred by a single-screw extruder and then the materials were layered onto a substrate plate for formation without an added intermediate stage.

Based on the results in phase I, it was demonstrated that the system was able to convert non-thixotropic feedstocks into thixotropic form in-situ within the process. Furthermore, one of the more important findings to emerge from Phase I is that the developed machine was capable of successfully extruding and depositing a stream of semi-solid alloy onto a stage, indicating the feasibility of the process. Nevertheless, several limitations to this pilot study need to be acknowledged. The major limitation of this study is that maintaining the steady-state rheological behaviour of semi-solid slurries within the extrusion compartment and before the deposition was challenging. Controlling the semi-solid alloy

with the properties of near sphere-shaped solid particles uniformly scattered in the liquid mixture is critical in providing controllable extrusion that, in turn, produces high-integrity and complex-shaped parts. In addition to the technical issues, precise process parameters were required, such as extrusion temperature, desired sharing rate and time. It was thought that a new mechanism is required, such as redesigning the current approach to specifically address the shortcomings of the existing mechanism. Hence, phase II has been proposed as an alternative methodology. Initially, thermodynamic simulations and DSC analysis were carried out to examine the alloy composition to ensure its suitability for the experimental examination. The results led to the conclusion that Zn-40Sn alloy was a proper candidate. The Zn-40Sn semi-solid alloy, in phase II, was obtained in the form of a billet by a partial remelting and an isothermal heating process of a distorted metallic feedstock. A piston-based instead of a single screw-based extruder was utilized to control the thixotropic feedstock. The pre-prepared feedstock with appropriate microstructure was reheated into a semi-solid state before being additively manufactured on a surface via the LEMA process. According to the results, it can be determined that the process that was adapted for the preparation of semi-solid billets by manipulating the deformation, partial remelting and holding of the material in the semi-solid state was effective in manufacturing high-quality thixotropic feedstock, resulting in a successful layered extrusion of Zn-40Sn metal alloys. The influence of process parameters such as nozzle diameter, distance between the nozzle and the substrate, extrusion speed and substrate velocity on the formation of a single layer were studied and found that they strongly affect the quality of the print shape. Furthermore, the result showed that the substrate pre-heating temperature improve the metallurgical bonding between the layers during the multilayer fabrication process. The integration of SSM processing and extrusion-based AM system has the potential not only to print Zn-Sn materials for electronic applications, but it would also be feasible to expand to other industrial alloys to create metallic components with good mechanical properties.

7.2 Comparison of Results between Phase I and Phase II

- Relationships between parameters:

Exploring relationships such as the "relationship between average grain size and shape factor" and the "effects of extrusion speed" is essential for understanding the behavior of semi-solid metal alloys during the extrusion process. However, it is important to note that the different material compositions between Phase I and Phase II contributed to the limited comparison of these relationships. In Phase I, the focus was primarily on establishing baseline parameters and validating the feasibility of the extrusion process for the Zn-30 wt.% Sn alloy. Detailed measurements of parameters such as

average grain size and shape factor were not conducted in this phase. However, Phase II involved a more comprehensive investigation into these relationships, particularly with the Zn-40 wt.% Sn alloy. The findings from Phase II provided more detailed insights into the effects of extrusion speed and other parameters on the microstructural properties of the alloys.

- Generalizability of results:

The results obtained from both Phase I and Phase II provide valuable insights into the behavior of semi-solid metal alloys during extrusion. While the specific measurements and parameters varied between the phases, the fundamental principles observed are likely applicable to other materials and processes. This generalizability is supported by findings in the existing literature, which validate the relevance and applicability of our results.

- Comparison with theoretical predictions and existing literature:

Throughout the study, experimental results were compared with theoretical predictions and existing literature. In Phase I, the focus was on validating the feasibility of the extrusion process for the Zn-30 wt.% Sn alloy. While specific comparisons with theoretical predictions were limited, the observed trends aligned with established principles in semi-solid processing. In Phase II, the selection of the Zn-40 wt.% Sn alloy was based on thermodynamic simulations and a review of existing literature. The experimental outcomes corroborated the theoretical predictions, demonstrating the suitability of the chosen alloy for the LEMA technique.

Main similarities between experimental results and existing literature included the influence of temperature and material composition on the extrusion process. Differences were mainly due to variations in experimental conditions, alloy composition, and measurement techniques. Discrepancies or deviations were explained by considering factors such as material properties, process parameters, and limitations of the experimental setup. Future work will focus on addressing the limitations identified in this research. This includes conducting more comprehensive experiments to establish clear relationships between process parameters and microstructural properties, as well as exploring alternative alloys and optimizing process parameters further.

7.3 Challenges and Limitations

This research has encountered several challenges and limitations, which have influenced the experimental process and the interpretation of results.

7.3.1 Material preparation challenges

A primary challenge in this research was the preparation of semi-solid thixotropic feedstock. While Phase II addressed this challenge more effectively than Phase I, difficulties persisted in achieving consistent microstructural properties in the feedstock. The process of partial re-melting and isothermal heating necessitated precise control of temperature and time, posing challenges in achieving consistency. Additionally, the deformation process required for obtaining the desired microstructure in the feedstock was not straightforward and demanded optimization.

7.3.2 Process control challenges:

Maintaining steady-state rheological behavior of semi-solid slurries during extrusion and deposition proved to be a significant challenge. Controlling properties such as particle size and distribution of the thixotropic feedstock within the extrusion compartment was difficult, leading to variations and inconsistencies in the extrusion process, thereby affecting the quality of printed parts. Achieving precise control over process parameters, including extrusion temperature, speed, and substrate velocity, also proved challenging and necessitated extensive experimentation

7.3.3 Interruptions in deposition process:

The LEMA system encountered interruptions in the deposition process due to the constant reloading of material feedstocks. These interruptions resulted in the cooling of the deposited part and extrusion, leading to inadequate bonding between layers. Maintaining a continuous supply of thixotropic feedstock to the machine was crucial for successful printing; however, the existing system lacked reliability in this aspect

7.3.4 Limited substrate movement:

The limited movement of the substrate in the X-Y directions posed a challenge to printing large and complex structures. The existing setup restricted the size and complexity of the printed parts, thus limiting the applicability of the LEMA process in certain scenarios. Although not implemented in this research, an enhanced machine setup with a motorized X-Y-Z movable platform could address this limitation.

7.3.5 Lack of mechanical property analysis:

While this research focused on the deposition process and microstructural analysis, limited mechanical property analysis was conducted. Comprehensive mechanical

testing of deposited parts, including yield strength, hardness, and tensile strength, would provide valuable insights into part performance and quality. The absence of such analysis limits the understanding of the suitability of the LEMA process for various applications

7.3.6 Scope and generalization:

The scope of this research was confined to the deposition of Zn-Sn alloys using the LEMA process. Although the findings have implications for other semi-solid alloys, generalizing the results to different materials necessitates further research. Additionally, exploring the applicability of the LEMA process to industrial-scale production and other metal alloys remains to be investigated

7.3.7 Overall research limitations:

The limitations of this research include the small-scale experimental setup, limited sample size, and lack of real-world application testing. These factors constrain the generalizability and practicality of the findings. Furthermore, the research primarily focused on process development and optimization, leaving room for further investigation into the broader implications and industrial applications of the LEMA process.

In conclusion, while this research has made significant strides in advancing the LEMA process for metal additive manufacturing, several challenges and limitations need to be addressed to realize its full potential. Further research and development are required to overcome these challenges and make the LEMA process a viable and competitive option in the field of metal AM.

7.4 Future Directions and Improvements

The findings and insights gained from this PhD research lay the groundwork for several potential future directions and improvements in the field of extrusion-based metal additive manufacturing using semi-solid thixotropic feedstock (LEMA). These future directions aim to address the challenges and limitations identified in this thesis and further advance the capabilities and applicability of the LEMA process.

7.4.1 Continuous material feed system

One of the main limitations identified in the developed process is the extrusion and deposition discontinuity, resulting in interruptions in the forming process and inadequate bonding between layers. Implementing a continuous material feed system would ensure a consistent supply of thixotropic feedstock to the machine

without the need for constant reloading. This system could involve the use of hoppers or reservoirs containing a sufficient amount of feedstock, continuously fed into the extrusion system. Automated sensors and control mechanisms could monitor the feedstock level and adjust the feed rate, ensuring uninterrupted printing.

7.4.2 Enhanced machine setup

The LEMA system encountered limitations due to its platform-moving mechanism in the x-y directions. To address this, upgrading the LEMA system with an advanced machine setup, incorporating a motorized X-Y-Z movable platform, would facilitate the printing of larger and more complex parts. This enhancement would significantly broaden the capabilities of the LEMA process, making it suitable for a wider range of applications across various industries

7.4.3 Substrate heating optimization:

Further research is needed to optimize substrate heating parameters for improved interlayer bonding. Investigating the effects of different heating temperatures and profiles on bonding strength and part quality would provide valuable insights. Additionally, integrating temperature monitoring and control systems into the LEMA setup would enhance process reliability.

7.4.4 Advanced process control

Enhancing process control mechanisms is crucial for achieving consistent and high-quality prints. Future research should focus on developing advanced control systems to regulate extrusion temperature, speed, and substrate movement more precisely. Implementing real-time monitoring and feedback mechanisms could help optimize process parameters and improve part quality

7.4.5 Mechanical property analysis:

Conducting comprehensive mechanical property analysis of printed parts is essential for evaluating their performance and suitability for different applications. Future research should include extensive testing of mechanical properties, such as tensile strength, fatigue resistance, and impact toughness, to assess the quality and reliability of LEMA-produced parts.

7.4.6 Exploration of alternative alloys:

Expanding the scope of research to include other semi-solid alloys, such as aluminium alloys, titanium alloys, and steel alloys, would broaden the applicability of the LEMA process. Investigating the feasibility of printing high-strength and high-performance alloys using LEMA could open up new opportunities in aerospace, automotive, and medical industries.

7.4.7 Heat transfer modelling:

Developing advanced heat transfer models to simulate the extrusion and deposition process would enhance the understanding and optimization of the LEMA system. By modeling the heat transfer between the extrusion nozzle, deposited layers, and substrate, researchers can predict the impact of process parameters and optimize material flow and deposition characteristics. For instance, Finite Element Analysis (FEA) could be employed to simulate the temperature distribution within the extrusion system and the substrate. Incorporating data on material properties, extrusion rates, and environmental conditions, these models could accurately predict temperature gradients and heat flow during deposition, enabling the optimization of extrusion parameters to minimize thermal gradients and improve bonding between layers

7.4.8 Interlayer bonding optimization

Improving interlayer bonding is essential for enhancing the mechanical properties and reliability of printed parts. Future work should investigate novel approaches to optimize interlayer bonding, such as modifying substrate temperature profiles, introducing interlayer bonding agents, or exploring post-processing techniques like laser re-melting. These approaches could help minimize defects and increase part strength

7.4.9 Real-world applications testing

Conducting real-world applications testing of LEMA-produced parts in relevant industrial settings is crucial for validating the process and its capabilities. Collaborating with industry partners to implement LEMA technology in practical applications, such as prototyping, tooling, and custom part manufacturing, would provide valuable feedback and insights for further improvement. In conclusion, the future directions and improvements outlined above aim to address the challenges and limitations identified in this research and to further enhance the capabilities and applicability of the LEMA process. By focusing on

continuous material preparation, advanced process control, interlayer bonding optimization, machine setup enhancement, substrate heating optimization, mechanical property analysis, exploration of alternative alloys, heat transfer modelling, and real-world applications testing, the LEMA process can become a competitive and viable option in the field of metal additive manufacturing.

8 PUBLICATIONS

1- Semisolid heat treatment processing window of Pb-40% Sn alloy for feedstock in the 3D printing thixo-forming process

9 REFERENCES

[1] D. Kirkwood, "Semisolid metal processing," *International Materials Reviews (UK),* vol. 39, no. 5, pp. 173-189, 1994.

[2] ASM Alloy Phase Diagram Database [Online] Available: https://www.asminternational.org/home/-/journal_content/56/10192/15469013/DATABASE.

[3] "Ceramic Band Heaters." http://heatandsensortech.com/products/ceramic-heaters/ (accessed 03/20/2018, 03/10/2018).

[4] K. Sołek and P. Kapranos, "Rheology of StelliteTM 21 Alloy in Semi-Solid State," 2016.

[5] 3DPrinting.com [Online] Available: https://3dprinting.com/what-is-3d-printing/

[6] C. J. Quaak, "Rheology of partially solidified aluminium alloys and composites," Doctoral Thesis, 1996-01-30.

[7] W. Associates. [Online] Available: https://wohlersassociates.com/press-releases/wohlers-report-2018-shows-dramatic-rise/

[8] "Additive Manufacturing Research , Loughborough University AM Research Group." http://www.lboro.ac.uk/research/amrg/about/the7categoriesofadditivemanufacturing/powderbedfusion/ (accessed 19/07/2018, 2018).

[9] A. de Figueredo, *Science and technology of semi-solid metal processing*. North American Die Casting Assoc., 2001.

[10] D. Zhang, "Thermodynamic characterisation of semi-solid processability in alloys based on AL-SI, AL-CU and AL-MG binary systems," University of Leicester, 2015.

[11] F. Esteve, D. Olivier, Q. Hu, and M. Baumers, "Micro-additive manufacturing technology," in *Micro-Manufacturing Technologies and Their Applications*: Springer, 2017, pp. 67-95.

[12] S. Ji, Z. Fan, and M. Bevis, "Semi-solid processing of engineering alloys by a twin-screw rheomoulding process," *Materials Science and Engineering: A,* vol. 299, no. 1-2, pp. 210-217, 2001.

[13] A. S. Ali, "Application of nanomaterials in environmental improvement," *Nanotechnology and the Environment,* 2020.

[14] S. Finke, W. Wei, and F. Feenstra, "Extrusion and deposition of semi-solid metals," in *Proc solid freeform fabrication symposium, Austin, TX*, 1999, pp. 9-11.

[15] W. Bleck, G. Hirt, and W. Püttgen, "Thixoforming of Steels-A Status Report," in *Materials science forum*, 2007, vol. 539: Trans Tech Publ, pp. 4297-4302.

[16] L. Waalkes, J. Längerich, F. Holbe, and C. Emmelmann, "Feasibility study on piston-based feedstock fabrication with Ti-6Al-4V metal injection molding feedstock," *Additive Manufacturing,* vol. 35, p. 101207, 2020.

[17] M. C. Flemings, "Behavior of metal alloys in the semisolid state," *Metallurgical transactions A,* vol. 22, no. 5, pp. 957-981, 1991.

[18] R. Decker *et al.*, "Thixomolding," in *Proceeding of Annual Meeting, International Magnesium Association*, 1990, vol. 47, pp. 106-116.

[19] W. Frazier, "Metal Additive Manufacturing: A Review," *Journal of Materials Engineering and Performance,* vol. 23, no. 6, pp. 1917-1928, 2014, doi: 10.1007/s11665-014-0958-z.

[20] J. Mireles, D. Espalin, D. Roberson, B. Zinniel, F. Medina, and R. Wicker, "Fused deposition modeling of metals," in *Proceedings of the Solid Freeform Fabrication Symposium, Austin, TX, USA*, 2012, pp. 6-8.
[21] H. Giberti, M. Strano, and M. Annoni, "An innovative machine for Fused Deposition Modeling of metals and advanced ceramics," in *MATEC web of conferences*, 2016, vol. 43: EDP Sciences, p. 03003.
[22] H. V. Atkinson, "Modelling the semisolid processing of metallic alloys," *Progress in Materials Science,* vol. 50, no. 3, pp. 341-412, 2005, doi: 10.1016/j.pmatsci.2004.04.003.
[23] M. S. Salleh, M. Z. Omar, J. Syarif, and M. N. Mohammed, "An Overview of Semisolid Processing of Aluminium Alloys," *ISRN Materials Science,* vol. 2013, 2013, doi: 10.1155/2013/679820.
[24] K. Satyanarayana, S. Ojha, D. N. N. Kumar, and G. Sastry, "Studies on spray casting of Al-alloys and their composites," *Materials Science and Engineering: A,* vol. 304, pp. 627-631, 2001.
[25] G. Hirt, L. Khizhnyakova, R. Baadjou, F. Knauf, and R. Kopp, "Semi-Solid Forming of Aluminium and Steel–Introduction and Overview," *Thixoforming: semi-solid metal processing,* pp. 1-27, 2009.
[26] F. Czerwinski, "Critical Assessment 32: Controling the melting behaviour of cast structures through solid-state deformation," *Materials Science and Technology,* vol. 35, no. 9, pp. 999-1006, 2019.
[27] W. Sames, F. A. List, S. Pannala, R. Dehoff, and S. S. Babu, "The metallurgy and processing science of metal additive manufacturing," in *Int. Mater. Rev.* vol. 61, ed, 2016, pp. 315-360.
[28] D. D. Lima, K. N. Campo, S. T. Button, and R. Caram, "3D thixo-printing: A novel approach for additive manufacturing of biodegradable Mg-Zn alloys," *Materials & design,* vol. 196, p. 109161, 2020.
[29] M. Ma and H. Zhang, "An experimental study of pneumatic extruding direct writing deposition-based additive manufacturing," *The International Journal of Advanced Manufacturing Technology,* vol. 97, no. 1-4, pp. 1005-1010, 2018.
[30] P. Hsieh, C. Tsai, B. Liu, W. Wei, A. Wang, and R. Luo, "3D printing of low melting temperature alloys by fused deposition modeling," in *2016 IEEE International Conference on Industrial Technology (ICIT)*, 2016: IEEE, pp. 1138-1142.
[31] D. Spencer and B., "Rheological behavior of Sn-15 pct Pb in the crystallization range," *Metallurgical and Materials Transactions,* 1972.
[32] J. Z. Li, M. R. Alkahari, N. A. B. Rosli, R. Hasan, M. N. Sudin, and F. R. Ramli, "Review of Wire Arc Additive Manufacturing for 3D Metal Printing," *International Journal of Automation Technology,* vol. 13, no. 3, pp. 346-353, 2019.
[33] S. Shimizu, H. Fujii, Y. Sato, H. Kokawa, M. Sriraman, and S. Babu, "Mechanism of weld formation during very-high-power ultrasonic additive manufacturing of Al alloy 6061," *Acta Materialia,* vol. 74, pp. 234-243, 2014.
[34] M. N. Mohammed, M. Z. Omar, M. S. Salleh, K. S. Alhawari, and P. Kapranos, "Semisolid Metal Processing Techniques for Nondendritic Feedstock Production," *The Scientific World Journal,* vol. 2013, 2013, doi: 10.1155/2013/752175.
[35] A. Jabbari and K. Abrinia, "A metal additive manufacturing method: semi-solid metal extrusion and deposition," *The International Journal of Advanced*

Manufacturing Technology, vol. 94, no. 9, pp. 3819-3828, 2018, doi: 10.1007/s00170-017-1058-7.
[36] M. Kiuchi and R. Kopp, "Mushy/ Semi- Solid Metal Forming Technology – Present and Future," *CIRP Annals - Manufacturing Technology,* vol. 51, no. 2, pp. 653-670, 2002, doi: 10.1016/S0007-8506(07)61705-3.
[37] C. Rice, P. Mendez, and S. Brown, "Metal solid freeform fabrication using semi-solid slurries," *JOM,* vol. 52, no. 12, p. 31, 2000.
[38] S. H. Masood and W. Q. Song, "Development of new metal/ polymer materials for rapid tooling using Fused deposition modelling," *Materials and Design,* vol. 25, no. 7, pp. 587-594, 2004, doi: 10.1016/j.matdes.2004.02.009.
[39] S. Gorsse, C. Hutchinson, M. Gouné, and R. Banerjee, "Additive manufacturing of metals: a brief review of the characteristic microstructures and properties of steels, Ti-6Al-4V and high-entropy alloys," *Science and Technology of advanced MaTerialS,* vol. 18, no. 1, pp. 584-610, 2017.
[40] W. Chen *et al.*, "Direct metal writing: Controlling the rheology through microstructure," *Applied Physics Letters,* vol. 110, no. 9, 2017, doi: 10.1063/1.4977555.
[41] K. Andrea Alice, G.-P. Marta, and R. S. Dolores, "Personalised 3D Printed Medicines: Which Techniques and Polymers Are More Successful?," *Bioengineering (Basel),* vol. 4, no. 4, p. 79, 2017, doi: 10.3390/bioengineering4040079.
[42] Z. Fan, "Semisolid metal processing," *International Materials Reviews,* vol. 47, no. 2, pp. 49-85, 2002, doi: 10.1179/095066001225001076.
[43] J. Gonzalez-Gutierrez, S. Cano, S. Schuschnigg, C. Kukla, J. Sapkota, and C. Holzer, "Additive Manufacturing of Metallic and Ceramic Components by the Material Extrusion of Highly- Filled Polymers: A Review and Future Perspectives," *Materials,* vol. 11, no. 5, 2018, doi: 10.3390/ma11050840.
[44] B. Hafner, "Scanning electron microscopy primer," *Characterization Facility, University of Minnesota-Twin Cities,* pp. 1-29, 2007.
[45] D. Deng, J. Moverare, R. L. Peng, and H. Söderberg, "Microstructure and anisotropic mechanical properties of EBM manufactured Inconel 718 and effects of post heat treatments," *Materials Science and Engineering: A,* vol. 693, pp. 151-163, 2017.
[46] K. Mumtaz and N. Hopkinson, "Selective laser melting of Inconel 625 using pulse shaping," *Rapid Prototyping Journal,* vol. 16, no. 4, pp. 248-257, 2010.
[47] D. Herzog, V. Seyda, E. Wycisk, and C. Emmelmann, "Additive manufacturing of metals," *Acta Materialia,* vol. 117, pp. 371-392, 2016, doi: 10.1016/j.actamat.2016.07.019.
[48] P. Mercelis and J. P. Kruth, "Residual stresses in selective laser sintering and selective laser melting," *Rapid prototyping journal,* 2006.
[49] D. Gu *et al.*, "Densification behavior, microstructure evolution, and wear performance of selective laser melting processed commercially pure titanium," *Acta materialia,* vol. 60, no. 9, pp. 3849-3860, 2012.
[50] B. A. Szost *et al.*, "A comparative study of additive manufacturing techniques: Residual stress and microstructural analysis of CLAD and WAAM printed Ti–6Al–4V components," *Materials & Design,* vol. 89, pp. 559-567, 2016.

[51] B. Vrancken, L. Thijs, J.-P. Kruth, and J. Van Humbeeck, "Heat treatment of Ti6Al4V produced by Selective Laser Melting: Microstructure and mechanical properties," *Journal of Alloys and Compounds,* vol. 541, pp. 177-185, 2012.
[52] T. Wohlers, "Wohlers Report 2019: Additive Manufacturing and 3D Printing, State of the Industry," Fort Collins, CO, USA,, 2019.
[53] P. Vora, K. Mumtaz, I. Todd, and N. Hopkinson, "AlSi12 in-situ alloy formation and residual stress reduction using anchorless selective laser melting," *Additive manufacturing,* vol. 7, pp. 12-19, 2015.
[54] L. E. Murr *et al.*, "Fabrication of metal and alloy components by additive manufacturing: examples of 3D materials science," *Journal of Materials Research and technology,* vol. 1, no. 1, pp. 42-54, 2012.
[55] J. Mireles *et al.*, "Development of a fused deposition modeling system for low melting temperature metal alloys," *Journal of Electronic Packaging,* vol. 135, no. 1, 2013.
[56] M. A. Gibson *et al.*, "3D printing metals like thermoplastics: Fused filament fabrication of metallic glasses," *Materials Today,* vol. 21, no. 7, pp. 697-702, 2018.
[57] G. Vijh, A. Gokhale, S. Mishra, V. Singh, and N. Viswanathan, "Solid freeform fabrication of aluminum alloy components: Numerical simulations," *Transactions of the Indian Institute of Metals,* vol. 62, pp. 291-294, 2009.
[58] Z. Li *et al.*, "Metallic slurry preparation and printability assessment for material extrusion additive manufacturing," *Additive Manufacturing Letters,* vol. 8, p. 100189, 2024.
[59] Y. Fei, J. Xu, D. Yao, and J. Zhou, "From semisolid metal processing to thixotropic 3D printing of metallic alloys," *Virtual and Physical Prototyping,* vol. 17, no. 3, pp. 489-507, 2022.
[60] S. Finke and F. Feenstra, "Solid freeform fabrication by extrusion and deposition of semi- solid alloys," *Journal of Materials Science,* vol. 37, no. 15, pp. 3101-3106, 2002, doi: 10.1023/A:1016137723481.
[61] A. Jabbari and K. Abrinia, "Developing thixo-extrusion process for additive manufacturing of metals in semi-solid state," *Journal of Manufacturing Processes,* vol. 35, pp. 664-671, 2018.
[62] C. Lieberwirth, A. Harder, and H. Seitz, "Extrusion based additive manufacturing of metal parts," *J. Mech. Eng. Autom,* vol. 7, no. 2, pp. 79-83, 2017.
[63] S. C. Altıparmak, V. A. Yardley, Z. Shi, and J. Lin, "Extrusion-based additive manufacturing technologies: State of the art and future perspectives," *Journal of Manufacturing Processes,* vol. 83, pp. 607-636, 2022.
[64] M. Agarwala, R. v. Weeren, A. Bandyopadhyay, P. Whalen, A. Safari, and S. Danforth, "Fused deposition of ceramics and metals: an overview," in *1996 International Solid Freeform Fabrication Symposium*, 1996.
[65] "ASTM F2792 . Standard Terminology for Additive Manufacturing Technologies. ASTM; 2014.," ed.
[66] D. S. Thomas and S. W. Gilbert, "Costs and cost effectiveness of additive manufacturing," *NIST special publication,* vol. 1176, p. 12, 2014.
[67] V. W. Kaufui and H. Aldo, "A Review of Additive Manufacturing," *ISRN Mechanical Engineering,* vol. 2012, 2012, doi: 10.5402/2012/208760.
[68] J. Corney, "Rapid prototyping: principles and applications," vol. 25, ed. Bedford: Emerald Group Publishing Limited, 2005, p. 339.

[69] H. Jan, P. Jouni, T. Jukka, and W. Manfred, "Rapid manufacturing in the spare parts supply chain; Alternative approaches to capacity deployment," *Journal of Manufacturing Technology Management,* vol. 21, no. 6, pp. 687-697, 2010, doi: 10.1108/17410381011063996.
[70] K. Salonitis and S. Al Zarban, "Redesign optimization for manufacturing using additive layer techniques," *Procedia CIRP,* vol. 36, pp. 193-198, 2015.
[71] S. B. S. B. R. K. Negi, "BASICS, APPLICATIONS AND FUTURE OF ADDITIVE MANUFACTURING TECHNOLOGIES: A REVIEW," *Journal of Manufacturing Technology Research,* vol. 5, no. 1/2, p. 75, 2013.
[72] K. S. Chan, M. Koike, R. L. Mason, and T. Okabe, "Fatigue life of titanium alloys fabricated by additive layer manufacturing techniques for dental implants," *Metallurgical and Materials Transactions A,* vol. 44, no. 2, pp. 1010-1022, 2013.
[73] N. Guo and M. C. Leu, "Additive manufacturing: technology, applications and research needs," *Frontiers of Mechanical Engineering,* vol. 8, no. 3, pp. 215-243, 2013.
[74] S. H. Huang, P. Liu, A. Mokasdar, and L. Hou, "Additive manufacturing and its societal impact: a literature review," *The International Journal of Advanced Manufacturing Technology,* vol. 67, no. 5-8, pp. 1191-1203, 2013.
[75] Q. Liu, M. C. Leu, and S. M. Schmitt, "Rapid prototyping in dentistry: technology and application," *The international journal of advanced manufacturing technology,* vol. 29, no. 3-4, pp. 317-335, 2006.
[76] R. Dhakshyani, Y. Nukman, N. A. Osman, and C. Vijay, "Preliminary report: rapid prototyping models for Dysplastic hip surgery," *Open Medicine,* vol. 6, no. 3, pp. 266-270, 2011.
[77] F. P. Melchels, J. Feijen, and D. W. Grijpma, "A review on stereolithography and its applications in biomedical engineering," *Biomaterials,* vol. 31, no. 24, pp. 6121-6130, 2010.
[78] K. S. Prakash, T. Nancharaih, and V. S. Rao, "Additive manufacturing techniques in manufacturing-an overview," *Materials Today: Proceedings,* vol. 5, no. 2, pp. 3873-3882, 2018.
[79] I. Gibson, *Additive manufacturing technologies [electronic resource] : rapid prototyping to direct digital manufacturing*. New York ; London: New York ; London : Springer, 2010, 2010.
[80] H. P. Le, "Progress and trends in ink-jet printing technology," *Journal of Imaging Science and Technology,* vol. 42, no. 1, pp. 49-62, 1998.
[81] A. T. Gaynor, N. A. Meisel, C. B. Williams, and J. K. Guest, "Multiple-material topology optimization of compliant mechanisms created via PolyJet three-dimensional printing," *Journal of Manufacturing Science and Engineering,* vol. 136, no. 6, 2014.
[82] H. Bikas, P. Stavropoulos, and G. Chryssolouris, "Additive manufacturing methods and modelling approaches: a critical review," *The International Journal of Advanced Manufacturing Technology,* vol. 83, no. 1-4, pp. 389-405, 2016.
[83] R. Singh, "Three dimensional printing for casting applications: A state of art review and future perspectives," in *Advanced Materials Research*, 2010, vol. 83: Trans Tech Publ, pp. 342-349.
[84] R. Singh, V. Singh, and M. S. Saini, "Experimental investigations for statistically controlled rapid moulding solution of plastics using polyjet printing," in *ASME*

International Mechanical Engineering Congress and Exposition, 2010, vol. 44274, pp. 1049-1053.
[85] A. A. Khalate, X. Bombois, R. Babuška, H. Wijshoff, and R. Waarsing, "Performance improvement of a drop-on-demand inkjet printhead using an optimization-based feedforward control method," *Control Engineering Practice,* vol. 19, no. 8, pp. 771-781, 2011.
[86] D. Eyers and K. Dotchev, "Technology review for mass customisation using rapid manufacturing," *Assembly Automation,* 2010.
[87] O. A. Mohamed, S. H. Masood, and J. L. Bhowmik, "Optimization of fused deposition modeling process parameters: a review of current research and future prospects," *Advances in Manufacturing,* vol. 3, no. 1, pp. 42-53, 2015.
[88] K. S. Boparai, R. Singh, and H. Singh, "Development of rapid tooling using fused deposition modeling: a review," *Rapid Prototyping Journal,* 2016.
[89] C. Körner, "Additive manufacturing of metallic components by selective electron beam melting—a review," *International Materials Reviews,* vol. 61, no. 5, pp. 361-377, 2016.
[90] E. C. e Costa, J. P. Duarte, and P. Bártolo, "A review of additive manufacturing for ceramic production," *Rapid Prototyping Journal,* 2017.
[91] F. Bos, R. Wolfs, Z. Ahmed, and T. Salet, "Additive manufacturing of concrete in construction: potentials and challenges of 3D concrete printing," *Virtual and Physical Prototyping,* vol. 11, no. 3, pp. 209-225, 2016.
[92] P. Parandoush and D. Lin, "A review on additive manufacturing of polymer-fiber composites," *Composite Structures,* vol. 182, pp. 36-53, 2017.
[93] T. D. Ngo, A. Kashani, G. Imbalzano, K. T. Nguyen, and D. Hui, "Additive manufacturing (3D printing): A review of materials, methods, applications and challenges," *Composites Part B: Engineering,* vol. 143, pp. 172-196, 2018.
[94] Y. Brif, M. Thomas, and I. Todd, "The use of high-entropy alloys in additive manufacturing," *Scripta Materialia,* vol. 99, pp. 93-96, 2015.
[95] C. Mikler *et al.*, "Laser additive manufacturing of magnetic materials," *Jom,* vol. 69, no. 3, pp. 532-543, 2017.
[96] S. Pauly *et al.*, "Processing metallic glasses by selective laser melting," *Materials Today,* vol. 16, no. 1-2, pp. 37-41, 2013.
[97] K. A. Mumtaz and N. Hopkinson, "Laser melting functionally graded composition of Waspaloy® and Zirconia powders," *Journal of materials science,* vol. 42, no. 18, pp. 7647-7656, 2007.
[98] D. Bourell *et al.*, "Materials for additive manufacturing," *CIRP Annals,* vol. 66, no. 2, pp. 659-681, 2017.
[99] F. Cabanettes *et al.*, "Topography of as built surfaces generated in metal additive manufacturing: a multi scale analysis from form to roughness," *Precision Engineering,* vol. 52, pp. 249-265, 2018.
[100] V. Bhavar, P. Kattire, V. Patil, S. Khot, K. Gujar, and R. Singh, "A review on powder bed fusion technology of metal additive manufacturing," in *4th International Conference and Exhibition on Additive Manufacturing Technologies-AM-2014, September*, 2014, pp. 1-2.
[101] H. Liu, T. Sparks, F. Liou, and D. M. Dietrich, "Residual stress and deformation modelling for metal additive manufacturing processes," in *Proceedings of the*

World Congress on Mechanical, Chemical, and Material Engineering (MCM 2015) Barcelona, Spain–July, 2015, pp. 20-21.

[102] K. Mumtaz, "Layered Extrusion of engineering Metal Alloys (LEMA) using Semi-Solid
Thixotropic Feedstock," ed.

[103] M. Baumers, C. Tuck, R. Hague, I. Ashcroft, and R. Wildman, "A comparative study of metallic additive manufacturing power consumption," in *Solid freeform fabrication symposium*, 2010, vol. 2009, pp. 278-288.

[104] M. Annoni, H. Giberti, and M. Strano, "Feasibility Study of an Extrusion- based Direct Metal Additive Manufacturing Technique," *Procedia Manufacturing,* vol. 5, pp. 916-927, 2016, doi: 10.1016/j.promfg.2016.08.079.

[105] D.-G. Ahn, "Direct metal additive manufacturing processes and their sustainable applications for green technology: A review," *International Journal of Precision Engineering and Manufacturing-Green Technology,* vol. 3, no. 4, pp. 381-395, 2016, doi: 10.1007/s40684-016-0048-9.

[106] D. D. Gu, W. Meiners, K. Wissenbach, and R. Poprawe, "Laser additive manufacturing of metallic components: materials, processes and mechanisms," *International Materials Reviews,* vol. 57, no. 3, pp. 133-164, 2012, doi: 10.1179/1743280411Y.0000000014.

[107] T. Himmer, T. Nakagawa, and M. Anzai, "Lamination of metal sheets," *Computers in Industry,* vol. 39, no. 1, pp. 27-33, 1999.

[108] D. I. Wimpenny, B. Bryden, and I. R. Pashby, "Rapid laminated tooling," *Journal of materials processing technology,* vol. 138, no. 1-3, pp. 214-218, 2003.

[109] B. Mueller and D. Kochan, "Laminated object manufacturing for rapid tooling and patternmaking in foundry industry," *Computers in Industry,* vol. 39, no. 1, pp. 47-53, 1999.

[110] Statista. Most used 3D printing technologies worldwide 2021 [Online] Available: https://www.statista.com/statistics/560304/worldwide-survey-3d-printing-top-technologies/

[111] W. Gao *et al.*, "The status, challenges, and future of additive manufacturing in engineering," *Computer-Aided Design,* vol. 69, pp. 65-89, 2015.

[112] S. Singh, G. Singh, C. Prakash, and S. Ramakrishna, "Current status and future directions of fused filament fabrication," *Journal of Manufacturing Processes,* vol. 55, pp. 288-306, 2020.

[113] S. Singh, S. Ramakrishna, and R. Singh, "Material issues in additive manufacturing: A review," *Journal of Manufacturing Processes,* vol. 25, pp. 185-200, 2017.

[114] M. Agarwala, R. Van Weeren, A. Bandyopadhyay, P. Whalen, A. Safari, and S. Danforth, "Fused deposition of ceramics and metals: an overview," in *Proceedings of the Solid Freeform Fabrication Symposium, Austin, Texas*, 1996.

[115] M. Jafari, W. Han, F. Mohammadi, A. Safari, S. Danforth, and N. Langrana, "A novel system for fused deposition of advanced multiple ceramics," *Rapid Prototyping Journal,* 2000.

[116] Ü. Çevik and M. Kam, "A review study on mechanical properties of obtained products by FDM method and metal/polymer composite filament production," *Journal of Nanomaterials,* vol. 2020, 2020.

[117] U. Scheithauer, T. Slawik, E. Schwarzer, H. Richter, T. Moritz, and A. Michaelis, "Additive manufacturing of metal-ceramic-composites by thermoplastic 3D-printing (3DTP)," *Journal of Ceramic Science and Technology,* vol. 6, no. 2, pp. 125-32, 2015.
[118] L. Novakova-Marcincinova, J. Novak-Marcincin, J. Barna, and J. Torok, "Special materials used in FDM rapid prototyping technology application," in *2012 IEEE 16th International Conference on Intelligent Engineering Systems (INES)*, 2012: IEEE, pp. 73-76.
[119] Y. Thompson, J. Gonzalez-Gutierrez, C. Kukla, and P. Felfer, "Fused filament fabrication, debinding and sintering as a low cost additive manufacturing method of 316L stainless steel," *Additive Manufacturing,* vol. 30, p. 100861, 2019.
[120] H. Ramazani and A. Kami, "Metal FDM, a new extrusion-based additive manufacturing technology for manufacturing of metallic parts: a review," *Progress in Additive Manufacturing,* pp. 1-18, 2022.
[121] A. I. Nurhudan, S. Supriadi, Y. Whulanza, and A. S. Saragih, "Additive manufacturing of metallic based on extrusion process: a review," *Journal of Manufacturing Processes,* vol. 66, pp. 228-237, 2021.
[122] H. Valkenaers, F. Vogeler, E. Ferraris, A. Voet, and J.-P. Kruth, "A novel approach to additive manufacturing: screw extrusion 3D-printing," in *Proceedings of the 10th International Conference on Multi-Material Micro Manufacture*, 2013: Research Publishing; Singapore, pp. 235-238.
[123] K. D. Migler and R. E. Ricker, "Measurement science roadmap for polymer-based additive manufacturing," 2016.
[124] B. N. Turner, R. Strong, and S. A. Gold, "A review of melt extrusion additive manufacturing processes: I. Process design and modeling," *Rapid Prototyping Journal,* vol. 20, no. 3, pp. 192-204, 2014, doi: 10.1108/RPJ-01-2013-0012.
[125] I. Gibson, D. W. Rosen, and B. Stucker, *Additive manufacturing technologies: rapid prototyping to direct digital manufacturing*. Springer Verlag, 2010.
[126] B. Reddy, N. Reddy, and A. Ghosh, "Fused deposition modelling using direct extrusion," *Virtual and Physical Prototyping,* vol. 2, no. 1, pp. 51-60, 2007.
[127] C. Suwanpreecha and A. Manonukul, "A Review on Material Extrusion Additive Manufacturing of Metal and How It Compares with Metal Injection Moulding," *Metals,* vol. 12, no. 3, p. 429, 2022.
[128] J. Gonzalez-Gutierrez *et al.*, "Models to predict the viscosity of metal injection molding feedstock materials as function of their formulation," *Metals,* vol. 6, no. 6, p. 129, 2016.
[129] K. Elkins, H. Nordby, C. Janak, R. W. Gray IV, J. Helge Bohn, and D. G. Baird, "Soft elastomers for fused deposition modeling," in *1997 International Solid Freeform Fabrication Symposium*, 1997.
[130] N. Kumar, P. K. Jain, P. Tandon, and P. M. Pandey, "Extrusion-based additive manufacturing process for producing flexible parts," *Journal of the Brazilian Society of Mechanical Sciences and Engineering,* vol. 40, no. 3, pp. 1-12, 2018.
[131] H. Valkenaers, F. Vogeler, A. Voet, and J.-P. Kruth, "Screw extrusion based 3D printing, a novel additive manufacturing technology," in *COMA'13*, 2013.
[132] A. Bellini, L. Shor, and S. I. Guceri, "New developments in fused deposition modeling of ceramics," *Rapid Prototyping Journal,* vol. 11, no. 4, pp. 214-220, 2005, doi: 10.1108/13552540510612901.

[133] N. Cruz, L. Santos, J. Vasco, and F. Barreiros, "Binder system for fused deposition of metals," in *Proceedings of the Euro PM2013, Congress & Exhibition, Gothenburg, Sweden*, 2013, pp. 15-18.
[134] I. Campbell and T. Wohlers. "Markforged: Taking a different approach to metal Additive Manufacturing." https://www.metal-am.com/wp-content/uploads/sites/4/2017/06/MAGAZINE-Metal-AM-Summer-2017-PDF-sp.pdf (accessed 10/03/2022.
[135] T. Wohlers. "Desktop Metal: A rising star of metal AM targets speed, cost and high-volume production." https://www.metal-am.com/wp-content/uploads/sites/4/2017/06/MAGAZINE-Metal-AM-Summer-2017-PDF-sp.pdf (accessed 10/03/2022.
[136] M. Vaezi, P. Drescher, and H. Seitz, "Beamless Metal Additive Manufacturing," *Materials,* vol. 13, no. 4, p. 922, 2020.
[137] A. Bandyopadhyay, R. K. Panda, V. F. Janas, M. K. Agarwala, S. C. Danforth, and A. Safari, "Processing of piezocomposites by fused deposition technique," *Journal of the American Ceramic Society,* vol. 80, no. 6, pp. 1366-1372, 1997.
[138] G. Wu, N. A. Langrana, R. Sadanji, and S. Danforth, "Solid freeform fabrication of metal components using fused deposition of metals," *Materials & Design,* vol. 23, no. 1, pp. 97-105, 2002.
[139] Y. Yu, F. Liu, and J. Liu, "Direct 3D printing of low melting point alloy via adhesion mechanism," *Rapid Prototyping Journal,* vol. 23, no. 3, pp. 642-650, 2017, doi: 10.1108/RPJ-12-2015-0185.
[140] N. Venkataraman *et al.*, "Feedstock material property–process relationships in fused deposition of ceramics (FDC)," *Rapid Prototyping Journal,* 2000.
[141] P. Kapranos, "Thixoforming of Aluminum A201-Expectations and Fulfilment," in *Solid State Phenomena*, 2019, vol. 285: Trans Tech Publ, pp. 476-488.
[142] P. Joly and R. Mehrabian, "The rheology of a partially solid alloy," *Journal of Materials Science,* vol. 11, no. 8, pp. 1393-1418, 1976.
[143] H. V. Atkinson, "Semisolid processing of metallic materials," *Materials Science and Technology,* vol. 26, no. 12, pp. 1401-1413, 2010.
[144] O. Lashkari and R. Ghomashchi, "The implication of rheology in semi- solid metal processes: An overview," *Journal of Materials Processing Tech.,* vol. 182, no. 1, pp. 229-240, 2007, doi: 10.1016/j.jmatprotec.2006.08.003.
[145] D. Brabazon, D. Browne, and A. Carr, "Mechanical stir casting of aluminium alloys from the mushy state: process, microstructure and mechanical properties," *Materials Science and Engineering: A,* vol. 326, no. 2, pp. 370-381, 2002.
[146] M. C. Flemings, *Solidification processing*. New York ; London (etc.): New York ; London etc. : McGraw-Hill, 1974, 1974.
[147] C. S. Rice, "Solid freeform fabrication using semi-solid processing," Massachusetts Institute of Technology, 1995.
[148] P. F. Mendez, "Joining metals using semi-solid slurries," Massachusetts Institute of Technology, 1995.
[149] P. Mendez, C. Rice, and S. Brown, "Joining using semisolid metals," *WELDING JOURNAL-NEW YORK-,* vol. 81, no. 9, pp. 181-S, 2002.
[150] S. B. Brown, "Method and apparatus for metal solid freeform fabrication utilizing partially solidified metal slurry," ed: Google Patents, 1997.

[151] P. F. Mendez and S. B. Brown, "Method and apparatus for metal solid freeform fabrication utilizing partially solidified metal slurry," ed: Google Patents, 1999.
[152] S. Finke, "Solid freeform fabrication of metal components by extrustion and deposition of semi-solid metals," Twente University Press (TUP), 2002. [Online]. Available: https://research.utwente.nl/en/publications/solid-freeform-fabrication-of-metal-components-by-extrustion-and-deposition-of-semisolid-metals(3ed1e8ad-a9d1-4db9-bocf-a6e0259e339a).html
[153] A. Pola, M. Tocci, and P. Kapranos, "Microstructure and properties of semi-solid aluminum alloys: a literature review," *Metals,* vol. 8, no. 3, p. 181, 2018.
[154] J. Mewis and N. J. Wagner, "Thixotropy," *Advances in Colloid and Interface Science,* vol. 147, pp. 214-227, 2009, doi: 10.1016/j.cis.2008.09.005.
[155] H. A. Barnes, "Thixotropy—a review," *Journal of Non-Newtonian Fluid Mechanics,* vol. 70, no. 1, pp. 1-33, 1997, doi: 10.1016/S0377-0257(97)00004-9.
[156] P. A. Joly, "Rheological properties and structure of a semi-solid tin-lead alloy," Massachusetts Institute of Technology, 1974.
[157] M. Modigell, A. Pola, and M. Tocci, "Rheological Characterization of Semi- Solid Metals: A Review," vol. 8, ed. Basel: MDPI AG, 2018, p. 245.
[158] N. H. Husain, A. H. Ahmad, and M. M. Rashidi, "An overview of thixoforming process," vol. 257, ed, 2017, p. <xocs:firstpage xmlns:xocs=""/>.
[159] C. Martin, P. Kumar, and S. Brown, "Constitutive modeling and characterization of the flow behavior of semi-solid metal alloy slurries—II. Structural evolution under shear deformation," *Acta metallurgica et materialia,* vol. 42, no. 11, pp. 3603-3614, 1994.
[160] H. F. Giles Jr, E. M. Mount III, and J. R. Wagner Jr, *Extrusion: the definitive processing guide and handbook*. William Andrew, 2004.
[161] A. Ahmad, S. Naher, and D. Brabazon, "Effects of cooling rates on thermal profiles and microstructure of aluminium 7075," *International Journal of Automotive and Mechanical Engineering,* vol. 9, p. 1685, 2014.
[162] T. Haga and P. Kapranos, "Simple rheocasting processes," *Journal of Materials Processing Technology,* vol. 130, pp. 594-598, 2002.
[163] E. Tzimas and A. Zavaliangos, "Evaluation of volume fraction of solid in alloys formed by semisolid processing," *Journal of Materials Science,* vol. 35, no. 21, pp. 5319-5330, 2000, doi: 10.1023/A:1004890711322.
[164] W. Wołczyński, W. Krajewski, R. Ebner, and J. Kloch, "The use of equilibrium phase diagram for the calculation of non-equilibrium precipitates in dendritic solidification. Theory," *Calphad,* vol. 25, no. 3, pp. 401-408, 2001.
[165] J.-O. Andersson, T. Helander, L. Höglund, P. Shi, and B. Sundman, "Thermo-Calc & DICTRA, computational tools for materials science," *Calphad,* vol. 26, no. 2, pp. 273-312, 2002.
[166] A. Megalingam, A. H. B. Ahmad, M. R. B. Maarof, and K. Sudhakar, "Viscosity measurements in semi-solid metal processing: current status and recent developments," *The International Journal of Advanced Manufacturing Technology,* pp. 1-25, 2021.
[167] S. Nafisi and R. Ghomashchi, *Semi-solid processing of aluminum alloys*. Springer, 2016.
[168] M. Flemings, R. Riek, and K. Young, "Rheocasting," *Materials Science and Engineering,* vol. 25, pp. 103-117, 1976.

[169] M. Rosso, "Thixocasting and rheocasting technologies, improvements going on," *Journal on Achievements in Materials and Manufacturing Engineering,* vol. 54, no. 1, pp. 110-119, 2012.
[170] G. Hirt and R. Kopp, *Thixoforming: Semi-solid metal processing*. John Wiley & Sons, 2009.
[171] S. Nafisi and R. Ghomashchi, "Semi-solid metal processing routes: an overview," *Canadian metallurgical quarterly,* vol. 44, no. 3, pp. 289-304, 2005.
[172] P. Prasad, S. Ray, J. Gaindhar, and M. Kapoor, "Relation between processing, microstructure and mechanical properties of rheocast Al-Cu alloys," *Journal of materials science,* vol. 23, no. 3, pp. 823-829, 1988.
[173] K. Ichikawa, S. Ishizuka, and Y. Kinoshita, "Stirring conditions and grain refinement in Al–Cu alloys by rheocasting," *Transactions of the Japan institute of metals,* vol. 28, no. 2, pp. 135-144, 1987.
[174] X. Pan, H. Zhang, A. Wang, B. Ding, K. Qiu, and Z. Hu, "Trend and development of semi-solid metal processing," *Journal of Materials Science and Technology,* vol. 16, no. 5, pp. 453-460, 2000.
[175] A. Mitsuru, S. Hiroto, H. Yasunori, S. Tatsuo, S. Satoru, and Y. Atsushi, "Method and apparatus for shaping semisolid metals," *UBE Industries Limited, Patent EP,* vol. 745694, p. A1, 1996.
[176] H. Kaufmann and P. J. Uggowitzer, "Fundamentals of the new rheocasting process for magnesium alloys," *Advanced engineering materials,* vol. 3, no. 12, pp. 963-967, 2001.
[177] S. P. Midson and A. Jackson, "A comparison of Thixocasting and Rheocasting," in *World Foundry Congress*, 2006, p. 10.
[178] K. P. Young, C. P. Kyonka, and J. A. Courtois, "Fine grained metal composition," ed: Google Patents, 1983.
[179] P. Kapranos, D. Kirkwood, and C. Sellars, "Thixoforming high melting point alloys into non-metallic dies," in *4 th International Conference on Semi-Solid Processing of Alloys and Composites*, 1996, pp. 306-311.
[180] E. Tzimas, *Evolution of microstructure and rheological behavior of alloys in the semisolid state*. Drexel University, 1997.
[181] J. C. Choi and H. J. Park, "Microstructural characteristics of aluminum 2024 by cold working in the SIMA process," *Journal of Materials Processing Technology,* vol. 82, no. 1-3, pp. 107-116, 1998.
[182] E. Tzimas and A. Zavaliangos, "Evolution of near-equiaxed microstructure in the semisolid state," *Materials Science and Engineering: A,* vol. 289, no. 1-2, pp. 228-240, 2000.
[183] P. Kapranos, D. Kirkwood, and C. Sellars, "Semi-solid processing of tool steel," *Le Journal de Physique IV,* vol. 3, no. C7, pp. C7-835-C7-840, 1993.
[184] D. Kirkwood, C. Sellars, and L. Boyed, "Thixotropic materials," *Patent NumberUS 5133811,* 1992.
[185] D. Liu, H. Atkinson, P. Kapranos, W. Jirattiticharoean, and H. Jones, "Microstructural evolution and tensile mechanical properties of thixoformed high performance aluminium alloys," *Materials Science and Engineering: A,* vol. 361, no. 1-2, pp. 213-224, 2003.

[186] Y. Wang, S. Zhao, and C. Zhang, "Grain refinement of aluminum alloy bar by a modified RAP process for semi-solid forming," *Materials Transactions,* p. M2016271, 2016.
[187] G. Yan, S. Zhao, S. Ma, and H. Shou, "Microstructural evolution of A356. 2 alloy prepared by the SIMA process," *Materials Characterization,* vol. 69, pp. 45-51, 2012.
[188] F. Czerwinski, "strain induced melt activation (SIMA): original concept, its impact and present understanding," *International Journal of Cast Metals Research,* pp. 1-8, 2020.
[189] F. Czerwinski, "Size evolution of the unmelted phase during injection molding of semisolid magnesium alloys," *Scripta materialia,* vol. 48, no. 4, pp. 327-331, 2003.
[190] Y. Zhang, Y. Liu, Q. Zhang, Z. Cao, X. Cui, and Y. Wang, "Microstructural evolution of thixomolded AZ91D magnesium alloy with process parameters variation," *Materials Science and Engineering: A,* vol. 444, no. 1-2, pp. 251-256, 2007.
[191] Y. Zhang, Y. Liu, Z. Cao, Q. Zhang, and L. Zhang, "Mechanical properties of thixomolded AZ91D magnesium alloy," *Journal of Materials Processing Technology,* vol. 209, no. 3, pp. 1375-1384, 2009.
[192] M. Mohammed, M. Omar, M. Salleh, K. Alhawari, and M. Abdelgnei, "An overview of semi-solid metal processing," *Australian Journal of Basic and Applied Sciences,* vol. 8, no. 19, pp. 369-373, 2014.
[193] H. V. Atkinson, "Alloys for semi-solid processing," in *Solid State Phenomena*, 2013, vol. 192: Trans Tech Publ, pp. 16-27.
[194] H. Atkinson, "Current status of semi-solid processing of metallic materials," in *Advances in Material Forming*: Springer, 2007, pp. 81-98.
[195] E. Cardoso Legoretta, H. Atkinson, and H. Jones, "Cooling slope casting to obtain thixotropic feedstock I: observations with a transparent analogue," *Full Set - Includes `Journal of Materials Science Letters',* vol. 43, no. 16, pp. 5448-5455, 2008, doi: 10.1007/s10853-008-2828-2.
[196] R. Kopp, D. Neudenberger, and G. Winning, "Different concepts of thixoforging and experiments for rheological data," *Journal of Materials Processing Tech.,* vol. 111, no. 1, pp. 48-52, 2001, doi: 10.1016/S0924-0136(01)00495-2.
[197] M. Salleh, M. Omar, J. Syarif, M. Mohammed, and K. Alhawari, "Thermodynamic simulation on thixoformability of aluminium alloys for semisolid metal processing," *International Journal of Mathematics and computers in simulation,* vol. 7, no. 3, pp. 286-293, 2013.
[198] Z. Chang, X. Wang, Y. Wu, L. Peng, and W. Ding, "Review on criteria for assessing the processability of semisolid alloys," *Materials Letters,* vol. 282, p. 128835, 2021.
[199] K. N. Campo, D. D. de Lima, É. S. N. Lopes, and R. Caram, "On the selection of Ti–Cu alloys for thixoforming processes: Phase diagram and microstructural evaluation," *Journal of materials science,* vol. 50, no. 24, pp. 8007-8017, 2015.
[200] Y. Liu, A. Das, and Z. Fan, "Thermodynamic predictions of Mg-Al-M (M= Zn, Mn, Si) alloy compositions amenable to semisolid metal processing," *Materials science and technology,* vol. 20, no. 1, pp. 35-41, 2004.
[201] A. A. Kazakov, "Alloy compositions for semisolid forming," *Advanced Materials & Processes,* vol. 157, no. 3, pp. 31-31, 2000.

[202] J. Patel, Y. Liu, G. Shao, and Z. Fan, "Rheo-processing of an alloy specifically designed for semi-solid metal processing based on the Al–Mg–Si system," *Materials Science and Engineering: A,* vol. 476, no. 1-2, pp. 341-349, 2008.
[203] E. Cerri, E. Evangelista, S. Spigarelli, P. Cavaliere, and F. DeRiccardis, "Effects of thermal treatments on microstructure and mechanical properties in a thixocast 319 aluminum alloy," *Materials Science and Engineering: A,* vol. 284, no. 1-2, pp. 254-260, 2000.
[204] E. Zoqui, "Alloys for semisolid processing," 2014.
[205] B. Hallstedt, D. Neuschütz, E. Balitchev, and H. Shimahara, "Semi- solid processing of alloys: Principles, thermodynamic selection criteria, applicability," vol. 46, ed, 2006, pp. 1852-1857.
[206] A. M. Camacho, H. Atkinson, P. Kapranos, and B. Argent, "Thermodynamic predictions of wrought alloy compositions amenable to semi-solid processing," *Acta Materialia,* vol. 51, no. 8, pp. 2319-2330, 2003.
[207] D. Liu, H. V. Atkinson, and H. Jones, "Thermodynamic prediction of thixoformability in alloys based on the Al–Si–Cu and Al–Si–Cu–Mg systems," *Acta Materialia,* vol. 53, no. 14, pp. 3807-3819, 2005.
[208] G. Govender, H. Möller, and U. A. Curle, "Alloy design for semi solid metal forming," in *Materials Science Forum*, 2014, vol. 783: Trans Tech Publ, pp. 136-141.
[209] S. Chayong, H. Atkinson, and P. Kapranos, "Thixoforming 7075 aluminium alloys," *Materials Science and Engineering: A,* vol. 390, no. 1-2, pp. 3-12, 2005.
[210] F. Czerwinski, "Semisolid processing of magnesium alloys: Progress and limitations," in *Solid State Phenomena*, 2019, vol. 285: Trans Tech Publ, pp. 489-494.
[211] L. Pasternak, R. Carnahan, R. Decker, and R. Kilbert, "Semi-solid production processing of magnesium alloys by thixomolding," *Processing of Semi-Solid Alloys and Composites,* pp. 159-169, 1992.
[212] L. Gan *et al.*, "Semi-solid processing of aluminum and magnesium alloys: Status, opportunity, and challenge in China," *Transactions of Nonferrous Metals Society of China,* vol. 31, no. 11, pp. 3255-3280, 2021.
[213] H. Patel, D. Chen, S. Bhole, and K. Sadayappan, "Microstructure and tensile properties of thixomolded magnesium alloys," *Journal of alloys and Compounds,* vol. 496, no. 1-2, pp. 140-148, 2010.
[214] A. Buhrig-Polaczek and J. Aguilar, "Materials development for semi-solid-metal processing (SSM)," *Proceeding of the 8^ th S2P. Cyprus,* 2004.
[215] J. Dutkiewicz, Ł. Rogal, K. Sołek, Z. Mitura, and P. Kapranos, "Thixoforming of spray formed M2 tool steel," *International Journal of Material Forming,* vol. 3, no. 1, pp. 755-758, 2010.
[216] P. Cezard and T. Sourmail, "Thixoforming of steel: a state of the art from an industrial point of view," in *Solid State Phenomena*, 2008, vol. 141: Trans Tech Publ, pp. 25-35.
[217] R. Kopp, J. Kallweit, T. Möller, and I. Seidl, "Forming and joining of commercial steel grades in the semi-solid state," *Journal of Materials Processing Technology,* vol. 130, pp. 562-568, 2002.
[218] M. Z. Omar, E. J. Palmiere, A. A. Howe, H. V. Atkinson, and P. Kapranos, "Thixoforming of a high performance HP9/ 4/ 30 steel," *Materials Science & Engineering A,* vol. 395, no. 1, pp. 53-61, 2005, doi: 10.1016/j.msea.2004.12.013.

[219] M. Omar, H. Atkinson, A. Howe, E. Palmiere, P. Kapranos, and M. Ghazali, "Solid–liquid structural break-up in M2 tool steel for semi-solid metal processing," *Journal of Materials Science,* vol. 44, no. 3, pp. 869-874, 2009.
[220] V. Pouyafar, S. Sadough, F. Hosseini, and A. Jabbari, "High temperature flow behaviour of semi-solid steel alloys," in *Solid State Phenomena*, 2013, vol. 192: Trans Tech Publ, pp. 365-369.
[221] M. Flemings, "Semi-solid forming: the process and the path forward," *Metallurgical Science and Tecnology,* vol. 18, no. 2, 2000.
[222] V. L. Dao, S. D. Zhao, W. J. Lin, and Y. Q. Chen, "Numerical simulation on thixocasting process of auto box-like," in *Advanced Materials Research*, 2012, vol. 341: Trans Tech Publ, pp. 177-182.
[223] H. V. Atkinson and P. J. Ward, "Flow visualization for semi-solid processing," *JOM,* vol. 58, no. 6, pp. 21-23, 2006.
[224] W. Winterbottom, "Semi-solid forming applications: high volume automotive products," *Metallurgical Science and Tecnology,* vol. 18, no. 2, 2000.
[225] W. Miller *et al.*, "Recent development in aluminium alloys for the automotive industry," *Materials Science and Engineering: A,* vol. 280, no. 1, pp. 37-49, 2000.
[226] P. Seo, H. Kim, and C. Kang, "Numerical integration design process to development of suspension parts by semi-solid die casting process," *Journal of Materials Processing Technology,* vol. 183, no. 1, pp. 18-32, 2007.
[227] Y. Birol, "Semi-solid processing of the primary aluminium die casting alloy A365," *Journal of Alloys and Compounds,* vol. 473, no. 1-2, pp. 133-138, 2009.
[228] K. A. Mumtaz, P. Vora, and N. Hopkinson, "A Method to Eliminate Anchors/Supports from Directly Laser Melted Metal Powder Bed Processes," ed, 2011.
[229] K. Rane and M. Strano, "A comprehensive review of extrusion-based additive manufacturing processes for rapid production of metallic and ceramic parts," *Advances in Manufacturing,* vol. 7, pp. 155-173, 2019.
[230] J. Costa, E. Sequeiros, M. T. Vieira, and M. Vieira, "Additive manufacturing: Material extrusion of metallic parts," *U. Porto Journal of Engineering,* vol. 7, no. 3, pp. 53-69, 2021.
[231] H. Gong, D. Snelling, K. Kardel, and A. Carrano, "Comparison of stainless steel 316L parts made by FDM-and SLM-based additive manufacturing processes," *Jom,* vol. 71, pp. 880-885, 2019.
[232] W. Zhou, R. Apkarian, Z. L. Wang, and D. Joy, "Fundamentals of scanning electron microscopy (SEM)," in *Scanning microscopy for nanotechnology*: Springer, 2006, pp. 1-40.
[233] S. Amelinckx, D. Van Dyck, J. Van Landuyt, and G. van Tendeloo, *Electron microscopy: principles and fundamentals*. John Wiley & Sons, 2008.
[234] P. J. Goodhew, J. Humphreys, and R. Beanland, *Electron microscopy and analysis*. CRC press, 2000.
[235] J. I. Goldstein, D. E. Newbury, J. R. Michael, N. W. Ritchie, J. H. J. Scott, and D. C. Joy, *Scanning electron microscopy and X-ray microanalysis*. Springer, 2017.
[236] A. Mohammed and A. Abdullah, "Scanning electron microscopy (SEM): A review," in *Proceedings of the 2018 International Conference on Hydraulics and Pneumatics—HERVEX, Băile Govora, Romania*, 2018, pp. 7-9.

[237] L. Reimer, "Scanning electron microscopy: physics of image formation and microanalysis," ed: IOP Publishing, 2000.
[238] M. E. Brown, *Introduction to thermal analysis: techniques and applications*. Springer Science & Business Media, 2001.
[239] V. S. Ramachandran, R. M. Paroli, J. J. Beaudoin, and A. H. Delgado, *Handbook of thermal analysis of construction materials*. William Andrew, 2002.
[240] J. D. Menczel, L. Judovits, R. B. Prime, H. E. Bair, M. Reading, and S. Swier, "Differential scanning calorimetry (DSC)," *Thermal analysis of polymers: Fundamentals and applications,* pp. 7-239, 2009.
[241] C. Schick, "Differential scanning calorimetry (DSC) of semicrystalline polymers," *Analytical and bioanalytical chemistry,* vol. 395, no. 6, p. 1589, 2009.
[242] W. J. Boettinger, U. R. Kattner, K.-W. Moon, and J. H. Perepezko, "DTA and heat-flux DSC measurements of alloy melting and freezing," in *Methods for phase diagram Determination*: Elsevier, 2007, pp. 151-221.
[243] H. E. Boyer and T. L. Gall, "Metals handbook; desk edition," 1985.
[244] F. M. Azizan, H. Purwanto, and M. Y. Mustafa, "Effect of adding Ag on tensile and microstructure properties of zinc alloy," *IJET-IJENS,* vol. 12, no. 03, pp. 78-84, 2012.
[245] M. Arif, M. Omar, and N. Muhamad, "Production of nondendritic semisolid ZA3 alloy through heat treatment," *Journal of Applied Sciences,* vol. 11, no. 2, pp. 323-329, 2011.
[246] M. Abou El-khair, A. Daoud, and A. Ismail, "Effect of different Al contents on the microstructure, tensile and wear properties of Zn-based alloy," *Materials Letters,* vol. 58, no. 11, pp. 1754-1760, 2004.
[247] J.-E. Lee, K.-S. Kim, K. Suganuma, J. Takenaka, and K. Hagio, "Interfacial properties of Zn–Sn alloys as high temperature lead-free solder on Cu substrate," *Materials Transactions,* vol. 46, no. 11, pp. 2413-2418, 2005.
[248] J.-E. Lee, K.-S. Kim, K. Suganuma, M. Inoue, and G. Izuta, "Thermal properties and phase stability of Zn-Sn and Zn-In alloys as high temperature lead-free solder," *Materials transactions,* vol. 48, no. 3, pp. 584-593, 2007.
[249] K. Suganuma, S.-J. Kim, and K.-S. Kim, "High-temperature lead-free solders: Properties and possibilities," *JOM Journal of the Minerals, Metals and Materials Society,* vol. 61, no. 1, p. 64, 2009.
[250] W. L. Santos, C. Brito, J. M. Quaresma, J. E. Spinelli, and A. Garcia, "Plate-like cell growth during directional solidification of a Zn–20wt% Sn high-temperature lead-free solder alloy," *Materials Science and Engineering: B,* vol. 182, pp. 29-36, 2014.
[251] S. A. Musa, M. A. A. Mohd Salleh, and S. Norainiza, "Zn-Sn based high temperature solder-A short review," in *Advanced Materials Research*, 2013, vol. 795: Trans Tech Publ, pp. 518-521.
[252] S. R. Chandrasekaran and B. K. Sharma, "From waste to resources: How to integrate recycling into the production cycle of plastics," in *Plastics to Energy*: Elsevier, 2019, pp. 345-364.
[253] J. H. Flynn, "Analysis of DSC results by integration," *Thermochimica acta,* vol. 217, pp. 129-149, 1993.
[254] C. Muthuraja, "Experimental investigation and thermodynamic prediction of new class of thixoformable magnesium alloys."

[255] Y. Birol, "Solid fraction analysis with DSC in semi-solid metal processing," *Journal of Alloys and compounds,* vol. 486, no. 1-2, pp. 173-177, 2009.
[256] A. Kroupa, "Modelling of phase diagrams and thermodynamic properties using Calphad method–Development of thermodynamic databases," *Computational Materials Science,* vol. 66, pp. 3-13, 2013.
[257] B. Jansson, B. Jönsson, B. Sundman, and J. Ågren, "The thermo calc project," *Thermochimica acta,* vol. 214, no. 1, pp. 93-96, 1993.
[258] S. Nafisi, D. Emadi, and R. Ghomashchi, "Semi solid metal processing: The fraction solid dilemma," *Materials Science and Engineering: A,* vol. 507, no. 1-2, pp. 87-92, 2009.
[259] D. Larouche, "Computation of solidification paths in multiphase alloys with back-diffusion," *Calphad,* vol. 31, no. 4, pp. 490-504, 2007.
[260] D. H. Kirkwood, C. M. Sellars, and L. G. Boyed, "Thixotropic materials," ed: Google Patents, 1992.
[261] F. Czerwinski, "Thermomechanical Processing of Metal Feedstock for Semisolid Forming: A Review," *Metallurgical and Materials Transactions B,* vol. 49, no. 6, pp. 3220-3257, 2018.
[262] Y. Xu, L. Hu, J. Jia, and B. Xu, "Microstructure evolution of a SIMA processed AZ91D magnesium alloy based on repetitive upsetting-extrusion (RUE) process," *Materials Characterization,* vol. 118, pp. 309-323, 2016.
[263] Pronterface. "https://www.pronterface.com/." (accessed 12/12, 2022).
[264] P. G. u. Repository. "https://github.com/kliment/Printrun." (accessed 12/12, 2022).
[265] Reprap. "https://reprap.org/wiki/RepRap." (accessed 12/12, 2022).
[266] X. F. Liu, S. N. A. Sunny, M. R. Shahriar, M. C. Leu, M. Cheng, and L. Hu, "Implementation of MTConnect for open source 3D printers in cyber physical manufacturing cloud," in *International Design Engineering Technical Conferences and Computers and Information in Engineering Conference*, 2016, vol. 50077: American Society of Mechanical Engineers, p. V01AT02A019.
[267] G. F. Vander Voort *et al.*, "ASM handbook," *Metallography and microstructures,* vol. 9, pp. 44073-0002, 2004.
[268] K. Ednie, "Metallographic preparation of soft materials: Lead alloys," *Materials Characterization,* vol. 36, no. 4-5, pp. 243-255, 1996.
[269] K. J. Puttlitz and K. A. Stalter, *Handbook of lead-free solder technology for microelectronic assemblies*. CRC Press, 2004.
[270] A. Handbook, "Metallography and microstructures of zinc and its alloys," *Microscopy,* vol. 132, p. 203, 1983.
[271] M. Chopra and R. Rauser, "Automatic metallographic preparation of low-concentration, directionally solidified lead-tin alloys," *Materials Characterization,* vol. 25, no. 3, pp. 311-323, 1990.
[272] A. Abedi, M. Shahmiri, B. A. Esgandari, and B. Nami, "Microstructural evolution during partial remelting of Al–Si alloys containing different amounts of magnesium," *Journal of Materials Science & Technology,* vol. 29, no. 10, pp. 971-978, 2013.
[273] S. Ji, A. Das, and Z. Fan, "Solidification behavior of the remnant liquid in the sheared semisolid slurry of Sn–15 wt.% Pb alloy," *Scripta materialia,* vol. 46, no. 3, pp. 205-210, 2002.

[274] M. C. Flemings, "Solidification processing," *Materials Science and Technology,* 2006.
[275] D. Manasijević, L. Balanović, I. Marković, M. Gorgievski, U. Stamenković, and K. Božinović, "Microstructure evaluation and thermal properties of Ag–Sb alloys," *Journal of Physics and Chemistry of Solids,* vol. 169, p. 110874, 2022.
[276] B. Smetana *et al.*, "Phase transition temperatures of Sn–Zn–Al system and their comparison with calculated phase diagrams," *Journal of thermal analysis and calorimetry,* vol. 110, no. 1, pp. 369-378, 2012.
[277] K. Suganuma, S.-J. Kim, and K.-S. Kim, "High-temperature lead-free solders: properties and possibilities," *Jom,* vol. 61, no. 1, pp. 64-71, 2009.
[278] X. Niu and K.-L. Lin, "The microstructure and mechanical properties of Zn-25Sn-XAl (X= 0–0.09 wt%) high temperature lead free solder," *Materials Science and Engineering: A,* vol. 677, pp. 384-392, 2016.
[279] R. Schmid-Fetzer, "Phase diagrams: the beginning of wisdom," *Journal of Phase Equilibria and Diffusion,* vol. 35, pp. 735-760, 2014.
[280] D. Manasijević, L. Balanović, I. Marković, M. Gorgievski, U. Stamenković, and K. Božinović, "Microstructure, melting behavior and thermal conductivity of the Sn–Zn alloys," *Thermochimica Acta,* vol. 702, p. 178978, 2021.
[281] Ł. Rogal, F. Czerwiński, L. Litynska-Dobrzyńska, P. Bobrowski, A. Wierzbicka-Miernik, and J. Dutkiewicz, "Effect of hot rolling and equal-channel angular pressing on generation of globular microstructure in semi-solid Mg-3% Zn alloy," in *Solid State Phenomena*, 2015, vol. 217: Trans Tech Publ, pp. 381-388.
[282] A. Bolouri, M. Shahmiri, and E. Cheshmeh, "Microstructural evolution during semisolid state strain induced melt activation process of aluminum 7075 alloy," *Transactions of Nonferrous Metals Society of China,* vol. 20, no. 9, pp. 1663-1671, 2010.
[283] A. Bolouri, M. Shahmiri, and C. G. Kang, "Coarsening of equiaxed microstructure in the semisolid state of aluminum 7075 alloy through SIMA processing," *Journal of Materials Science,* vol. 47, pp. 3544-3553, 2012.
[284] C.-P. Wang, Z.-J. Tang, H.-S. Mei, L. Wang, R.-Q. Li, and D.-F. Li, "Formation of spheroidal microstructure in semi-solid state and thixoforming of 7075 high strength aluminum alloy," *Rare Metals,* vol. 34, pp. 710-716, 2015.
[285] G. Chen, J. Jiang, Z. Du, Q. Cao, H. Li, and X. Zhang, "Formation of Fine Spheroidal Microstructure of Semi-Solid Al–Zn–Mg–Cu Alloy by Hyperthermally and Subsequent Isothermally Reheating," *Journal of Materials Science & Technology,* vol. 29, no. 10, pp. 979-982, 2013.
[286] H. Mohammadi, M. Ketabchi, and A. Kalaki, "Microstructure evolution of semi-solid 7075 aluminum alloy during reheating process," *Journal of materials engineering and performance,* vol. 20, pp. 1256-1263, 2011.
[287] J.-l. Fu, K.-k. Wang, X.-w. Li, and H.-k. Zhang, "Microstructure evolution and thixoforming behavior of 7075 aluminum alloy in the semi-solid state prepared by RAP method," *International Journal of Minerals, Metallurgy, and Materials,* vol. 23, pp. 1404-1415, 2016.
[288] J.-L. Fu and K.-K. Wang, "Formation of spheroidal microstructure of semisolid Al–Zn–Mg–Cu alloy prepared by RAP and modified SIMA," *Rare Metals,* pp. 1-11, 2018.

[289] Q. Chen, Z. Zhao, G. Chen, and B. Wang, "Effect of accumulative plastic deformation on generation of spheroidal structure, thixoformability and mechanical properties of large-size AM60 magnesium alloy," *Journal of Alloys and Compounds,* vol. 632, pp. 190-200, 2015.
[290] Y. Hu, Y.-y. Liu, L.-z. Zhao, Y.-c. Tang, H.-t. Jiao, and D.-j. Liu, "Investigation on microstructures and properties of semi-solid Al80Mg5Li5Zn5Cu5 light-weight high-entropy alloy during isothermal heat treatment process," *China Foundry,* vol. 19, no. 6, pp. 519-527, 2022.
[291] N. A. Sukindar, M. Ariffin, B. H. T. Baharudin, C. N. A. Jaafar, and M. I. S. Ismail, "Analyzing the effect of nozzle diameter in fused deposition modeling for extruding polylactic acid using open source 3D printing," *Jurnal Teknologi,* vol. 78, no. 10, 2016.
[292] R. F. Quero, G. D. da Silveira, J. A. F. da Silva, and D. P. de Jesus, "Understanding and improving FDM 3D printing to fabricate high-resolution and optically transparent microfluidic devices," *Lab on a Chip,* vol. 21, no. 19, pp. 3715-3729, 2021.
[293] P. Geng *et al.*, "Effects of extrusion speed and printing speed on the 3D printing stability of extruded PEEK filament," *Journal of Manufacturing Processes,* vol. 37, pp. 266-273, 2019.
[294] E. N. Udofia and W. Zhou, "Microextrusion based 3D printing–a review," in *2018 International Solid Freeform Fabrication Symposium*, 2018: University of Texas at Austin.
[295] C. S. Rice, "Semi-Solid Metal Freeform Fabrication-Phase I Final Report for Period September 4, 1999--June 14, 2000," Semi-Solid Technologies, Inc., Cambridge, MA (US), 2000.
[296] S. Nafisi and R. Ghomashchi, "The microstructural characterization of semi-solid slurries," *Jom,* vol. 58, pp. 24-30, 2006.
[297] Z. Fan, G. Liu, and Y. Wang, "Microstructure and mechanical properties of rheo-diecast AZ91D magnesium alloy," *Journal of materials science,* vol. 41, pp. 3631-3644, 2006.
[298] S. Hassas-Irani, A. Zarei-Hanzaki, B. Bazaz, and A. A. Roostaei, "Microstructure evolution and semi-solid deformation behavior of an A356 aluminum alloy processed by strain induced melt activated method," *Materials & Design (1980-2015),* vol. 46, pp. 579-587, 2013.
[299] J. Xiong, G. Zhang, and W. Zhang, "Forming appearance analysis in multi-layer single-pass GMAW-based additive manufacturing," *The International Journal of Advanced Manufacturing Technology,* vol. 80, pp. 1767-1776, 2015.
[300] X. Fang *et al.*, "Study on metal deposit in the fused-coating based additive manufacturing," *Procedia Cirp,* vol. 55, pp. 115-121, 2016.

APPENDICES

Appendix 1: Calculations used for Solid/Liquid Fraction

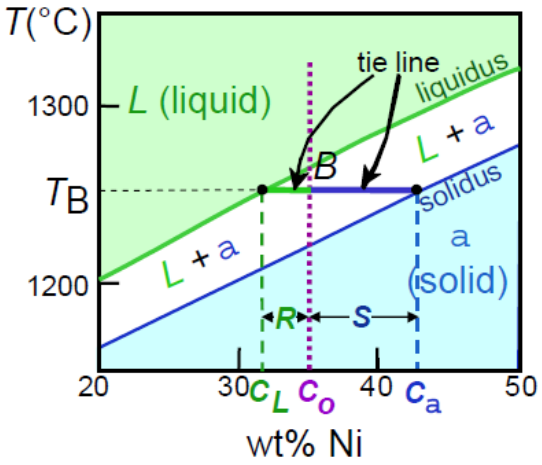

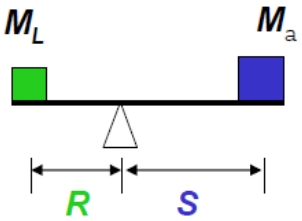

$$M_a \; S = M_L \; R$$

$$W_L = \frac{M_L}{M_L + M_a} = \frac{S}{R+S} = \frac{C_a - C_0}{C_a - C_L}$$

$$W_a = \frac{R}{R+S} = \frac{C_0 - C_L}{C_a - C_L}$$

Appendix 2: Piston-Based design

Cylinder Barrel

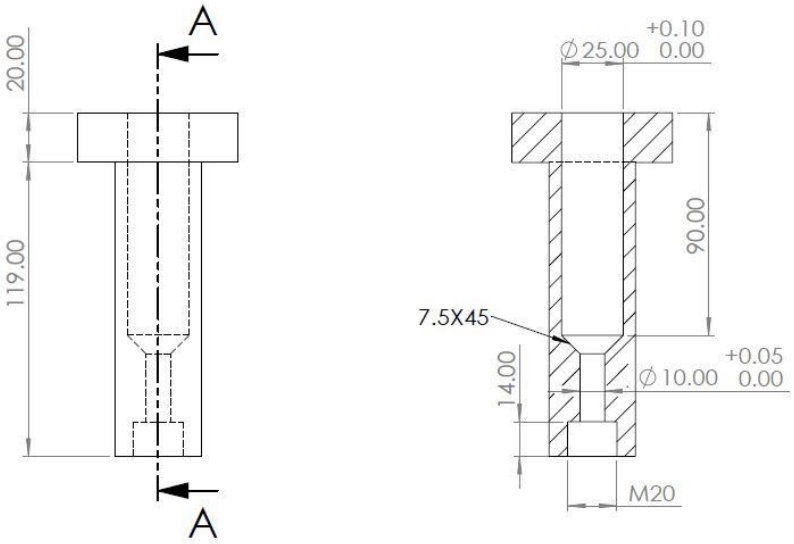

Piston

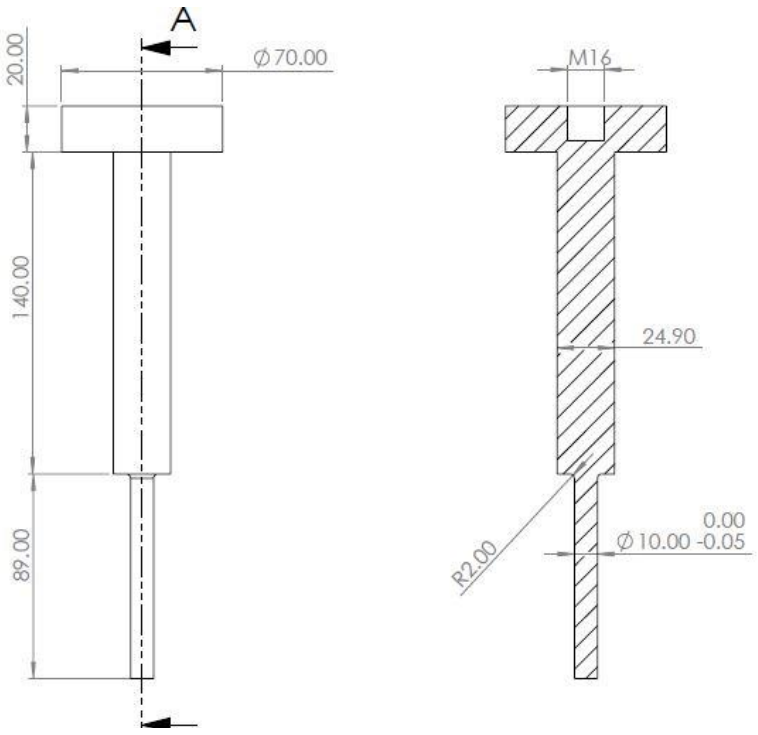

Nozzle tip

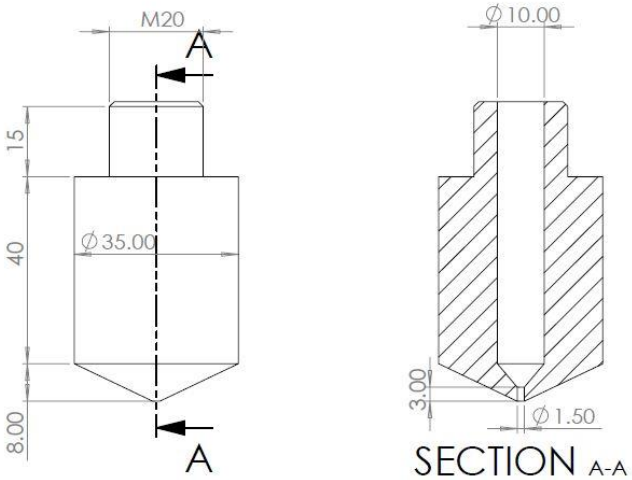

Appendix 3: Extrusion frame

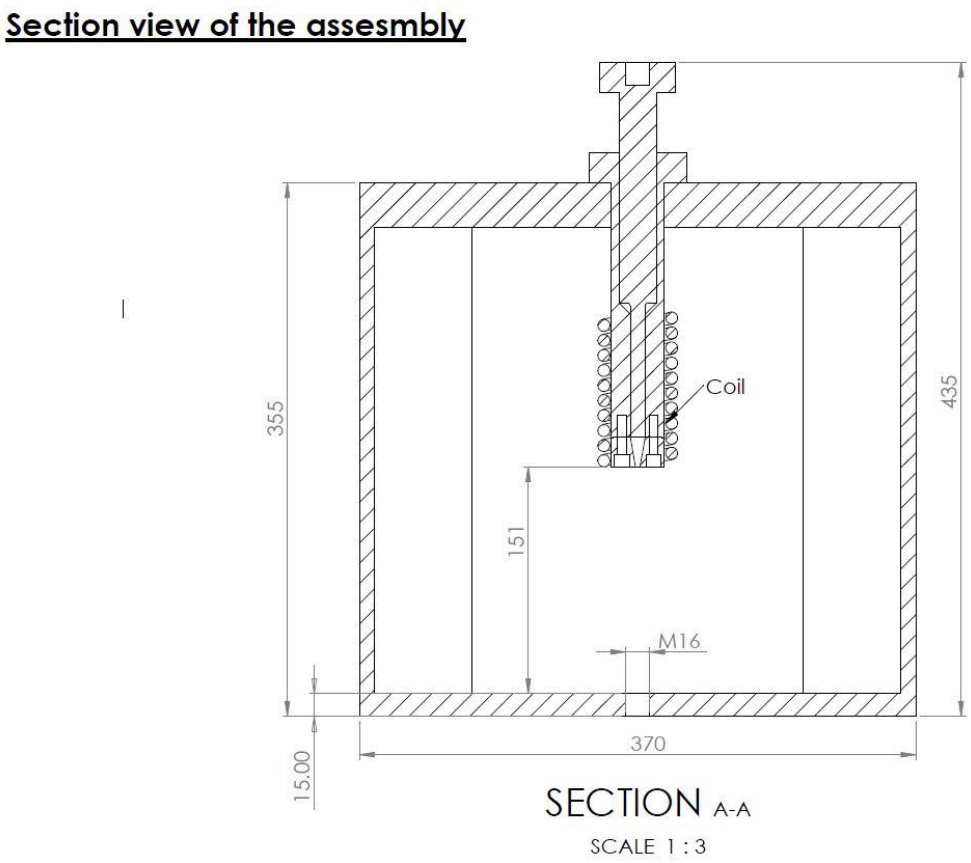

Appendix 4: LEMA system Phase II